ILMATIETEEN LAITOS
METEOROLOGISKA INSTITUTET
FINNISH METEOROLOGICAL INSTITUTE

150
CONTRIBUTIONS

VARIABILITY AND LINKAGES OF AEROSOL PROPERTIES BETWEEN SUB-URBAN AND HIGH ALTITUDE ENVIRONMENTS IN NORTHERN INDIA

RAKESH K HOODA

FINNISH METEOROLOGICAL INSTITUTE
CONTRIBUTIONS

No. 150

VARIABILITY AND LINKAGES OF AEROSOL PROPERTIES BETWEEN SUB-URBAN AND HIGH ALTITUDE ENVIRONMENTS IN NORTHERN INDIA

Rakesh K Hooda

Institute for Atmospheric and Earth System Research/Physics
Faculty of Science, University of Helsinki, Finland

Academic dissertation
To be presented with the permission of the Faculty of Science
of the University of Helsinki, for public criticism in the Aura Hall
of Finnish Meteorological Institute, Erik Palménin aukio 1
FI-00560 Helsinki, on March 27, 2019 at 12 o'clock noon.

Finnish Meteorological Institute
Helsinki, 2019

Author's Address: Atmospheric Aerosols
Finnish Meteorological Institute
P.O. Box 503
FI-00101 Helsinki, Finland
e-mail Rakesh.K.Hooda@fmi.fi

Supervisors: Academy Professor Markku Kulmala, Ph.D.
Institute for Atmospheric and Earth System Research/Physics
Faculty of Science, University of Helsinki, Finland

Professor Heikki Lihavainen, Ph.D.
SIOS Knowledge Centre
Longyearbyen, Norway
and
Atmospheric Composition Research Unit
Finnish Meteorological Institute
Helsinki, Finland

Docent Antti Hyvärinen, Ph.D.
Atmospheric Aerosols
Finnish Meteorological Institute
Helsinki, Finland

Reviewers: Professor Jyrki M. Mäkelä, Ph.D.
Faculty of Engineering and Natural Sciences
Physics Unit, Aerosol Physics laboratory
Tampere University, Finland

Senior Scientist Julia Schmale, Ph.D.
Molecular Cluster and Particle Processes
Paul Scherrer Institute, Villigen, Switzerland

Opponent: Professor Örjan Gustafsson, Ph.D.
Department of Environmental Science and Analytical Chemistry
Bolin Centre for Climate Research
University of Stockholm, Sweden

Custos: Professor Veli-Matti Kerminen, Ph.D.
Institute for Atmospheric and Earth System Research/Physics
Faculty of Science, University of Helsinki, Finland

ILMATIETEEN LAITOS
METEOROLOGISKA INSTITUTET
FINNISH METEOROLOGICAL INSTITUTE

Published by Finnish Meteorological Institute
(Erik Palménin aukio 1), P.O. Box 503
FIN-00101 Helsinki, Finland

Series title, number and report code of publication
Contributions 150
Date: March 2019

Author(s)

Rakesh K Hooda

Title
Variability and linkages of aerosol properties between sub-urban and high altitude environments in Northern India

Abstract

Atmospheric aerosol particles are linked to visibility reduction and adverse health effects, and radiation balance of the Earth— directly by reflecting and absorbing solar radiation and indirectly by influencing the cloud properties and processes and, possibly, by changing the heterogeneous chemistry of reactive gaseous species. Atmospheric aerosols are the most uncertain driver of global climate change.

The South–Asian region has been increasingly recognized as one of the global hotspots of aerosols; and Indo Gangetic Plains (IGP) is one among them with complex geography, heterogeneity in sources and varying atmospheric dynamics. These factors make IGP's aerosol and pollution very difficult to characterize. So far, long-term regional observations of aerosol properties have been scarce in this region, but argued necessary in order to bring the knowledge of regional and global distribution of aerosols further. In this context, regional studies of aerosol properties their dynamics and atmospheric processes are very important areas of investigation to better estimate the climatic importance of submicron aerosol particles. Moreover regional studies over IGP-Himalayas domain are inevitable to know how trans-Himalayan valleys are acting as conduits for aerosol and pollution transport from the plains to the Himalayas.

Therefore, in this thesis we studied these issues by applying basic to state-of-the-art instrumentation in two different environments, plains—Gual Pahari, and Himalayan foothills— Mukteshwar; to obtain physical and optical properties of submicron particles. Additionally, we used meteorological parameters, emissions and process modelling to determine local and regional scale transport of atmospheric aerosols.

The work carried out as part of the thesis infers four main conclusions, 1) Simultaneous long-term measurements at both the environments in Northern India region are useful to establish linkages between sub-urban environment and high altitude sites. One site represents a source region, while another characterize as a receiver site of atmospheric pollutants; 2) A distinct cycle of aerosol properties, both seasonal and diurnal, is present and provides information of driving factors of aerosol variability at both the sites; 3) The contribution of regional sources seem to dominate over the local /sub-urban sources, in the IGP region boundary layer; 4) Aerosol properties and specific humidity "passive tracer" based analysis clearly reveal that the mountainous terrain sites are under the influence of air from the plains due to convective transport processes enhanced by local and mesoscale topography.

The results presented in this thesis are particularly useful, first, when examining the linkages of aerosol properties variability between two different environments. The second, in determining for instance local versus regional influences, and pollutants reaching high altitude sites which can be explained by boundary layer dynamics processes, especially in the mountain terrain where the modelled mixing layer depths have uncertainties.

This work outlines future direction of multi-points measurements on vertical profile of atmospheric particles and local boundary layer over mountainous terrain where the atmospheric structure becomes much more complicated. Additionally, investigations including isotope-based analysis and modelling work over the Himalayan region are desirable to be able to describe better the transport of atmospheric aerosols from IGP to high altitudes and further up to Himalayan ice-pack and glaciers where aerosol deposition could have serious environmental impacts.

Publishing unit
Finnish Meteorological Institute, Atmospheric Aerosols

Classification (UDC)
551.510.4
551.583.1

Keywords
Aerosol properties, atmospheric dynamics, regional transport, Indo-Gangetic Plains, Himalayan foothills

ISSN and series title
0782-6117 Finnish Meteorological Institute Contributions

ISBN (paperback) 978-952-336-069-3
ISBN (pdf) 978-952-336-070-9

Language
English

Pages
115

Contents

List of Figures

List of Tables

List of Acronyms

α_{abs}	Absorption Ångström Exponent
ABC	Atmospheric Brown Clouds
ABL	Atmospheric Boundary Layer
AL	Aerosol Layer
APS	Aerosol Particle Sizer
ARB	Auto-Regressive Bootstrap
AV	Advective Venting
BC/eBC	Black Carbon / equivalent Black Carbon
CBL	Convective Boundary Layer
CCN	Cloud Condensation Nuclei
CPF	Conditional Probability Function
DMA	Differential Mobility Analyzer
DMPS	Differential Mobility Particle Sizer
D_a	Aerodynamic diameter
D_p	Particle diameter
ECHAM-HAM	Global aerosol-climate model
ECLIPSE	Evaluating the Climate and Air Quality Impacts of Short-Lived Pollutants project
ECMWF	European Centre for Medium-Range Weather Forecasts
ENSO	El Niño–Southern Oscillation
EUCAARI	European Integrated project on Aerosol, Cloud, Climate, and Air Quality Interactions project
FLEXTRA	FLEXible TRAjectory model
FMI	Finnish Meteorological Institute
GAW	Global Atmosphere Watch
GDAS	Global Data Assimilation System
GLS	Generalized Least Square
GMD	Geometric Mean Diameter
HEPA	High Efficiency Particulate Air filter
HYSPLIT	Hybrid Single Particle Lagrangian Integrated Trajectory Model
IGP	Indo Gangetic Plains
IIASA	International Institute for Applied Systems Analysis
IPCC	Intergovernmental Panel on Climate Change
LIDAR	Light Detection and Ranging
LMS	Least-Mean Square
MAAP	Multi-Angle Absorption Photometer
MCV	Mountain-Cloud Venting
MK	Mann-Kendall
MMH	Maximum Mixing Height
MODIS	Moderate Resolution Imaging Spectroradiometer
MV	Mountain Venting
Nacc	Accumulation-mode; >100 nm
Nait	Aitken-mode; 25–100 nm (typically)

NCR	National Capital Region
Nnuc	Nucleation-mode; 10–25 nm
NPF	New Particle Formation
Ntot	Total particle number concentration
OC	Organic Carbon
OM	Organic Matter
PBL	Planetary Boundary Layer
PMx	Particulate matter with an aerodynamic diameter smaller than x µm
PMx-y	Particulate matter with an aerodynamic diameter between x and y µm
PMF	Positive Matrix Factorization
rBC	refractory Black Carbon
REMO-HAM	Regional aerosol-climate model
RH	Relative Humidity
SOA	Secondary Organic Aerosol
SOC	Secondary Organic Carbon
SOP	Standard Operating Procedure
SP2	Single Particle Soot Photometer
SSA	Single Scattering Albedo
TERI	The Energy and Resources Institute
TOC	Total Organic Carbon
VOC	Volatile Organic Compounds
WHO	World Health Organization
WMO	World Meteorological Organization

Acknowledgements

To start for an academic goal, when I was on the verge to move ahead of a young professional level, only possible for me, was due to support of my dear family and the blessings of the Almighty. Nevertheless, I am thankful for the opportunity granted to me for working with the best fraternity in atmospheric aerosol science led by Acad. Prof. Markku Kulmala and associated by Prof. Veli-Matti Kerminen and my supervisors in Finnish Meteorological Institute, Prof. Heikki Lihavainen and Dr. Antti Hyvärinen. Thank you, Heikki, for hiring and believing in me and for all the support and guidance endeavored over the years. My young supervisor, mentor and friend since beginning of work in India, Antti, who have had made this work possible through his positive vibes, great technical supervision, funding applications, and many scientific/non-scientific discussions we have had during the course of this work both in India and Finland. I will forever be grateful to my first *guru*, Dr. A. Vinod Kumar, Bhabha Atomic Research Centre, India, for introducing me to atmospheric aerosols in the field and playing with computational modelling. I extend my gratitude to Dr. Antti (Katja) Lauri for the support and direction in completion of academic credits to reach to this stage of today. My sincere thanks are due to the pre-examiners, Prof. Jyrki M. Mäkelä and Dr. Julia Schmale for their insightful review and constructive comments. I highly appreciate that Prof. Örjan Gustafsson has kindly promised to my official Opponent in the public examination of this thesis.

The work presented in this thesis had been carried out at the Finnish Meteorological Institute and with concurrent visits to my home country institute, The Energy and Resources Institute. I thank both the organizations, Dr. Petteri Taalas, Dr. R. K. Pachauri, Prof. Yrjö Viisanen, Dr. T. S. Panwar, and Prof. Ari Laaksonen; and of course, the successive administrative establishment at both the institutions for providing me the opportunity to work in the corresponding institutes.

I really want to thank all the colleagues and research collaborators in the institutions, both in India and Finland and other parts of the world, who directly or indirectly were engaged with me during persuasion of this work. Special thank goes to Timo, Ved, Mika, Rawat, Eija, and Tomi who played an important role during the course of this research. I also extend my gratitude to my co-authors for their suggestions and comments on the research articles included in this thesis, perhaps not to forget to mention Niku, Ville, Ewan, Martine, Joni, Hannele, David, John, Mika, and Stefania. I appreciate the companionship of my FMI colleagues and friends for their support.

It is my duty to acknowledge the funding agencies and institutions I have worked in: Ministry for Foreign Affairs of Finland; the European Commission; Academy of Finland; Business Finland; Ministry of Science and Technology, India; and of course, Finnish Meteorological Institute and The Energy and Resources Institute.

Having said in preface of this acknowledgment, if it was not the continuous support and encouragement of my family this thesis would not have been completed. I would like to thank my parents for believing in me. I am blessed to have my parents-in-law who gave love and consistent support in every way. And, it is my fortune to have a lovely wife Vineeta who has had endured the situation in which I could concentrate on my work, and her role and sacrifices in taking alone the responsibility of our children Armaan and Akshat is beyond writing here. She also supported and pushed me forward during the completion phase of this work. In a way, she deserves not a thanks when this thesis is her achievement.

Rakesh K Hooda
Helsinki, 08 March 2019

List of publications

This thesis consists of of an introductory review and five research articles. The introduction contains scope and objectives, background for the studies and main results reached in the articles. The research articles are cited according to their numerals in the introductory review.

Paper 1 (P1)
Panwar, T. S., R. K. Hooda, H. Lihavainen, A. P. Hyvärinen, V. P. Sharma, and Y. Viisanen (2013), Atmospheric aerosols at a regional background Himalayan site—Mukteshwar, India, *Environ. Monit. Assess.*, 185(6), 4753–4764, doi: 10.1007/s10661-012-2902-8.

Paper 2 (P2)
Hooda, R. K., A.-P. Hyvärinen, M. Vestenius, S. Gilardoni, V. P. Sharma, E. Vignati, M. Kulmala, and H. Lihavainen (2016), Atmospheric aerosols local-regional discrimination for a semi-urban area in India, *Atmos. Res.*, 168, 13–23, doi:10.1016/j.atmosres.2015.08.014.

Paper 3 (P3)
Raatikainen, T., A.-P. Hyvarinen, J. Hatakka, T. S. Panwar, R. K. Hooda, V. P. Sharma, and H. Lihavainen (2014), The effect of boundary layer dynamics on aerosol properties at the Indo-Gangetic plains and at the foothills of the Himalayas, *Atmos. Environ.*, 89, 548–555, doi:10.1016/j.atmosenv.2014.02.058.

Paper 4 (P4)
Hooda, R. K., N. Kivekäs, E. O'Connor, M. Collaud Coen, J.-P. Pietikäinen, V. Vakkari, J. Backman, E. Asmi, M. Komppula, H. Korhonen, A.-P. Hyvärinen, H. Lihavainen (2018), Driving factors of aerosol properties over the foothills of central Himalayas based on 8.5 years continuous measurements, *J. Geophys. Res.*, 123 (23), 13421–13442, doi: 10.1029/2018JD029744.

Paper 5 (P5)
Raatikainen, T., D. Brus, R. K. Hooda, A.-P. Hyvärinen, E. Asmi, V. P. Sharma, A. Arola, and H. Lihavainen (2017), Size-selected black carbon mass distributions and mixing state in polluted and clean environments of northern India, *Atmos. Chem. Phys.*, 17(1), 371–383, doi:10.5194/acp-17-371-2017.

1. Introduction

Atmospheric aerosol is a major player leading positive and negative radiative balance of the Earth's climate and triggering cloud formation, and also influencing the visibility and having adverse health effects on humans. Studying its properties and processes is thus an important field of scientific research. In very remote areas such as Antarctica, the aerosol concentrations are observed as low as some tens of particles per cubic centimeter (e.g., Koponen et al., 2003). In remote areas in mountainous environments such as Mukteshwar (2180 m) in India (**Paper 1**) and Jungfraujoch (3579 m) in Switzerland (Bukowiecki et al., 2016), the particle number concentrations reach to several thousands. But, in polluted megacities such as Delhi in the Indo Gangetic Plain (IGP), particle number concentrations further elevate to several hundreds of thousands per cubic centimeter (e.g., Mönkkönen et al., 2005; **Paper 2**).

The mixture of high concentrations of aerosol particles, their precursors and reactive trace gases form persistent haze layers, commonly referred as Atmospheric Brown Clouds (ABC) spanning vast areas of the globe (Kaufman et al., 2002; Ramanathan & Crutzen, 2003).

The ABC generally denotes natural aerosols such as mineral dust and sea salt, and anthropogenic black carbon, resuspended dust and fly ash particles in addition to aerosols generated due to chemical reactions involving pollutant gases, such as nitrogen oxides, sulfur dioxide, ammonia, ozone and hundreds of organic gases and acids (Ramanathan & Crutzen, 2003). The major sources of these anthropogenic constituents are combustion of biofuels used in cooking and heating practices, open biomass burning activities, and fossil fuels used broadly throughout different economic sectors (Andreae & Crutzen, 1997; Gustafsson et al., 2009). The ABC mixture not only scatter but absorb solar radiation, and change the radiation fluxes at the surface and the top of the atmosphere (Ramanathan et al., 2001).

The large emissions of aerosols and their precursors along with unique meteorology of the tropics and the subtropics (including southern Asia) are important reasons of haze problem in this part of the globe. In India over the Gangetic-Himalayan region, these spatio-temporally diversified emissions are coupled with varying atmospheric dynamics, such as contrasting monsoons and varying Atmospheric Boundary Layer (ABL). All of this, together with the complex topography makes this region's aerosol very difficult to fingerprint and model, and to implement effective mitigation strategies (Moorthy et al., 2016).

In recent times the most polluted cities in the world are located in Northern India (WHO, 2016) and are often characterized by ABC formation (Lelieveld et al., 2001; Ramanathan et al., 2007) extending from late fall and winter until spring. The ABC exerts an increase in atmospheric stability and the reduction in rainfall over the South Asia region (Ganguly et al., 2012; Ramanathan et al., 2007; Rosenfeld, 2000), and ultimately both these effects can enhance the lifetime of aerosols. Furthermore, the ABC mixture consisting of black carbon and other light absorbing impurities are also connected in large-scale environmental effects, such as melting of the Himalayan glaciers (e.g., Menon et al., 2010). There is thus a critical need to better quantify the role and nature of aerosols in the region since their ability to modify climate depends on atmospheric abundance over time as well as their chemical, physical, and optical properties; uncertainties on all of which are large in the region.

The polluted air comprising ABC mixture can be transported via convective mixing from the plains and valleys to high altitude mountain sites (Baltensperger et al., 1997). But, there has been a lack of long-term measurements of aerosol properties in the southern Asia, especially from background areas in India. These are set of questions motivated to collect the longest time-series data for investigating

atmospheric aerosol heterogeneity in the Gangetic–Himalayan region, and further to determine the effect of boundary layer dynamics and the transport of aerosol pollution from the IGP to the foothills of the Himalayas.

This thesis deals therefore with the heterogeneity of aerosol behaviour due to local and regional emissions, and influence of boundary layer dynamics which directly govern the strength of different aerosol properties and processes. Here, the focus is set on two different environments, one in the plains and the other in Himalayas.

The aims of this work by relying on field experiments over these two different environments have been;

1. to establish a measurement station in the foothills of central Himalayas for characterization background aerosols and their trends (**Papers 1 & 4**),
2. to determine the seasonal and diurnal cycles of aerosol particles in two different environments in Northern India (**Papers 1 & 2**),
3. to segregate the local and regional emission sources of aerosol particles and finding driving factors of variabilities in aerosol properties (**Papers 2, 4 & 5**),
4. to formulate a linkage in the transport of atmospheric aerosol from the plains towards Himalayas (**Papers 3 & 4**).

2. Background

Aerosol originate from different sources, are exposed to different kinds of processes in the atmosphere, and are removed from it by various sinks. An overview of major sources, properties, processes, sinks, and the impacts of aerosols is given in section 2.1. This is followed by section 2.2 with a brief discussion on the effect of boundary layer dynamics in modulating aerosols concentrations over the plains and the mountainous terrain.

2.1 Atmospheric aerosols

An aerosol is technically defined as a suspension of liquid or solid particles in a gas, and individual aerosol particles in atmospheric science are usually characterized mostly by size and composition (Seinfeld and Pandis, 2006).

The major emission sources of anthropogenic primary particles (directly emitted) are agricultural operations, combustion of wood and fossil fuels, construction and demolition activities, road dust resuspension and industrial processes. Conversely, the main natural sources of primary particles to global emissions are mineral dust (originating from arid and semi-arid regions) and sea salt (emitted from the oceans by evaporated sea spray) (Seinfeld and Pandis, 2006). Noticeably in anthropogenic primary particles category, the combustion processes are the only contributor to light absorbing constituents e.g., black carbon (BC) together with organic component "brown carbon" (Gustafsson and Ramanathan, 2016).

The emission sources of anthropogenic secondary aerosol particles (formed in the atmosphere) include emissions from motor vehicles, smoke through domestic heating using coal or wood, open waste burning and stubble burning, or forest fires, and gaseous vegetative emissions. Typically natural sources of secondary aerosols are the biosphere that emit volatile organic compounds (VOC) which oxidizes and are able to form new particles.

The size of aerosol particles ranges from less than nanometer to hundreds of micrometer. In general, the aerosol size distribution is characterized by different size modes, which are specific concerning their different transformation and removal processes and sources. The particle size ranges of aerosol are typically: <25 nm particles (nucleation-mode) represent the most recently formed aerosol particles; 25–100 nm particles (Aitken-mode) represent fresher aerosol particles no more than a few days old; and 100 nm to 2.5 μm particles (accumulation-mode) are representative of aged aerosol particles (Seinfeld & Pandis, 2006). However, in studying the aerosol particle health effects, mass concentration of particulate matter (Pope et al., 2002) is still in common use (WHO, 2016), and the first and fundamental separation is made between the fine mode (D_p < 2.5 μm) and the coarse mode particulate matter (D_p > 2.5 μm).

The size of a particle is determined by condensation, evaporation and in-cloud reactions. Condensation and its reverse process, evaporation, change the size, mass and chemical composition of airborne particles. The primary emissions and new particle formation (gas-to-particle conversion and photochemical reactions) play an important role in escalation of particle number concentration, while a decrease in particle number concentration is governed by coagulation and wet- and dry deposition. Coagulation is a process where the collision and adhesion of aerosol particles resulting into a decrease in particle number concentration and an increase in particle size. Thus, these processes in total have a significant role in atmospheric aerosol dynamics. The aerosol particles those are smaller than 100 nm have shorter lifetimes in lower troposphere, although higher in the upper atmosphere, i.e., in stratosphere and mesosphere, where the aerosol particles may stay up to a year or even longer (Seinfeld & Pandis, 2006). Due to shorter lifetime of aerosol particles in contrast to anthropogenic carbon dioxide emissions that persists for hundreds of years (Archer et al., 2009), the aerosols are defined as important short-lived climate forcing agents. This means that spatial and temporal variability of aerosol particles is much higher than many other climate impacting agents (e.g., Kaufman et al., 2002), and the changes in emissions can be rapidly seen through variations in aerosol concentration levels (**Paper 4**). In addition to this, several aerosol emission sources could have a significant seasonality at regional scale, for instance biomass burning and mineral dust in IGP and southwest Asia regions (**Papers 2 & 4**). Not only seasonality in aerosol sources, but seasonal pattern in synoptic scale atmospheric circulation, e.g. summer monsoon that does also affect aerosol removal (**Paper 4**). This underlines the need for long-term observations covering seasonal cycle in order to do a comprehensive analysis of aerosol particle properties and their interactions in the atmosphere.

Aerosols exist in the atmosphere in a variety of composite structures: externally mixed, internally mixed, coated particles or most likely a combination of all of these. The aerosol composition is dependent on its age in the atmosphere and it varies as more and more condensable matter, especially sulphates and organics, condense on the particles due to mixing/coating (Gustafsson and Ramanathan, 2016). The external mixing is generally more reasonable for freshly emitted aerosol, while the internal mixing is associated with aged aerosol that had the time to form the coating around the core. Internally mixed primary aerosols can be produced at the source if more than one component is involved in the creation of the aerosol. Even if the particles are individually pure when first produced, there are numerous processes in the atmosphere that will convert an external mixture to an internal mixture. The freshly-emitted particles form external mixtures with pre-existing particles, where the aerosol particles of the same size have different compositions (**Paper 5**). The condensation and evaporation processes reduce these composition differences until the mixing state starts to be more uniform, with different compounds internally mixed in the particles.

In terms of impacts, atmospheric aerosol particles perturb the radiative energy budget of the Earth's climate system (IPCC, 2007) fundamentally in a two-fold way–

First, directly through interaction with radiation (aerosol-radiation interactions– REari) formerly known as direct radiative effect, where the change in radiative flux is caused by the combined scattering and absorption of radiation by anthropogenic and natural aerosols. The magnitude of this effect depends mainly on the aerosol composition (refractive index), its size distribution and concentration, and on the surface albedo (or reflectance) below the aerosol. The REari is close to being an observable quantity, yet our knowledge of aerosol and environmental characteristics needed to quantify the aerosol-radiation interactions at the global scale remains incomplete (IPCC, 2013). In general, the REari at the surface is negative and can be much stronger than the REari at the top of atmosphere over regions where aerosols are absorbing (IPCC, 2013). In India, over central and eastern parts and IGP, the atmospheric warming due to aerosols are higher in comparison to seen over peninsular, western parts and over island locations. The BC aerosols contributes more than half of the total warming during winter except over Himalayas and west India (Nair et al, 2016).

Second, indirectly by aerosol-cloud interactions (and also by aerosol–cryosphere; not explained here) where aerosol particles act as condensation nuclei for cloud droplets. In absence of such cloud condensation nuclei (CCN) no clouds could be formed in atmospheric conditions. And the diameter of the aerosol particle is the most important aerosol property deciding whether a particle can act as a CCN or not (e.g., Andreae and Rosenfeld, 2008). In aerosol-cloud interaction, when atmospheric aerosol influence the albedo is called cloud albedo effect (Lohmann and Feichter, 2005) and also known as the first indirect effect (Ramaswamy et al., 2001) or the Twomey effect (Twomey, 1977. While atmospheric aerosol when affects lifetime of clouds is called cloud lifetime effect (Lohmann and Feichter, 2005) and also known as the second indirect effect or Albrecht effect (Ramaswamy et al., 2001). So, the aerosol indirect effect is based on microphysical properties of clouds such as the number of CCN in a cloud and a higher number of CCN can lead to smaller cloud droplets. The smaller cloud droplets have a higher optical depth and hence a higher reflectivity and lifetime of clouds (Andreae and Rosenfeld, 2008). Eventually, a higher cloud cover and brighter clouds will reflect a larger fraction of incoming solar radiation back to space, i.e, in a net cooling effect in terms of the Earth's radiative budget (IPCC, 2007; Seinfeld 2011). Notably, in 2013, IPCC reported that in their earlier assessments the radiative implications of aerosol–cloud interactions are considered as two complementary processes—albedo and lifetime effects—that together amplify forcing. However, recent work at the process scale has identified compensating adjustments that make the system less susceptible to perturbation than might have been expected based on the earlier albedo and lifetime effects. Therefore, elevation in aerosol emissions can result in either an increase or a decrease in aerosol–cloud related forcing depending on the particular environmental conditions (IPCC, 2013). In total, the indirect effects are still not fully understood.

In 2013 assessment report, IPCC concluded that the radiative forcing from emissions of well-mixed greenhouse gases (CO_2, CH_4, N_2O, and Halocarbons) for 2011 relative to 1750 is 2.83 (2.54–3.12) W m^{-2}. On the other hand, the radiative forcing of the total aerosol effect in the atmosphere, which includes cloud adjustments (excluding BC on snow and ice) due to aerosols, is estimated with a 5–95% uncertainty between –0.1 and –1.9 W m^{-2} with a most likely value of –0.9 W m^{-2} [medium confidence]. The likely range of this forcing is between –0.4 and –1.5 W m^{-2}, and results from a negative forcing from most aerosols and a positive contribution from black carbon absorption of solar radiation. There is high confidence that aerosols and their interactions with clouds have offset a substantial portion of global mean forcing from well-mixed greenhouse gases. The overall impact of present-day

atmospheric aerosols is estimated to be cooling, globally counter balancing a significant fraction of the warming associated with greenhouse gases (IPCC, 2013). In total, aerosol still continue to contribute the largest uncertainty to the total radiative forcing estimate. The uncertainties in the direct and indirect aerosol climate effects are estimated to be close to the net heating effect of carbon dioxide and methane in the year 2100 climate projection (IPCC, 2007; 2013).

Besides impact on climate, the aerosols have adverse effects on human health, since particles can enter the human respiratory and cardiovascular system, and may cause inflammation and even damage of cells and organs (e. g., Franklin et al., 2008; Pope et al., 2002). Total global deaths attributable to ambient $PM_{2·5}$ increased from 3·5 million in 1990 to 4·2 million in 2015, 59% of are in east and south Asia (Butt et al., 2017; Cohen et al., 2017; Guo et al., 2018). In year 2016, WHO has reported that 10 out of the world's 20 most polluted cities are located in South Asia. The lifespans of about 660 million people is estimated to shorten by about 3 years in this region due to poor air quality (Greenstone et al., 2015). However, the effects of particle composition and size distribution on human health have yet to be fully elucidated (e.g., Davidson et al., 2005). Visibility degradation is another example of the impact of air pollution on the environment (e.g., Charlson, 1969; Malm et al., 1994; Roessler and Faxvog, 1981).

2.2 Boundary layer dynamics

The atmospheric boundary layer (ABL) is the atmospheric layer that interacts directly with the Earth's surface on a time scale of a few hours or less, and during convective conditions, ABL is referred as convective boundary layer (CBL). The development of ABL plays a key role in the distribution of atmospheric constituents (Stull, 1988).

In flat terrain, the CBL grows by upward sensible heat flux at the surface and downward sensible heat flux (entrainment) at the top of the CBL. The convergence of the sensible heat flux causes the CBL to warm and grow in depth (e.g., De Wekker and Kossmann, 2015). On the other hand, over mountainous terrain, the atmospheric structure becomes much more complicated and even a universal definition of CBL height over mountains remains an ambiguous issue (e.g., De Wekker and Kossmann, 2015; Serafin et al., 2018). Transport and mixing processes, such as those related to mountain waves (Smith et al., 2007) and thermally driven wind systems (Zardi & Whiteman, 2013) among others, affect CBL variability significantly (Fig. 1).

The atmospheric thermal and dynamic factors, e.g., air temperature and wind speed basically drives the ABL, and also controls feedback between atmospheric aerosol loading and ABL height. The more ambient aerosols accumulate, the less solar radiation reaches to surface resulting a disadvantageous effect on surface air temperature as well as a positive impact on ambient relative humidity, which restricts the development of ABL. The low ABL height in turn forces the accumulation of aerosol particles in the high relative humidity and shallow atmosphere. This is a case recognized in the IGP region mainly during post-monsoon and winter seasons (**Papers 2 & 3**). However, this scientific issue involves many complicated atmospheric processes remaining poorly understood. In order to that the temporal variability and the vertical distribution of aerosol concentrations at different altitudes are important to study. This can give an understanding of changes in the aerosol properties at plains within the ABL and transport of aerosol to the mountains as a function of ABL growth (**Papers 3 & 4**).

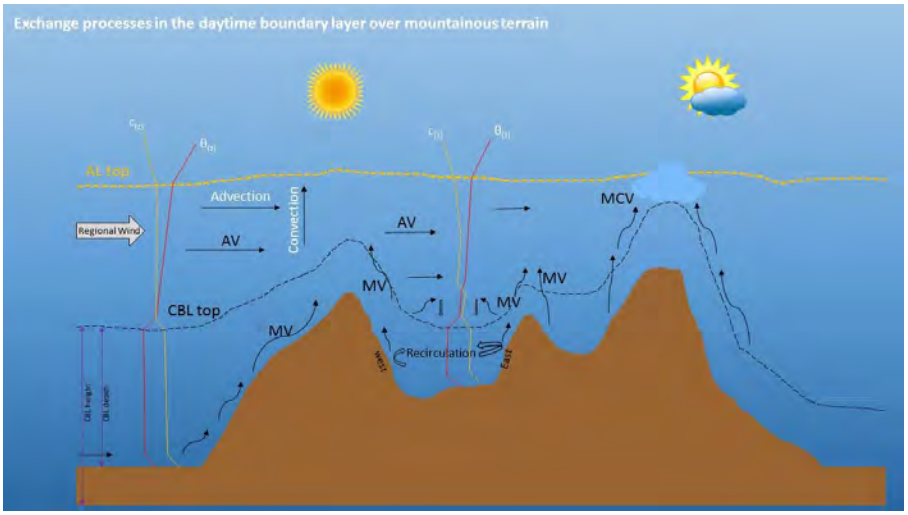

Figure 1. Schematic illustration of mountain induced exchange processes between the convective boundary layer and the overlying atmosphere. AV= Advective venting; MV= Mountain venting; MCV= Mountain-cloud venting. Vector indicates airflow, whereas c(z) and θ(z) indicate vertical profiles of pollutant concentration and potential temperature, respectively. The dotted and dashed line indicate the top of the aerosol layer (AL) and the CBL, respectively (modified from De Wekker and Kossmann, 2015).

3. Methods and material

3.1 Observation sites

As part of this thesis work, the measurements were carried out at two locations (Fig. 2). The first observation site was a background location in Mukteshwar (29°26´N, 79°37´E), about 250 km east of New Delhi in India. The site has a 180° view of the Himalayan ranges west, north and east of the site; the nearest high peaks are approximately 90 km NE of the site. The area surrounding the site consists of low mountains (peaks 1,500–2,500 m asl) between the IGP (100–200 m asl) and the Himalayas (peaks 6,000–8,000). The Indian Himalayan region is part of the Third Pole which encompasses the Himalaya-Hindu Kush mountain range and the Tibetan Plateau because its ice fields contain the largest reserve of fresh water outside the Polar Regions. The combination of snowmelt, ice melt, and rain from the Indian Himalayas forms the source of the Indus, Ganges, and Brahmaputra, and six other large rivers in Asia. More than 750 million people live within the Indus, Ganges, and Brahmaputra basins, including an estimated 200 million living in the headwater regions (Shresta et al., 2015).

The measurement site in Mukteshwar was located at 2180 m asl in a rural region in the foothills of southern Himalayas. The nearest population centers to observatory are the town of Almora (1650 m asl, 16 km N, population ~34 000) and the city of Haldwani (424 m asl, 32 km SW, population ~150 000). The major metropolitan city Delhi, located in the IGP region (215 m asl, 250 km SW), has a population of ~16.8 million (Census of India, 2011). Since the location is a remote place with minimal local emissions, we believe that the site represented, to the extent possible, a regional background in India (**Paper 4**).

The second measurement site was located in outskirts of Delhi at Gual Pahari (28°26'N, 77°09'E, 243 m asl) about 25 km south of New Delhi (Kulmala et al., 2009; Hyvärinen et al., 2010; **Paper 2**). The surroundings represent a semi-urban environment and is located in the densely populated IGP region.

The site is mostly influenced by large-scale anthropogenic emission sources (biomass burning, fossil-fuel combustion and industrial activities) within the IGP and mineral dust transported from western India. The IGP region is one of the most populated with over 900 million inhabitants. It is both highly fertile agricultural belt and a rapidly developing region of the Indian subcontinent, and increasingly recognized to be among the global hotspots of aerosols and trace gases (Moorthy et al., 2016).

The simultaneous measurements focusing on these two different environments: polluted IGP and relatively clean Himalayan foothills provide experimental information about the processes affecting the transport of atmospheric aerosol from the plains towards Himalayan foothills (**Papers 3 & 4**). The elevation profile (Fig. 2) shows Mukteshwar is closer to the plains than the high mountains of the Himalayas, and the distance between the two stations is about 270 km. It is however studied that aerosols from the plains can have an effect on concentration levels at high altitude sites in the Himalayas (Bonasoni et al., 2010; **Papers 3, 4 & 5**). Moreover, due to wintertime shallow boundary layer and confined dispersion of aerosol particles due to Himalayan mountain range parallel to the IGP, aerosols are restricted to lower atmosphere. This atmospheric dynamics and a complex geographic location of IGP therefore could be one of the reasons of high concentration of anthropogenic aerosols.

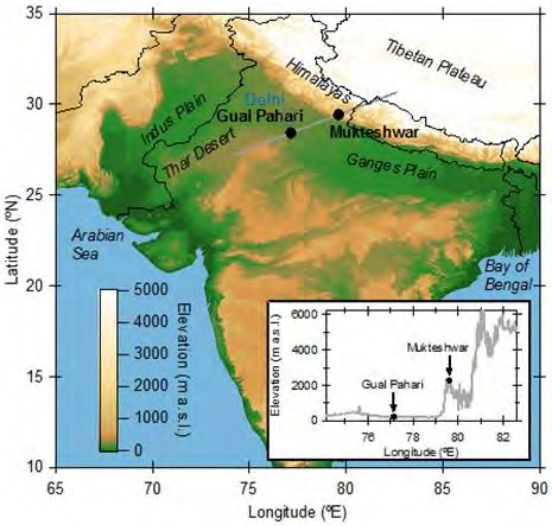

Figure 2. Location of measurement stations in mountains at Mukteshwar (black solid marker) and in plains at Gual Pahari (black solid marker). The elevation of Mukteshwar is 2180 m asl and Gual Pahari is 243 m asl, and distance between Mukteshwar and Gual Pahari is 270 Km. Delhi is shown with blue open marker (modified from Paper 3).

In addition to this, a low-elevation and gently sloping middle and lower reaches of the Indus and Ganges river basins in the IGP make this region susceptible to commonly windblown dust originated from the arid and desert regions of southwest Asia and Thar Desert (e.g., El-Askary et al., 2006). It blankets IGP and Himalayan foothills during March to June period (e.g., Kumar et al., 2015; **Paper 4**). Also, the anthropogenic emission in terms of agriculture residue burning are noticed to be a major attributor to atmospheric aerosols over the region. This activity of residue burning lasts for about a month each in pre- and post-monsoon seasons to prepare the soil for sowing next crop when agriculture residue is generated due to combine harvesters. It has previously been highlighted that this

smoke of agriculture residue burning during post-monsoon generally blankets nearly the whole IGP region from west to east (e.g., Badarinath et al., 2009; Singh and Kaskaoutis, 2014) during adverse seasonal meteorological conditions (calm to weak winds and relatively low boundary layer height and insufficient dilution, all following intense monsoons in the months prior). Figure 3 shows the bulk of the plume clearly sourced from fires in specific areas in Northern India. The pollution over the IGP region, however, is a combination of biomass burning, open-waste burning, vehicular pollution, and emissions from coal-based power plants (e.g., Prasad et al., 2012; **Paper 2)**. Moreover, in the course of certain circumstances, these plumes can even get transported over the Himalayan foothills (Bonasoni et al., 2010; **Paper 4**).

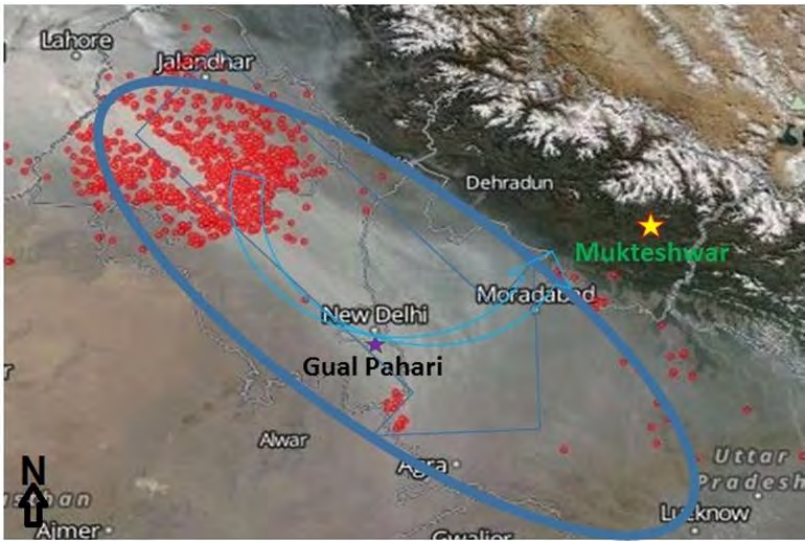

Figure 3. Satellite image from Aqua — MODIS (Moderate Resolution Imaging Spectroradiometer) showing the transport of plumes from agriculture residue burning in northern India toward the east of the Indo-Gangetic plain (IGP) on 31st Oct 2017. The red solid circles show predominant areas of agriculture residue burning. The measurement locations Mukteshwar and Gual Pahari are shown with star marker. On the very next day, the same plume formed intense smog and fog over the IGP shown with blue circle (modified from Singh and Kaskaoutis, 2014). The two arrows show that regional weather patterns typically funnel this smoke to the IGP from west to east and in certain circumstances these plumes can even get transported over the Himalayan foothills. Source: https://earthobservatory.nasa.gov/images/stubble-burning-in-northern-india (accessed on 09.10.2018)

In light of different major sources of aerosols in the IGP region, the knowledge on spatial and temporal distribution of surface emissions, and evaluating their evolution over time is essential for a comprehensive assessment of air quality and climate change issues at regional scale. The emissions of SO_2 (e.g., IIASA, 2015), NOx (e.g., Li et al., 2017) and $PM_{2.5}$ (Butt et al., 2017) have increasing trends, and sulphate mainly from energy production and industries has also showed a steep increasing trend after 2007 (IIASA, 2015). Conversely, emissions of BC and OM (organic matter) from domestic sector in India has showed a slight decreasing or stable trend. Figure 4 drawn based on emission estimations by IIASA, (2015) shows lower levels of BC emissions at Mukteshwar in comparison to IGP region (represented by Gual Pahari). The emission levels are almost stable at Mukteshwar over the study period, while at Gual Pahari an increase is seen in year 2014 with respect to the base year 2005 (**Paper 4**).

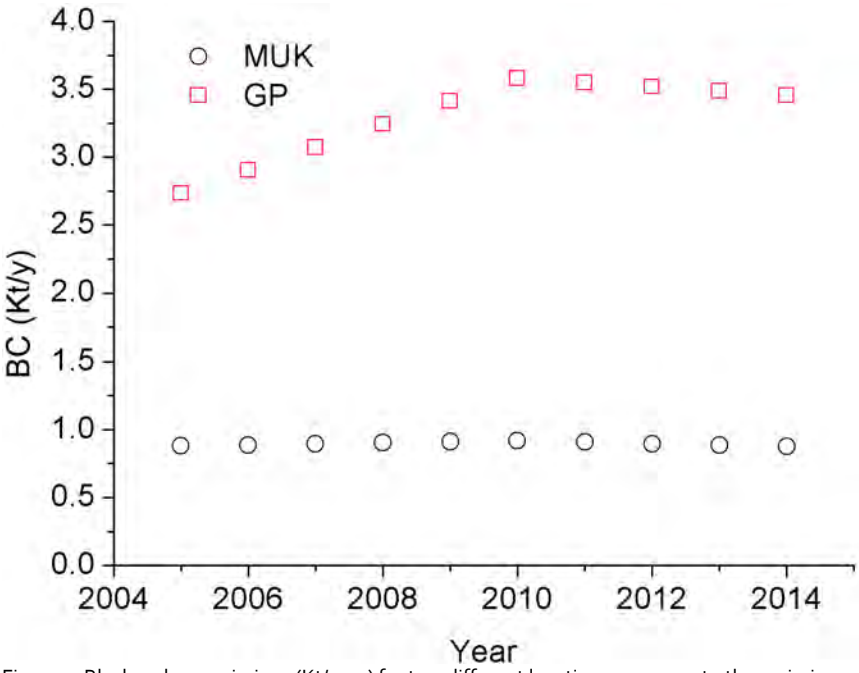

Figure 4. Black carbon emissions (Kt/year) for two different locations, one near to the emission sources in IGP (represented by Gual Pahari-GP) and second in the foothills of Himalayas (represented by Mukteshwar-MUK) (adapted from Paper 4 Supporting Information).

3.2 Field experiments

In order to initiate a long-term aerosol measurement program many issues need careful considerations with respect to administrative support and of course in terms of technical services. The administrative and infrastructural services could be in form of available resources (power supply, network connection, local supporting staff etc.), security and stationing of instruments, etc. The technical services are in form of defining the goal of the measurements, listing of instrumentation to be installed, preparing standard operating procedure (SOP), training of local staff, and daily maintenance of the station/instruments and keep a record of activities in the form of station logbook, etc. This approach gets complicated when the start of measurements is in foothills of Himalayas, a remote station such as Mukteshwar. However, this was achieved successfully with a collaboration of the Finnish Meteorological Institute (FMI) and The Energy and Resources Institute (TERI), a local partner. The level and number of problems decreased drastically when the measurements were operational at Gual Pahari near to Delhi in collaboration with the same local partner institute, and of course improved also at Mukteshwar with due course of time resulting a data coverage between 70% and 80% over the years.

The instruments for long-term measurements at Mukteshwar and Gual Pahari were selected in a way to automatically restart after a power failure, and the data logging programing was done accordingly. This practice minimizes the work of on-site maintenance personnel, though was required to visit the station daily and practically for cleaning of aerosol inlets and impactor plates, checking

measurements flow, aerosol device zero levels and replacing filter tape when necessary. The visits of researchers from FMI were every 1 to 3 month time to make full calibration of the instruments, for example, nephelometer full calibration (span calibration gas CO_2), however, automatic zero calibration (with HEPA filter) was made every three hours. The PM monitors calibration using a set of reference mass filters, verifying continuous power supply and inventorying the stock of spare parts necessary to an uninterrupted measurement were the part of responsibilities of local staff. The FMI researchers were available online and also on phone to provide instructions to correct the fault, noticed if any, on daily basis.

3.2.1 Measurements

In Mukteshwar, the measurement station was made of stone and had four rooms, of which the instrument room was air conditioned to about 20 °C. The station building was on the top of a hill above the surrounding nearby areas (**Papers 1 & 4**). The next requirement was using an inlet for aerosol measurement that meets certain design guidelines so that undisturbed aerosol is delivered to measurement instrumentation (WMO/GAW, 2003). In substance, the ambient air sampling scheme and sample air conditioning (drying) were adhered with the recommendations of WMO (WMO/GAW, 2003). The instruments were shipped to Mukteshwar in June 2005 and after a gestation period of 3 months, the systematic and long-term measurements of aerosol properties were started in Sept 2005 and are operational till the writing of this thesis with some intermittent breaks due to requirement of instruments for campaign based studies in India particularly at Gual Pahari (Hyvärinen et al., 2009; Komppula et al., 2009; **Papers 1, 4 & 5**). The station was established by FMI and is now fully handed over to the local partner TERI, but a technical support from FMI is still provided.

In Gual Pahari, the station was built in a standard 20 feet sea container with air conditioning, thermal insulation between outer and inner walls, an internal electricity board and UPS's for power stabilization. In addition, the container was shaded with a light tent to prevent excessive heating by direct sunlight. The container was prepared at FMI with the required instruments and shipped to India in late 2007 under the EUCAARI project (Kulmala et al., 2009). The measurements were carried out from December 2007 to January 2010 (Hyvärinen et al., 2010; **Papers 2 & 3**). The measurements were also carried out both in Gual Pahari and Mukteshwar sites for studying the mixing state of absorbing aerosol (black carbon) (**Paper 5**). Substantively, the technical arrangements at Gual Pahari were similar to Mukteshwar.

3.2.2 Instruments

Both the stations, Mukteshwar and Gual Pahari, had similar instrumentation including Particulate Mass (PM) monitors (Thermo Scientific, beta attenuation) for measuring $PM_{2.5}$ and PM_{10} mass concentrations, nephelometer (Ecotech) for aerosol scattering, Differential Mobility Particle Sizer (DMPS) systems for sub-micron particle number size distributions (10–800 nm), Aerosol Particle Sizer (APS, TSI 3321) for particle number size distribution (0.5–10 μm) and Vaisala WXT/Milos weather stations for meteorological parameters. The absorption coefficient and aerosol equivalent black carbon (eBC, refers to the optical absorption methods) were measured from the $PM_{2.5}$ inlet with a Magee Scientific 7-wavelength aethalometer at 370, 470, 520, 590, 660, 880, and 950 nm (in Mukteshwar. The eBC absorbs light at all seven wavelengths, but is the sole absorbent at 880 nm, thus, aethalometer gives directly the black carbon concentrations from the 880 nm measurement. However,

the aethalometer has been observed with a number of artefacts, such as the multiple scattering on the filter paper and filter paper loading. These artefacts had been corrected for Mukteshwar measurements following adequate methods as explained in Hyvärinen et al., 2009 and **Paper 4.** In Gual Pahari, eBC was measured from the PM10 inlet by a Multi-Angle Absorption Photometer (MAAP, Thermo Scientific; 637 nm wavelength). The measured eBC concentration was corrected for a measurement artefact of the MAAP (Hyvärinen et al., 2013), and later used in **Papers 2 & 3**. In addition, the refractory black carbon (rBC) concentrations and mixing state parameters were also measured during the year 2013 and also in 2014 at both Mukteshwar and Gual Pahari minimum for 2 months period successively at each site during pre-monsoon period. It was done by using state-of-the-art instrumentation setup and first time in India, a Single Particle Soot Photometer (SP2; Revision C* with 8 channels) manufactured by Droplet Measurement Technologies (Boulder, CO, USA) which was connected to a DMA (**Paper 5**). A summary of the instruments is listed in Table 1.

At Mukteshwar, the inlet system mounted 1.5–2m above the roof and 4–5m above ground level included separate inlets for the PM monitors and a joint PM10 inlet with a PM2.5 cyclone (Rupprecht & Patashnick) for the aethalometer, nephelometer and DMPS. In addition to the aerosol measurements; ambient temperature, relative humidity, solar irradiation, both wind direction and speed were also measured with MILOS500+ sensors weather station. The temporal measurement resolution was 5 min for the aerosol properties and 1 min for meteorological parameters (**Papers 1 & 4**).

At Gual Pahari, a range of instruments were utilized within the period of the EUCAARI project, but part of that data is used for this thesis work (**Papers 2, 3 & 4**). The foremost is a Dichotomous Partisol-Plus Sequential Air Sampler which was mounted near the container and sample was taken at 2 m above the ground level (**Paper 2**). The sampling of 24 hours simultaneous ambient fine (PM2.5) and coarse (PM2.5–10) aerosol every 6 days from April 2008 to March 2009 was carried out subjected to chemical speciation including ions, organic and elemental carbons (**Paper 2)**. The fine and coarse particles were collected on 47 mm quartz filter at a flow rate of 16.7 l/min, and the negative artefacts (losses of volatile species such as ammonium and nitrate) and positive artefacts (absorption on the collection substrate of semi-volatile species such as low molecular weight organics) were corrected (Gilardoni et al., 2011; Vecchi et al., 2009; **Paper 2**). The ambient temperature, relative humidity, rain intensity, wind direction and wind speed were also measured with WXT weather station. The sensor was mounted 3m above the container roof. The other measurements conducted during the period of the EUCAARI project are for example with DMPS, nephelometer (Hyvärinen et al., 2010), and Cimel sunphotometer and the PollyXT LIDAR (Komppula et al., 2012), and had been presented in our previous publications.

Table 1. Summary of instrument used both in Mukteshwar and Gual Pahari, the parameters measured and their physical, chemical and optical properties measurements/derived.

Instrument	***Parameter***	***Property***	***Derived variable***
Particulate Mass (PM) monitors (Thermo Scientific, beta attenuation)	PM2.5	Mass concentration (Fine particulate matter in health studies)	Mass concentration of particle size fraction with an aerodynamic diameter smaller than 2.5 μm
Particulate Mass (PM) monitors (Thermo Scientific, beta attenuation)	PM10	Mass concentration (Respirable suspended particulate matter in context of health studies)	Mass concentration of particle size fraction with an aerodynamic diameter smaller than 10 μm

Dichotomous Partisol-Plus Sequential Air Sampler	Fine (PM2.5) and coarse (PM2.5–10)	Filter based mass deposition and gravimetric mass	Chemical speciation including ions, organic carbon and elemental carbon
Differential Mobility Particle Sizer (DMPS)	Particle number size distributions (10–800 nm)	Size distribution	Particle number size distribution typically in size ranges: the nucleation, Aitken and accumulation mode. Total number concentration and geometric mean diameter. The particle mass distribution, assuming spherical particles and a gravimetric density of 1.77 g cm^{-3}
Aerosol Particle Sizer (APS, TSI 3321)	Particle number size range 0.5–10 μm	Size distribution	Volume size distribution
Vaisala WXT/Milos weather stations	Meteorological parameters	Ambient temperature, relative humidity, solar irradiation, both wind direction and speed	Specific humidity, wind variability (turbulence)
Integrating Nephelometer (Ecotech M 9003) (σsp) at λ=525 nm	Scattering coefficient	Aerosol scattering	Total scattering and submicron scattering fraction with PM2.5 inlet system
Seven-wavelength (370 nm to 950 nm) Aethalometer (Magee Scientific AE-31)	Absorption coefficient (σap) and equivalent black carbon (eBC) at λ=880 nm (refers to the optical absorption methods)	Aerosol absorption and black carbon concentration	The single scattering albedo (SSA) using measured σsp (λ= 525 nm) and σap (λ=520 nm), and absorption Ångström exponent (αabs) that describes the spectral dependence of light absorption by the aerosol
Multi-Angle Absorption Photometer (MAAP, Thermo Scientific; 637 nm wavelength)	Absorption coefficient	Aerosol black carbon concentration	
Single Particle Soot Photometer (SP2; Revision C* with 8 channels) manufactured by Droplet Measurement Technologies (Boulder, CO, USA)	refractory black carbon (rBC) concentrations	Mixing state parameters including rBC number fractions and rBC mass in each particle	rBC mixing state and comparing the differential mobility analyzer (DMA) selected particle size with that measured by the SP2 gives additional information about particle morphology

For quality assurance and quality control of the data generated at both the sites, the raw data was first examined visually and clear outliers were removed. During data processing, the meteorological parameters and aerosol properties were averaged to 1-hour resolution, taking into account only those hours when more than 50% of time was covered by valid measurements. The hourly data was then used in all further calculations (**Papers 1, 2 & 3**) unless a high time resolution data for any specific analysis was required, e.g., meteorological data (**Paper 4**); and refractory black carbon (rBC) concentrations and mixing state parameters (**Paper 5**).

3.3 Meteorological characteristics

As typical for the Indian sub-continent, the weather exhibits a clear seasonal pattern. The seasonal classification adopted for Mukteshwar and Gual Pahari is winter (December to February), pre-monsoon (March to May), monsoon (July to August), post-monsoon/autumn (October to November). The months of June and September are a mix of dry and rainy periods with transitional synoptic weather conditions and synoptic scale circulation, hence classified as transition months in our analysis. Broadly, the differentiation of pre- and post-monsoon in India are based on arrival and withdrawal phase of the classified precipitation level, and that might differ across the years. The southwest flow of humid air over India is a main feature of the monsoon period. But, sometimes it is weakened by induction of stronger and/or more frequent dry northwesterly winds of continental origin over western India (Kaskaoutis et al., 2012), resulting in anomalies in precipitation level.

In monsoon, typical southwest and southeast monsoon winds are observed both at Gual Pahari and Mukteshwar. During other seasons a distinct pattern in both wind speed and direction manifests a topography difference between Mukteshwar and Gual Pahari. Notably, at Mukteshwar mountain/valley wind patterns prevail the diurnal cycle across the seasons including monsoon, and the wind directions are consistent with the alignment of the mountain ridges (**Paper 4**). Hourly average wind speed generally below 2 m/s at Mukteshwar indicates weak horizontal transport (**Papers 3 & 4**). Since both wind direction and speed depend on local topography (**Papers 2 & 3**), therefore the specific humidity as a passive tracer is utilized (**Paper 4**) for studying boundary layer dynamics (e.g., Kowol-Santen et al., 2001; Weigel et al., 2007), and trajectory analysis is used to examine the possible origin of air masses (**Papers 3 & 4**).

In figure 5, temperature, relative humidity and wind speed for example of winter season are shown for both the locations. Temperature has similar diurnal cycles, but the absolute values are lower in Mukteshwar due to the higher altitude. In Gual Pahari, cold temperature is recorded during winter season and a high diurnal variation in temperature during pre-monsoon has been observed. This difference in temperature leads to a highly dynamic boundary layer characteristics in the IGP region, which drives a confined mixing of pollutants during winter season whilst in pre-monsoon season an efficient vertical mixing (Hyvärinen et al., 2010; **Papers 2 & 3**). The temperature minima and RH maxima are seen at the same time for Gual Pahari across the seasons. The RH is less variable at Mukteshwar than of Gual Pahari.

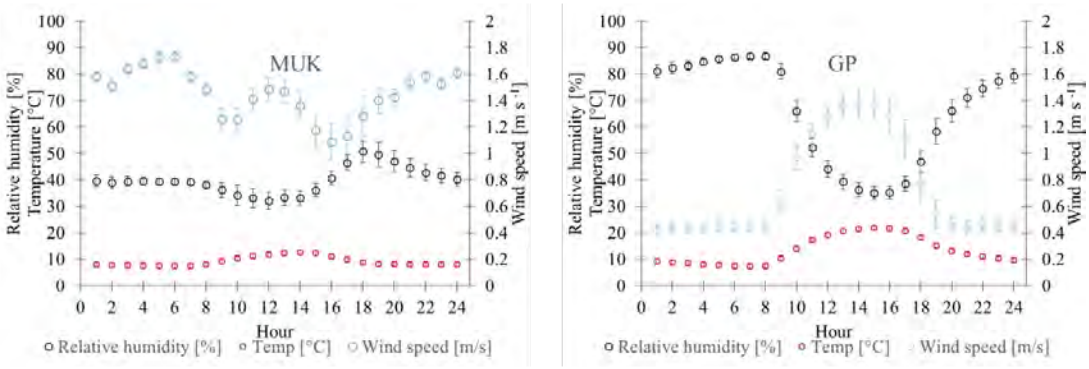

Figure 5. Diurnal mean relative humidity, temperature and wind speed at Mukteshwar (left) and Gual Pahari (right) during winter season. The error bars indicate 95% confidence values for relative humidity, temperature and wind speed.

The 5-day back trajectories were calculated using the HYSPLIT 4.9 (Draxler and Hess, 1998; Stein et al., 2015) for every three hours (the temporal resolution of the GDAS data) at Mukteshwar and FLEXTRA model (Stohl et al., 1995; Stohl and Seibert, 1998) using data from the European Centre for Medium-Range Weather Forecasts (ECMWF) at Gual Pahari, for the respective measurement periods. Even if Mukteshwar and Gual Pahari trajectory directions are similar (e.g., Komppula et al., 2009; **Papers 2, 3 & 4**), average trajectory altitudes, total lengths and mixing heights (or ABL, PBL) shows that air masses could have different origin. During the monsoon season both sites have air masses mainly from southwest and southeast (Arabian Sea and Bay of Bengal, respectively), but in other seasons westerly air masses prevail (Fig. 6). During the post-monsoon and winter seasons, more than 70% of time Mukteshwar air masses are originating from altitudes well above the Gual Pahari maximum mixing height (MMH) (**Paper 4**). The average trajectory altitude are also greater than the trajectory end point altitude indicating that air masses are descending while approaching the Mukteshwar station. Finally, the longest trajectory lengths indicate that Mukteshwar air masses are also originating from the free troposphere where wind speeds are commonly high. These observations show that Mukteshwar air could be relatively clean (**Paper 1**) while the limited mixing in Gual Pahari allows the buildup of high aerosol concentrations during the post-monsoon season and winter (**Papers 2 & 3**). During pre-monsoon the MMH increases (**Paper 4**) and eventually exceeds the average trajectory altitude at Mukteshwar. The situation is similar during the monsoon season when air masses approaching Mukteshwar are actually ascending (average altitudes below the end point altitudes) from altitudes similar to the MMH, indicating Mukteshwar and Gual Pahari air masses have similar origin. It is usually due to prevailing cyclonic circulation in this region during the pre-monsoon and monsoon seasons (**Papers 3 & 4**). In total, Mukteshwar air masses are practically always crossing the IGP, which is here represented by Gual Pahari (**Paper 4**).

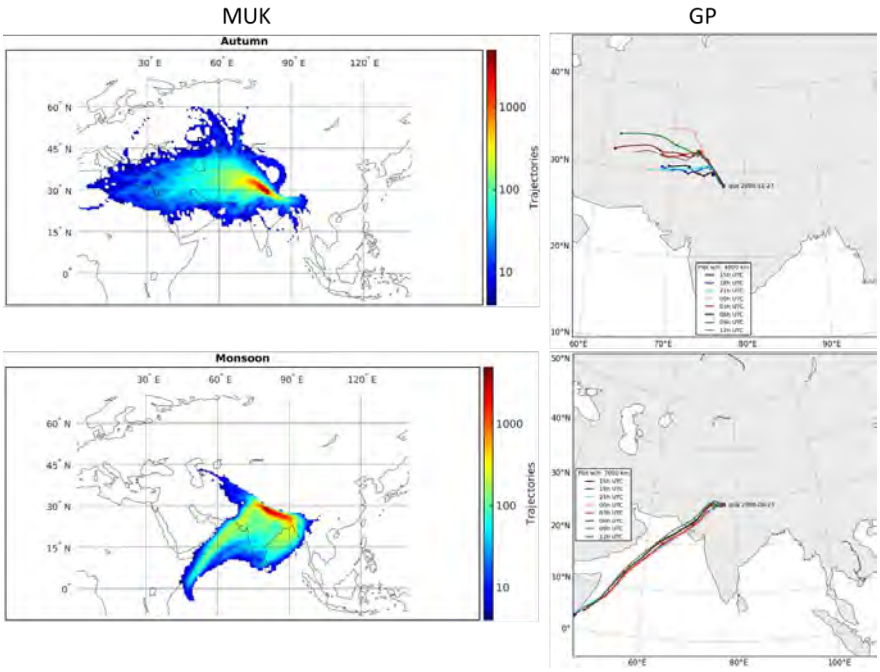

Figure 6. The 5-day long backward air mass trajectory for the autumn and monsoon seasons as frequency distribution for Mukteshwar (left) and as typical example days for Gual Pahari (right). The 5-day back trajectories are calculated with HYSPLIT (at Mukteshwar) and FLEXTRA (at Gual Pahari) for the respective measurement periods.

4. Results and Discussion

The mass concentration of PM10, PM2.5, eBC and rBC, number size distributions (10–800 nm), geometric mean diameter (GMD) and absorption and scattering coefficients are the aerosol properties included in this work (Table 1). The number size distribution was divided further into three characteristic particle size ranges of aerosol, 10–25 nm particles (nucleation-mode 'Nnuc'), 25–90 nm particles (Aitken-mode 'Nait'), 90–800 nm particles (accumulation-mode 'Nacc'). The sum of the particle number concentrations in the three particle size ranges is termed total number concentration (Ntot). The single scattering albedo (SSA) and absorption Ångström exponent (α_{abs}) were also estimated using absorption and scattering coefficients. Studying mass concentrations of PM10, PM2.5 and eBC inculcate broadly the effects on health and environment, while rBC reveals mixing state of BC that helps in evaluating micro-physical characterization and potential impact of BC on climate. The number size distribution and the ratio of various size modes can be utilized to examine age of the aerosols and also in fingerprinting distance of various aerosol sources. The GMD expresses the lognormal size distribution and enlightens growth and potential shrinkage of particles. In optical properties, SSA is an important parameter which explains absorbing/scattering nature of aerosols and generally used for estimating direct radiative effect of aerosol, while α_{abs} is used to characterize the absorbing species which tells nature of the emitting source.

4.1 Spatio-temporal distribution of aerosol properties

In general, number concentrations correlate with mass concentrations unless particles due to new particle formation (NPF) attribute dominantly. Similarly, scattering and spectral absorption coefficients correlate with the total aerosol (PM10 or Ntot) and eBC mass concentrations, respectively. So the diurnal cycles of the mass concentrations are broadly identical to those of aerosol optical properties and number concentrations (**Papers 3 & 4**). Previously, similar results have been presented in our publications (Hyvärinen et al., 2009, 2010; Komppula et al., 2009).

The PM10 & PM2.5 annual average mass concentrations of 40 μg/m^3 and 25 μg/m^3 at Mukteshwar and 215 μg/m^3 and 125 μg/m^3 at Gual Pahari, respectively, are among the highest concentrations in comparable environments all around the world (Hyvärinen et al., 2010; WHO, 2016; **Papers 2, 3 & 4**). The mass concentration values exhibit a pronounced month dependent diurnal cycle at both the stations (Fig. 7). This is an expected result due to a high contrast in the rainy and the dry seasons' meteorology. High pre-monsoon and low monsoon season aerosol concentrations are common for both the sites, however, at Gual Pahari the level of concentration is relatively higher across the seasons. This high level concentration behavior mainly during winter, and partly in the post-monsoon is explained potentially by the meteorological situations. In winter, the surface-based inversion layer is at low altitudes and has a weaker development of the ABL compared to the other seasons. Notably, the low ABL height or stable atmospheric conditions in the night time during winter season in turn forces the accumulation of aerosol particles at Gual Pahari. The nocturnal high concentrations in particular are genesis of an increase in wastes burning such as grass, dry leaves, wood, solid-waste etc. for getting warmth against cold weather during the winter in northern part of India (Ganguly et al., 2006; Hyvärinen et al., 2010; **Paper 2**). On the other hand, in post-monsoon season high concentration levels are mainly due to regional smoke plumes and secondary aerosols (**Paper 2**). Kaskaoutis et al., (2014) reported thick smoke/hazy aerosol layer below 2.5 km in the atmosphere during post-monsoon which covers nearly the whole IGP. Furthermore, across the seasons a broad peak between about 07:00–09:00 AM is consistent with the rush-hour traffic in the National Capital Region (NCR) Delhi. So, the peak might be a result of local traffic emissions combined with poor dispersion conditions for aerosols due to shallow boundary layer (Hyvärinen et al., 2010; **Papers 2 & 3**).

At Mukteshwar both PM10 & PM2.5 concentrations are modulated with respect to air masses from the plains (**Papers 1 & 4**). The low concentrations during night and morning hours infer very weak contribution of local anthropogenic emissions (Fig. 7), hence referred as a cleaner location. But, when ABL height increases during the pre-monsoon season, polluted air masses from the IGP reach the Mukteshwar site, the aerosol concentrations become nearly equal until the end of monsoon season. Conversely, during post-monsoon and winter seasons the concentration levels at Mukteshwar are relatively low because about 70% of the Mukteshwar air masses originate mostly from altitudes well above the Gual Pahari maximum mixing height (MMH) (**Paper 4**).

The long data-set of aerosol properties in particular at Mukteshwar enables investigating the trends in aerosol properties (**Paper 4**). The statistical methods used to analyze the trends of aerosol parameters and to verify the sensitivity of the trends results were the seasonal Mann-Kendall (MK) test, the Sen's slope estimator and least-mean square (LMS) (Collaud Coen et al., 2013), and a generalized least square trends with either autoregressive or block bootstrap confidence intervals (GLS/ARB) (Asmi et al., 2013), respectively. Trend analysis at Mukteshwar shows statistically significant (95% confidence level) negative trend of -2.3 μgm^{-3}/year for PM2.5 and -2.7 μgm^{-3}/year for

PM10, with both LMS and GLS/ARB methods. But, MK analysis results into a statistically insignificant trend for both PM2.5 and PM10. The trend analysis result of Ntot has a positive slope, but not with a statistically significant result (**Paper 4**).

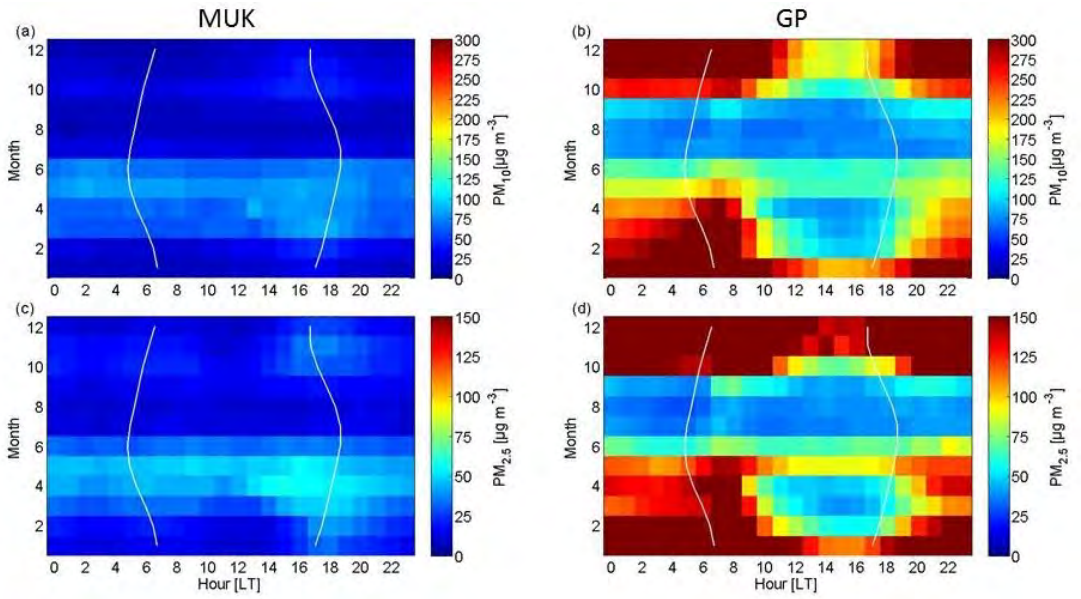

Figure 7. Seasonal-mean diurnal variations for PM10 and PM2.5 at Mukteshwar and Gual Pahari. The sunrise and sunset time is shown with the white lines.

The eBC mass concentration annual average are 1.0 and 12.0 µg/m^3 at Mukteshwar and Gual Pahari, respectively. The eBC at Gual Pahari is high during the winter and post-monsoon seasons (**Papers 2 & 3**), and the diurnal values peaks during morning and evening hours were observed due to localized traffic and cooking activities (Hyvärinen et al., 2010). The eBC concentration maxima at Mukteshwar towards the afternoon in all seasons except monsoon in contrary indicates a relatively weak contribution of local activities compared to contribution of regional polluted air masses (**Papers 1 & 4**).The seasonal-mean diurnal pattern of eBC is seemed to be different than PM mass concentrations at both the locations. Possible explanations for these differences include the influence of substantial carbonaceous fraction in PM mass. In Gual Pahari, the carbonaceous matter contributes the largest mass fraction to the atmospheric aerosol (i.e., >30% organic carbon (OC)) across the seasons. Further, mass species characterization in fine mode (PM2.5) at Gual Pahari shows 46% secondary organic carbon (SOC) in total organic carbon (TOC) (**Paper 2**). This suggests the condensation of SOC on fine size particles can occur more rapidly leading to fast growth of aerosols in the region, and that might be the driving factor of differing seasonal- mean diurnal cycles of the PM concentration than those of eBC concentration (**Paper 4**). These result underline importance of estimating OC levels in addition to eBC estimations over IGP-Himalayan region since in climatic perspective emissions of OC causes a negative forcing (except its brown carbon component), while emissions of eBC lead to positive forcing

via aerosol–radiation interactions. Moreover, broadly warming due to eBC at top of atmosphere is fully compensated or overwhelmed by the cooling effect due to OC aerosols (IPCC, 2013).

In case of rBC, the campaign average rBC mass concentrations at Mukteshwar and Gual Pahari are of similar levels to that of eBC with 1.0 and 11 μg/m^3, respectively. Further, the number fraction of rBC-containing particles is higher in Gual Pahari as compared to Mukteshwar, but individual rBC-containing particles and their size distributions are fairly similar at both the sites (**Paper 5**). The rBC mass concentrations are about 10 times higher in Gual Pahari than those at Mukteshwar which are consistent with the eBC mass concentrations, however, a high variability of rBC mass concentrations is observed in their diurnal cycles at both the sites.

The SSA values at Mukteshwar are relatively close to each other across the seasons (0.82 to 0.84) (**Paper 4**), indicating equal changes in source strength or removal processes of absorbing and scattering types of aerosols. But, a clear difference is observed in SSA during the March and November eBC peaks. In March, the mean SSA decreases from 0.85 to 0.81 as the BC-rich aerosol reaches Mukteshwar, and the low values of SSA indicate the dominance of absorbing rather than scattering material. On the other hand, in November a small increase is seen in SSA in the afternoon hours likely due to emissions of secondary organic aerosol (SOA) precursors and SOA formation in crop-residue burning plumes (Vakkari et al., 2018) that might make a larger contribution in November as compared to March (**Paper 4**). Moreover, α_{abs} at Mukteshwar has small diurnal changes across the seasons, but a high α_{abs} concurrently with low SSA suggesting less scattering nature of the particles in winter (**Paper 4)**. The SSA and α_{abs} were not estimated from our work in Gual Pahari, however, Soni et al. (2010) reported annual average SSA 0.70 with only slight variations across the seasons in Delhi. The α_{abs} remained close to unity throughout the year in their study which strongly indicates the absorption at Delhi aerosol is mainly due to the abundance of black carbon of fossil fuel origin.

4.2 Regional and local influences of emission sources

The air mass movement depicted with either backward trajectories or wind vector can explain identification of the origin of the emission sources. At Gual Pahari, the spatial sectoral contribution of different sources were resolved by using receptor modelling tool PMF (Positive Matrix Factorization) in combination with conditional probability function (CPF) analysis of backward trajectories as well as wind vector. The trajectory approach identified the predominance of regional transport of sea-salt enriched mineral dust from Arabian Sea and Thar Desert during the pre-monsoon season. The surface wind direction approach captured reasonably well the influence of local origin sources particularly in winter season. Substantively, both the approaches indicate that the air masses at Gual Pahari are reached mainly from north and west directions and cross-through not only the dense populated areas, but also the small-scale industrial zones (**Paper 2**).

At Mukteshwar similarly to Gual Pahari, except in monsoon, the north and west sectors predominate throughout the year. These source sectors retain a homogeneity (**Paper 4**) which manifests the fact that the aerosol properties over the remote sites in India might have similar pattern; however, may vary in magnitude, depending on strength of the local emission sources (e.g., Bonasoni et al., 2008; Chatterjee et al., 2012; Hyvärinen et al., 2009; Komppula et al., 2009; Nair et al., 2012; Pant et al., 2006; **Papers 3 & 4**).

In addition to air mass origins using backward trajectories or wind vector, the ratio of aerosol properties also helps to infer the origin via characteristics of sources. The fraction of eBC in PM which is higher in Gual Pahari most likely indicating to local anthropogenic emissions from biomass burning, agriculture residue burning, cooking and road traffic (e.g., Beegum et al., 2009; Hyvärinen et al., 2010; **Paper 2**). Figure 8 illustrates the relative frequency distribution of the ratio of hourly values of eBC to PM2.5 during the entire measurement period at Mukteshwar and Gual Pahari. The eBC/PM2.5 ratio about 0.10 at Gual Pahari suggests occurrence of some major anthropogenic activities such as combustion of fossil fuel and biomass burning in the IGP region (**Paper 2**). At Mukteshwar, on average about 3.5% of black carbon mass contributes to total PM2.5 and which is mostly due to regional air masses (**Papers 4 & 5**).

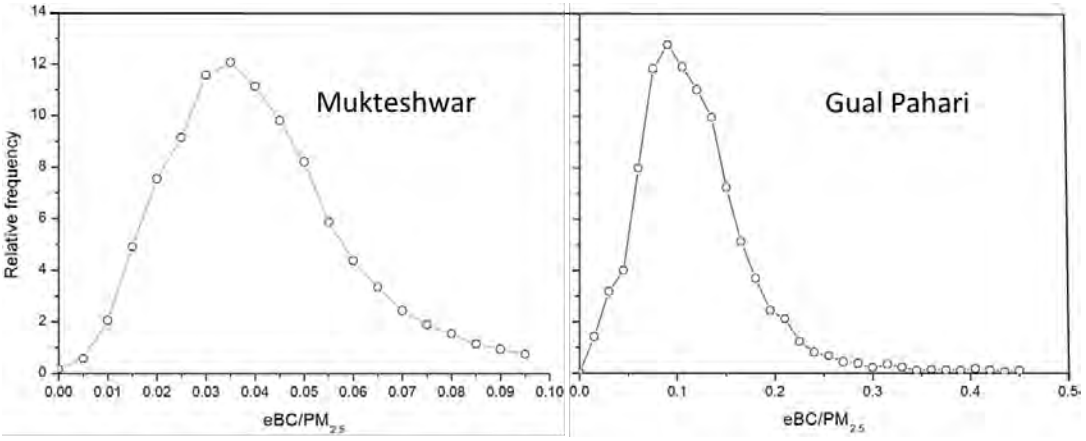

Figure 8. Relative frequency distribution of the ratio of the hourly values of eBC/PM2.5 at Mukteshwar and Gual Pahari.

In figure 9a, the particle volume size distribution with a peak at diameter of about 0.78 µm obtained from APS in conjunction with PMF analysis at Gual Pahari suggests secondary aerosols and vehicular emissions predominate in the fine mode (PM2.5) of particulate matter (**Paper 2**). This further indicates that formation of secondary aerosol at Gual Pahari is primarily due to rich availability of precursors reaching from distant or local anthropogenic emissions and of course conducive meteorology plays its role into that substantially. The work of **paper 5**, where evaluation of size-selected rBC core size distributions (Fig. 9 b) further suggests that at Gual Pahari rBC core size distribution is mostly unimodal (mode at about 180 nm) and that at Mukteshwar is clearly bimodal (smaller mode at about 110 nm and other dominating mode at about 210 nm). But, in general the mode at about 200 nm and thinly coated seems to be quite similar for Gual Pahari and Mukteshwar. In additional analysis related to rBC, it is revealed that the trends in the rBC mixing state parameters are similar for Gual Pahari and Mukteshwar, which indicate fairly dominancy of local and regional rBC sources. The individual particles are also seem to be similar in Gual Pahari and Mukteshwar, although relatively a large fraction of the particles contain rBC in Gual Pahari than in Mukteshwar. The plausible explanation of these similarities could be that some aerosol sources are common for the whole region (e.g., agriculture residue and biofuel burning and cooking), and second, a significant fraction of rBC observed at Mukteshwar is originated from the densely populated IGP represented by Gual Pahari in our work (**Papers 4 & 5**).

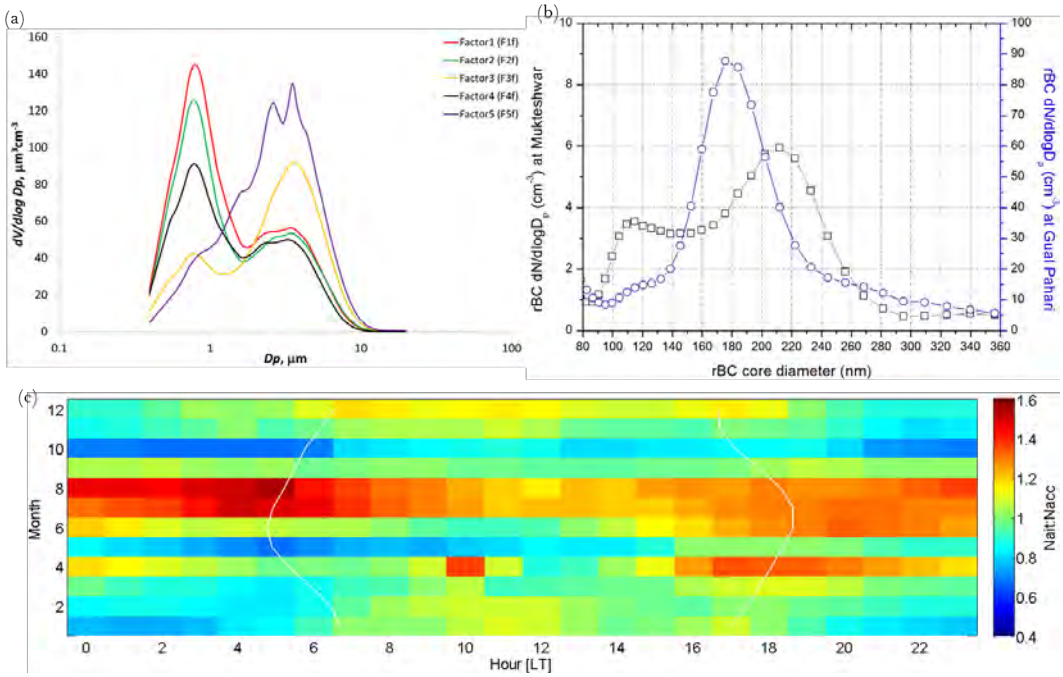

Figure 9. (a) Typical volume size distribution observed with APS during periods dominated by five factors in fine mode identified with receptor model at Gual Pahari (adapted from Paper 2); (b) the campaign average of rBC core number size distributions from Mukteshwar and Gual Pahari (modified from Paper 5); (c) Seasonal-diurnal ratio of modal particle number concentration at Mukteshwar (adapted from Paper 4 Supporting Information). The sunrise and sunset time is shown with the white lines.

As explained briefly in previous sections that Mukteshwar area is often under the influence of regional air pollution plumes containing biomass burning and aged combustion-derived aerosols. In light of that aging of primary aerosols or qualitative identification of distance of various aerosol sources is interpreted by examining the ratio between the particle size number concentrations, e.g., Nait/Nacc (Fig. 9 c). A high Nait/Nacc ratio, in absence of NPF event, indicates primary aerosol emissions mainly from combustion-derived sources or that efficient wet scavenging process prevails. In contrast a low ratio is an indication of aged aerosols and emissions from a distant source (as seen in Fig. 9 c, May and October). At Mukteshwar, the attribution of NPF to total number concentration of aerosol during pre-monsoon is also dominant in addition to regional emissions (**Paper 4**), while in post-monsoon a larger GMD infers to relatively higher contribution of regional combustion aerosols than in pre-monsoon (**Paper 4**). The Nait/Nacc ratio from 0.5 upto 5 at Gual Pahari has indicated the presence of NPF, preference of the accumulation mode removal by wet deposition, and that the aerosols are fresh rather than aged (Hyvärinen et al., 2010). However, during end period of the rainy seasons, Nait/Nacc when starts to decrease showed that the aerosols has begun to age again.

In total, the morning and evening activities such as biomass burning and cooking has a significant influence on aerosol concentration levels in addition to the regional sources contributions at Gual Pahari, and the daytime minima is due to the increased vertical mixing (**Papers 2 & 3**). In Mukteshwar, aerosol concentration has maxima in the afternoon most likely due to the transport of polluted air masses from the IGP (**Papers 3, 4 & 5**). The findings in the present work indicate that aerosols particles

at the both the sites, Mukteshwar and Gual Pahari, have similar type of local and regional emission sources.

4.3 Relationship in aerosol and boundary layer over Himalayan foothills and the plains

In the plains, the relationship between aerosol concentration and ABL is inversely proportional. The ABL growth rate is affected primarily by the characteristics of the surface-based temperature inversion at sunrise and the upward sensible heat flux at the surface. The strength of the elevated temperature inversion causes evolution of ABL and eventually convection of aerosol. However, subsidence at the top of ABL slows down its growth rate resulting to accumulation of aerosol. The situation is complicated in IGP when more ambient aerosols accumulate resulting less solar radiation to surface, hence, a decrease in surface air temperature successively with an increase in ambient relative humidity restrict the development of ABL. Eventually, the low ABL height in turn forces the accumulation of aerosol particles in the high relative humidity and shallow atmosphere. This is the case at Gual Pahari in the IGP region has been manifested mainly during post-monsoon and winter seasons (Figs. 7 b & d; **Papers 2 & 3**). The limited vertical mixing and significant local and regional sources thus resulting to highest aerosol concentrations at Gual Pahari during post-monsoon and winter seasons. In contrary during the pre-monsoon day time when sun radiation and the temperature are high, a decrease in aerosol concentrations occur due to dispersion build upon convective mixing and boundary layer evolution (Hyvärinen et al., 2010; **Papers 2 & 3**).

In case of high altitude mountain sites it has previously been shown that convective mixing can transport polluted air from valleys and plains (Baltensperger et al., 1997; Collaud Coen et al., 2018). In light of the results on both diurnal and seasonal aerosol concentration cycles at Mukteshwar which are temporally opposite to Gual Pahari, it has been imperative to examine the aerosol variability with respect to the boundary layer evolution. In **Paper 3**, it has been identified that aerosol patterns at Mukteshwar are concurrent to deepening of boundary layer in the plains which infers the transport of polluted air from IGP (represented by Gual Pahari) to Mukteshwar. During pre-monsoon distinctly the aerosol mass concentrations in Mukteshwar approach those at Gual Pahari when the convergence of the sensible heat flux causes the ABL to warm and grow in depth in the IGP. The diurnal cycle of aerosol properties is observed with similar characteristics at Mukteshwar across the years (Figs. 7 a & c; **Paper 4**). In total, when ABL height increases during the day, dispersion decreases aerosol concentrations at Gual Pahari and consequently concentrations first decrease in Mukteshwar due to dilution, but a clear increase is seen later in the afternoon when polluted air masses reach the station level. Such delay is expected because polluted air masses are most likely originating from the IGP, a few tens of kilometers SW from the Mukteshwar station.

The ratios of Mukteshwar/Gual Pahari monthly average PM2.5 and scattering coefficient concentration as a function of the average ABL height show significant correlation coefficient values in dry months. This reveals aerosol concentrations at Mukteshwar are depending strongly on ABL dynamics (**Paper 3**). The correlation is clear even if it does not account for the horizontal transport and the distance between the stations is about 270 km. This further indicates that Gual Pahari is a good representative of the IGP and vertical mixing is important (**Papers 2 & 4**). However Mukteshwar/ Gual Pahari eBC ratio, which is only weakly dependent on the ABL height indicating that Gual Pahari eBC concentrations depend mainly on the local eBC emissions. In addition, the mixing of eBC is not as effective as that of the other aerosol types. This is due to the fact that all eBC sources are at the local level and it is confirmed by when no change of rBC core diameters in rBC-containing particles being

estimated at Gual Pahari and Mukteshwar. It could have been expected that rBC core size decreases when secondary organic aerosol and sulphate condense to existing particle during their transport to Mukteshwar, but this effect is not clearly seen (**Paper 5**).

The results so far show qualitatively that transport of polluted air from Gual Pahari to Mukteshwar takes place (**Paper 3**), it is known however that modeled mixing layer depths have uncertainties, especially in the mountain environment (Lehner and Rotach, 2018; Rotach et al., 2015). Therefore in **paper 4** to overcome this uncertainty factor, the observed surface meteorological variables (due to the absence of direct measurements of the mixing layer depth) are utilized to determine the likely influence of boundary layer transport and compared with the modelled mixing layer depth. In wind parameters, the wind direction variability (δWD) and relative wind speed variability (δWSr) were used. The δWD was calculated as the average of the absolute differences in wind direction from 1 minute to the next during the given hour. The δWSr was calculated similarly to δWD, but divided by the average wind speed of that hour in order to retrieve a proxy that was independent of the mean wind speed. In addition, the variability in specific humidity was obtained by subtracting the monthly mean diurnal minima from the monthly mean diurnal cycle and denoted as ∂q. Figs. 10 a & c show that the simultaneous observations at Mukteshwar and Gual Pahari has a distinct seasonal pattern of specific humidity (q), but ∂q is temporally opposite at Mukteshwar and Gual Pahari. In Mukteshwar (Fig. 10 b), q is gained, while a loss is estimated for Gual Pahari (Fig. 10 d). The changes are dominant in dry months and during afternoon hours that last till night (**Paper 4**).

In summary, the variability in winds and q, with a high variability indicates turbulence, and hence an actively mixing boundary layer. The variability in both wind speed and direction and q is much higher during the day, a consequence of the daytime convectively-driven turbulent boundary layer (Stull, 1988). The strength of the turbulent mixing, indicated by the variability in each parameter, is determined by the sensible heat fluxes arising from the solar irradiance. During the monsoon season, the diurnal pattern is heavily suppressed and at night time the wind direction is from SE since the summer monsoon circulation in India is more synoptic in scale, and there is also more night time variability in both wind speed and direction compared to other seasons. Further, the solar irradiance at the surface is much reduced during summer monsoon, producing weaker surface-driven convective mixing and hence the daytime variability in the winds and in q is not as strong as in the pre- and post-monsoon seasons (**Paper 4**).

A relative strength of boundary layer mixing, however, alone is not sufficient to infer the mixing layer depth. Therefore it is imperative to determine whether aerosol measurements at Mukteshwar are influenced by transport from the plains (IGP) through an additional parameter. The fraction of Mukteshwar air originating from the plains referred as Φq (Fig. 10 e) was then estimated (methodology in **Paper 4**) by utilizing q hourly values of Mukteshwar and Gual Pahari. It is a much clearer indicator as explained in **Paper 4**, since this uses the property that q is a conserved variable and is usually locally well-mixed. Elevated values of Φq correspond very well with the observed 1.5–2 times increase in aerosol properties at Mukteshwar seen in the early to late-afternoon (**Papers 1, 3, 4 & 5**). However, a weak peak in the morning is attributed to transport of air from the local valley while the boundary layer is still growing and the strong peak in the late-afternoon relates to daytime transport of moist air masses from lower altitude, mixed with the valley air (Fig. 10 e). Furthermore, different threshold values of 'Φq' (0.25, 0.5 and 0.75) are compared to the maximum mixing depth (model based) in terms of the fraction of the days when Mukteshwar is under the influence of air from the plains (**Paper 4**). The result remarkable shows the mixing of air masses in pre- and post-monsoon is predominant (Figure 7 a & c) when the observation stations in foothills of Himalayas (e.g., Mukteshwar) are

influenced by air masses transported from the plains below (IGP). This is in agreement with previous findings that high regional pollution can be seen in dry months at elevated sites when the boundary layer is deep enough (Collaud Coen et al., 2013).

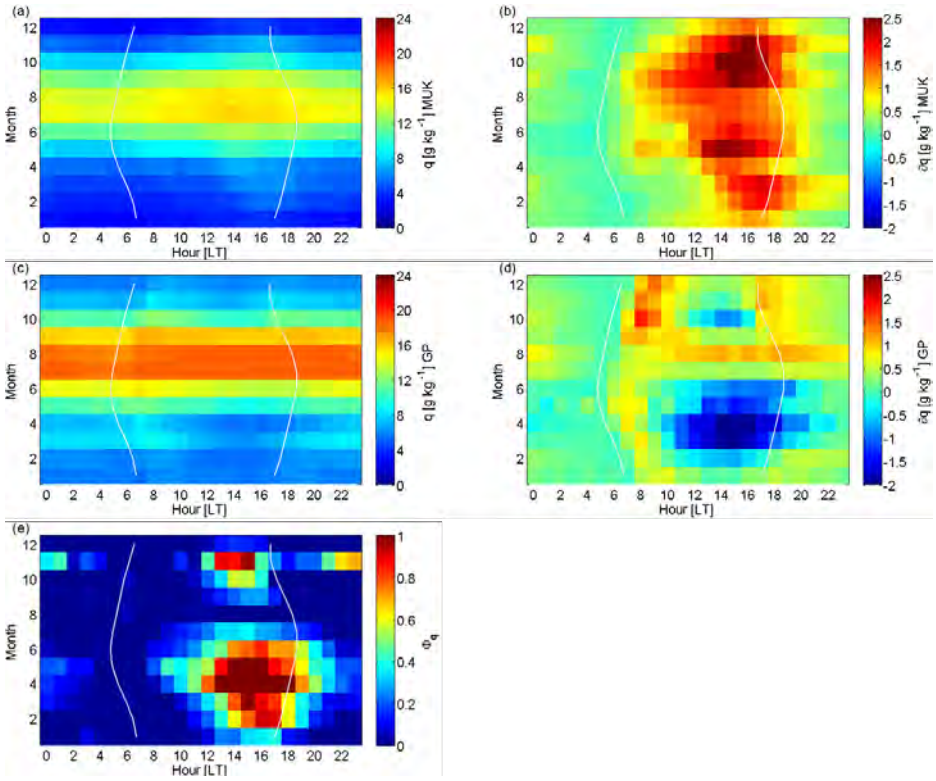

Figure 10. (a & c) Monthly-mean diurnal specific humidity at Mukteshwar and Gual Pahari, respectively; (b & d) variability ∂q at Mukteshwar and Gual Pahari (represents IGP), respectively, indicating turbulence and moreover, opposite temporal features in the variability of specific humidity for Mukteshwar and Gual Pahari, negligible variability during night time and in monsoon season; (e) 'Φq' a clearer indicator for air mass transport to Mukteshwar from the plains in IGP (adapted from Paper 4).

4.4 Factors of aerosol variability

The main factors and causes identified at Mukteshwar and Gual Pahari that modulate annual, seasonal or diurnal cycles of the aerosols properties at these sites are for example, the boundary layer dynamics (explained in previous section), southwest monsoon, NPF and local and regional emission sources such as biomass burning, transported mineral dust, agriculture-residue & open waste burning, etc. (**Papers 1, 2, 3, 4 & 5**).

At Gual Pahari, broad similarities are identified when using trajectories and wind direction, but wind direction did not correlate clearly with any of the aerosol properties, which indicates that there are very few, or none, disturbing local sources (Hyvärinen et al., 2010; **Paper 2**). Thus we can assume that

the aerosols at Gual Pahari are broadly representative of the regional scale emissions. On the other hand, in the foothills of Himalayas at Mukteshwar, the vertical transport of pollution, in addition to the horizontal winds, from the plains has been a common explanation of modulating aerosol concentrations (**Papers 3 & 4**). Moreover, an interesting finding in **paper 4** is in form of identifying a decrease in interannual tendency of ABL (using modelled mixing layer depth) air transport to Mukteshwar from the IGP. It is notably a demanding future work to investigate its reasons and linkages with aerosol variability in the Himalayan region.

Previously, Hyvärinen et al. (2011 a, b) have shown that both at Gual Pahari and Mukteshwar the major aerosol sink is rainy season which creates efficient wet deposition in the area. This decreases the fraction of particle mass in the PM2.5 size range, thus the scattering and absorbing coefficients are decreasing too. But, the average coarse mode concentrations are not affected so much due to wet deposition, indicating the rains are sporadic in nature, and outside the rain period the coarse mode (seen from the APS and PM data) has a potential to build up again more rapidly than the secondary aerosol mass in the fine mode. Over the period of monsoon, the aerosol concentration as a function of the total local rainfall decreases by 55–70% compared to the pre-monsoon average concentrations at both Mukteshwar and Gual Pahari. However, Gual Pahari which is located in NCR close to New Delhi makes it more susceptible to regional vehicular emissions, which in part may explain the less effective decrease of eBC during the monsoon. It has also been observed that the aerosol concentration even during monsoon are so high in Delhi region, although the monsoon is claimed to be the cleanest season in India (Hyvärinen et al., 2011 a, b). The levels of PM concentrations at Gual Pahari even during monsoon season are not in compliance to the WHO (World Health Organization) 24 h guideline of 25 μgm^{-3} (Hyvärinen et al., 2011 a, b; **Papers 1, 2 & 4**). In Mukteshwar, although the 24 h PM2.5 concentrations are nearly always below the Indian National Air Quality Standard of 60 μgm^{-3} during the monsoon season, but violates the WHO 24 h guideline at many occasions.

A clear dip in GMD (Fig. 11; **Paper 4**) during monsoon season at Mukteshwar manifests a decreasing pattern of aerosol particles. It also corroborates with the finding of removal of particles due to cloud processes and wet scavenging by rain, which are more efficient for aerosol particles at Mukteshwar and Gual Pahari also (Hyvärinen et al., 2011 a, b). Figure 11 shows a clear dip in GMD values due to effect of monsoon on GMD via wet deposition of aerosol, and another dip during pre-monsoon season due to NPF events, a source of nucleated particles. The monthly frequency of NPF event days (Dal Maso et al., 2005; Neitola et al., 2011) has clearly showed a peak in afternoon during March-April both at Mukteshwar and Gual Pahari. The attribution of NPF to Ntot during pre-monsoon is noticeable in spite of a significant contribution of regional natural and anthropogenic emissions at both the sites (Hyvärinen et al., 2010; **Paper 4**).

At Mukteshwar, the analysis in **Paper 4** reveals that NPF events during the pre-monsoon months occurred roughly every third day, but less frequently during other seasons. In post-monsoon, less air from the plains and eventually less precursors might be a reason of much fewer NPF events. Moreover, during post-monsoon and winter the high GMD values indicate dominancy of other possible sources of aged aerosols and infrequent NPF days. The results on NPF frequency in Mukteshwar are in corroboration with Nieminen et al. (2018), where they have also reported that at the majority of measurement sites in the Northern Hemisphere including Mukteshwar, the NPF frequency has a strong seasonal variability. At the measurement sites analyzed in their study, NPF occurs most frequently in March–May (on about 30% of the days) and least frequently in December–February (about 10% of the days).

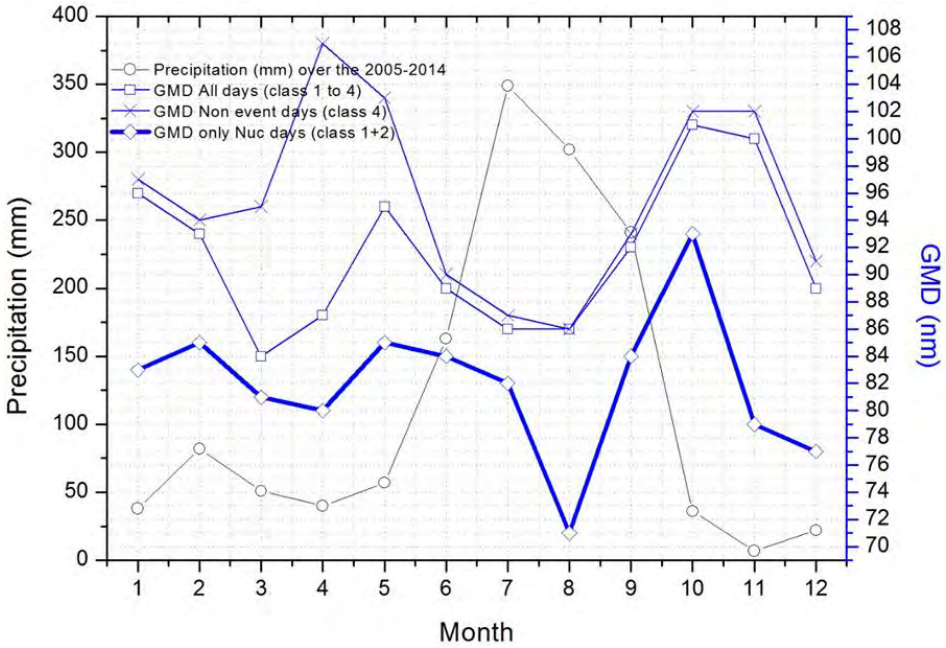

Figure 11. Monthly GMD (nm) for all days and only nucleation event days as a function of precipitation (mm) at Mukteshwar.

In addition to modulations caused by rainy periods and NPF events, the aerosol concentrations are predominantly elevated during pre-monsoon season due to intense dust storms originated from the arid and desert regions of southwest Asia, Arabia and Thar desert (e.g., Duchi et al., 2014; El-Askary et al., 2006). The prevailing meteorological conditions and the marine humidity during early monsoon periods are the factors that differentiate the air masses, along with the fact that during pre-monsoon; there is large amount of dust at middle and upper levels of the troposphere that is also transported over to IGP and further upto Mukteshwar (**Paper 4**). This results into elevated fractions of the coarse mode, PM2.5–10 at both the stations (Hyvärinen et al., 2011 a; **Papers 1, 2 & 4**).

Although Mukteshwar is often under the influence of regional air masses transport from the IGP region, as discussed in previous sections, that results into contribution of biomass burning aerosols (Komppula et al., 2009; **Papers 3 & 4**) and aged combustion-derived aerosols (Komppula et al., 2009; **Papers 4 & 5**). But, in order to assess modulation due to strength of emissions, the absolute emissions at Mukteshwar are estimated and found to be lesser in comparison to emissions over NCR (represented by Gual Pahari) (**Paper 4**). A comparison of the modeled and measured eBC concentrations at Mukteshwar with the ECHAM-HAM and REMO-HAM models, using the same emission inventory, shows an overestimation in ECHAM-HAM and relatively better result with the REMO-HAM. Notwithstanding, the regional climate model has also problems in capturing the orographic influence accurately. It highlights that transport and representation of the valley wind influence to ABL could be the main reason of poor performance of climate models in mountainous environment (**Paper 4**). Conversely, at Gual Pahari both models are able to capture the observed eBC concentrations much more reliably. This is indicating that the emission inventory does not have

significant biases and the interannual variability in aerosol properties at Gual Pahari relates reasonably well with the emission strength over IGP region.

5. Review of papers and author's contribution

Paper 1 (P1) reports continuous aerosols measurements of PM2.5, PM10 and eBC at Mukteshwar for the first 3 years and detailed out a baseline information for both diurnal and annual aerosol concentration cycles and compared with Indian ambient air quality standards. The outcome and the outlook are described in Table 2. I carried out the data analysis and contributed substantially in writing of the text. The data is further utilized in papers 3 and 4.

Paper 2 (P2) describes a sequential filter-based gravimetric measurement using artefact corrected methods and followed by chemical analysis. The source region discrimination is detailed out using conditional probability functions with receptor modelling, and validation through volume size distribution. The sources are identified in fine and coarse mode of PM. In this work I contributed towards installation of the measurements, daily maintenance, did all the data analysis, and wrote most of the text.

Paper 3 (P3) observes the transport of pollution by comparing simultaneous measurements of more than two years at both the stations including meteorological parameters and aerosol mass concentrations. The comparison shows that aerosol concentrations at the foothills of Himalayas are correlated with the boundary layer height. I contributed to the field measurements, improving the data analysis method and wrote part of the text.

Paper 4 (P4) presents the first step towards the use of observed surface meteorological variables in the absence of direct measurements of the mixing layer depth to determine the likely influence of boundary layer transport to Mukteshwar which is qualitatively identified in paper 3. The results are obtained to investigate that the mountainous terrain site (Mukteshwar) is under the influence of air from the plains due to convective transport processes that are enhanced by local and mesoscale topography, and leading to pronounced valley/mountain winds and consequently to ABL air lifting from the plains below. The transport from plains is evident in seasonal-diurnal patterns observed at Mukteshwar. I contributed in designing the data analysis, did a major part of the data analysis and writing of the paper.

Paper 5 (P5) contains the description of state-of-the-art method of measuring size selected black carbon mass distribution and mixing state in polluted and clean environments in India. The results show that refractory black carbon concentrations are about 10 times higher in polluted environment than those at a cleaner site, and which are consistent with black carbon observation utilized in papers 2, 3 & 4. A detail examination revealed that the refractory black carbon particles are most likely to contain non-refractory materials such as sulphate and organics, but the exact volume fractions could not be quantified because these particles are not spherical. In this paper, I participated in designing the study, did a major part of the measurements and the related data analysis in the paper, and contributed in writing.

A simplified summary of connections between the work carried out over the years and included as part of this thesis are capitulated in Table 2.

Table 2. Summary of linkage in research papers those included in the thesis.

Research Article	*Objectives*	*Primary input*	*Secondary input*	*Outcome*	*Outlook*
P1 Atmospheric aerosols at a regional background Himalayan site—Mukteshwar, India	Baseline concentration in foothills of Himalayas	Real-time state-of-the-art continuous long-term data		Aerosol concentrations are significant even in background regions	Elevated RH occurs with air masses moving uphill, and to create larger database; **Addressed in Paper 4**
P2 Atmospheric aerosols local-regional discrimination for a semi-urban area in India	Concentration and sources in Indo-Gangetic Plain	Artefacts corrected physical and chemical data; Source Receptor model	FLEXTRA model trajectories calculations; MAAP black carbon artefact corrected data (other paper)	Mass and size distribution for sources identification and quantification	Detailed micro-physical properties of key pollutant (black carbon); **Addressed in Paper 5**
P3 The effect of boundary layer dynamics on aerosol properties at the Indo-Gangetic plain and at the foothills of the Himalayas	Transport of aerosol	Simultaneous aerosol measurements at cleaner and polluted environments, Model based boundary layer dynamics	FLEXTRA & ECMWF Model based trajectories and boundary layer heights	Boundary layer dynamics has major role in aerosol transport to cleaner environments	Mountain and valley winds circulations can be an enhancing factor in transport of pollution from plains; **Addressed in Paper 4**
P4 Driving factors of aerosol properties over the foothills of central Himalayas based on 8.5 years continuous measurements	Aerosol temporal variability and its driving factors, trends analysis, aerosol transport processes, and testing aerosol-climate models for the reproducibility of aerosol variability	Longest-time series data, detailed meteorological information and the emissions	HYSPLIT & GDAS based trajectories and boundary layer heights calculations, ECHAM-HAMMOZ and REMO-HAM models, ECLIPSE emission inventory, Precipitation and ENSO phase details	Synthesis of a micro-meteorology approach using turbulence and specific humidity as proxies for diurnal boundary layer influence over a complex topography	Detailed micro-physical properties of aerosol to be parametrized into indigenous aerosol-climate models and to reduce the uncertainties at a regional scale

P5 Size-selected black carbon mass distributions and mixing state in polluted and clean environments of northern India	New and detailed information about the black carbon mass distribution, mixing state and morphology in cleaner and polluted environments	State-of-the-art measurement set-up by using size-selective (DMA) particles before SP2		Particles at both sites have similar local and regional sources but aerosol are also transported from polluted to cleaner environments	The particle structure remains unknown. Additional high quality multi-point measurements are required for assessing and improving the performance of aerosol-climate models predictions at regional level

6. Summary and conclusions

In this thesis the aerosol properties in two different environments and their spatio-temporal variability are presented. On one hand, the longest time-series data of in situ measurements of aerosol properties is utilized, for the first time in India, to determine the diurnal-seasonal cycles, inter-annual variability and trend analysis. On the other hand, the closely associated continuous measurements and intensive campaigns data with state-of-the-art instrumentation is utilized followed by modelling approach to evaluate relationship between aerosol properties and transported air masses from plains to high altitude sites.

Our main conclusions are as follows:

1. Simultaneous measurements at both—a polluted and cleaner environments are useful for a comprehensive analysis.

The high time resolution data set of more than two years of simultaneous measurements reveals an opposite pattern in diurnal cycles of aerosol properties at Mukteshwar and Gual Pahari. The concentration of aerosol properties is about 10 times higher in polluted environment, Gual Pahari, than those at cleaner, Mukteshwar. The size-selected black carbon mass distribution determined in terms of refractory black carbon (rBC) shows consistency with eBC concentrations in both the environments. Noticeably in the present work, a statistically significant (95% confidence level) negative trend of -2.3 $\mu g/m^3$ /year and -2.7 $\mu g/m^3$/year for PM2.5 and PM10, respectively, is estimated at Mukteshwar, and on average the inter-annual variability of both PM2.5 and Ntot is ± 20%. The first aim of this thesis work is accomplished with long-term continuous measurements of about 8.5 years at a cleaner environment, Mukteshwar. It provided information on background aerosol properties, trends in aerosol concentrations and properties, and data for validating models. Moreover, Mukteshwar station provided possibilities for studying the influence of regional sources and processes.
The present work highlights the fact that in health perspective, the PM10 and PM2.5 at both Mukteshwar and Gual Pahari are in exceedance to the WHO (World Health Organization) 24 h guideline of 25 μgm^{-3}. This shows that even in background regions that are far away from major

pollution sources or urban areas, the aerosol concentrations are high. Thus, to address how future emission scenarios can work in pollution controlling and climate policy framework at regional scale, there is need of many more observatory sites, continuous long-term measurements, quantification of nature and role of aerosols with the models predictions.

2. A distinct cycle of aerosol properties is observed at polluted site near Delhi as well as at a relatively cleaner in the foothills of central Himalaya.

A distinct diurnal and seasonal pattern of aerosol properties is observed at both the sites, but temporally opposite. During post-monsoon and winter, high aerosol concentrations are found at Gual Pahari, while less at Mukteshwar. In pre-monsoon the levels are again opposite in magnitude when high at Mukteshwar or almost equal at both the sites. It is observed that the concentration levels of extensive aerosol properties at Mukteshwar are consistently high over the course of the day with 1.5–2 times higher values in early to late-afternoon than during the night. But, in monsoon the aerosol concentrations are minimum both at Mukteshwar and Gual Pahari. These variabilities across the seasons indicate that the foothill sites are correlated with the spatially averaged ABL height, and together with the favorable synoptic scale atmospheric circulation, suggesting air mass transport from the plains. The climate models simulations also predict the distinct seasonal cycles of measured eBC concentrations at Gual Pahari, while at Mukteshwar climate models could not. The possible reasoning of the poor performance of model predictions at Mukteshwar might be due to the incapability to capture the transport and representation of the valley wind influence to ABL. It is noted, however, that our observations are restricted to only one site in each environment, hence multi-point measurements are needed to add to our observations and modelling comparison. This will give an improved explanation on spatially and temporal variation of the emissions and their optimized reduction strategies which could be helpful to equilibrium air quality and climate change prospects over the entire region.

3. The regional sources attributions seem to dominate over the local sources, at least in the IGP region boundary layer.

The high aerosol concentrations at Gual Pahari are found mainly during post-monsoon and winter seasons and at Mukteshwar these are high during pre-monsoon. This suggests an opposite seasonal pattern in the aerosol properties and the reason could be either contribution of different local sources or may be common regional sources but differ in magnitude due to varying transport processes. The eBC/PM2.5 ratio of 0.035 at Mukteshwar and 0.10 at Gual Pahari is suggesting substantial difference in local anthropogenic activities between the two locations. But, rBC mixing state parameters reveal that the trends of these parameters are similar for Gual Pahari and Mukteshwar, which indicate fairly identical local and regional rBC sources. Moreover, the similar characteristics of individual particles in Gual Pahari and Mukteshwar indicate firstly that some aerosol sources are common for the whole region (e.g., agriculture residue and biofuel burning and cooking), and secondly a significant fraction of rBC observed at Mukteshwar is originated from the densely populated IGP represented by Gual Pahari.

The elevated fractions of the coarse mode, PM2.5–10 at both the stations suggesting contribution of transported dust over to IGP and further upto Mukteshwar when the prevailing meteorological conditions and the marine humidity differentiate the air masses during pre-monsoon. Thus, regionally

transported pollutant laden air masses from IGP to Himalayan foothills are playing an important role than the local sources or from other parts of the Indian subcontinent. So, more surface in situ measurements including isotopic-based source apportionment and validation with satellite retrieved information of aerosol properties at different locations and altitude would shed light onto this subject comprehensively. In this way, the coverage will be from local to regional scale in the Gangetic-Himalayan domain.

4. The mountainous terrain sites are under the influence of air from the plains due to convective transport processes enhanced by local and mesoscale topography.

The significant correlation values (0.95, p >0.05) of Mukteshwar to Gual Pahari aerosol properties ratio as a function of ABL height show that unlikely the horizontal transport, the distance between the stations which is about 270 km does not matter. Broadly this implies that Gual Pahari is a good representative of the IGP and vertical mixing is important. Build upon this result, the observed surface meteorological variables both at Gual Pahari and Mukteshwar are utilized to investigate that the mountainous terrain site (Mukteshwar) is likely under the influence of air from the plains. This happened due to convective transport processes that are enhanced by local and mesoscale topography, and leading to pronounced valley/mountain winds and consequently to ABL air lifting from the plains below. The high variability in winds and specific humidity has indicated turbulence and hence an actively mixing boundary layer. But, the relative strength of boundary layer mixing alone is not sufficient to infer the mixing layer depth and hence determine the fraction of Mukteshwar air originating from the plains (referred as Φq). This parameter Φq is a much clearer indicator to elucidate the fraction of Mukteshwar air. The elevated values of Φq correspond very well with the observed 1.5–2 times increase in all extensive aerosol properties at Mukteshwar seen in the early to late-afternoon corroborates reasonably well the fact of influence of air from the plains to high altitude sites.
Substantially, the mixing of air masses between plains and high altitude sites via vertical and horizontal transport is significant in pre- and post-monsoon. The monsoon season is not captured well either with specific humidity proxy or with the modeled mixing layer depth. But, the ABL seasonal influence explained in this work is a step forward to more accurately describe the mesoscale transport of aerosols in models which are used to predict the concentrations at high altitude sites over the Himalayan region. Nonetheless, a direct measurement data of ABL for a complex terrain would be more sensitive to pin down these processes in detail before parametrizing the climate models.

To summarize, the scientific work carried out as part of this thesis is ranging from macro to a micro scale. The work is starting from baseline observations that provide a basis to quantify the driving factors of variability in aerosol properties and the trends analysis; and micro level scale through characterization of individual particles of key pollutant species (Fig. 12). The work also enlightens the fact that how dynamics of aerosol behaviour and meteorological variables is taking place in one of aerosol's complex regions in South Asia, and their evolution in future. But, the questions are unavoidable on investigating the climate effects of aerosol on hydrological cycle, aerosol-monsoon interaction and effects of aging and coatings on eBC absorption enhancement in receptor locations, such as Himalayan glaciers. The idea is fascinating in determining absorbing aerosols (eBC, brown carbon (BrC) and mineral dust)) deposition on the India-Himalayan ice-pack and glaciers based on long-term measurements via isotope fingerprinting and eventually to estimate radiative forcing of absorbing aerosols due to the emissions of southern Asian region. However, to be able to describe the

impacts and to assess the radiative forcing due to absorbing aerosols and its-induced snow albedo reduction in snow on third pole "Hindukush–Himalayas", a multi-institutional effort based on multiple measurement stations is needed. It is also be noted that the vertical profile of concentrations and aging processes of absorbing aerosols are likely to vary depending on the environment.

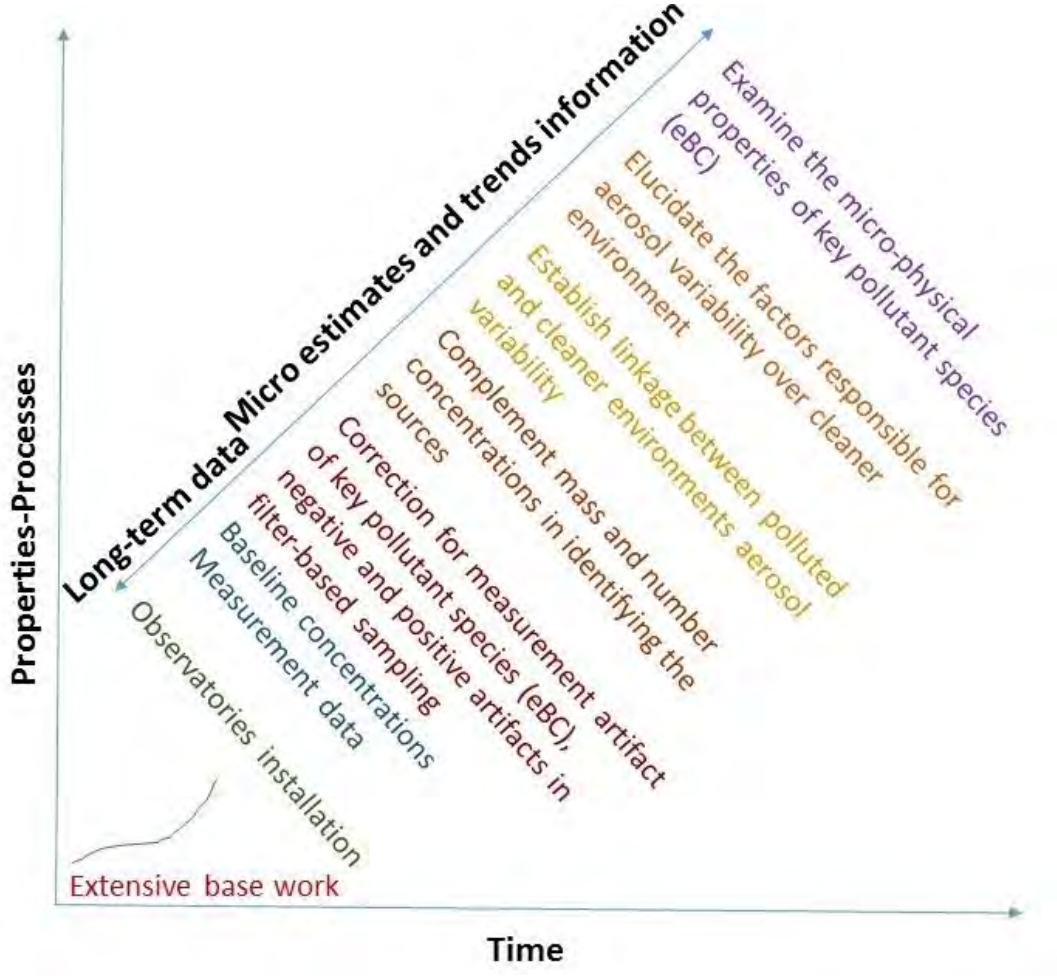

Figure 12. Schematic of development in research work carried out at Mukteshwar and Gual Pahari over the years.

7. Bibliography

Andreae, M. O., and Crutzen. P. J. (1997). Atmospheric aerosols: Biogeochemical sources and role in atmospheric chemistry. Science, 276,1052-1058.

Andreae, M.O., and Rosenfeld, D. (2008). Aerosol-cloud-precipitation interactions. Part 1. The nature and sources of cloud-active aerosols. Earth Science Reviews, 89, 13-41.

Archer, D., Eby, M., Brovkin, V., Ridgwell, A., Cao, L., Mikolajewicz, U., et al. (2009). Atmospheric Lifetime of Fossil Fuel Carbon Dioxide. Annual Review of Earth and Planetary Sciences, 37:1, 117-134.

Asmi, A., Collaud Coen, M., Ogren, J. A., Andrews, E., Sheridan, P., Jefferson, A., et al. (2013). Aerosol decadal trends – Part 2: In situ aerosol particle number concentrations at GAW and ACTRIS stations. Atmospheric Chemistry and Physics, 13(2), 895–916, doi:10.5194/acp-13-895-2013.

Badarinath, K. V. S., S. K. Kharol, and Sharma, A. R., et al. (2009). Long-range transport of aerosols from agriculture crop residue burning in Indo-Gangetic Plains—A study using LIDAR, ground measurements and satellite data. Journal of Atmospheric and Solar-Terrestrial Physics, 71 , 112 – 120 .

Baltensperger, U., Gäggeler, H. W., Jost, D. T., Lugauer, M., Schwikowski, M., Weingartner, E., & Seibert, P. (1997). Aerosol climatology at the high-alpine site Jungfraujoch, Switzerland. Journal of Geophysical Research, 102(D16), 19707–19715, doi:10.1029/97JD00928.

Beegum, S.N., Moorthy, K.K., Babu, S.S., Satheesh, S., Vinoj, V., Badarinath, K., Safai, P., Devara, P., Singh, S., Vinod, Dumka, U., Pant, P. (2009). Spatial distribution of aerosol black carbon over India during pre-monsoon season. Atmospheric Environment 43, 1071–1078.

Bonasoni , P. , et al. (2010). Atmospheric brown clouds in the Himalayas: First two years of continuous observations at the Nepal Climate Observatory Pyramid (5079 m). Atmospheric Chemistry and Physics, 10 ,7515 – 7531 .

Bukowiecki, N., Ernest, W., Gysel, M., Collaud Coen, M. and Z., Paul and Herrmann, E., Steinbacher, M., Gäggeler, H. W., and Baltensperger, U. (2016). A Review of More than 20 Years of Aerosol Observation at the High Altitude Research Station Jungfraujoch, Switzerland (3580 m asl). Aerosol and Air Quality Research, 16(3), 764–788, doi:10.4209/aaqr.2015.05.0305.

Butt, E. W., Turnock, S. T., Rigby, R., Reddington, C. L., Yoshioka, M., Johnson, J. S., Regayre, L. A., Pringle, K. J., Mann, G. W., and Spracklen, D. V. (2017). Global and regional trends in particulate air pollution and attributable health burden over the past 50 years. Environmental Research Letters, 12(10), 104017.

Census of India. 2011. Provisional population totals: rural-urban distribution Volume 2, Issue 1 of Census of India, 2011, India. Office of the Registrar General & Census Commissioner, India.

Charlson, R. J. (1969). Atmospheric visibility related to aerosol mass concentration: review. Environmental Science & Technology, 3, 913-918, doi:10.1021/es60033a002.

Chatterjee, A., Ghosh, S.K., Adak, A., Singh, A.K., Devara, P.C.S., and Raha, S. (2012). Effect of Dust and Anthropogenic Aerosols on Columnar Aerosol Optical Properties over Darjeeling (2200 m asl), Eastern Himalayas, India. PLoS One (7): e40286. doi.org/10.1371/journal.pone.0040286

Cohen, A. J., Brauer, M., Burnett, R., Anderson, H. R., Frostad, J., Estep, K., et al. (2017). Estimates and 25-year trends of the global burden of disease attributable to ambient air pollution: an analysis of data from the Global Burden of Diseases Study 2015. The Lancet, 389(10082), 1907–1918, doi:10.1016/S0140-6736(17)30505-6.

Collaud Coen, M., Andrews, E., Asmi, A., Baltensperger, U., Bukowiecki, N., Day, D., et al. (2013). Aerosol decadal trends – Part 1: In situ optical measurements at GAW and IMPROVE stations. Atmospheric Chemistry and Physics, 13(2), 869–894, doi:10.5194/acp-13-869-2013.

Collaud Coen, M., Andrews, E., Aliaga, D., Andrade, M., Angelov, H., Bukowiecki, N., et al. (2018). Identification of topographic features influencing aerosol observations at high altitude stations. Atmospheric Chemistry and Physics, 18(16), 12289–12313, doi:10.5194/acp-18-12289-2018.

Dal Maso, M., Kulmala, M., Riipinen, I., Wagner, R., Hussein, T., Aalto, P. P., and Lehtinen, K. E. J. (2005). Formation and growth of fresh atmospheric aerosols: eight years of aerosol size distribution data from SMEAR II, Hyytiälä, Finland. Boreal Environment Research, 10, 323–336.

Davidson, C., Phalen, R., and Solomon, P. (2005). Airborne particulate matter and human health: A review. Aerosol Science and Technology, 39, 737–749.

De Wekker, S. F. J. and Kossmann, M. (2015). Convective Boundary Layer Heights Over Mountainous Terrain—A Review of Concepts. Frontiers of Earth Science, 3, 77, doi:10.3389/feart.2015.00077.

Draxler, R. R., and Hess, G. D. (1998). An Overview of the HYSPLIT_4 Modelling System for Trajectories, Dispersion, and Deposition. Australian Meteorological Magazine, 47, 295–308.

Duchi, R., Cristofanelli, P., Marinoni, A., Bourcier, L., Laj, P., and Calzolari, F. (2014). Synoptic-scale dust transport events in the southern Himalaya. Aeolian Research, 13, 51–57, doi:10.1016/j.aeolia.2014.03.008.

El-Askary, H., Gautam, R., Singh, R. P., and Kafatos, M. (2006). Dust storms detection over the Indo-Gangetic basin using multi sensor data. Advances in Space Research, 37(4), 728–733, doi:10.1016/j.asr.2005.03.134.

Franklin, M., Koutrakis, P., and Schwartz, J. (2008). The Role of Particle Composition on the Association Between PM2.5 and Mortality. Epidemiology. 19(5):680-689, SEP 2008; DOI: 10.1097/EDE.0b013e3181812bb7.

Ganguly, D., Jayaraman, A., Rajesh, T. A., Gadhavi, H. (2006). Wintertime aerosol properties during foggy and non-foggy days over urban center Delhi and their implications for shortwave radiative forcing. Journal of Geophysical Research, 111:D15217. doi: 10.1029/2005JD007029.

Ganguly, D., Rasch, P. J., Wang, H., and Yoon, J. (2012). Fast and slow responses of the South Asian monsoon system to anthropogenic aerosols. Geophysical Research Letters, 39(18), doi:10.1029/2012GL053043.

Gilardoni, S., Vignati, E., Marmer, E., Cavalli, F., Belis, C., Gianelle, V., Loureiro, A., and Artaxo, P. (2011). Sources of carbonaceous aerosol in the Amazon basin. Atmospheric Chemistry and Physics, 11, 2747–2764.

Greenstone, M., Nilekani, J., Pande, R., Ryan, N., Sudarshan, A., and Sugathan, A. (2015). Lower pollution, longer lives. Economic and Political Weekly, 8, 40–46.

Guo, H., Kota, S. H., Chen, K. , Sahu, S. K., Hu, J., Ying, Q., Wang, Y., and Zhang, H. (2018). Source contributions and potential reductions to health effects of particulate matter in India. Atmospheric Chemistry and Physics, 18(20), 15219–15229, doi:10.5194/acp-18-15219-2018.

Gustafsson, Ö., Krusa, M., Zencak, Z., Sheesley, R. J., Granat, L., et al. (2009). Brown clouds over South Asia: Biomass or fossil fuel combustion. Science 323(5913), 495–498. doi:10.1126/science.1164857.

Gustafsson, Ö., and Ramanathan, V. (2016). Convergence on climate warming by black carbon aerosols. Proceedings of the National Academy of Sciences of the United States of America, 113(16), 4243, doi:10.1073/pnas.1603570113.

Hyvärinen, A.-P., Lihavainen, H., Komppula, M., Sharma, V. P., Kerminen, V.-M., Panwar, T. S., and Viisanen, Y. (2009), Continuous measurements of optical properties of atmospheric aerosols in Mukteshwar, northern India. Journal of Geophysical Research, 114, D08207, doi:10.1029/2008JD011489.

Hyvärinen, A.-P., Lihavainen, H., Komppula, Panwar, T. S., Sharma, V. P., Hooda, R. K., and Viisanen, Y. (2010), Aerosol measurements at the Gual Pahari EUCAARI station: preliminary results from in-situ measurements. Atmospheric Chemistry and Physics, 10(15), 7241–7252, doi:10.5194/acp-10-7241-2010.

Hyvärinen, A.-P., Raatikainen, T., Brus, D., Komppula, M., Panwar, T. S., Hooda, R. K., et al. (2011a). Effect of the summer monsoon on aerosols at two measurement stations in Northern India – Part 1: PM and BC concentrations. Atmospheric Chemistry and Physics, 11(16), 8271–8282, doi:10.5194/acp-11-8271-2011.

Hyvärinen, A.-P., Raatikainen, T., Komppula, M., Mielonen, T., Sundström, A.-M., Brus, D., et al (2011b). Effect of the summer monsoon on aerosols at two measurement stations in Northern India – Part 2: Physical and optical properties. Atmospheric Chemistry and Physics, 11(16), 8283–8294, doi:10.5194/acp-11-8283-2011.

Hyvärinen, A.-P., Vakkari, V., Laakso, L., Hooda, R. K., Sharma, V. P., Panwar, T. S., et al. (2013). Correction for a measurement artifact of the Multi-Angle Absorption Photometer (MAAP) at high black carbon mass concentration levels. Atmospheric Measurement Techniques, 6(1), 81–90, doi:10.5194/amt-6-81-2013.

IIASA, 2015; http://www.iiasa.ac.at/web/home/research/researchPrograms/air /Global_emissions.html, accessed in June 2015.

IPCC, 2007, Climate Change 2007: The Physical Science Basis. Contribution of Working Group I to the Fourth Assessment Report of the Intergovernmental Panel on Climate Change (S. Solomon, D. Qin, M. Manning, Z. Chen, M. Marquis, K.B. Averyt, M. Tignor and H.L. Miller (eds)), Cambridge University Press, Cambridge, United Kingdom and New York, NY, USA.

IPCC, 2013, Climate Change 2013: The Physical Science Basis. Contribution of Working Group I to the Fifth Assessment Report of the IPCC, (eds Stocker, T.F.et al.), Cambridge University Press, Cambridge, United Kingdom and New York, NY, US.

IPCC, 2018, Summary for Policymakers of IPCC Special Report on Global Warming of 1.5°C approved by Governments. 48th Session of the IPCC on 1 - 5 October 2018, Republic of Korea.

Kaskaoutis, D. G., Gautam, R., Singh, R. P., Houssos, E. E., Goto, D., Singh, S., et al. (2012). Influence of anomalous dry conditions on aerosols over India: Transport, distribution and properties. Journal of Geophysical Research: Atmospheres, 117(D9), doi:10.1029/2011JD017314.

Kaskaoutis, D. G., Kumar, S., Sharma, D., Singh, R. P., Kharol, S. K., Sharma, M., et al. (2014). Effects of crop residue burning on aerosol properties, plume characteristics, and long-range transport over northern India. Journal of Geophysical Research: Atmospheres, 119, 5424–5444, doi:10.1002/2013JD021357.

Kaufman, Y. J., Tanre, D., and Boucher, O. (2002). A satellite view of aerosols in the climate system. Nature, 419, 215–223.

Komppula, M., Lihavainen, H., Hyvärinen, A.-P., Kerminen, V.-M., Panwar, T. S., Sharma, V. P., and Viisanen, Y. (2009). Physical properties of aerosol particles at a Himalayan background site in India. Journal of Geophysical Research: Atmospheres, 114, D12202, doi:10.1029/2008JD011007.

Komppula, M., Mielonen, T., Arola, A., Korhonen, K., Lihavainen, H., Hyvärinen, A.-P., et al. (2012). Technical Note: One year of Raman-lidar measurements in Gual Pahari EUCAARI site close to New Delhi in India – Seasonal characteristics of the aerosol vertical structure. Atmospheric Chemistry and Physics, 12(10), 4513–4524, doi:10.5194/acp-12-4513-2012.

Koponen, I. K., Virkkula, A., Hillamo, R., and Kerminen, V.-M., and Kulmala, M. (2003). Number size distributions and concentrations of the continental summer aerosols in Queen Maud Land, Antarctica. Journal of Geophysical Research: Atmospheres, 108, D18, 4587, doi:10.1029/2003JD003614, 2003.

Kowol-Santen, J., M. Beekmann, S. Schmitgen, and Dewey, K. (2001). Tracer analysis of transport from the boundary layer to the free troposphere. Geophysical Research Letters, 28(15), 2907–2910, doi:10.1029/2001GL012908.

Kulmala, M., Asmi, A., Lappalainen, H. K., Carslaw, K. S., Pöschl, U., Baltensperger, U., et al. (2009). Introduction: European Integrated Project on Aerosol Cloud Climate and Air Quality interactions (EUCAARI) – integrating aerosol research from nano to global scales. Atmospheric Chemistry and Physics, 9(8), 2825–2841, doi:10.5194/acp-9-2825-2009.

Kumar, S., Kumar, S., Kaskaoutis, D. G., Singh, R. P., Singh, R. K., Mishra, A. K., et al. (2015). Meteorological, atmospheric and climatic perturbations during major dust storms over Indo-Gangetic Basin. Aeolian Research, 17, 15–31, doi:10.1016/j.aeolia.2015.01.006.

Lehner, M., and Rotach, M. W. (2018). Current Challenges in Understanding and Predicting Transport and Exchange in the Atmosphere over Mountainous Terrain. Atmosphere, 9(7), 276, https://doi.org/10.3390/atmos9070276.

Lelieveld, J., Crutzen, P. J., Ramanathan, V., Andreae, M. O., Brenninkmeijer, C. A. M., Campos, T., et al. (2001). The Indian Ocean Experiment: Widespread Air Pollution from South and Southeast Asia. Science, 291(5506), 1031, doi:10.1126/science.1057103.

Li, C., McLinden, C., Fioletov, V., Krotkov, N., Carn, S., Joiner, J., et al. (2017). India is overtaking China as the World's largest emitter of anthropogenic sulfur dioxide. Scientific Reports, 7(1), 14304, doi:10.1038/s41598-017-14639-8.

Lohmann U., and Feichter J. (2005). Global indirect aerosol effects: A review. Atmospheric Chemistry and Physics, 5(3), 715–737, doi:10.5194/acp-5-715-2005.

Malm W., Sisler J., Huffman D., Eldred R., and Cahill T. (1994). Spatial and seasonal trends in particle concentration and optical extinction in the United States. Journal of Geophysical Research: Atmospheres, 99(D1), 1347–1370, doi:10.1029/93JD02916, 1994.

Menon, S., et al. (2010). Black carbon aerosols and the third polar ice cap. Atmospheric Chemistry and Physics, 10 (10):4559–4571.

Mönkkönen, P, Koponen, I. K., Lehtinen, K. et al., (2005). Measurements in a highly polluted Asian mega city: Observations of aerosol number size distributions, modal parameters and nucleation events. Atmospheric Chemistry and Physics, 5:, 57–66.

Moorthy, K. K., Satheesh, S. K., Sarin, M. M., and Panday, A. K. (2016). South Asian aerosols in perspective: Preface to the special issue. Atmospheric Environment, 125, 307–311, doi:10.1016/j.atmosenv.2015.10.073.

Nair, V. S., Solmon, F., Giorgi, F., Mariotti, L., Babu, S. S., Moorthy, K. K. (2012). Simulation of South Asian aerosols for regional climate studies. Journal of Geophysical Research: Atmospheres, 117 (D04209), doi:10.1029/2011JD016711.

Nair, V. S., Babu, S. S., Manoj, M. R., Moorthy, K. K., Chin, M. (2016). Direct radiative effects of aerosols over South Asia from observations and modeling. Climate Dynamics, DOI 10.1007/s00382-016-3384-0.

Neitola, K., Asmi, E., Komppula, M., Hyvärinen, A.-P., Raatikainen, T., Panwar, T. S., et al. (2011). New particle formation infrequently observed in Himalayan foothills – why?, Atmospheric Chemistry and Physics, 11(16), 8447–8458, doi:10.5194/acp-11-8447-2011.

Nieminen, T., Kerminen, V.-M., Petäjä, T., Aalto, P. P., Arshinov, M., Asmi, E., et al. (2018). Global analysis of continental boundary layer new particle formation based on long-term measurements. Atmospheric Chemistry and Physics, 18(19), 14737–14756, doi:10.5194/acp-18-14737-2018.

Pant, P., Hegde, P., Dumka, U. C., Sagar, R., Satheesh, S. K., Moorthy, K. K., Saha, A., and Srivastava, M. K. (2006). Aerosol characteristics at a highaltitude location in central Himalayas: Optical properties and radiative forcing. Journal of Geophysical Research: Atmospheres, 111, D17206, doi:10.1029/2005JD006768.

Pope III C., Burnett R., Thun M., Calle E., Krewski D., Ito K., and Thurston G. (2002). Lung cancer, cardiopulmonary mortality, and long-term exposure to fine particulate air pollution. Journal of the American Medical Association, 287(9), 1132–1141.

Prasad, A. K., Singh, R. P., and Kafatos, M. (2012). Influence of coal-based thermal power plants on the spatial–temporal variability of tropospheric NO_2 column over India. Environmental Monitoring and Assessment, 184, 1891 – 1907, doi: 10.1007/s10661-011-2087-6.

Ramanathan, V., Crutzen, P. J., Lelieveld, J., Mitra, A. P., Althausen, D., Anderson, J., et al. (2001). Indian Ocean Experiment: An integrated analysis of the climate forcing and effects of the great Indo-Asian haze. Journal of Geophysical Research: Atmospheres, 106(D22), 28371–28398, doi:10.1029/2001JD900133.

Ramanathan, V., and Crutzen, P. J. (2003). New Directions: Atmospheric Brown "Clouds". Atmospheric Environment. 37(28), 4033–4035, doi:10.1016/S1352-2310(03)00536-3.

Ramanathan, V., Li, F., Ramana, M. V., Praveen, P. S., Kim, D., Corrigan, C. E., Nguyen, H., et al. (2007). Atmospheric brown clouds: Hemispherical and regional variations in long-range transport, absorption, and radiative forcing. Journal of Geophysical Research: Atmospheres, 112(D22), doi:10.1029/2006JD008124.

Ramaswamy V., Boucher O., Haigh J., Hauglustaine D., and Haywood J. (2001). Radiative Forcing of Climate Change, Cambridge University Press, Cambridge, United Kingdom and New York, NY, USA.

Roessler, D. M., and Faxvog, F. R. (1981). Visibility in absorbing aerosols. Atmospheric Environment (1967), 15(2), 151–155, doi:10.1016/0004-6981(81)90006-8.

Rosenfeld, D. (2000). Suppression of Rain and Snow by Urban and Industrial Air Pollution. Science, 287(5459), 1793, doi:10.1126/science.287.5459.1793.

Rotach, M. W., Gohm, A., Lang, M. N., Leukauf, D., Stiperski, I., & Wagner, J. S. (2015). On the Vertical Exchange of Heat, Mass, and Momentum over Complex Mountainous Terrain. Frontiers in Earth Science, 3, 76, doi:10.3389/feart.2015.00076.

Seinfeld, J., & Pandis, S. (2006). Atmospheric Chemistry and Physics: From air pollution to climate change, II edition, John Wiley & Sons, Inc.

Seinfeld, J.H. (2011). Insights on Global Warming. AIChE Journal, 57, 3259-3284, doi: 10.1002/aic.12780.

Serafin, S., Adler, B., Cuxart, J., et al. (2018), Exchange Processes in the Atmospheric Boundary Layer Over Mountainous Terrain. Atmosphere, 9(3), 102, https://doi.org/10.3390/atmos9030102.

Shresta, A., Agrawal, N., Alfthan, B., Bajracharya, S., Maréchal, J., and Oort, B. (2015). The Himalayan climate and water atlas: Impact of climate change on water resources in five of Asia's major river basins. Nepal: ICIMOD.

Singh, R. P. and Kaskaoutis, D. G. (2014). Crop Residue Burning: A Threat to South Asian Air Quality. EOS Trans. AGU, 95(37), 333–334.

Smith, R. B., Doyle, J. D., Jiang, Q., and Smith, S.A. (2007). Alpine gravity waves: lessons from MAP regarding mountain waves generation and braking. Quarterly Journal of the Royal Meteorological Society, 133,917–936.doi:10.1002/qj.103.

Soni, K., Singh, S., Bano, T., Tanwar, R. S., Nath, S., and Arya, B. C. (2010). Variations in single scattering albedo and Angstrom absorption exponent during different seasons at Delhi, India. Atmospheric Environment, 44(35), 4355–4363, doi:10.1016/j.atmosenv.2010.07.058.

Stein, A. F., Draxler, R. R., Rolph, G. D., Stunder, B. J. B., Cohen, M. D., and Ngan, F. (2015). Noaa's hysplit atmospheric transport and dispersion modeling system. Bulletin of the American Meteorological Society, 96(12), 2059–2077, doi:10.1175/BAMS-D-14-00110.1.

Stohl, A., Wotawa, G., Seibert, P., Kromp-Kolb, H. (1995). Interpolation errors in wind fields as a function of spatial and temporal resolution and their impact on different types of kinematic trajectories. Journal of Climate and Applied Meteorology, 34, 2149–2165.

Stohl, A., and Seibert, P. (1998). Accuracy of trajectories as determined from the conservation of meteorological tracers. Quarterly Journal of the Royal Meteorological Society, 124, 1465–1484.

Stull, R. B. (1988). An introduction to boundary layer meteorology. Atmospheric Sciences Library, Kluwer Academic Publishers, Dordrecht, 666pp.

Twomey, S. (1977). Influence of pollution on shortwave albedo of clouds. Journal of the Atmospheric Sciences, 34(7), 1149–1152.

Vakkari, V., Beukes, J. P., Dal Maso, M., Aurela, M., Josipovic, M. and van Zyl, P. G. (2018). Major secondary aerosol formation in southern African open biomass burning plumes. Nature Geoscience, 11, 580–583, doi:10.1038/s41561-018-0170-0.

Vecchi, R., Valli, G. Fermo, P., D'Alessandro, A., Piazzalunga, A., Bernardoni,V. (2009). Organic and inorganic sampling artefacts assessment. Atmospheric Environment, 43, 1713–1720.

Weigel, A. P., Chow, F. K., and Rotach, M. W. (2007). The effect of mountainous topography on moisture exchange between the "surface" and the free atmosphere. Boundary-Layer Meteorology, 125,227–244.doi:10.1007/s10546-006- 9120-2.

WHO. WHO global urban ambient air pollution database (update 2016). http://www.who.int/phe/health_topics/outdoorair/ databases/cities/en/ (accessed Sept 29, 2017).

WMO/GAW. (2003). Aerosol Measurement Procedures, Guidelines and Recommendations, Edition 2003, GAW Report No. 153, http://library.wmo.int/pmb_ged/wmo-td_1178.pdf.

Zardi, D., and Whiteman, C. D. (2013). "Diurnal mountain wind systems," in Mountain Weather Research and Forecasting: Recent Progress and Current Challenges, Eds F. Chow, S. F. J. De Wekker, and B. Synder (New York, NY: Springer), 35–119.

8. Reprints of the articles (five)

Environ Monit Assess (2013) 185:4753–4764
DOI 10.1007/s10661-012-2902-8

Paper 1 (P1)

Atmospheric aerosols at a regional background Himalayan site—Mukteshwar, India

T. S. Panwar · Rakesh K. Hooda · H. Lihavainen · A. P. Hyvarinen · V. P Sharma · Y. Viisanen

Received: 18 November 2010 / Accepted: 24 September 2012 / Published online: 17 November 2012

Abstract Continuous aerosol measurements were made at a regional background station (Mukteshwar) located in a rural Himalayan mountain terrain from December 2005 to December 2008 for a period of 3 years. The average concentrations of particulate matter less than or equal to 10 μm (PM_{10}), particulate matter less than or equal to 2.5 μm ($PM_{2.5}$) and black carbon (BC) are 46.0, 26.6 and 0.85 μg/m^3 during the study period. Majority of the PM_{10} values lie below 100 μg/m^3 while majority of the $PM_{2.5}$ values lie below 30 μg/m^3. It is further seen that during the monsoon months, especially July and August, the average values are comparatively low. It is also noted that the $PM_{2.5}/PM_{10}$ ratios between 0.50 and 0.75 have the maximum frequency distribution in the data set. Furthermore, the monthly mean ratio of BC to $PM_{2.5}$ mass lies between 3.0 and 7.5 % during the study period. Though the average PM_{10} and $PM_{2.5}$ concentrations during the study period are less than the respective Indian ambient air quality standards, however, they are still above the WHO guidelines and would have adverse health impacts. This shows that even in rural/background regions that are far away from major pollution sources or urban areas, the aerosol concentrations are significant and require long-term monitoring, source quantification and aerosol model simulations.

Keywords Background site · Fine particulate matter · Black carbon · Long-range transport · $PM_{2.5}/PM_{10}$ ratio

T. S. Panwar (✉) · R. K. Hooda · V. P. Sharma
The Energy and Resources Institute, IHC,
Lodi Road,
New Delhi 110003, India
e-mail: tspanwar@hotmail.com

R. K. Hooda · H. Lihavainen · A. P. Hyvarinen · Y. Viisanen
Finnish Meteorological Institute,
PO Box 503, 00101 Helsinki, Finland

R. K. Hooda
Department of Physics, University of Helsinki,
PO Box 64, 00014 Helsinki, Finland

Background

Atmospheric aerosol is linked to visibility reduction, adverse health effects and heat balance of the Earth, directly by reflecting and absorbing solar radiation and indirectly by influencing the properties and cloud processes and, possibly, by changing the heterogeneous chemistry of reactive greenhouse gases (IPCC 2007). The size distribution of atmospheric aerosols, together with their composition, sources and sinks, play a key role in understanding and managing aerosol effects on health, visibility and climate (Kim et al. 2001; Pope and Dockery 2006; Hand and Malm 2007; Lokman et al. 2008; Anderson 2009). Given the increased toxicity of fine ($PM_{2.5}$) and ultrafine particles and the role of ultrafine particles in particle-related premature deaths and morbidity (Donaldson et al. 2002), the abundance of these particles after nucleation is

considered a potential human health hazard. In addition, the growth of nuclei from a few nanometers to optically active and efficient cloud condensation nuclei has important implications for visibility and climate (Kulmala et al. 2004).

The fine ($PM_{2.5}$) and coarse ($PM_{10–2.5}$) particles are relatively different in their physical and chemical compositions. They generally originate from different sources or by different activities within the same source. Coarse particles are normally generated by mechanical activities such as grinding or wind blowing and are dominated by materials of geological origin (Chow 1995). Fine particles mainly consist of secondary particles which are formed in the atmosphere by chemical reactions and primary organic carbon and elemental carbon (Oanh et al. 2006).

In India, particulate matter pollution is widespread across many ambient air-quality monitoring stations. The Central Pollution Control Board is executing a nation-wide programme of ambient air-quality monitoring known as National Air Quality Monitoring Programme. These ambient air-quality monitoring stations (more than 375) are mainly located in cities/towns. In Delhi, the daily mean concentration of particulate matter less than or equal to 10 μm (PM_{10}) over the period 2000–2006 was as high as 234 μg/m^3 (Kandlikar 2007). Many authors from India expressed concern regarding high particulate matter concentration in Indian cities (Bhanarkar et al. 2002; Mitra and Sharma 2002).

However, there are very limited observations in rural/background sites. Gajananda et al. (2005) indicated that the 8-year average (1996–2003) of total suspended particulate at Mohal (Kullu) was 78.4 μg/m^3 and 66.9 μg/m^3 at Manali in northwestern Himalayan region. Kumar and Sarin (2009) reported mass concentrations of fine particulate matter less than or equal to 2.5 μm ($PM_{2.5}$) and coarse ($PM_{10–2.5}$) mode aerosols to vary from 1.6 to 46.1 and 2.3 to 102 μg/m^3, respectively over the annual seasonal cycle during 2007 at a high-altitude site (Mt. Abu) in a semi-arid region.

The average concentration of fine (aerodynamic diameter less than 2.5 μm) mode aerosol at a high-altitude station in northeastern Himalayas (Darjeeling) during January–December 2005was found to be 29.5±20.8 μg/m^3 varying between 3.6 and 61 μg/m^3, whereas coarse (aerodynamic diameter of more than 2.5 μm) mode aerosol ranged between 5.4 and 32 μg/m^3 with an average of 19.6±11.1 μg/m^3 (Chatterjee et al. 2010). The large variation in concentrations of both fine and coarse mode aerosol during the entire study period could be due to the thermodynamic conditions in the planetary boundary layer (PBL), which either favour or adversely affect pollutants dispersion. Ambient weather conditions, such as air temperature, relative humidity (RH) and shortwave radiation, could also influence the chemical reactions leading to secondary aerosol formation.

In addition to contribution from local sources, long-range-transported aerosol particles are a potential contributor to episodic aerosol events in megacities globally, as well as over the Himalayan region (Ramanathan et al. 2007; Gautam et al. 2009; Ferhat et al. 2009; Komppula et al. 2009; Hyvarinen et al. 2009; Raatikainen et al. 2011).

To address the data gap of limited observation in background areas, and to the study the physical, chemical and radiative properties of the aerosols, their variability with the season, as well as long-term trends, The Energy and Resources Institute in collaboration with the Finnish Meteorological Institute started an aerosol laboratory at Mukteshwar, Uttarakhand in September 2005.

The measurement site at Supi, Mukteshwar, which represents a regional background station, is located in a rural mountain terrain at a height of about 2,180 m. Further details regarding the measurement site are provided in Hyvarinen et al. (2009) and Komppula et al. (2009). The climatological data (1951–1980) at Mukteshwar observatory located a few kilometres away from the station, indicate that the mean daily minimum and daily maximum temperature vary from 9.0 to 18.3 °C, annual total rainfall is 1,296.6 mm, average number of rainy days are 77.6 and the mean wind speed is 3.5 m/s (IMD 1999).

The physical properties of aerosol particles indicate a seasonal cycle in measured aerosols in terms of particle number concentrations (Komppula et al. 2009) during the period from November 2005 to November 2008 at the same measurement station. Likewise, the optical properties of aerosols were studied for the period September 2005 to September 2007 and it indicates that though the aerosol concentrations were somewhat lower than those measured closer to urban areas in India, some optical parameters have a noticeable resemblance to those measured elsewhere in India (Hyvarinen et al. 2009). The present study

focuses on the analysis of the mass concentrations of particulate matter, including their seasonal cycle during the study period, i.e. from December 2005 to December 2008.

The information regarding the fine particulate matter (aerosols) compiled in the study would be helping in subsequent assessment of health and climatic impacts as well. As is already known, the pollution aerosols have impacts on human health and regional climate. Most of these aerosols originate from incomplete combustion, being capable of carrying variety of toxic chemicals with them and small enough to penetrate deep into human lung. In addition to their adverse health impacts, the possible climatic impacts associated with these aerosols are surface radiative cooling and heating of the lower atmosphere.

Methodology

Measurement/instrument details

The measurement site (Fig. 1) is located in Mukteshwar (29°47′ N, 79°65′ E), Uttarakhand, in northern India. The surroundings represent an Indian rural mountain terrain, 2,180 m above sea level in the Himalayan region. The closest towns are Nainital located about 25 km

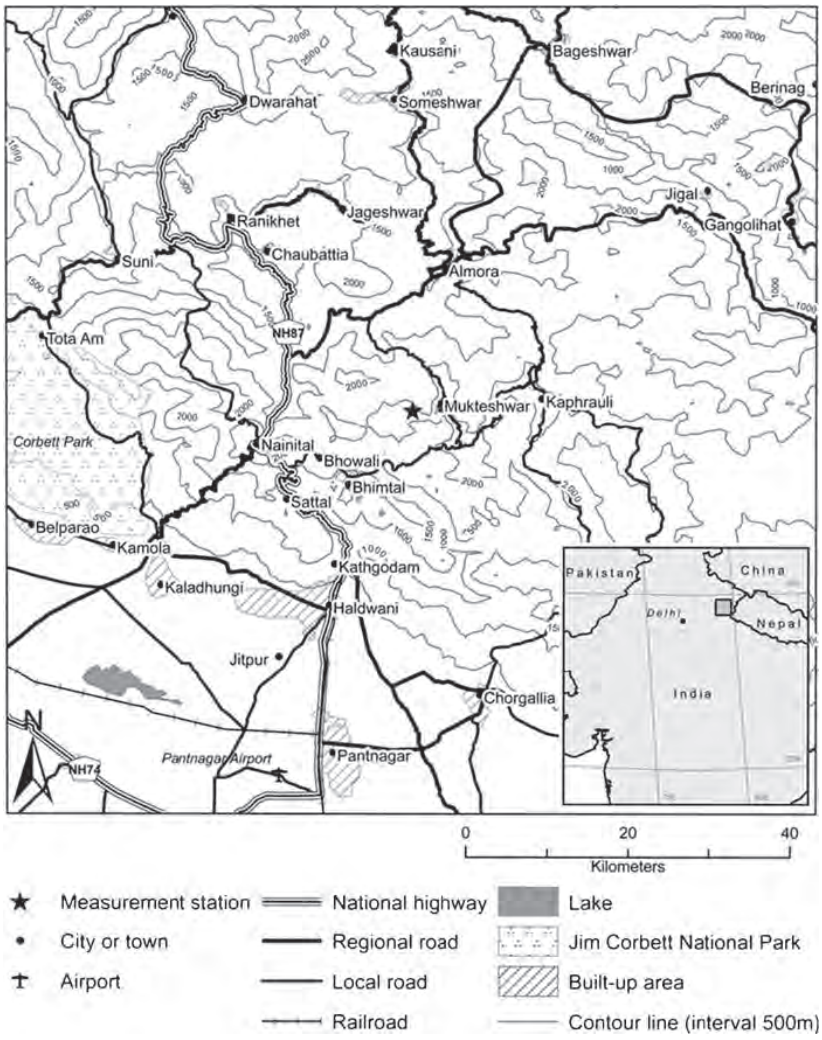

Fig. 1 Location map of the Mukteshwar measurement site

southwest of the station (population of 40,000, Census of India 2001) and Almora located about 20 km north of the station (population of 31,000, Census of India 2001). There are no major local pollution sources, except limited burning over the fields after rainy season. The station is surrounded by an agricultural test field. No major local pollution sources are known to affect the site. The details regarding the measurement site are provided in Hyvarinen et al. (2009) and Komppula et al. (2009). Since the location is one of the remote places in India with minimal local emissions, we believe that the site represents, to the extent possible, a regional background in the Indian atmosphere.

PM_{10} and $PM_{2.5}$ measurements were carried out using real-time particulate monitors (FH 62 I-R) manufactured by Thermo Electron Corporation. Pre-separators (PM_{10} and $PM_{2.5}$ inlets) are used for the measurement of different particulate fractions. The monitoring mechanism is based on the method of radiometric dust measurement that utilises the beta-attenuation by a two-beam compensation method for continuous mass determination of the dust sampled on a filter. A high measurement stability is achieved, because for each measurement value, simultaneously a reference value is determined in separate measuring section. This reference section and the measuring section are physically interconnected, having an equal effect from ambient temperature and pressure fluctuations in both system parts. This is basic condition for precise and steady compensation (Thermo Electron Corporation 2003).

During the sampling, the accumulated particle mass on a filter is measured and displayed simultaneously. The air flow rate (1 m^3/h) is recorded on-line and regulated. From the speed of mass growing and the airflow rate, the dust concentration is calculated. The measuring range of this instrument is 0–5,000 $\mu g/m^3$. The influence of unsteady humidity in ambient air as well as the danger of water condensation in the sampling tube is prevented through the employment of an inlet heater. Measurements were recorded for a time resolution of 5 min duration. PM impactor plates were cleaned on a regular monthly basis. In addition, standard procedure for calibration of the particulate monitoring instrument was carried out by using a set of basic calibration (mica) foils.

The measurement period considered for the present analysis is from December 2005 to December 2008. However, it is noted that there are considerable gaps in the monitored data due as instruments suffered from malfunctions, though in general the data during the year 2006 and second half of 2008 were relatively better. Periodical and routine calibration and flow checks of the instruments were carried out to maintain the data reliability and precision. Furthermore, the months considered for various seasons are as follows: summer (March–May), monsoon (June–September), post-monsoon (October–November) and winter (December–February).

The warmest month was June with an average temperature of 17.8 °C, while January was the coldest month (average temperature, 7.3 °C). The average RH varied from the winter low of 40 % to the monsoon high of 88 %. The predominant wind direction during the measurement period was the sector 300–330° with about a 14 % total contribution. Winds were rarely blowing from the directions 210–270°, as this sector is upslope from the station. The average wind speed was about 1.3 m/s and the average air pressure was about 785 hPa. A backward trajectory analysis was also performed for air masses arriving at the station in the earlier articles (Komppula et al. 2009; Hyvarinen et al. 2009). The air masses were distributed to five different sectors. In general, most of the trajectories were of westerly origin, but during the rainy season the dominating air mass trajectories came from east. RH is the meteorological parameter that could be utmost correlating with the PM concentrations, which is related to boundary layer evolution. Elevated RH occurs with air masses moving uphill. Daytime transport of moist air masses from lower altitudes is an additional explanation for the observations. This is discussed in Raatikainen et al. (2011), where it is shown that specific humidity and RH cycles are correlated in Mukteshwar.

Data screening

The data set comprising 5-min average recorded data was first cleaned based on the operational status codes of the instrument. Only normal operation, i.e. values with zero status code were selected for further analysis. Next, outliers and inconsistent data points were removed taking into consideration very high concentration values, and cross reference to log books for the period when the instrument was not functioning properly. Also, zero concentration values and data values corresponding to sudden spikes (less than 10 min duration) were considered as outliers. However, peaks/spikes for a longer period (for several hours) were

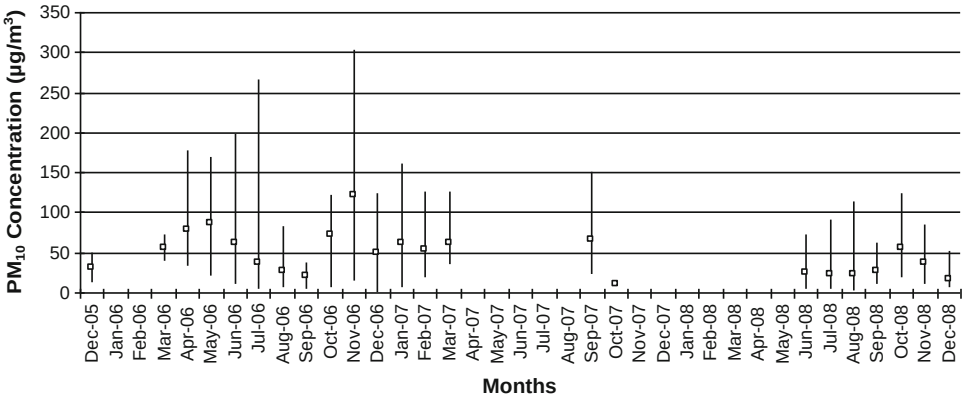

Fig. 2 Monthly average PM_{10} concentration along with minimum and maximum values (based on 24-h average data) at Mukteshwar

considered as normal data, which may be due to some episodic plume conditions in the vicinity of measurement location.

Results and discussions

PM_{10} concentration

Figure 2 shows the monthly average PM_{10} concentration obtained at Mukteshwar during the study period. It is seen that majority of the values (96 %) are below 100 µg/m^3, with an equal percentage (48 % each) in the range 50–100 µg/m^{3}and below 50 µg/m^3. It is further seen that during the rainy months, especially July, August and September 2006 and 2008, the average values are comparatively lower due to washout effect. A similar observation was made by Komppula et al. (2009) whereby during the rainy season the particle number concentrations decreased to less than half of that observed prior to the rainy season. A comparison against the 24-hourly annual ambient air quality standard of 100 µg/m^3 indicates that a majority of the values are in compliance against the standard. Likewise, a comparison against the annual ambient air-quality standard of 60 µg/m^3 indicates that in the year 2006, the annual average value of 50 µg/m^3 was below the standard. However, the annual value in 2008 was 30.2 µg/m^3, which was just half of the standard value. It

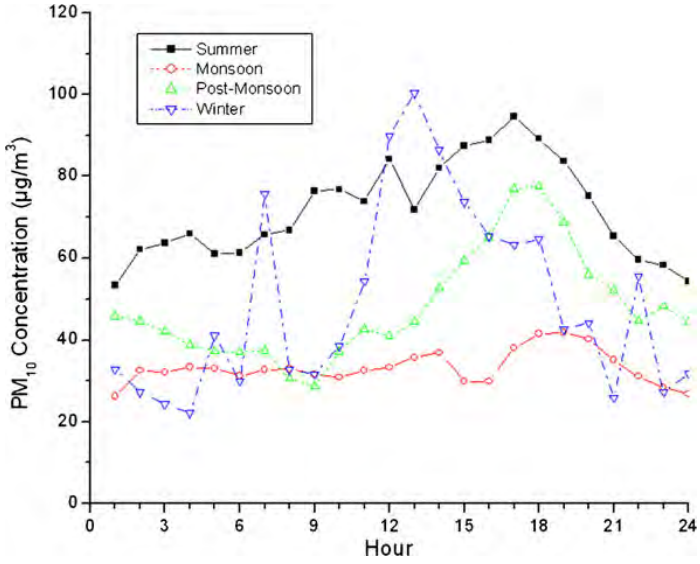

Fig. 3 Diurnal variation of PM_{10} concentration across different seasons during the study period

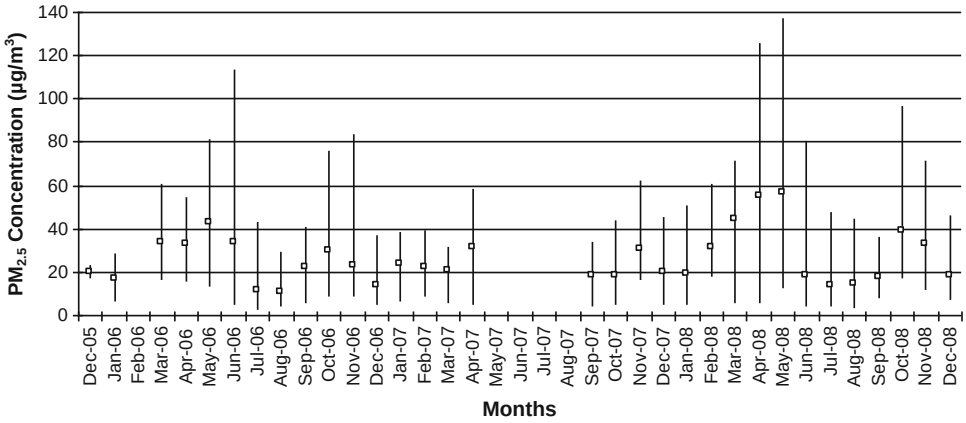

Fig. 4 Monthly average $PM_{2.5}$ concentration along with minimum and maximum values (based on 24-h average data) at Mukteshwar

may be noted here that the months such as April and May which show the highest values are missing in 2008. Furthermore, the range of 1-h average data is very large, varying from a few microgrammes per cubic metre to as high as 650 µg/m^3.

Figure 3 shows that in general, the PM_{10} concentrations are maximum in summer and minimum in the monsoon season, with the post-monsoon season showing intermediate values. However, the winter season values show large variations and the peak is observed around noon time. This is in agreement with the explanation provided by Pant et al. (2006) and Komppula et al. (2009) which states that after the sunrise, the heating of the land surface results in convection, which gradually raises the inversion to higher altitudes, leading to increased vertical mixing that brings up the air with high aerosol concentration to higher levels. However, the peak concentrations in summer and post-monsoon are observed in late afternoon/evening due to enhanced local activities such as cooking mainly burning biomass along with a gradually decreasing mixing height. Unfortunately, the PM_{10} instrument suffered from malfunctions, such that no firm conclusion regarding dust particles can be made.

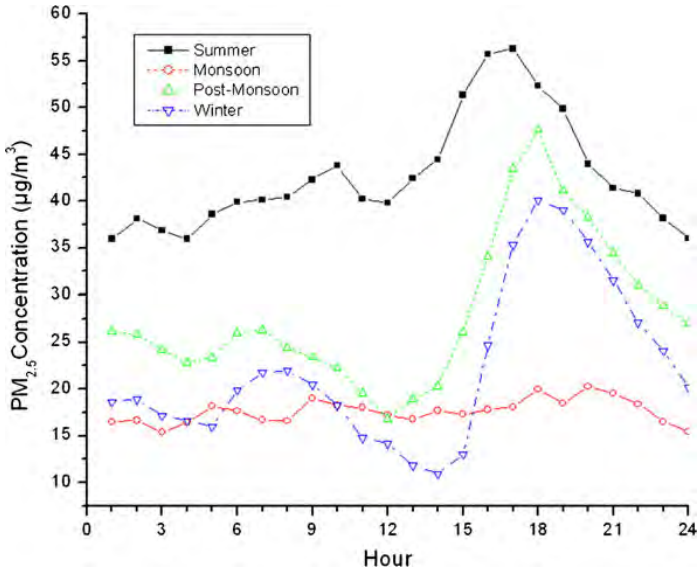

Fig. 5 Diurnal variation of $PM_{2.5}$ concentration across different seasons during the study period

$PM_{2.5}$ concentration

Figure 4 shows the monthly average $PM_{2.5}$ concentration obtained at Supi, Mukteshwar during the study period. It is seen that majority of the average values (63 %) lie below 30 μg/m^3, followed by 37 % that lie in the range 30–60 μg/m^3. It is seen that during the summer months, especially April and May, the average values are comparatively higher while during the monsoon season (especially July and August), there is a sharp reduction. Subsequently, during the post-monsoon season (October–November), the values show an increase. However, December again shows a dip in the concentration values. Since the station is at an altitude, particulate pollution seems to reside partly below the measurement station (Hyvarinen et al. 2009; Gehrig and Buchmann 2003) and may be responsible for the decrease in December. A comparison against the 24-hourly ambient air-quality standard of 60 μg/m^3 indicates that all the average values are in compliance against the standard, though on a few individual days the values did exceed the standards. A comparison against the annual ambient air-quality standard of 40 μg/m^3 indicates that the annual average values in the years 2006 (13.6 μg/m^3), 2007 (20.1 μg/m^3) and 2008 (30.2 μg/m^3) showed no violations. Also, the

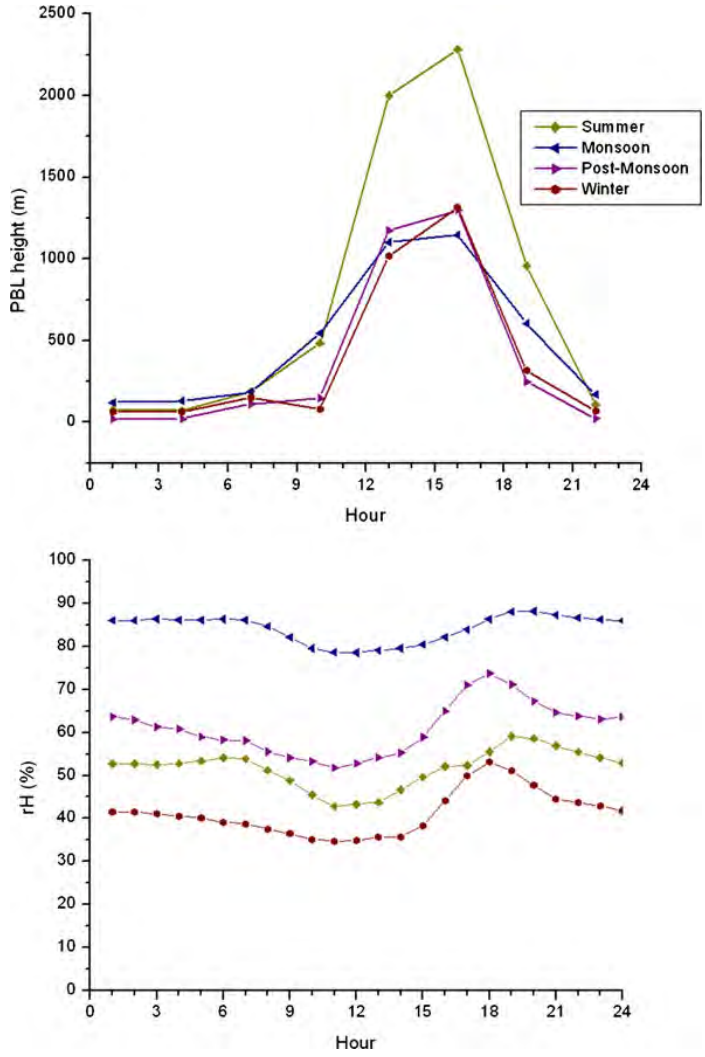

Fig. 6 Diurnal variation of PBL height and RH across different seasons during the study period

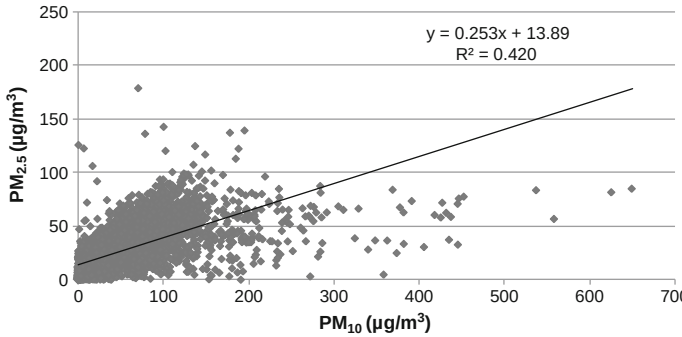

Fig. 7 Scatter plot for the simultaneous hourly $PM_{2.5}$ and PM_{10} concentration values at Mukteshwar for the entire study period

range of the 1-h average data is large, varying from a few microgrammes per cubic metre to as high as 376 µg/m^3.

Figure 5 shows that the $PM_{2.5}$ concentrations are maximum in summer and post-monsoon season. This is broadly in agreement with the observations of Komppula et al. (2009) regarding higher particle number concentrations observed during March–May whereby newly formed particles may have been transported from other areas within the moving air masses. During post-monsoon season (October–November), Komppula et al. (2009) observed higher particle number concentrations, larger mean particle diameter and inferred a high contribution from long-range transported combustion particles based on trajectory analysis.

Figure 5 further shows that the monsoon season has minimum values and does not show any significant diurnal variation. However, the winter season values show large diurnal variations and the peak is observed in the evening. In general, the pattern observed could be explained due to a combined effect of boundary layer evolution and daily activity pattern such as cooking and heating. Komppula et al. (2009) too observed that the main diurnal pattern of the particle number concentration showed an increase from morning to the evening and settled to lower levels again during the night.

The PBL height (Raatikainen et al. 2011) has a significant impact on aerosol concentrations. The concentration cycle is based on mixing of local clean air masses with polluted air masses from plains when the PBL height and RH are high. As seen in Fig. 5, $PM_{2.5}$ concentrations are decreased in the morning simply due to dilution. The $PM_{2.5}$ concentrations start to increase with a delay of few hours when the polluted air masses reach the station height. The sharp peak from 1,500 to 2,300 h are seen when the polluted and clean air masses are well mixed. The same mixing can be observed in the case of RH. As discussed in the measurement details, the increased boundary layer brings up moist air from below (Fig. 6). This creates a strong correlation between RH and PM concentrations, and gives further support to the proposed long-range transport contribution towards PM concentrations.

Comparison of $PM_{2.5}$ and PM_{10} concentration

A scatter plot diagram is prepared for the simultaneous hourly $PM_{2.5}$ and PM_{10} concentration values at Supi,

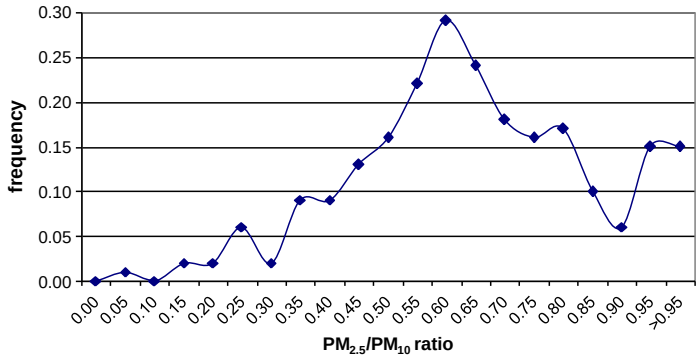

Fig. 8 Frequency distribution of the ratio of the daily values of $PM_{2.5}/PM_{10}$

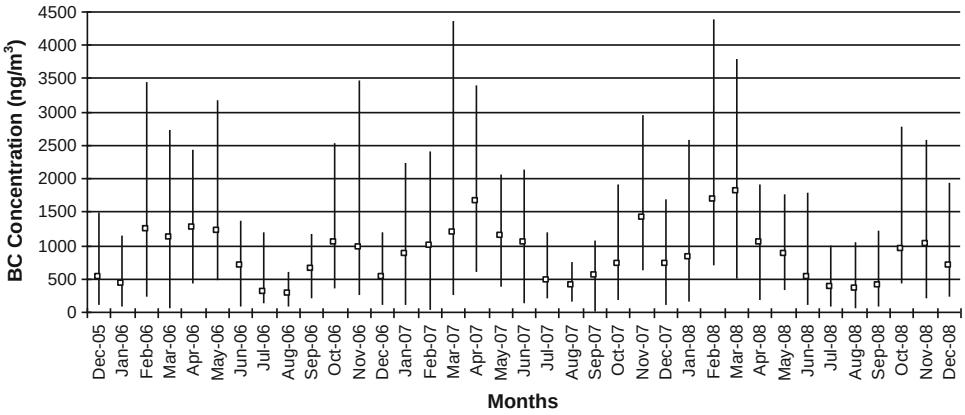

Fig. 9 Monthly average BC concentration along with minimum and maximum values (based on 24-h average data) at Mukteshwar

Mukteshwar for the entire study period December 2005–December 2008 (Fig. 7).

Figure 7 shows that majority of the PM_{10} values are below 200 μg/m^3 and the corresponding $PM_{2.5}$ values are below 100 μg/m^3. Furthermore, Fig. 8 shows the frequency distribution of the ratio of the daily values of $PM_{2.5}/PM_{10}$ during the entire measurement period. It is noted that the $PM_{2.5}/PM_{10}$ ratios between 0.50 and 0.75 have the maximum frequency distribution in the given data set. This ratio is calculated for the days when both $PM_{2.5}$ and PM_{10} data are available.

Black carbon concentration

Figure 9 shows the monthly average black carbon (BC) concentration obtained at Supi, Mukteshwar during the study period. It is seen that majority of the average values lie below 1,000 ng/m^3, though there are some values lying in the range 1,000–2,000 ng/m^3 as well. The maximum value based on 24-h average is 4,364 ng/m^3. It is seen that the summer months have high values while monsoon months show a sharp reduction. A similar seasonal cycle is observed across different years. Further, the range of the 1-h average

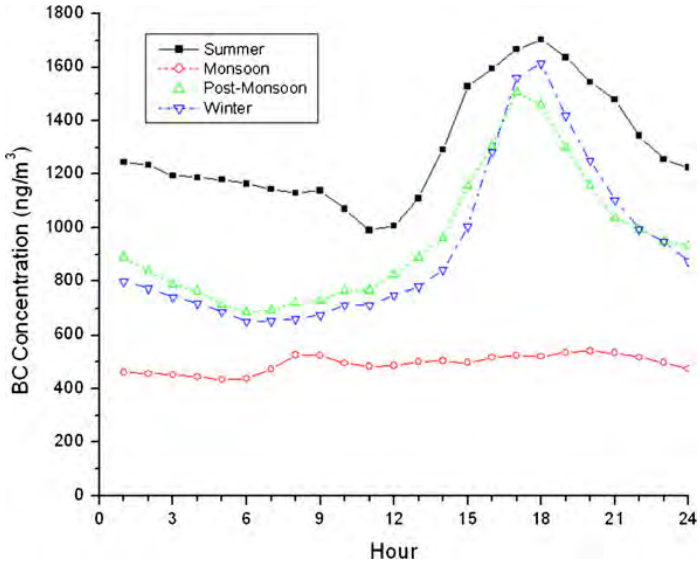

Fig. 10 Diurnal variation of BC concentration across different seasons during the study period

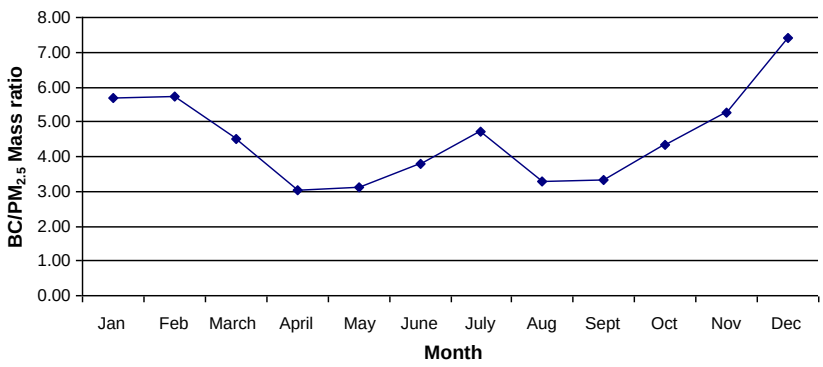

Fig. 11 Percentage share of BC in $PM_{2.5}$ mass

data is large, varying from a few ng/m^3 to as high as 7,000 ng/m^3.

As observed in the earlier cases, the seasonal concentration of BC shows maximum values during the summer season and the minimum values in the monsoon season (Fig. 10). The values during post-monsoon and winter season are close to each other. Further, the diurnal peak is observed towards the evening in all seasons except monsoon. It may be noted that the $PM_{2.5}$ and BC follow a similar pattern, which is an indication that the sources for these particles are similar; based on mixing of local clean air masses with polluted air masses from plains when the PBL is high. Moreover, the contribution of local activities seems to be relatively weak compared with the long-range transport.

Share of BC in $PM_{2.5}$ mass

BC aerosols are produced due to incomplete combustion of fossil fuels as well as biomass burning. Major urban centres such as Delhi have high BC concentrations as well as high BC to particulate matter ratios. Ganguly et al. (2006) have reported average value of BC mass concentration during the campaign period in December 2004 at Delhi to be 29±14 μg/m^{3}and the ratio of BC to PM_{10} to be in the range of 4–15 %. Likewise, Niranjan et al. (2006) showed that at Kharagpur the share of the BC aerosol to fine mode aerosol (<1 μm) was consistently 10 %, which is typical of an urban location. In contrast, Hyvarinen et al. (2009) shows the BC monthly mean concentration at this background rural site to be in the range 0.3–1.4 μg/m^3. Figure 11 shows that the monthly mean ratio of BC to $PM_{2.5}$ mass lie between 3.0 and 7.5 % during the study period. Here, monthly ratios are calculated taking into consideration only those days that had simultaneous BC and $PM_{2.5}$ values reported. In general, it is observed that the winter months have a higher ratio of BC to $PM_{2.5}$ since the biomass burning is more due to heating requirements. However, as compared with urban areas, this site has lower share of BC indicating that fossil fuel combustion activity levels are limited in this area.

Mean concentrations of PM_{10}, $PM_{2.5}$ and BC

The average concentrations of PM_{10}, $PM_{2.5}$ and BC are 46.0, 26.6 and 0.85 μg/m^3 (Table 1). The average PM_{10} concentration during the entire study period is three fourths of the annual ambient air quality standard (60 μg/m^3) prescribed in India. The average $PM_{2.5}$ concentration is more than half of the annual ambient air quality standard (40 μg/m^3) prescribed in India. Though these values are less than the ambient standards, however, they are still above the WHO guidelines (20 and 10 μg/m^3 for PM_{10} and $PM_{2.5}$, respectively) (WHO 2005) and would have adverse health impacts.

Table 1 Annual statistical values of PM_{10}, $PM_{2.5}$ and BC concentrations

	PM_{10} (μg/m^3)	$PM_{2.5}$ (μg/m^3)	BC (ng/m^3)
N (days)	418	802	1,037
Mean	46.0	26.6	849.0
Median	34.7	21.9	670.0
Max	303.4	137.0	4,364.1
Min	0.5	2.3	6.7
SD	41.0	19.3	661.0

Conclusions

Particulate matter (aerosol) measurements made at a regional background station (Mukteshwar) located in a rural Himalayan mountain terrain from December 2005 to December 2008 indicate that the average concentrations of PM_{10}, $PM_{2.5}$ and BC are 46.0, 26.6 and 0.85 μg/m^3during the study period. This shows that even in rural/background regions that are far away from major pollution sources or urban areas, the aerosol concentrations are significant. Though these values are less than the ambient air quality standards in India, however, they are still above the WHO guidelines and may have adverse health impacts. The high $PM_{2.5}/PM_{10}$ ratio indicates the dominance of finer fractions and consequently higher associated health implications. Furthermore, monthly mean ratio of BC to $PM_{2.5}$ mass lie between 3.0 and 7.5 % during the study period.

It is also seen that boundary layer evolution is an important factor for both diurnal and annual aerosol concentration cycles which are clearly supporting the previous conclusions from studies at same location. Moreover, the transport of pollutions is especially important in case of Mukteshwar where local aerosol sources can be considered relatively weak. This summary is based on the $PM_{2.5}$, BC and PM_{10} mass concentrations, which have the best data coverage from a background station in this area.

Thus, efforts should be made to address the long-range transport as well as local sources of pollution and policies should be designed that will minimise emissions of pollutants in urban/industrial areas far away. It may also be mentioned that background monitoring stations should be expanded in order to have a larger database over a longer time period, including its chemical characterisation. Efforts are also required for identifying and quantifying the local/long-range sources as well as appropriate aerosol model simulations.

Acknowledgements This work was supported by the Finnish Meteorological Institute by funding from the Ministry of Foreign Affairs of Finland. The authors would like to acknowledge Timo Anttila for technical assistance during the site visits and D.S. Rawat for valuable routine upkeep of the instruments.

References

Anderson, H. R. (2009). Air pollution and mortality. *Atmospheric Environment, 43*, 142–152.

Bhanarkar, A. D., Gajghate, D. G., & Hasan, M. Z. (2002). Air pollution concentration in Haryana sub-region, India. *Bulletin of Environmental Contamination and Toxicology, 69*, 690–695.

Chatterjee, A., Adak, A., Singh, A. K., Srivastava, M. K., Ghosh, S. K., Tiwari, S., et al. (2010). Aerosol chemistry over a high altitude station at Northeastern Himalayas, India. *PLoS One, 5*(6), e11122.

Chow, J. C. (1995). Measurements methods to determine compliance with ambient air quality standards for suspended particles. *Journal of Air and Waste Management Association, 45*, 320–382.

Donaldson, K., Brown, D., Clouter, A., Duffin, R., MacNee, W., Renwick, L., et al. (2002). The pulmonary toxicology of ultrafine particles. *Journal of Aerosol Medicine, 15*(2), 213–220.

Ferhat, K., Ismail, A., & Omar, A. (2009). Long range potential source contributions of episodic aerosols events to PM_{10} profile of a megacity. *Atmospheric Environment, 43*, 5713–5722.

Gajananda, K., Kuniyal, J. C., Momin, G. A., Rao, P. S. P., Safai, P. D., Tiwari, S., et al. (2005). Trend of atmospheric aerosols over the north western Himalayan region, India. *Atmospheric Environment, 39*, 4817–4825.

Ganguly, D., Jayaraman, A., Rajesh, T. A., & Gadhavi, H. (2006). Wintertime aerosol properties during foggy and nonfoggy days over urban center Delhi and their implications for shortwave radiative forcing. *Journal of Geophysical Research, III*, D15217. doi:10.1029/2005JD007029.

Gautam, R., Hsu, N. C., Lau, K. M., Tsay, S. C., & Kafatos, M. (2009). Enhanced pre-monsoon warming over the Himalayan–Gangetic region from 1979 to 2007. *Geophysical Research Letters, 36*, L07704. doi:10.1029/2009GL037641.

Gehrig, R., & Buchmann, B. (2003). Characterising seasonal variations and spatial distribution of ambient PM_{10} and $PM_{2.5}$ concentrations based on long-term Swiss monitoring data. *Atmospheric Environment, 37*, 2571–2580.

Hand, J. L., & Malm, W. C. (2007). Review of aerosol mass scattering efficiencies from ground-based measurements since 1990. *Journal of Geophysical Research, 112*, D16203. doi:10.1029/2007JD008484.

Hyvarinen, A. P., Lihavainen, H., Komppula, M., Sharma, V. P., Kerminen, V. M., Panwar, T. S., et al. (2009). Continuous measurements of optical properties of atmospheric aerosols in Mukteshwar, northern India. *Journal of Geophysical Research, 114*, D08207. doi:10.1029/2008JD011489.

IMD. (1999). *Climatological tables of observatories in India, 1951–1980* (p. 782). New Delhi: India Meteorological Department. Controller of Publications, Meteorological Department, Govt. of India.

IPCC. (2007). *Fourth assessment report*. Cambridge: CambridgeUniversity Press. Section 2.2.

Kandlikar, M. (2007). Air pollution at a hotspot location in Delhi: detecting trends, seasonal cycles and oscillations. *Atmospheric Environment, 41*, 5934–5947.

Kim, Y. J., Kim, K. W., & Oh, S. J. (2001). Seasonal characteristics of haze observed by continuous visibility monitoring in the urban atmosphere of Kwangju, Korea. *Environmental Monitoring and Assessment, 70*, 35–46.

Komppula, M., Lihavainen, H., Hyvarinen, A. P., Kerminen, V. M., Panwar, T. S., Sharma, V. P., et al. (2009). Physical

properties of aerosol particles at a Himalayan background site in India. *Journal of Geophysical Research, 114*, D12202. doi:10.1029/2008JD011007.

Kulmala, M., Vehkamäki, H., Petäjä, T., DalMaso, M., Lauri, A., Kerminen, V. M., et al. (2004). Formation and growth rates of ultrafine atmospheric particles: a review of observations. *Journal of Aerosol Science, 35*(2), 143–176.

Kumar, A., & Sarin, M. M. (2009). Mineral aerosols from western India: temporal variability of coarse and fine atmospheric dust and elemental characteristics. *Atmospheric Environment, 43*, 4005–4013.

Lokman, H. T., Alagha, O., Karaca, F., Gurdal, T., & Nilufer, E. (2008). Particulate matter ($PM_{2.5}$, $PM_{10–2.5}$ and PM_{10}) and children's hospital admissions for asthma and respiratory outcomes: a bidirectional case-crossover study. *Journal of Toxicology and Environmental Health, 71*, 512–520.

Mitra, A. P., & Sharma, C. (2002). Indian aerosols: present status. *Chemosphere, 49*, 1175–1190.

Niranjan, K., Sreekanth, V., Madhavan, B. L., & Krishna Moorthy, K. (2006). Wintertime aerosol characteristics at a north Indian site Kharagpur in the Indo-Gangetic plains located at the outflow region into Bay of Bengal. *Journal of Geophysical Research, III*, D24209. doi:10.1029/2006JD007635.

Oanh, N. T. K., Upadhyay, N., Zhuang, Y.-H., Hao, Z.-P., Murthy, D. V. S., Lestari, P., et al. (2006). Particulate air pollution in six Asian cities: spatial and temporal distributions, and associated sources. *Atmospheric Environment, 40*, 3367–3380.

Pant, P., Hegde, P., Dumka, U. C., Sagar, R., Satheesh, S. K., Moorthy, K. K., et al. (2006). Aerosol characteristics at a high altitude location in central Himalayas: optical properties and radiative forcing. *Journal of Geophysical Research, III*, D17206. doi:10.1029/2005JD006768.

Pope, C. A., III, & Dockery, D. W. (2006). Health effects of fine particulate air pollution: lines that connect. *Journal of the Air & Waste Management Association, 56*, 709–742.

Raatikainen, T., Hyvärinen, A.-P., Hatakka, J., Panwar, T. S., Hood, Rakesh, K., et al. (2011). Comparison of aerosol properties from the Indian Himalayas and the Indo-Gangetic plains. *Atmospheric Chemistry and Physics Discussion, 11*, 1–37.

Ramanathan, V., Li, F., Ramana, M. V., Siva, P. S., Kim, D., et al. (2007). Atmospheric brown clouds: hemispherical and regional variations in long range transport, absorption and radiative forcing. *Journal of Geophysical Research, 112*, D24S91. doi:10.1029/2006JD008124.

Thermo Electron Corporation. (2003). *Operating manual, particulate monitoring instrument FH62 I-R*. Ref. No 42545/10. Pp. 173.

WHO. (2005). *WHO air quality guidelines for particulate matter, ozone, nitrogen dioxide and sulfur dioxide, global update 2005, summary of risk assessment*. Report No. WHO/SDE/PHE/OEH/06.02.

Atmospheric Research 168 (2016) 13–23

Contents lists available at ScienceDirect

Atmospheric Research

journal homepage: www.elsevier.com/locate/atmos

Atmospheric aerosols local–regional discrimination for a semi-urban area in India

R.K. Hooda [a,b,*], A.-P. Hyvärinen [a], M. Vestenius [a], S. Gilardoni [c,1], V.P. Sharma [b], E. Vignati [c], M. Kulmala [d], H. Lihavainen [a]

[a] Finnish Meteorological Institute, P.O. Box 503, FIN-00101 Helsinki, Finland
[b] The Energy and Resources Institute, IHC, Lodhi Road, New Delhi -110003, India
[c] European Commission, Joint Research Centre, 21027 Ispra, Italy
[d] Department of Physics, University of Helsinki, P.O. BOX 64, 00014 Helsinki, Finland

ARTICLE INFO

Article history:
Received 23 November 2014
Received in revised form 11 August 2015
Accepted 17 August 2015
Available online 29 August 2015

Editor: J.L. Sanchez

Keywords:
Source region
Volume size-distribution
Secondary organic carbon
Aerosol

ABSTRACT

In the European Integrated project on Aerosol Cloud Climate and Air Quality interactions (EUCAARI), measurements were carried out with a sequential filter-based aerosol sampler and on-line instruments for aerosol composition and behaviour at Gual Pahari, close to New Delhi. In fine mode ($PM_{2.5}$), the secondary organic carbon (SOC) to total organic carbon ratio was 46%. This indicated that condensation of SOC on fine size particles could occur rapidly which may be related to the growth of aerosols and the potential to the size of cloud condensation nuclei in the region.

Source region discrimination was improved significantly through coupling conditional probability functions with receptor modelling, and validation through volume size distribution. The air masses from industrial and dense populated regions show a mix of local as well as regional emissions to fine mode aerosols. The back-trajectory analysis captured the long-range transport of sea-salt aerosols enriched with mineral dust. The surface wind directions identified the influence of local emission activities.

1. Introduction

Atmospheric aerosols affect the quality of human life in many different ways such as health, visibility and climate change. To the climate, aerosol influence the Earth's radiation balance directly by scattering and absorbing solar radiations, and indirectly by acting as cloud condensation nuclei (CCN) (Charlson et al., 1992). However, still the largest uncertainty is in predicting the radiative forcing and future climate due to interaction between atmospheric aerosols and climate system (IPCC, 2013; Andreae and Rosenfeld, 2008). Furthermore, better understanding and quantification of the above aerosol effects requires information on how different sources and atmospheric transformation processes modify the aerosol properties when transport through vertical and horizontal layers in a local, regional and global domain.

The Indo-Gangetic Plain (IGP) region is having large local air pollution emissions from transport, industries, energy production, domestic, residue burning and re-suspended dust (Prasad et al., 2006; Rengarajan et al., 2007; CPCB, 2010; Guttikunda and Calori, 2013). In addition, the IGP is affected by mineral dust in pre-monsoon season. The transport and occurrence of IGP pollutants over foothills of the Himalayan region have also been presented (Raatikainen et al., 2014).

There were local scale initiatives over an air pollution 'hot spot' location in the IGP i.e. Delhi, to control these emissions. Different measures have had been implemented such as conversion of fuel from high sulphur diesel to compressed natural gas (CNG) in year 2000–2002, metro rail system (year 2002–2008), and relocation of industries (year 1996–2000). These initiatives had helped during their inception years. At present, almost all these emission control measures have fallen short in keeping up with the growing local and regional emissions which led to degradation in air quality and increasing health risk. Moreover, when meteorological conditions block the dispersal of aerosols, their high concentration impairs visibility and has a respiratory health threat (HEI, 2010). Thus, there is a need to analyse the aerosol composition to study the behaviour and source-sectors discrimination to control these emissions.

A one-year size-segregated aerosol data was measured at a semi-urban site, Gual Pahari, in IGP from April 2008 to March 2009 as a part of the European Integrated project on Aerosol Cloud Climate and Air Quality interactions (EUCAARI) (Kulmala et al., 2011), that includes particulate mass, elemental and organic carbon, and water soluble ions measured through appropriate techniques to understand atmospheric aerosol behaviour. The purpose of including India along with China, South Africa and Brazil under the EUCAARI project was to expand

* Corresponding author at: Finnish Meteorological Institute, P.O.Box 503, FIN-00101 Helsinki, Finland. Tel.: +358 50 401 4544.
E-mail address: rakesh.hooda@fmi.fi (R.K. Hooda).
[1] Currently at: ISAC-CNR, via Gobetti 101, 40129 Bologna, Italy.

http://dx.doi.org/10.1016/j.atmosres.2015.08.014
0169-8095/

the European activities of aerosol measurements outside Europe and to provide useful reference for evaluating European conditions.

2. Methods

2.1. Site description and aerosol composition

The measurement site was located in Gual Pahari (28°26′N, 77°09′E, 243 m above sea level), Gurgaon, about 25 km south of New Delhi. The 24 h ambient fine ($PM_{2.5}$) and coarse ($PM_{2.5-10}$) aerosols were sampled simultaneously every 6 days using a Dichotomous Partisol-Plus Sequential Air Sampler (Yeatts et al., 2007). The sample was taken at 2 m above the ground. In addition to the filter sampler, the station had a comprehensive set of ground-level *in-situ* aerosol and remote sensing measurements (Hyvärinen et al., 2010; Komppula et al., 2012). In this work, we utilised online $PM_{2.5}$ and PM_{10} measurements (Thermo Scientific SHARP Monitors model 5030), aerosol black carbon measurements (Thermo Scientific Multi-Angle Absorption Photometer, MAAP), and size distribution (TSI Aerodynamic Particle Sizer, APS). Ambient temperature, relative humidity, rain intensity, wind direction and wind speed were also measured (Vaisala WXT 510 weather transmitter) at a height of about 10 m above the ground. A more detailed presentation of the sampling location and instrumentation can be found in Hyvärinen et al. (2010) and Komppula et al. (2012).

The fine and coarse particles were collected on 47 mm quartz filter at a flow rate of 16.7 lpm. Aerosol sampling on quartz filters is subject to negative artefacts (losses of volatile species such as ammonium and nitrate) and positive artefacts (absorption on the collection substrate of semivolatile species such as low molecular weight organics) (Turpin et al., 1994; Vecchi et al., 2009). To correct negative sampling artefacts due to the volatilisation of ammonium and nitrate, a Whatman 41 paper filter was placed on the back of each quartz filter used to sample fine particles. Fine ammonium and nitrate concentration were calculated as the sum of ammonium and nitrate on quartz and on the paper filter concentration (Putaud et al., 2004). To avoid positive sampling artefacts, active carbon honeycomb denuders were placed upstream of the filter to remove semi volatile organic species, while denuders coated with sodium chloride and nitric acid were employed to remove nitric acid and ammonia, respectively (Gilardoni et al., 2011).

PM collected on filters was determined gravimetrically with a microbalance in a clean room after conditioning at a controlled relative humidity (20%–30%) and temperature (20–25 °C) for 24 h.

Filters were analysed for organic carbon (OC), elemental carbon (EC), and major water-soluble inorganic ions (sulphate, nitrate, chloride, ammonium, sodium, potassium, calcium and magnesium). OC and EC were quantified on quartz filters with a Sunset Lab Thermal/Optical Carbon Analyser using the EUSAAR-2 protocol (Cavalli et al., 2010). The heating protocol was modified with longer heating step to ensure the complete evolution of the carbon fractions. A punch of each quartz and paper filter was extracted with ultrapure mQ water and the extracts were analysed by ion chromatography to quantify the water-soluble inorganic species (Metrohm 861 Advanced Compact ion chromatographer equipped with an 813 Compact Auto-sampler, Micro Devices Metrohm Limited). For quality control purposes, an aliquot of standard reference material SRM 2694 (simulated rain water) was analysed simultaneously with each sample batch and the agreement between measured and certified concentrations was verified (Gilardoni et al., 2011).

2.2. Source region characterisation

Receptor model (Positive matrix factorization, PMF) (Paatero and Tapper, 1994; Paatero, 1997) a commonly employed method was used for apportionment of source strength using speciation data. EPA PMF 3.0 program (EPA, 2008a) was applied to fine and coarse mode aerosol annual data (11 species, $n = 52$). Each data point was individually weighted using the estimated analytical uncertainty and the method detection limit (Gilardoni et al., 2011; Polissar et al., 1998; Norris et al., 2008). A 7% of fine and 13% of coarse mode aerosol data was below limit of quantification (LOQ) or missing values. Missing values were substituted by medians of the adjacent four values (Huang et al., 1999), and these values were down-weighted by assigning uncertainty with ten times the median concentration. Values below LOQ were replaced with half of the LOQ, and corresponding uncertainty value at 5/6 times the LOQ (Polissar et al., 1998; Evans and Jeong, 2007). A 5% extra modelling uncertainty was used for all species in PMF runs.

Air-mass backward (120 h) trajectories were calculated for every 3 h with the FLEXTRA model (Stohl et al., 1995; Stohl and Seibert, 1998) as described in Hyvärinen et al., 2010 and Raatikainen et al., 2014. Hourly local wind vectors were calculated using local wind direction and speed, similarly as described in Vestenius et al., 2011. Wind direction and trajectories were classified as four main sectors: north (315–45°), east (45–135°), south (135–225°) and west (225–315°).

The conditional probability function (CPF) was applied on resolved source contributions differently for back-trajectories (CPF_T) and wind directions (CPF_W).

CPF is defined with the following equation:

$$CPF = \frac{m_{\Delta\theta}}{n_{\Delta\theta}} \quad (1)$$

where $m_{\Delta\theta}$ is the number of times the average trajectory vectors (3-hourly) and the wind direction vectors (1-hourly) that fall in the sector $_{\Delta\theta}$ in each sampling day and exceed the threshold criteria (80th percentile) of the daily source contribution, while $n_{\Delta\theta}$ is the total number of vectors that fall in the same trajectory sector and the wind direction sector (Kim et al., 2003; Vestenius et al., 2011).

3. Results and discussion

3.1. Trajectories and meteorology

Seasons were classified as summer (March–May), monsoon (June–September), post-monsoon (October–November) and winter (December–February). According to the trajectory analysis, during summer, 43% of the air masses came from the wide western sector between NW (i.e. dust areas) and SW (i.e. Arabian Sea). These mixed air mass patterns have also been similarly seen by Lodhi et al., 2013. In monsoon, air masses were mainly from the W–SW sector (i.e. Arabian Sea) with a small fraction from the E–SE sector (i.e. Bay of Bengal). The post-monsoon and the winter had similar patterns, mainly from the NW sector. The post-monsoon period also had a small contribution from the E–SE sector. The typical seasonal behaviour of air-mass trajectories for summer season (22-04-2008), monsoon season (23-06-2008) and post-monsoon season (27-11-2008) are illustrated in Fig. 4 (discussion in Section 3.4).

In the winter, the coldest nights reached as low as 1.5 °C. The maximum temperature for the hourly data set was 42.4 °C in summer. The diurnal average temperature varied from 8.5 to 34.3 °C during the measurement period. Maximum relative humidity reached nearly 97% during most of the night time in post-monsoon and winter months. On the other hand, the relative humidity in daytime never reached 90%. The average height of planetary boundary layer (PBL) above ground level at Gual Pahari during the measurement period was 540 m (for detailed calculations see Raatikainen et al., 2014). The highest diurnal variation in the temperature during the summer season in the IGP creates a highly dynamic boundary layer and efficient vertical mixing of pollutants (Hyvärinen et al., 2010; Raatikainen et al., 2014).

3.2. PM concentrations

The annual range of size-resolved gravimetric mass concentration from filters was 7–293 μgm^{-3} (average: $77 \pm 46\ \mu gm^{-3}$, $n = 52$) and 7–108 μgm^{-3} (average: $44 \pm 25\ \mu gm^{-3}$, $n = 52$), for $PM_{2.5}$ and $PM_{2.5-10}$ aerosols, respectively. The coefficient of determination (r^2) (square of the correlation coefficient) between filter and online measurements of the PM concentrations were 0.58 and 0.53 for $PM_{2.5}$ and PM_{10}, respectively. PM_{10} on filter samples is the sum mass concentration of $PM_{2.5}$ and $PM_{2.5-10}$ aerosols. It was observed that PM values were clearly higher from the online instruments. Masses yielded from filter samples and those from online instruments were $PM_{2.5} = 77 \pm 46$; 118 ± 76 and $PM_{10} = 121 \pm 71$; 177 ± 93, respectively. The details are provided as Supplementary material. The mass concentration from filter samples and online instruments showed a similar seasonal variation for both $PM_{2.5}$ and PM_{10}. The daily average gravimetric mass concentration of $PM_{2.5}$ was $145 \pm 80\ \mu gm^{-3}$ (post-monsoon) and $92 \pm 30\ \mu gm^{-3}$ (winter). More than 50% filter sampling days (27/52) in a one-year time have had concentration levels that exceed standards (CPCB, 2009) in India, which is 60 μgm^{-3} for $PM_{2.5}$ (daily ambient air quality standard in India).

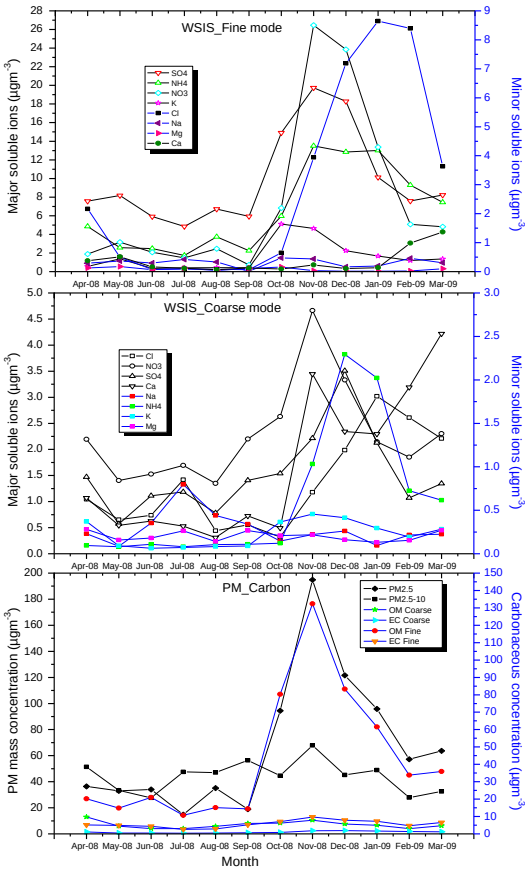

Fig. 1. Monthly (April 2008–March 2009) variation of chemical species in $PM_{2.5}$ (fine mode) and $PM_{2.5-10}$ (coarse mode) at Gual Pahari, WSIS = Water soluble ionic species; Y-axis depict major ($Y_{Primery}$) and minor ($Y_{Secondary}$) soluble ions with black and blue colour, respectively; and PM mass with black colour and carbonaceous concentration with blue colour.

A very distinct seasonal variation is seen for $PM_{2.5}$ concentrations (Fig. 1). The seasonal average mass concentrations for $PM_{2.5}$ were higher during post-monsoon and winter season compared to that during the summer season (Table 1). This may be due to low and stable boundary layer height, which limits vertical mixing of aerosols in the region during winter and post-monsoon seasons. The shallow boundary layer and colder temperatures during winter facilitate trapping of pollutants, and this results in the confinement of aerosols near the surface. Concentrations decrease in March–June, which could be due to increase in temperature and boundary layer height that allows significant dispersion and vertical mixing of aerosols. The lowest concentrations during rainy months (June to August/Sept) were due to scavenging through wet deposition. Similar observations were made for the mass and number size distribution at the same location (Hyvärinen et al., 2010), and have been corroborated through following studies (Srivastava et al., 2012; Ram et al., 2012) carried out for another sampling sites in IGP. The $PM_{2.5}$ mass accounted for 24%–74% of the PM_{10} mass (Fig. 2), with an annual average of 57%. The highest values were observed in post-monsoon and winter, and the lowest values in monsoon season. These seasonal variations of ratio of $PM_{2.5}$ to PM_{10} are due to the fact that enhanced combustion sources were contributing more to $PM_{2.5}$ during winter (Aggarwal et al., 2013). But, in summer, natural $PM_{2.5-10}$ aerosols transport (sea salt and mineral dust) (Habib et al., 2006) and wet deposition during monsoon (Seinfeld and Pandis, 2006; Croft et al., 2009) were quite effective.

3.3. Species characterisation

Carbonaceous species (OM (organic mass) + EC) formed 74% of the annual average mass of $PM_{2.5}$, while in $PM_{2.5-10}$ their proportion was 14%. In addition to filter samples, BC was measured using online instrument. The comparison of the filter-based EC and online based BC is supplemented (Supplementary material). Equivalent BC concentration is calculated from absorption coefficient measured by MAAP and assuming constant optical properties, i.e. using a single mass absorption cross section (MAC) during the entire campaign. The low r^2 value (0.33, Fig. S3) calculated over the entire dataset might be explained by a non-constant MAC over the campaign. The seasonal variability of OC was seen very clearly in $PM_{2.5}$ as well as in $PM_{2.5-10}$. The concentration of OC was quite high as compared with EC. The ratio of OC to EC for $PM_{2.5}$ was 4.2 and 3.5 for $PM_{2.5-10}$. The OC and EC contributions were found to be higher in $PM_{2.5}$ (Fig. 1). EC accounted for 6% of PM_{10}, 9% of $PM_{2.5}$, and 2% of $PM_{2.5-10}$ (Fig. 2). OM (OM = 1.8 × OC for the $PM_{2.5}$ and 1.4 × OC for the $PM_{2.5-10}$) accounted for 65% of $PM_{2.5}$ mass and 12% of $PM_{2.5-10}$ mass. Higher OM was observed during the winter and post-monsoon period. This could be due to the enhanced combustion sources (e.g., residential heating and waste burning) and stagnant meteorological conditions during the colder season (Ram et al., 2010; Aggarwal et al., 2013). A factor of 1.8 and 1.4 are commonly used for converting measured OC to OM in an urban (semi-urban) atmosphere for $PM_{2.5}$ and $PM_{2.5-10}$, respectively (Turpin and Lim, 2001; Guinot et al., 2007). We adopted these factors since those are the best available for $PM_{2.5}$ and $PM_{2.5-10}$ in a semi-urban area. In another study for the Indian urban region (e.g., Aggarwal et al., 2013) they adopted 1.6 as a factor to convert OC to OM for PM_{10}. However, the value of the factor multiplier under different situations remains the subject of current research (Chow et al., 2015).

The high carbonaceous fraction in $PM_{2.5}$ implies to further estimate secondary organic carbon (SOC) fraction. Using an approach widely adopted in the literature (Turpin and Lim, 2001; Snyder et al., 2009), secondary organic carbon was estimated using the following equation:

$$(SOC) = (OC) - \left[\frac{(OC)}{(EC)}\right]_{Min} * (EC) \quad (2)$$

Table 1
Statistical summary of surface chemistry measurements for size and seasonal variations.

Chemical species	Summer[a]			Monsoon[a]			Post-monsoon[a]			Winter[a]		
	Mean/Med	SD	Range	Mean/Med	SD	Range	Mean/Med	SD	Range	Mean/Med	SD	Range
Coarse mode												
Coarse ($PM_{2.5-10}$) (μgm^{-3})	39/34	28	14–71	45/45	29	18–75	56/59	23	22–80	41/43	16	18–61
OC (μgm^{-3})	4.5/4.9	2.1	1.9–6.3	2.9/2.9	0.9	2.1–4.0	5.0/5.5	1.8	2.2–6.6	3.3/2.9	1.0	2.1–4.5
EC (μgm^{-3})	0.9/0.9	0.2	0.6–1.2	0.5/0.5	0.2	0.3–0.6	1.4/1.1	0.5	1.0–2.1	1.6/1.6	0.4	1.1–2.2
Cl^- (μgm^{-3})	1.30/1.25	0.49	0.81–1.88	0.79/0.61	1.04	0.16–1.90	0.75/0.77	0.48	0.25–1.43	2.54/2.27	1.37	1.28–4.77
NO_3^- (μgm^{-3})	1.97/2.04	0.58	1.26–2.51	1.69/1.49	1.25	0.68–3.07	3.65/3.18	1.80	1.70–5.90	2.44/2.47	1.24	0.82–4.24
SO_4^{2-} (μgm^{-3})	1.13/1.15	0.43	0.65–1.60	1.12/1.05	0.77	0.49–1.89	1.88/1.69	0.74	1.02–2.85	2.23/1.97	1.07	1.10–3.72
Na^+ (μgm^{-3})	0.18/0.20	0.09	0.07–0.25	0.48/0.44	0.31	0.26–0.83	0.18/0.11	0.15	0.04–0.35	0.19/0.19	0.09	0.09–0.29
NH_4^+ (μgm^{-3})	0.26/0.20	0.15	0.17–0.48	0.10/0.11	0.03	0.07–0.12	0.58/0.29	0.54	0.11–1.26	1.68/1.78	0.93	0.60–2.85
K^+ (μgm^{-3})	0.25/0.24	0.12	0.12–0.39	0.08/0.07	0.04	0.04–0.12	0.41/0.30	0.35	0.16–0.99	0.30/0.31	0.09	0.21–0.42
Mg^{2+} (μgm^{-3})	0.24/0.24	0.08	0.15–0.33	0.21/0.19	0.17	0.09–0.39	0.21/0.23	0.07	0.12–0.30	0.15/0.14	0.05	0.09–0.23
Ca^{2+} (μgm^{-3})	1.94/2.05	0.66	1.07–2.59	0.55/0.46	0.44	0.26–1.04	1.97/1.95	0.50	1.31–2.65	2.61/2.18	1.17	1.52–4.45
Fine mode												
Fine ($PM_{2.5}$) (μgm^{-3})	44/44	21	21–68	26/23	16	15–45	145/130	83	48–256	92/90	30	52–123
OC (μgm^{-3})	13.1/12.9	4.8	7.9–18.0	8.5/7.0	6.5	4.3–16.1	59.1/56.2	26.2	27.2–89.5	33.1/36.4	11.9	15.7–45.1
EC (μgm^{-3})	5.6/5.8	2.7	2.4–8.2	3.8/3.2	2.3	2.6–6.7	8.4/8.6	2.6	4.6–11.5	6.6/7.1	2.4	3.2–9.7
Cl^- (μgm^{-3})	2.10/1.15	2.41	0.52–5.57	0.08/0.07	0.06	0.04–0.15	2.30/2.35	1.58	0.75–4.43	8.08/8.44	4.66	2.05–13.51
NO_3^- (μgm^{-3})	3.29/2.83	1.43	2.15–4.94	1.68/1.62	1.00	0.89–2.78	16.64/10.61	11.33	8.20–35.48	14.10/14.87	5.09	7.62–20.41
SO_4^{2-} (μgm^{-3})	7.99/7.03	3.66	4.73–12.25	5.85/5.92	2.27	3.61–8.15	17.33/15.06	9.34	8.67–32.62	12.00/11.53	4.25	7.70–17.96
Na^+ (μgm^{-3})	0.32/0.34	0.19	0.12–0.52	0.26/0.25	0.08	0.20–0.33	0.46/0.50	0.29	0.15–0.83	0.27/0.32	0.16	0.09–0.45
NH_4^+ (μgm^{-3})	4.95/4.87	2.06	2.90–7.17	2.54/2.28	1.19	1.70–3.78	9.73/8.93	3.28	6.09–13.69	11.72/11.42	2.20	9.42–14.89
K^+ (μgm^{-3})	1.10/1.10	0.78	0.30–1.96	0.40/0.36	0.16	0.28–0.59	4.88/3.56	4.56	1.59–12.60	1.70/1.82	0.54	0.92–2.23
Mg^{2+} (μgm^{-3})	0.13/0.09	0.10	0.06–0.27	0.08/0.07	0.08	0.03–0.17	0.09/0.04	0.14	0.02–0.34	0.02/0.02	0.01	0.01–0.04
Ca^{2+} (μgm^{-3})	0.75/0.42	0.82	0.22–1.91	0.12/0.10	0.08	0.07–0.22	0.16/0.17	0.05	0.07–0.22	0.41/0.11	0.64	0.09–1.55

[a] Summer (March–May), Monsoon (June–September), Post-monsoon (October–November) and Winter (December–February).

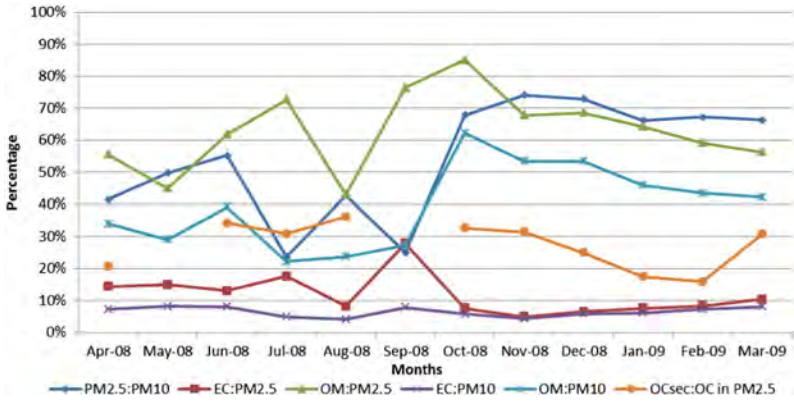

Fig. 2. Particulate mass and carbonaceous fraction ratio in aerosols at Gual Pahari.

The formula assumes that all the OC not related to the EC is secondary. This could work for $PM_{2.5}$ but does not hold for $PM_{2.5-10}$ where primary biogenic particles might be present (Turpin and Lim, 2001). $[(OC)/(EC)]_{Min}$ in the range of 1.1 to 1.5 was estimated for the rural and urban European sites (Turpin and Huntzicker, 1995; Castro et al., 1999). In our study, the values 1.0 ± 0.8 to 3.3 ± 2.3 estimated for different seasons could arise due to seasonal variations in the source strength and meteorology as well as the chemical mechanism involving production of SOC from oxidation products (Pandis et al., 1992; Miyazaki et al., 2009).

SOC was 46% of the annual average of the total OC in $PM_{2.5}$ and was 54% in post-monsoon and 37% in winter. The high SOC percentage in summer and monsoon seasons may be attributed to biogenic emissions (Kulmala et al., 2011). These high SOC in form of condensed vapours may also be related to new particle formation and growth, which may be responsible for the increase in cloud condensation nuclei in the area (e.g., Hyvärinen et al., 2010). Rengarajan et al. (2011) estimated the concentration of SOC by the same method, which accounts for ~25% of the total OC in $PM_{2.5}$ during the winter season at Ahmedabad, located in a semi-arid region of western India, about 900 km from Delhi.

Water soluble ionic species (WSIS) comprised 44% and 18% of the annual average gravimetric $PM_{2.5}$ and $PM_{2.5-10}$ mass, respectively. SO_4^{2-}, NH_4^+ and NO_3^- were dominant ions with 37% of $PM_{2.5}$ mass and followed by Cl^- and K^+ (4% and 2%, respectively). However, in $PM_{2.5-10}$ mass SO_4^{2-}, NH_4^+ and NO_3^- comprised 9%. The species such as Ca^{2+} (4%), Mg^{2+}, Na^+ and Cl^- were seen with a total of 8% in $PM_{2.5-10}$ due to contribution of dust and sea salt, respectively. The abundance of SO_4^{2-} and NO_3^- secondary aerosols in $PM_{2.5}$ ionic mass was high throughout the year. This suggests that contribution of combustion sources (fossil fuel) in forming secondary prime pollutants is significant in the region (Rengarajan et al., 2007; Miyazaki et al., 2009) and moreover, low boundary layer conditions enhance the concentration further. The seasonal distribution of ionic species shows peak concentrations in post-monsoon and winter periods as seen through Fig. 1.

Moreover, the reconstructed mass (RM) for $PM_{2.5}$ was formulated as the following equation (Chow et al., 2015);

$$RM = [NH4] + [SO4] + [NO3] + [Cl] + [Na] + [Mg] + [K] + [Ca] + (1.8 \times [OC]) + [EC] \quad (3)$$

This fulfilled 128 ± 72% for $PM_{2.5}$. The high estimated uncertainties of some of the analysed water soluble species and OM factor may result into average mass reconstruction more than $PM_{2.5}$ average mass. However, mass closure result is in corroboration to earlier studies (e.g., Chowdhury et al., 2007; Malm et al., 2005; Andrews et al., 2000). For $PM_{2.5-10}$, the same equation was applied with a multiplier of 1.4[OC]. This fulfilled 46 ± 38%, which could be due to a deficit in the reconstructed mass of chemical species where the undefined mass significantly pertains to geological minerals, trace elements and oxalate. The composition data of insoluble fraction was not analysed.

3.4. Source region (SR) discrimination

The receptor modelling solutions are shown in Table S1 (as Supplementary material). The three-factors ($p = 3$) solution for coarse mode ($PM_{2.5-10}$) and five-factors ($p = 5$) solution for fine mode ($PM_{2.5}$) were the most feasible results. The model reproduced total mass for fine mode quite effectively (slope = 0.77; $r^2 = 0.81$) (Fig. S4) but not so well for coarse mode (slope = 0.35; $r^2 = 0.31$). This comparison between the analysed values (input data) and the predicted values (modelled) is useful to determine if the model fits the individual species well (EPA, 2008b). The modelled percentage mass distributions for fine mode ($PM_{2.5}$) and for coarse mode ($PM_{2.5-10}$) are shown in Fig. S5. The details are provided as Supplementary material.

The receptor modelling factors were coupled with CPF_T and CPF_W analysis to identify spatial sectors for atmospheric aerosols in the region. For five-factors in the receptor model to fine mode, 68%–76% of the time CPF_T hits mainly SW–NW sectors and CPF_W depicts NW–SW and NE–SE sectors for 58%–78%. For the coarse mode, the scenario was relatively similar to fine mode except the intensity. CPF_T hits mainly SW–NW sectors for 74%–93% of the time and CPF_W are mainly from NW–SW and NE–SE sectors for 74%–77% for three receptor model factors (Fig. 3).

The dispersion sectors (SR) for sources types to fine and coarse mode aerosols are shown below:

3.4.1. Fine mode aerosols

SR-I:

CPF_T (Fig. 3) pointed to mix impact of farther emissions from industrial areas in SW, NW and NE sectors. However, CPF_W showed predominant emissions from all directions (e.g., Guttikunda and Calori, 2013). A case day (27-11-2008) was identified with the highest loading in receptor model fine factor 1 ($F1_f$) (Fig. 4). This trajectory zone has showed the prevailing conditions for secondary aerosols formation (Miyazaki et al., 2009).

$F1_f$ has loadings of 68%, 53% and 23% for SO_4^{2-}, NH_4^+, NO_3^-, respectively. These could be identified as secondary aerosols (Aneja et al., 2006; Kulshrestha et al., 2009). Secondary SO_4^{2-} has accounted as a long-range transport tracer (Takiguchi et al., 2008; Hand et al., 2012). The presence of NH_4^+ and NO_3^-, which are related to combustion processes

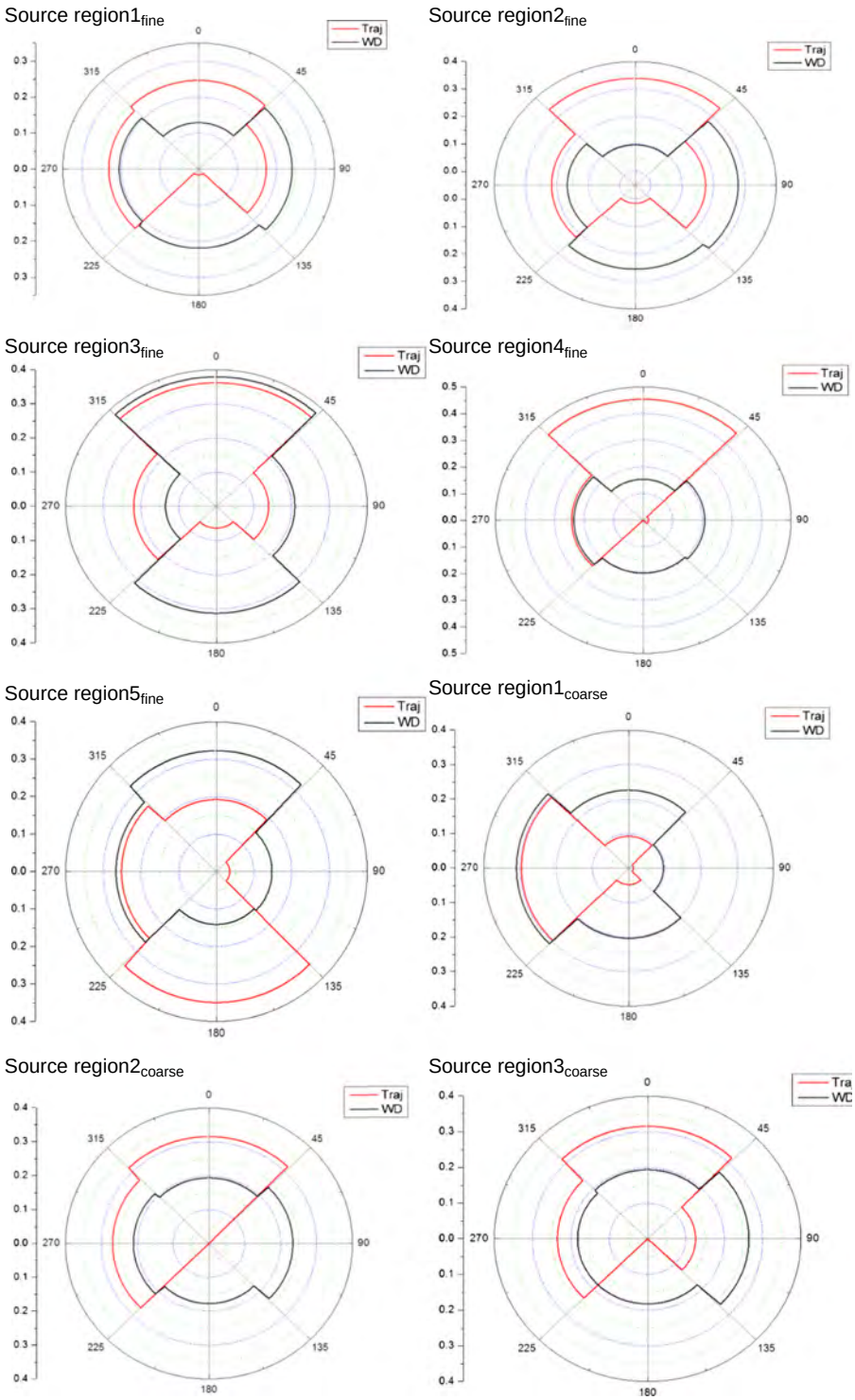

Fig. 3. CPF analyses with trajectory and wind direction for receptor model identification in fine and coarse aerosol modes (scale is of magnitude of CPF value); Trajectory is in red and wind direction is in black colour. Radial distance defined by the magnitude of CPF value and the angle ($\Delta\theta$) derived from the back-trajectory and/or wind direction.

(biomass and biofuel) (Aggarwal et al., 2013), and also secondary aerosols, shows that there is local as well as regional transport.

SR-II:

The CPF_T analysis influenced by NW–NE and SW–NW sectors indicates transport of air parcels through northeast and south of Delhi. However, CPF_W shows much overlap directions with a lesser magnitude (Fig. 3). However, a case day (27-11-2008) with the highest loading in receptor model fine factor 2 ($F2_f$) showed that air mass carrying fine mode aerosols travelled 240–140 km in a day from the north and as high as 5000 m asl (Fig. 4). Eventually, it appears that emissions to fine mode were a mix of local as well as regional origin, which agrees with earlier findings (Komppula et al., 2012). These mixed air masses may also result into formation of secondary aerosols (Miyazaki et al., 2009). $F2_f$ with 63%, 62%, 55% and 34% of NO_3^-, OC, K^+, and EC respectively, likely represents a mix of combustion sources (domestic, industrial, transport and biomass) (Andreae and Merlet, 2001; Streets et al., 2003). Less than expected NH_4^+ loading in this factor profile could be due to shifting of domestic cooking fuel from cow dung to LPG around 95% in urban and semi-urban population (CPCB, 2010; Bansal et al., 2013).

SR-III:

CPF_T analysis shows trajectories from the north-eastern and western sector (Fig. 3). The major contributions could be from Delhi and National Highway 8 (Delhi–Jaipur), whereby heavy diesel trucks are plied in a very high volume (Guttikunda and Calori, 2013). However, CPF_W points towards NE–SE and SW which are influenced by a nearby major link road. A case day (22-04-2008) with the highest loading in receptor model fine factor 3 ($F3_f$) (Fig. 4) shows that air parcels of 500 m asl elevated up to 4500 m asl might be originated in the western sector and in localised NE side.

$F3_f$ has 83%, 59%, 43%, 40% and 30% loadings of Ca^{2+}, EC, K^+, Na^+ and OC, respectively, which could be related to road traffic sources (combination of re-suspended road dust and tail-pipe emissions) (Watson and Chow, 2000). The mass concentration of marker species such as EC, K^+, Ca^{2+} and Na^+ is small and stable throughout the year to fine mode (Figs. 1, 2 and Fig. S5). Nevertheless, these marker species could represent to a mix of fresh biomass combustion emissions and soil but these sources are relatively seasoned in India with high peaks (Habib et al., 2006).

SR-IV:

CPF_T and CPF_W analyses show multiple sources to factor 4 ($F4_f$) from northeastern and western sectors (Fig. 3). In case days (e.g., 02-01-2009), CPF_T shows that air parcels starting from 1000 m and 2000 m asl could have different origins of emissions (Nair et al., 2007; Guttikunda and Calori, 2013) and overlap after a certain time. The trajectories advections were not only through the industrial and power plant regions in western–northern India but also the dense populated areas.

$F4_f$ is represented by 85% of Cl^- and 24% of NH_4^+. The multiple sources of Cl^- possibly have major contributions of ammonia through neutralisation of hydrochloric acid to form ammonium chloride, or combustion activities (coal and biomass) (Speciate USEPA, 1999; Reddy and Venkataraman, 2002; Shapiro et al., 2007; Akagi et al., 2011; Behera et al., 2013; Guttikunda and Calori, 2013) and secondary formation of ammonium nitrate and ammonium chloride (Marley and Gaffney, 2004). It is difficult to draw any conclusion in explaining which is more important, the primary or secondary emissions source. The factor profile concentration for NH_4^+ cannot be ignored as being also emitted from crop residue burning (Badarinath et al., 2006) having r^2 value of 0.43 with K.

SR-V:

The spatial discrimination to factor ($F5_f$) was very clear. CPF_T and CPF_W analyses show (Fig. 3) prevailing NW–SW air parcels. The case day (23-06-2008) was evaluated further (Fig. 4) and which corroborates to the long-range transport of dust and mix with sea-salts. On the basis of chemical–physical properties and air–mass back trajectories, the Arabian Sea; southwest Asian basins; and Thar Desert had been presented for the long-range transport of sea-salt enriched with mineral dust during pre-monsoon season (Moorthy et al., 1993; Moorthy et al., 2004; Chinnam et al., 2006; Prasad and Singh, 2007). It has been found that the back-trajectories starting at very low heights as well as of 500 m asl overlap and show the same origin and transport. Komppula et al. (2012) at the same sampling location have observed higher values of single scattering albedo at 532 nm for lower aerosol layers associated with the presence of maritime aerosols. Moreover, with backward trajectory analysis (case day 13-07-2008, which fall in monsoon season) had been shown that the air masses arrived at 500 m and 1000 m height had crossed over the Arabian Sea.

$F5_f$ shows characteristics of natural mineral dust and sea-salt by having loading of 79%, 32%, 14% and 10% for Mg^{2+}, Na^+, Ca^{2+} and SO_4^{2-}, respectively. These mineral dust aerosols enter the atmosphere through wind erosion of desert regions and disturbed soils (Miller et al., 2004; Tegen and Fung, 1994). A contribution of SO_4^{2-} with Na^+, Mg^{2+} also refers to aged sea-salt (Hwang and Hopke, 2007; Tiwari et al., 2009). The average ratio of Cl^-/Na^+ in the aerosols (1.22 w/w) is about the same as that of seawater (1.16 w/w) for the case day. However, average ratio of Mg^{2+}/Na^+ in the aerosols (0.93 w/w) is higher than for seawater (0.13 w/w) for the case day which could be attributed to mineral dust.

3.4.2. Coarse mode aerosols

SR-I:

CPF_T and CPF_W analyses (Fig. 3) along with the case day evaluation (Fig. 4) for coarse factor ($F1_c$) are found to be similar to $F5_f$. APS data (Section 3.5) were also examined for discrimination of this spatial sector for coarse mode aerosols.

$F1_c$ is having loadings of 75%, 72%, 61%, and 55% for Mg^{2+}, Na^+, OC, and NO_3^-, respectively. These marker species are commonly attributed to terrestrial dust, partially aged sea-salt and mixed with combustion activities (industries). The ratio of fine mode to coarse mode aerosols for high factor loading days have also been examined and found that the days fall mostly in pre-monsoon season and with a ratio of >0.65. The contribution of fine mode to coarse mode fraction is very high; therefore, the long- range transport of dust cannot be ignored.

SR-II:

CPF_T and CPF_W analyses point towards northeastern and northwestern sectors (Fig. 3). However, besides broad similarities, CPF_T analysis shows NE direction as a major sector. This overwhelms the possibilities to present the factor ($F2_c$) with sea-salt aerosols. $F2_c$ has loadings of 77%, 59% for Cl^-, Ca^{2+}, respectively and with each 25% for Mg^{2+} and Na^+. This may represent a mix of open waste burning and soil sources (Akagi et al., 2011). Ca^{2+}-abundant particles in coarse mode ($PM_{2.5-10}$) can also be originated from local construction activities, which occurred heavily in the region through to the end of 2008 preparation for the Commonwealth Games (Guttikunda and Calori, 2013).

SR- III:

The CPF_T analysis shows that air parcels from NE and NW sectors, while CPF_W shows local air blows (Fig. 3). Factor 3 ($F3_c$) was found to be a mixed source of incomplete combustion of biomass/agriculture residue and re-suspension dust of fuel oil combustion (motor vehicles) (Watson and Chow, 2000; Badarinath et al., 2006; Akagi et al., 2011; Sillapapiromsuk et al., 2013) with trace marker loadings of 100%, 61%, 58% and 52% for NH_4^+, K^+, SO_4^{2-} and EC, respectively.

3.5. Volume size distribution and receptor model

A very crucial and complementary information was obtained from APS for particle volume size distribution (size range 0.5–10 μm). For calculating the average volume size distribution, quality assured 1 h of APS data was used. The volume size distribution for each size bin measured by the instrument is calculated from the particle number in the

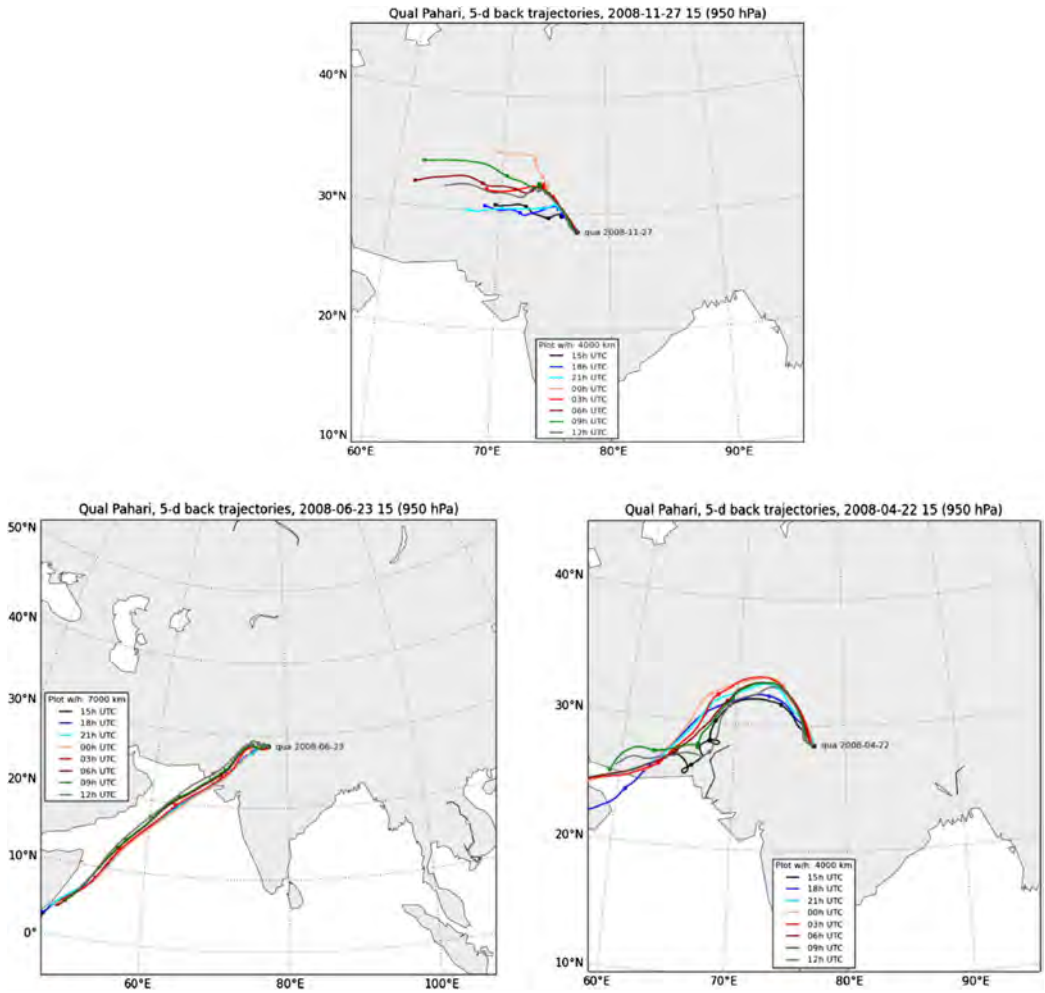

Fig. 4. 5-day calculated backtrack trajectories from case days during 2008–2009 in Gual Pahari.

bin and assuming spherical particles (additional information for data processing, see Hyvärinen et al., 2010). Following the PMF analysis, days for each receptor model factor (high loadings (11 out of 52 days)) were first clubbed together, and the final average for the volume size distribution characterising each fine and coarse mode receptor model factor were calculated from these days and the daily APS data (Fig. 5). The APS data clearly supports the findings of receptor model factors identification and spatial sector discrimination.

For fine mode (Fig. 5a), the particle volume distribution for factor 1($F1_f$) produced on average the highest volume peak at a diameter of about 0.78 μm, followed by factor 2($F2_f$), factor 4($F4_f$), factor 3($F3_f$), and factor 5($F5_f$). Factor 1($F1_f$), 2($F2_f$) and 4($F4_f$) showed similar bimodal distributions with higher volume concentration in fine mode and lesser in coarse mode fractions, while for factor 3($F3_f$), a small peak (0.78 μm) in fine mode attributed to vehicle exhaust and another high peak in coarse mode (3.5 μm) likely due to re-suspended road dust. Factor 5($F5_f$) clearly showed bi-modal volume distribution in coarse mode fraction.

For coarse mode factors as shown in Fig. 5b, the particle volume distribution increased with a diameter from about 2 μm to about 5 μm. As expected, mineral dust/aged sea-salt ($F1_c$) produced the highest coarse mode volume peak and appeared in bi-modal distribution. This was followed by factor 3($F3_c$) and factor 2($F2_c$).

The volume size distributions for the factors with the dust element in fine mode ($F5_f$ and $F3_f$) correspond with the volume–size distribution of factor $F1_c$ (dust) in the coarse mode. Similarly, volume size distributions for factors $F4_f$ and $F2_f$ correspond to those for factors $F2_c$ and $F3_c$ from coarse mode, respectively.

4. Conclusions

Aerosol characteristics and chemical speciation was studied to understand aerosol behaviour from the data set collected over one year. The present work at a background receptor location to Delhi and surroundings has importance in assessing benefits and the current status of different managerial and technical measures taken in the past years (1996–2008) to control the air emissions.

The coupling of conditional probability function (CPF: CPF_T and CPF_W) analysis with receptor modelling tool (PMF) and validation through volume size distribution (APS) has improved geographical

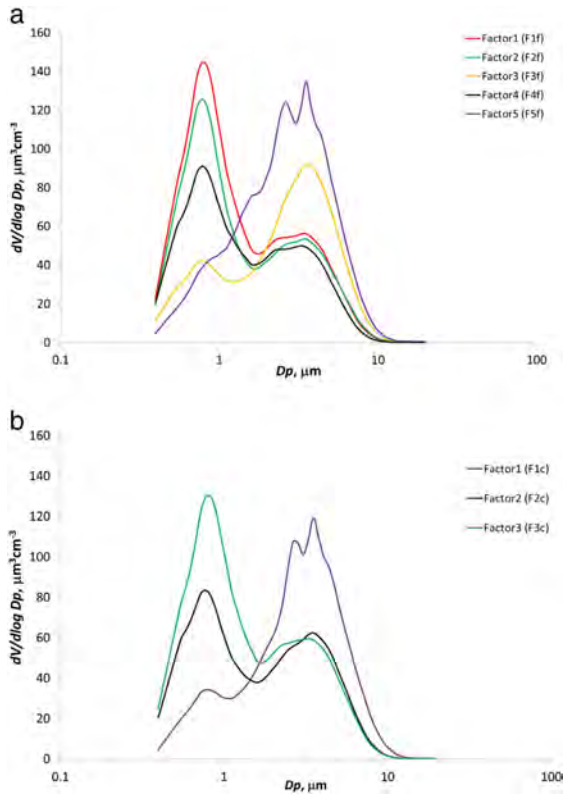

Fig. 5. Typical volume size distribution observed with APS during periods dominated by receptor model factor in, a) Fine and, b) Coarse aerosol mode.

discrimination significantly than using either independently. Approach in present study shows 68%–76% of CPF_T hits mainly SW–NW sectors and CPF_W analysis depicts NW–SW and NE–SE sectors for 58%–78% of the time for five factors to fine mode aerosols. For coarse mode aerosols, the scenario was relatively similar to fine mode aerosols except the intensity. CPF_T hits mainly SW–NW sectors for 74%–93% time and CPF_W are mainly from NW–SW and NE–SE sectors for 74%–77% of the time for three factors. The trajectories advections were through not only the industrial and power plant regions in western India and in northern India but also the dense populated areas at regional level. The spatial discrimination of long-range transport of sea-salt enriched with mineral dust from Arabian Sea and Thar Desert was identified during the pre-monsoon season. The surface wind directions captured the emission activities at a local scale. The overlapping and clustering of spatial sectors in terms of source origin is also seen. Overlapping is shown by different source origins and mixed during transport before reaching the receptor point, while clustering is shown through same spatial sector for different size mode fraction of aerosols. Therefore, the approach of CPF_T and CPF_W work as complementary to each other and endorse the precise outcome.

From a health perspective, more than 50% of the days exceeded the daily $PM_{2.5}$ concentration limit value despite various control measures in and around Delhi. It shows that $PM_{2.5}$ is a respiratory health threat in the region. In climatic perspective, high OC composition in fine as well as in coarse mode fraction showed the possibility that combustion sources and meteorological conditions lead to high concentration of secondary organic carbon (important roles of both biogenic and anthropogenic emissions in SOC formation). These condensable organic compounds can contribute to new particle formation, the increased enhanced growth of aerosols, and eventually an increase in the cloud condensation nuclei concentration. For future studies, inclusion of the estimation of detailed microphysical properties (effective radius, effective density, refractive index, hygroscopicity) in terms of seasonally and monthly averaged optical data along with chemical data would be of great value to aerosol related -climate-air quality linkages in IGP region.

Acknowledgements

This work was supported by the EC 6th Framework programme project EUCAARI (036833-2), European Commission, the Ministry of Foreign Affairs of Finland and the Academy of Finland as part of the Centre of Excellence programme (project no 1118615). Special recognition goes to T.S. Panwar for his direction, Timo Anttila and Ari Halm from FMI for technical assistance and TERI's Gual Pahari retreat staff for routine maintenance of instruments. The authors also wish to thank Pentti Paatero for his recommendations on PMF methodology (Paatero, 2013).

Appendix A. Supplementary data

Supplementary data to this article can be found online at http://dx.doi.org/10.1016/j.atmosres.2015.08.014.

References

Aggarwal, S.G., Kawamura, K., Umarji, G.S., Tachibana, E., Patil, R.S., Gupta, P.K., 2013. Organic and inorganic markers and stable C-, N-isotopic compositions of tropical coastal aerosols from megacity Mumbai: sources of organic aerosols and atmospheric processing. Atmos. Chem. Phys. 13, 4667–4680.
Akagi, S.K., Yokelson, R.J., Wiedinmyer, C., Alvarado, M.J., Reid, J.S., Karl, T., Crounse, J.D., Wennberg, P.O., 2011. Emission factors for open and domestic biomass burning for use in atmospheric models. Atmos. Chem. Phys. 11, 4039–4072.
Andreae, M.O., Merlet, P., 2001. Emission of trace gases and aerosols from biomass burning. Glob. Biogeochem. Cycles 15, 955–966.
Andreae, M.O., Rosenfeld, D., 2008. Aerosol-cloud-precipitation interactions. Part 1. The nature and sources of cloud-active aerosols. Earth-Sci. Rev. 89, 13–41.
Andrews, E., Saxena, P., Musarra, S., Hildemann, L.M., Koutrakis, P., McMurry, P.H., 2000. Concentration and composition of atmospheric aerosols from the 1995 SEAVS experiment and a review of the closure between chemical and gravimetric measurements. J. Air Waste Manage. Assoc. 50, 648–664.
Aneja, V.P., Wang, B., Tong, D.Q., Kimball, H., Steger, J., 2006. Characterization of major chemical components of fine particulate matter in North Carolina. J. Air Waste Manag. Assoc. 56, 1099–1107.
Badarinath, K.V.S., Kiran Chand, T.R., Prasad, K.V., 2006. Agriculture crop residue burning in the Indo-Gangetic Plains — a study using IRS-P6 AWiFS satellite data. Curr. Sci. 91, 1085–1089.
Bansal, M., Saini, R.P., Khatod, D.K., 2013. Development of cooking sector in rural areas in India — a review. Renew. Sust. Energ. Rev. 17, 44–53.
Behera, S.N., Betha, R., Balasubramanian, R., 2013. Insights into chemical coupling among acidic gases, ammonia and secondary inorganic aerosols. Aerosol Air Qual. Res. 13, 1282–1296.
Castro, L.M., Pio, C.A., Harrison, M.R., Smith, D.J.T., 1999. Carbonaceous aerosol in urban and rural European atmospheres: estimation of secondary organic carbon concentrations. Atmos. Environ. 33, 2771–2781.
Cavalli, F., Viana, M., Yttri, K.E., Genberg, J., Putaud, J.P., 2010. Toward a standardised thermal-optical protocol for measuring atmospheric organic and elemental carbon: the EU- SAAR protocol. Atmos. Meas. Tech. 3, 79–89.
Charlson, R.J., Schwartz, S.E., Hales, J.M., Cess, R.D., Coakley, J.A., Hansen, J.E., Hofmann, D.J., 1992. Climate forcing by anthropogenic aerosols. Science 255, 423–430.
Chinnam, N., Dey, S., Tripathi, S.N., Sharma, M., 2006. Dust events in Kanpur, northern India: chemical evidence for source and implications to radiative forcing. Geophys. Res. Lett. 33, L08803. http://dx.doi.org/10.1029/2005GL025278.
Chow, J.C., Lowenthal, D.H., Chen, L.-W., Wang, X., Watson, J.G., 2015. Mass reconstruction methods for $PM_{2.5}$: a review. Air Qual. Atmos. Health 8, 243–263.
Chowdhury, Z., Zheng, M., Schauer, J.J., Sheesley, R.J., Salmon, L.G., Cass, G.R., Russell, A.G., 2007. Speciation of ambient fine organic carbon particles and source apportionment of $PM_{2.5}$ in Indian cities. J. Geophys. Res. 112, D15303. http://dx.doi.org/10.1029/2007JD008386.
CPCB, 2009. National Ambient Air Quality Standards, Notification, Central Pollution Control Board, Government of India, New Delhi, India.
CPCB, 2010. Air Quality Monitoring, Emission Inventory and Source Apportionment Study for Indian Cities. Central Pollution Control Board, Government of India, New Delhi, India.

Croft, B., Lohmann, U., Martin, R.V., Stier, P., Wurzler, S., Feichter, J., Posselt, R., Ferrachat, S., 2009. Aerosol size-dependent below-cloud scavenging by rain and snow in the ECHAM5-HAM. Atmos. Chem. Phys. 9, 4653–4675.

EPA, 2008a. PMF Model, Version 3. http://www.epa.gov/heasd/products/pmf/pmf.html last accessed in 2014.

EPA, 2008b. Positive Matrix Factorization (PMF) 3.0 Fundamentals & User Guide Washington.

Evans, G.J., Jeong, C.-H., 2007. Data Analysis and Source Apportionment of $PM_{2.5}$ in Golden, British Columbia using Positive Matrix Factorization (PMF), SOCAAR Report No.: CR-WB-2007-02.

Gilardoni, S., Vignati, E., Marmer, E., Cavalli, F., Belis, C., Gianelle, V., Loureiro, A., Artaxo, P., 2011. Sources of carbonaceous aerosol in the Amazon basin. Atmos. Chem. Phys. 11, 2747–2764.

Guinot, B., Cachier, H., Oikonomou, K., 2007. Geochemical perspectives from a new aerosol chemical mass closure. Atmos. Chem. Phys. 7, 1657–1670.

Guttikunda, S.K., Calori, G., 2013. A GIS based emissions inventory at 1 km × 1 km spatial resolution for air pollution analysis in Delhi, India. Atmos. Environ. 67, 101–111.

Habib, G., Venkataraman, C., Chiapello, I., Ramachandran, S., Boucher, O., Reddy, M.S., 2006. Seasonal and inter-annual variability in absorbing aerosols over India derived from TOMS: relationship to regional meteorology and emissions. Atmos. Environ. 40, 1909–1921.

Hand, J.L., Schichtel, B.A., Malm, W.C., Pitchford, M.L., 2012. Particulate sulfate ion concentration and SO_2 emission trends in the United States from the early 1990s through 2010. Atmos. Chem. Phys. 12, 10353–10365.

HEI, 2010. Outdoor air pollution and health in the developing countries of Asia: a comprehensive review. Special Report 18. Health Effects Institute, Boston, USA.

Huang, S., Rahn, K.A., Arimoto, R., 1999. Testing and optimizing two factor — analysis techniques on aerosol at Narragansett, Rhode Island. Atmos. Environ. 33, 2169–2185.

Hwang, I., Hopke, P.K., 2007. Estimation of source apportionment and potential source locations of PM2.5 at a west coastal IMPROVE site. Atmos. Environ. 41, 506–518.

Hyvärinen, A.-P., Lihavainen, H., Komppula, M., Panwar, T.S., Sharma, V.P., Hooda, R.K., Viisanen, Y., 2010. Aerosol measurements at the Gual Pahari EUCAARI station: preliminary results from in-situ measurements. Atmos. Chem. Phys. 10, 7241–7252.

IPCC, 2013. Summary for Policymakers. In: Stocker, T.F., Qin, D., Plattner, G.-K., Tignor, M., Allen, S.K., Boschung, J., Nauels, A., Xia, Y., Bex, V., Midgley, P.M. (Eds.), Climate Change 2013: The Physical Science Basis. Contribution of Working Group I to the Fifth Assessment Report of the Intergovernmental Panel on Climate Change. Cambridge University Press, Cambridge, United Kingdom and New York, NY, USA.

Kim, E., Hopke, P.K., Edgerton, E.S., 2003. Source identification of Atlanta aerosol by positive matrix factorization. J. Air Waste Manag. Assoc. 53, 731–739.

Komppula, M., Mielonen, T., Arola, A., Korhonen, K., Lihavainen, H., Hyvärinen, A.-P., Baars, H., Engelmann, R., Althausen, D., Ansmann, A., Muller, D., Panwar, T.S., Hooda, R.K., Sharma, V.P., Kerminen, V.-M., Lehtinen, K.E.J., Viisanen, Y., 2012. Technical note: one year of Raman-lidar measurements in Gual Pahari EUCAARI site close to New Delhi in India — seasonal characteristics of the aerosol vertical structure. Atmos. Chem. Phys. 12, 4513–4524.

Kulmala, M., Asmi, A., Lappalainen, H.K., Baltensperger, U., Brenguier, J.-L., Facchini, M.C., Hansson, H.-C., Hov, Ø., O'Dowd, C.D., Poschl, U., Wiedensohler, A., Boers, R., Boucher, O., de Leeuw, G., Denier van den Gon, H., Feichter, J., Krejci, R., Laj, P., Lihavainen, H., Lohmann, U., McFiggans, G., Mentel, T., Pilinis, C., Riipinen, I., Schulz, M., Stohl, A., Swietlicki, E., Vignati, E., Amann, M., Ammann, M., Alves, C., Arabas, S., Artaxo, P., Beddows, D.C.S., Bergstrom, R., Beukes, J.P., Bilde, M., Burkhart, J.F., Canonaco, F., Clegg, S., Coe, H., Crumeyrolle, S., D'Anna, B., Decesari, S., Gilardoni, S., Fischer, M., Fjæraa, A.M., Fountoukis, C., George, C., Gomes, L., Halloran, P., Hamburger, T., Harrison, R.M., Herrmann, H., Hoffmann, T., Hoose, C., Hu, M., Horrak, U., Iinuma, Y., Iversen, T., Josipovic, M., Kanakidou, M., Kiendler-Scharr, A., Kirkevag, A., Kiss, G., Klimont, Z., Kolmonen, P., Komppula, M., Kristjansson, J.-E., Laakso, L., Laaksonen, A., Labonnote, L., Lanz, V., Lehtinen, K.E.J., Makkonen, R., McMeeking, G., Merikanto, J., Minikin, A., Mirme, S., Morgan, W.T., Nemitz, E., O'Donnell, D., Panwar, T.S., Pawlowska, H., Petzold, A., Pienaar, J.J., Pio, C., Plass-Duelmer, C., Prevot, A.S.H., Pryor, S., Reddington, C.L., Roberts, G., Rosenfeld, D., Schwarz, J., Seland, Ø., Sellegri, K., Shen, X.J., Siebert, H., Sierau, B., Simpson, D., Sun, J.Y., Topping, D., Tunved, P., Vaattovaara, P., Vakkari, V., Veefkind, J.P., Visschedijk, A., Vuollekoski, H., Vuolo, R., Wehner, B., Wildt, J., Woodward, S., Worsnop, D.R., van Zadelhoff, G.-J., Zardini, A.A., Zhang, K., van Zyl, P.G., Kerminen, V.-M., Carslaw, K.S., Pandis, S.N., 2011. General overview: European Integrated project on Aerosol Cloud Climate and Air Quality interactions (EUCAARI) — integrating aerosol research from nano to global scales. Atmos. Chem. Phys. 11, 13061–13143. http://dx.doi.org/10.5194/acp-11-13061-2011.

Kulshrestha, U.C., Raman, R.S., Kulshrestha, M.J., Rao, T.N., Hazarika, P.J., 2009. Secondary aerosol formation and identification of regional source locations by PSCF analysis in the Indo-Gangetic region of India. J. Atmos. Chem. 63, 33–47.

Lodhi, N.K., Naseema, S.B., Singh, S., Kumar, K., 2013. Aerosol climatology at Delhi in the western Indo-Gangetic Plain: microphysics, long-term trends, and source strengths. J. Geophys. Res. 118, 1361–1375. http://dx.doi.org/10.1002/jgrd.50165.

Malm, W.C., Day, D.E., Carrico, C., Kreidenweis, S.M., Collett Jr., J.L., McMeeking, G., Lee, T., Carrillo, J., Schichtel, B., 2005. Intercomparison and closure calculations using measurements of aerosol species and optical properties during the Yosemite aerosol characterization study. J. Geophys. Res. 110, D14302. http://dx.doi.org/10.1029/2004JD005494.

Marley, N.A., Gaffney, J.J., 2004. Sixth Conference on Atmospheric Chemistry: Air Quality in Megacities; Seattle, Washington.

Miller, R.L., Tegen, I., Perlwitz, J., 2004. Surface radiative forcing by soil dust aerosols and the hydrologic cycle. J. Geophys. Res. 109, D04203. http://dx.doi.org/10.1029/2003JD004085.

Miyazaki, Y., Aggarwal, S.G., Singh, K., Gupta, P.K., Kawamura, K., 2009. Dicarboxylic acids and water-soluble organic carbon in aerosols in New Delhi, India in winter: characteristics and formation processes. J. Geophys. Res. 114, D19206. http://dx.doi.org/10.1029/2007JD009116.

Moorthy, K.K., Nair, P.R., Prasad, B.S.N., Muralikrishnan, N., Gayathri, H.B., Murthy, B.N., Niranjan, K., Babu, V.R., Satyanarayana, G.V., Agashe, V.V., Aher, G.R., Singh, R., Srivastava, B.N., 1993. Results from the MWR Network of IMAP. Indian J. Radio Space Phys. 22, 243–258.

Moorthy, K.K., Babu, S.S., Satheesh, S.K., 2004. Aerosol characteristics and radiative impacts over the Arabian Sea during the inter-monsoon season: results from ARMEX field campaign. J. Atmos. Sci. 62, 192–206.

Nair, V.S., Moorthy, K.K., Alappattu, D.P., Kunhikrishnan, P.K., George, S., Nair, P.R., Babu, S.S., Abish, B., Satheesh, S.K., Tripathi, S.N., Niranjan, K., Madhavan, B.L., Srikant, V., Dutt, C.B.S., Badarinath, K.V.S., Reddy, R.R., 2007. Wintertime aerosol characteristics over the Indo-Gangetic Plain (IGP): impacts of local boundary layer processes and long-range transport. J. Geophys. Res. 112, D13205. http://dx.doi.org/10.1029/2006JD008099.

Norris, G., Vedantham, R., Wade, K., Brown, S., Pouty, J., Foley, C., Martin, L., 2008. EPA Positive Matrix Factorization (PMF) 3.0 Fundamentals & User Guide.

Paatero, P., 1997. Least square formulation of robust non-negative factor analysis. Chemom. Intell. Lab. Syst. 37, 23–35.

Paatero, P., 2013. Personal communication.

Paatero, P., Tapper, U., 1994. Positive matrix factorization: a non-negative factor model with optimal utilization of error estimates of data values. Environmetrics 5, 111–126.

Pandis, S.N., Harley, R.A., Cass, G.R., Seinfeld, J.H., 1992. Secondary organic aerosol formation and transport. Atmos. Environ. 26, 2269–2282.

Polissar, A.V., Hopke, P.K., Paatero, P., Malm, W.C., Sisler, J.F., 1998. Atmospheric aerosol over Alaska-2. Elemental composition and sources. J. Geophys. Res. 103, 19045–19057.

Prasad, A.K., Singh, R.P., 2007. Changes in aerosol parameters during major dust storm events (2001–2005) over Indo-Gangetic Plains using AERONET and MODIS data. J. Geophys. Res. 112, D09208. http://dx.doi.org/10.1029/2006JD007778.

Prasad, A.K., Singh, R.P., Kafatos, M., 2006. Influence of coal based thermal power plants on aerosol optical properties in the Indo-Gangetic basin. Geophys. Res. Lett. 33, L05805. http://dx.doi.org/10.1029/2005GL023801.

Putaud, J.-P., Van Dingenen, R., Dell'Acqua, A., Raes, F., Matta, E., Decesari, S., Facchini, M.C., Fuzzi, S., 2004. Size-segregated aerosol mass closure and chemical composition in Monte Cimone (I) during MINATROC. Atmos. Chem. Phys. 4, 889–902.

Raatikainen, T., Hyvärinen, A.-P., Hatakka, J., Panwar, T.S., Hooda, R.K., Sharma, V.P., Lihavainen, H., 2014. The effect of boundary layer dynamics on aerosol properties at the Indo-Gangetic plains and at the foothills of the Himalayas. Atmos. Environ. 89, 548–555.

Ram, K., Sarin, M.M., Tripathi, S.N., 2010. 1 year record of carbonaceous aerosols from an urban location (Kanpur) in the Indo-Gangetic Plain: characterization, sources and temporal variability. J. Geophys. Res. 115, D24313. http://dx.doi.org/10.1029/2010JD014188.

Ram, K., Sarin, M.M., Tripathi, S.N., 2012. Temporal trends in atmospheric $PM_{2.5}$, PM_{10}, elemental carbon, organic carbon, water-soluble organic carbon, and optical properties: impact of biomass burning emissions in the Indo-Gangetic Plain. Environ. Sci. Technol. 46, 686—695. http://dx.doi.org/10.1021/es202857w.

Reddy, M.S., Venkataraman, C., 2002. Inventory of aerosol and sulphur dioxide emissions from India: I-fossil fuel combustion. Atmos. Environ. 36 (4), 677–697.

Rengarajan, R., Sarin, M.M., Sudheer, A.K., 2007. Carbonaceous and inorganic species in atmospheric aerosols during wintertime over urban and high-altitude sites in North India. J. Geophys. Res. 112, D21307. http://dx.doi.org/10.1029/2006JD008150.

Rengarajan, R., Sudheer, A.K., Sarin, M.M., 2011. Aerosol acidity and secondary organic aerosol formation during wintertime over urban environment in western India. Atmos. Environ. 45 (11), 1940–1945.

Seinfeld, J.H., Pandis, S.N., 2006. Atmospheric Chemistry and Physics from Air Pollution to Climate Change. John Wiley Sons, Inc., New York.

Shapiro, J.B., Simpson, H.J., Griffin, K.L., Schuster, W.S.F., 2007. Precipitation chloride at West Point, NY: seasonal patterns and possible contributions from non-seawater sources. Atmos. Environ. 41, 2240–2254.

Sillapapiromsuk, S., Chantara, S., Tengjaroenkul, U., Prasitwattanaseree, S., Prapamontol, T., 2013. Determination of PM_{10} and its ion composition emitted from biomass burning in the chamber for estimation of open burning emissions. Chemosphere 93, 1912–1919.

Snyder, D.C., Rutter, A.P., Collins, R., Worley, C., Schauer, J.J., 2009. Insights into the origin of water soluble organic carbon in atmospheric fine particulate matter. Aerosol Sci. Technol. 43, 1099–1107.

SPECIATE, 1999. Software Version 3.1, User Guide and Program; U.S. Environmental Protection Agency, Durham, NC.

Srivastava, A.K., Singh, S., Tiwari, S., Bisht, D.S., 2012. Contribution of anthropogenic aerosols in direct radiative forcing and atmospheric heating rate over Delhi in the Indo-Gangetic Basin. Environ. Sci. Pollut. Res. 19, 1144–1158.

Stohl, A., Seibert, P., 1998. Accuracy of trajectories as determined from the conservation of meteorological tracers. Q. J. R. Meteorol. Soc. 124, 1465–1484.

Stohl, A., Wotawa, G., Seibert, P., Kromp-Kolb, H., 1995. Interpolation errors in wind fields as a function of spatial and temporal resolution and their impact on different types of kinematic trajectories. J. Appl. Meteorol. 34, 2149–2165.

Streets, D.G., Yarber, K.F., Woo, J.-H., Charmichael, G.R., 2003. Biomass burning in Asia: annual and seasonal estimates and atmospheric emissions. Glob. Biogeochem. Cycles 17, 1099. http://dx.doi.org/10.1029/2003GB002040.

Takiguchi, Y., Takami, A., Sadanaga, Y., Lun, X., Shimizu, A., Matsui, I., Sugimoto, N., Wang, W., Bandow, H., Hatakeyama, S., 2008. Transport and transformation of total reactive nitrogen over the East China Sea. J. Geophys. Res. 113, D10306. http://dx.doi.org/10.1029/2007JD009462.

Tegen, I., Fung, I., 1994. Modeling of mineral dust in the atmosphere: sources, transport, and optical thickness. J. Geophys. Res. 99 (D11), 22,897–22,914. http://dx.doi.org/10.1029/94JD01928.

Tiwari, S., Srivastava, A.K., Bisht, D.S., Behura, S., Chate, D.M., Bano, T., Singh, S., Srivastava, M.K., Padmanabhamurty, B., 2009. Black carbon and chemical characteristics of PM_{10} and $PM_{2.5}$ at an urban site of North India. J. Atmos. Chem. 62 (3), 193–209. http://dx.doi.org/10.1007/s10874-010-9148.

Turpin, B.J., Huntzicker, J.J., 1995. Identification of secondary organic aerosol episodes and quantitation of primary and secondary organic aerosol concentrations during SCAQS. Atmos. Environ. 29, 3527–3544.

Turpin, B.J., Lim, H.-J., 2001. Species contributions to $PM_{2.5}$ mass concentrations: revisiting common assumptions for estimating organic mass. Aerosol Sci. Technol. 35, 602–610.

Turpin, B.J., Huntzicker, James J., J. J., Hering S. V., 1994. Investigation of organic aerosol sampling artifacts in the Los Angeles basin. Atmos. Environ. 28, 3061–3071.

Vecchi, R., Valli, G., Fermo, P., D'Alessandro, A., Piazzalunga, A., Bernardoni, V., 2009. Organic and inorganic sampling artefacts assessment. Atmos. Environ. 43, 1713–1720.

Vestenius, M., Leppänen, S., Anttila, P., Kyllönen, K., Hatakka, J., Hellen, H., Hyvärinen, A., Hakola, H., 2011. Background concentrations and source apportionment of polycyclic aromatic hydrocarbons in South-Eastern Finland. Atmos. Environ. 45, 3391–3399.

Watson, J.G., Chow, J.C., 2000. Reconciling Urban Fugitive Dust Emissions Inventory and Ambient Source Contribution Estimates: Summary of Current Knowledge and Needed Research DRI Document No. 6110.4F.

Yeatts, K., Svendsen, E., Creason, J., Alexis, N., Herbst, M., Scott, J., Kupper, L., Williams, R., Neas, L., Cascio, W., Devlin, R.B., Peden, D.B., 2007. Coarse particulate matter ($PM_{2.5-10}$) affects heart rate variability, blood lipids, and circulating eosinophils in adults with asthma. Environ. Health Perspect. 115, 5.

Atmospheric Environment 89 (2014) 548–555

Contents lists available at ScienceDirect

Atmospheric Environment

journal homepage: www.elsevier.com/locate/atmosenv

The effect of boundary layer dynamics on aerosol properties at the Indo-Gangetic plains and at the foothills of the Himalayas

T. Raatikainen [a,*], A.-P. Hyvärinen [a], J. Hatakka [a], T.S. Panwar [b,1], R.K. Hooda [a,b], V.P. Sharma [b], H. Lihavainen [a]

[a] Finnish Meteorological Institute, Erik Palménin aukio 1, P.O. Box 503, 00101 Helsinki, Finland
[b] The Energy and Resources Institute (TERI), Darbari Seth Block, IHC Complex, Lodhi Road, New Delhi 110 003, India

HIGHLIGHTS

- We compare aerosol properties from Himalayan foothills and Indo-Gangetic plains.
- The data set contains more than two years of simultaneous measurements.
- Aerosols are transported from the plains to the Himalayan foothills.
- Boundary layer dynamics can explain the observed aerosol concentrations.

ARTICLE INFO

Article history:
Received 8 October 2013
Received in revised form
19 February 2014
Accepted 25 February 2014
Available online 26 February 2014

Keywords:
Aerosol
India
Himalayas
Brown cloud

ABSTRACT

Previous studies have noted that aerosols originating from the polluted Indo-Gangetic plains can reach high altitudes at the Indian Himalayas and thereby have an effect on the south Asian monsoon. Here we examine the transport of pollutions by comparing aerosol properties from a Himalayan foothill measurement site and a site at the Indo-Gangetic plains. Gual Pahari is a polluted semi-urban background measurement site at the Indo-Gangetic plains close to New Delhi and Mukteshwar is a relatively clean background measurement site at the foothills of the Himalayas about 270 km NE from Gual Pahari and about 2 km above the nearby plains. The data set has more than two years of simultaneous measurements including meteorological parameters and aerosol mass concentrations. Modeled backward trajectories and Planetary Boundary Layer (PBL) heights are also used to examine the origin or air masses and the extent of the vertical mixing. The comparison shows that aerosol concentrations at the foothill site are correlated with the average PBL height. Together with the favorable synoptic scale circulation, this suggests a contribution of air mass transport from the plains.

1. Introduction

During the dry winter and spring months, large area of the Indian subcontinent is covered by a few kilometer thick pollution layer commonly known as the south Asian brown cloud (Ramanathan et al., 2001, 2005, 2007; Gautam et al., 2009). The main components of the brown cloud are mineral dust from natural sources, and black carbon, sulfate and organic aerosol mainly from anthropogenic sources such as biomass burning, energy production, industry and transportation. Due to the dense population, regional dust sources (e.g. the Thar Desert), meteorological conditions, and the blocking effect of the Himalayas, the highest aerosol concentrations are typically seen at the Indo-Gangetic plains in the northern India (Singh et al., 2004; Sarkar et al., 2006; Bollasina et al., 2008; Gautam et al., 2009; Dey and Di Girolamo, 2010).

Aerosols have adverse health effects and also their direct effects on visibility and surface radiation can be easily observed. In addition, there are observational and modeling evidence of the effect of aerosols on the regional climate and especially on the monsoon cycle (e.g. Ramanathan et al., 2001, 2005; Menon et al., 2002; Chung et al., 2002; Lau et al., 2006; Satheesh et al., 2008; Bollasina et al., 2008, 2011; Gautam et al., 2009; Kuhlmann and Quaas, 2010; Ganguly et al., 2012; Turner and Annamalai, 2012). This is especially important as these densely populated areas in the south Asia are dependent on monsoon rains. On the other hand, floods due to

* Corresponding author.
E-mail address: tomi.raatikainen@fmi.fi (T. Raatikainen).
[1] Present address: WWF India, Lodhi Road, New Delhi 110 003, India.

http://dx.doi.org/10.1016/j.atmosenv.2014.02.058
1352-2310/

excessive monsoon rains can be devastating as was seen in the Indus River valley in Pakistan during the 2010 monsoon season and in northern India during the 2013 monsoon season. Predicting how the monsoon cycle changes with changing global climate and anthropogenic aerosol emissions is challenging due to several uncertainties such as the spatial and temporal distributions of aerosols and their direct and indirect effects on clouds and precipitation (e.g. Turner and Annamalai, 2012; Ganguly et al., 2012; Sajani et al., 2012).

Aerosol concentrations and composition have been measured in several intensive field campaigns such as INDOEX (Ramanathan et al., 2001), ICARB (Moorthy et al., 2008) and CAIPEEX-IGOC (Srivastava et al., 2014). There are also satellite measurements (e.g. Gautam et al., 2009; Dey and Di Girolamo, 2010; Kuhlmann and Quaas, 2010) and long-term data sets from ground stations (e.g. Hyvärinen et al., 2009; Ram et al., 2010; Marinoni et al., 2010). The latter includes two well-equipped aerosol measurement stations at Gual Pahari and Mukteshwar, which were established by the Finnish Meteorological Institute (FMI) in co-operation with the Energy and Resources Institute of India (TERI). The Gual Pahari station is close to New Delhi at the Indo-Gangetic plains (Hyvärinen et al., 2010) and the Mukteshwar station (Hyvärinen et al., 2009; Komppula et al., 2009) is in a less polluted environment at the foothills of the Himalayas about 270 km NE from Gual Pahari and about 2 km above the nearby plains.

In general, boundary layer has the highest aerosol concentrations, but boundary layer height depends on season and additional pollution layers, especially dust and black carbon, have been observed at altitudes up to 8 km (e.g. Satheesh et al., 2008; Gautam et al., 2009; Kuhlmann and Quaas, 2010; Gobbi et al., 2010; Brun et al., 2011; Babu et al., 2011; Komppula et al., 2012; Srivastava et al., 2011, 2012b, 2012a). High altitude pollution layers can be observed at Himalayan stations such as the Nepal Climate Observatory-Pyramid located at 5079 m altitude (Decesari et al., 2010; Marinoni et al., 2010; Sellegri et al., 2010; Gobbi et al., 2010). However, at lower altitudes at the foothills of the Himalayas where stations such as Mukteshwar (Hyvärinen et al., 2009) and Manora Peak (Dumka et al., 2008; Ram et al., 2010; Srivastava et al., 2011) are located, boundary layer dynamics and transport of pollutions from the nearby plains can be more important for aerosol concentrations (e.g. Pant et al., 2006; Dumka et al., 2008; Komppula et al., 2009; Hyvärinen et al., 2009, 2010; Ram et al., 2010; Brun et al., 2011; Gautam et al., 2011; Srivastava et al., 2012b).

The effect of boundary layer dynamics and especially the transport of aerosol pollutions from the Indo-Gangetic plains to the foothills of the Himalayas is the main topic of this study. When most previous studies are based on observations from a single station or the data does not cover a full year, we are comparing two simultaneous long term (from December 2007 to January 2010) data sets of aerosol concentrations and meteorological parameters from two stations representing the Indo-Gangetic plains and the foothills of the Himalayas.

2. Measurement sites and instrumentation

Aerosol concentrations and optical properties as well as basic meteorological parameters were measured at two stations in northern India. Fig. 1 shows locations of the Mukteshwar, Nainital (29.47° N, 79.65° E, 2180 m above sea level) and Gual Pahari, Gurgaon (28.43° N, 77.15° E, 243 m above sea level) stations. The distance between the stations is about 270 km, but the Mukteshwar station is located at the foothills of the Himalayas, an area representing Indian rural background, and Gual Pahari is at the densely populated Indo-Gangetic plains about 40 km south from New Delhi

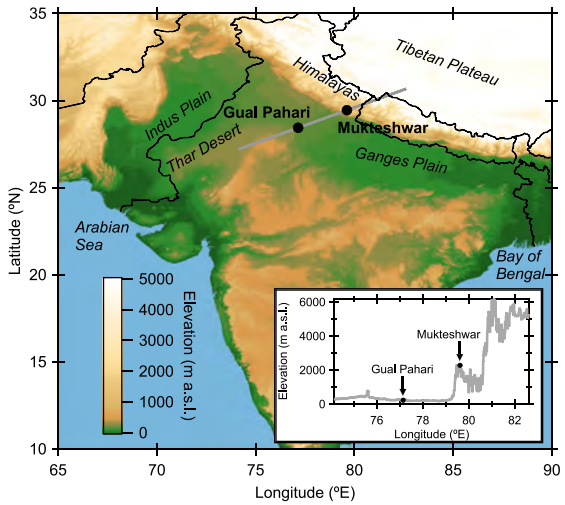

Fig. 1. Locations of the Gual Pahari and Mukteshwar stations in the northern India. The terrain elevation (meters above sea level, m a.s.l.) map is from the Global Land One-kilometer Base Elevation (GLOBE) Digital Elevation Model (GLOBE Task Team, 1999). Terrain elevation profile is also shown for the gray vector crossing the station coordinates.

in a semi-urban environment. As can be seen from the elevation profile shown in Fig. 1, Mukteshwar is closer to the plains than the high mountains of the Himalayas, which means that pollutions from the plains are likely to have an effect on aerosol concentrations. Mukteshwar and Gual Pahari measurements were started in September 2005 and December 2007, respectively, and Gual Pahari measurements ended in January 2010. We are therefore limited to the common time period from December 2007 to January 2010.

As described in our previous publications (Hyvärinen et al., 2009, 2010; Komppula et al., 2009), the stations had similar instrumentation including Particulate Mass (PM) monitors (Thermo Scientific, beta hybrid mass monitors) for measuring $PM_{2.5}$ and PM_{10} mass concentrations, nephelometers from Ecotech for aerosol scattering, Vaisala WXT weather stations, and Differential Mobility Particle Sizer (DMPS) systems for sub-micron particle number size distributions. Aerosol equivalent (refers to the optical absorption method) black carbon (EBC) concentration was measured from the $PM_{2.5}$ inlet by an aethalometer (Magee Scientific; 880 nm wavelength) in Mukteshwar. In Gual Pahari, however, that was measured from the PM_{10} inlet by a Multiangle Absorption Photometer (Thermo Scientific; 637 nm wavelength). The measured EBC concentration was corrected for a measurement artifact of the Multiangle Absorption Photometer (Hyvärinen et al., 2013). The rest of the data is limited to either one of the stations, so it will not be considered here.

The raw data was first examined visually and clear outliers were removed and then hourly averages were calculated while requiring 50% minimum data coverage. This hourly data was then used in all further calculations. The same 50% minimum data coverage was required for monthly and seasonal averages, but not for annual and diurnal cycles as these are averages of more than two years of data. All time values are in local time (UTC + 5.5 h) and concentrations are at the STP conditions (273.15 K and 1013.25 hPa), which were calculated using constant station temperatures (both thermostated to 298.15 K) and monthly averaged station pressures. The actual sample temperatures and pressures can deviate from the assumed

mean values, but the possible bias is insignificant compared with the observed variability of the aerosol parameters.

3. Results and discussion

Part of the data has been presented in our previous publications: Hyvärinen et al. (2009) presented the Mukteshwar measurements including meteorological parameters, trajectory analysis and aerosol properties from the first years of measurements, which do not include the current time period (from December 2007 to January 2010), and Hyvärinen et al. (2010) did the same for the Gual Pahari measurements. Panwar et al. (2013) focused on Mukteshwar EBC, $PM_{2.5}$ and PM_{10} concentrations measured until December 2008. Komppula et al. (2009) focused on Mukteshwar size distributions and Neitola et al. (2011) further examined those with the focus on new particle formation. Hyvärinen et al. (2011a, b) focused on the effect of monsoon on aerosol properties at Gual Pahari and Mukteshwar. Here we are examining the effect of boundary layer dynamics on Gual Pahari and Mukteshwar aerosol properties by comparing measured aerosol parameters, meteorological data, Planetary Boundary Layer (PBL) heights and backward trajectories from both sites.

Aerosol properties depend strongly on season which are here defined as winter, pre-monsoon, monsoon and post-monsoon. The winter season has fixed days extending from December to February, but each monsoon season has an onset and a withdrawal date. The exact days are approximated from the India Meteorological Department (IMD) monsoon onset and withdrawal maps. In the first year of our study period, monsoon onset was 16 June 2008 and withdrawal day was 28 September 2008 for both sites (Tyagi et al., 2009). In the next year onset dates were 29 June 2009 and 30 June 2009 for Mukteshwar and Gual Pahari, respectively, and the withdrawal day was again the same 28 September 2009 (Tyagi et al., 2010). For simplicity, however, the same day (29 June 2009) is selected as the onset date for the 2009 monsoon season. These monsoon onset and withdrawal dates define the end and start of the pre-monsoon and post-monsoon seasons, respectively.

3.1. Meteorological data

Meteorological data was presented by Hyvärinen et al. (2009) and Hyvärinen et al. (2010), so only the temperature and relative humidity (RH) are shown in Fig. 2. Temperatures had similar annual and diurnal cycles, but the absolute values were lower in Mukteshwar due to the higher altitude. Relative humidities (RH) were also similar during the wet monsoon season and the dry pre-monsoon season, but clear differences were seen especially during winter. When Gual Pahari RH could be explained by the diurnal temperature cycle, which is shown in Fig. 3, Mukteshwar RH was generally lower and more variable. Even if a diurnal RH cycle was observed, the diurnal temperature variations were too low to explain it and also the temperature minimum and RH maximum were not seen at the same time (Fig. 3). Similar diurnal RH cycles, which also correlated with aerosol concentrations, have been seen at other stations located at elevated altitudes close to the Indo-Gangetic plains (e.g. Gautam et al., 2011; Dumka et al., 2008), and the typical explanation was that the humid air masses observed in the daytime were originating from lower altitudes.

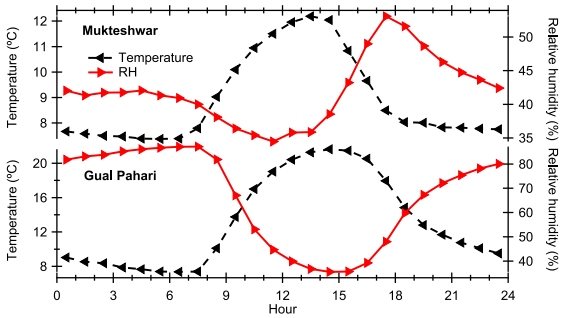

Fig. 3. Diurnal temperature (left scales) and relative humidity (right scales) cycles for Mukteshwar (top) and Gual Pahari (bottom) during winter (December–February).

Wind directions and speeds were also measured and these are shown in Hyvärinen et al. (2009, 2010). Hourly average wind speeds were generally below 2 m s^{-1} indicating weak horizontal transport. Although typical SE monsoon winds were observed at both measurement sites, mountain/valley wind patterns dominated the diurnal wind pattern at Mukteshwar. The observed mountain/valley wind pattern showed that easterly winds dominated during the days and the wind direction was reversed during nights, which is consistent with local topography instead of that related to the Himalayan mountains. Because both the wind direction pattern and wind speed depend on local topography, we have used trajectory analysis to examine the origin of air masses.

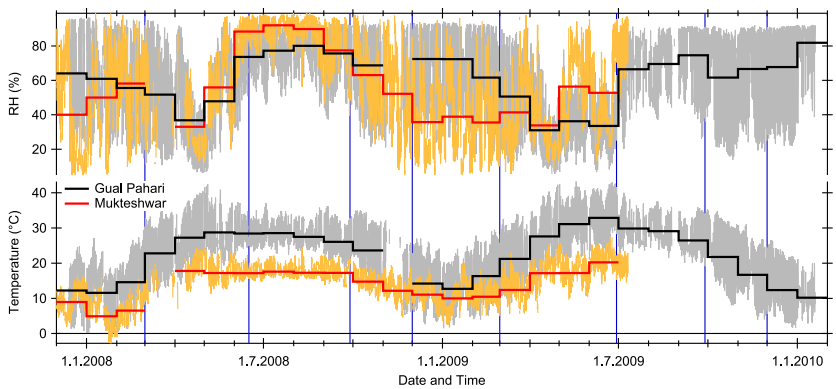

Fig. 2. Hourly (thin lines) and monthly (thick lines) averages of RH (%) and temperature (°C) for Gual Pahari and Mukteshwar. Seasons are indicated by the vertical lines.

3.2. Trajectories and boundary layer heights

Five days long backward trajectories were calculated for every 3 h with the FLEXTRA model (Stohl et al., 1995; Stohl and Seibert, 1998). The model was run in three dimensions with modeled vertical velocities. The European Centre for Medium-Range Weather Forecasts (ECMWF) data (operational archive, ensemble forecast at 00 and 12 h UTC, +3, +6, +9 h) had one degree grid resolution and 62 vertical levels for the northern hemisphere. The initiation, or the end point in the case of backward calculations, pressure levels were 950 hPa and 750 hPa for Gual Pahari and Mukteshwar, respectively; these were about 20–40 hPa lower than the surface air pressures at the stations. Calculated average altitudes above sea level (a.s.l.) and total trajectory lengths are shown in Fig. 4. Trajectory sector probabilities shown in Hyvärinen et al. (2009) and Komppula et al. (2009) were similar for both sites: during the monsoon season both sites had air masses mainly from the Bay of Bengal (SE) direction and westerly air masses dominated during the other seasons. Specifically, this means that Mukteshwar air masses were practically always crossing the Indo-Gangetic plains, which is here represented by the Gual Pahari station. Planetary Boundary Layer (PBL) heights above ground level (a.g.l.) are also shown in Fig. 4. The station PBL heights were calculated from the same unit degree resolution ECMWF data used in the trajectory calculations as 1/distance weighted averages of the PBL heights at the four closest grid points. It is known that modeled backward trajectories and PBL heights have uncertainties especially at the mountain environment. However, in the absence of direct PBL height measurements and knowing the uncertainties related to the surface winds, using modeled PBL heights and trajectories is justified at least to show the seasonal and diurnal trends.

Even if Gual Pahari and Mukteshwar trajectory directions were similar (Hyvärinen et al., 2009; Komppula et al., 2009), average trajectory altitudes and total lengths and PBL heights showed that air masses could have different origin. During the post-monsoon season and winter, Mukteshwar air masses were originating from altitudes well above the Gual Pahari maximum PBL height. The average trajectory altitude was also greater than the trajectory end point altitude shown by the green line in Fig. 4 (in the web version), which meant that air masses were descending while approaching the station. Finally, the longest trajectory lengths indicated that Mukteshwar air masses were originating from the free troposphere where wind speeds are commonly higher. These three observations showed that Mukteshwar air could be relatively clean while the limited mixing in Gual Pahari allowed the buildup of high aerosol concentrations during the post-monsoon season and winter. Mukteshwar received polluted air masses from the plains during the pre-monsoon season when the maximum PBL height increased and eventually exceeded the average trajectory altitude. The situation was similar during the monsoon season when air masses approaching Mukteshwar were actually ascending (average altitudes below the end point altitudes) from altitudes similar to the maximum PBL height. This indicated that Mukteshwar and Gual Pahari air masses had similar origin during the pre-monsoon and monsoon seasons.

Trajectory lengths and average altitudes did not have clear diurnal variations, because these are integrated or averaged over the total trajectory length of five days. PBL heights, on the other hand, had clear diurnal cycles which were related to the solar heating. These diurnal cycles will be shown with aerosol mass concentrations.

3.3. Aerosol properties

Aerosol measurements included PM_{10}, $PM_{2.5}$ and equivalent black carbon (EBC) mass concentrations, number size distributions (10–800 nm), and absorption and scattering coefficients. New particle formation had a clear effect on the concentration of the smallest particles (Neitola et al., 2011), but otherwise number concentrations correlated with mass concentrations. Similarly, scattering and absorption coefficients correlated with the total aerosol and EBC mass concentrations, respectively. Because of their similarity with the mass concentrations, we are not presenting size distribution, scattering or absorption data here.

Mass concentration time series are shown in Fig. 5. High pre-monsoon and low monsoon season aerosol concentrations were common for both sites, but significantly higher aerosol concentrations were seen at Gual Pahari during the post-monsoon season and winter. This is in good agreement with the trajectory and PBL height data shown in the previous section. Mukteshwar air masses were originating from higher altitudes during the post-monsoon season and winter while pollutions were accumulated to the

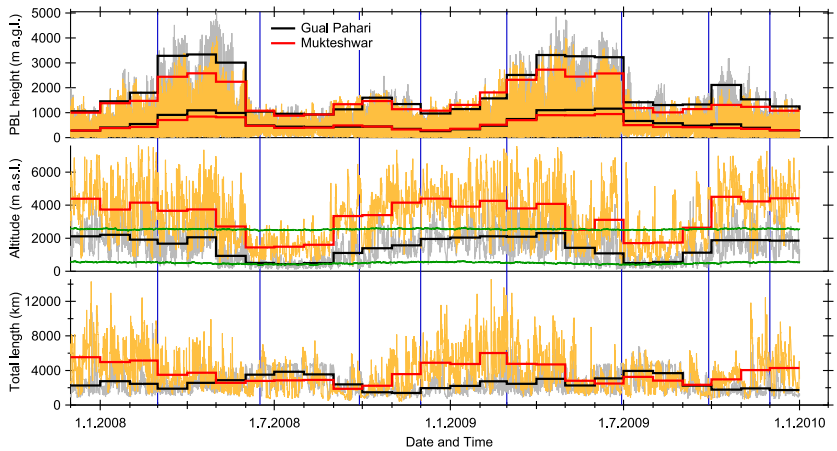

Fig. 4. Planetary Boundary Layer (PBL) heights above ground level (a.g.l.), average trajectory altitudes above sea level (a.s.l.) and total trajectory lengths. Monthly averages of the data are shown with the thick lines. Monthly averages of the daily maximum PBL heights are also shown for the PBL heights (the higher thick lines). The thin horizontal lines in the average altitude graph represent trajectory altitudes at the station coordinates. Seasons are indicated by the vertical lines.

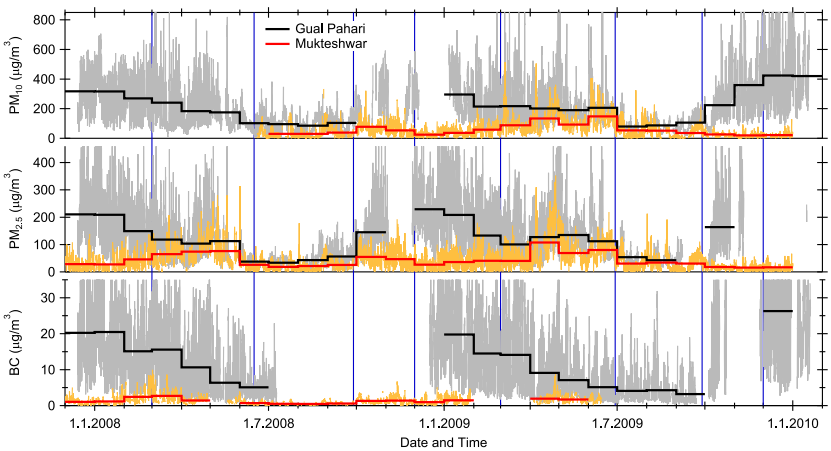

Fig. 5. Hourly (thin lines) and monthly (thick lines) average PM_{10} (μg m^{-3}), $PM_{2.5}$ (μg m^{-3}) and equivalent black carbon (EBC) concentrations (μg m^{-3}). The highest PM_{10} (up to 1985 μg m^{-3}), $PM_{2.5}$ (up to 1454 μg m^{-3}) and EBC (up to 78 μg m^{-3}) mass concentration peaks are not shown. Seasons are separated by vertical lines.

Indo-Gangetic plains. When mixing increased during the pre-monsoon season, polluted air masses from the plains reached the Mukteshwar station and aerosol concentrations became similar until the end of the monsoon season.

In general, EBC concentrations were relatively (e.g. EBC/PM_{10}) higher in Gual Pahari most likely due to local anthropogenic emissions from biomass burning, agriculture residue burning, cooking and road traffic (e.g. Beegum et al., 2009; Srivastava et al., 2012b). Annual cycles of EBC seemed to be different than those of PM_{10} and $PM_{2.5}$, but the EBC data coverage was too low to draw firm conclusions.

EBC is not included due to the lower data coverage, but diurnal cycles of PM_{10}, $PM_{2.5}$ and PBL heights are shown in Fig. 6. In general, diurnal cycles of the mass concentrations were similar to those of aerosol optical properties, number concentrations and EBC mass concentrations, which have been shown in our previous publications (Hyvärinen et al., 2009, 2010; Komppula et al., 2009; Panwar et al., 2013; Hooda et al., 2014). Morning and evening activities such as biomass burning and cooking (Hooda et al., 2014) cause the observed peaks in Gual Pahari, and the daytime minimum is seen due to the increased vertical mixing. In Mukteshwar, aerosol concentrations had the maximum in the afternoon most likely due to the transport of polluted air masses from the Indo-Gangetic plains. PM_{10} and $PM_{2.5}$ concentration cycles were otherwise similar except that $PM_{2.5}$ decreased and PM_{10} increased around noon in Mukteshwar during the winter and post-monsoon season. The increase in coarse particles matched with the maximum vertical mixing, so it could have been caused by dust originating from higher altitudes

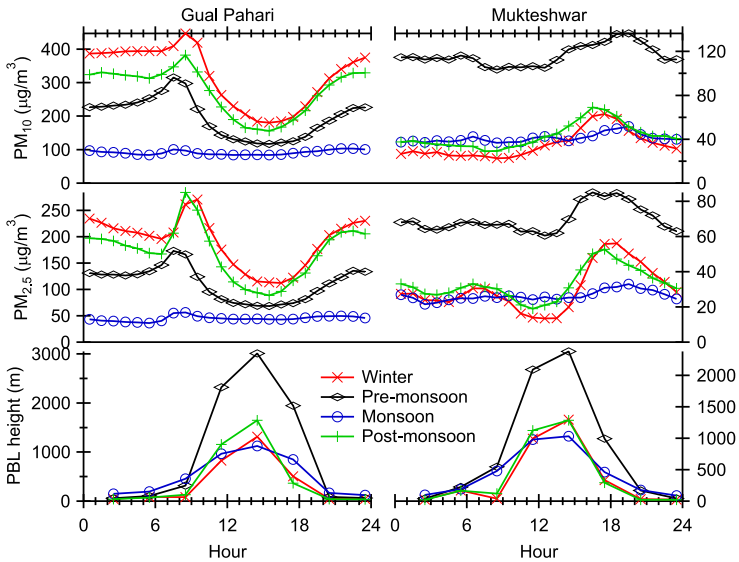

Fig. 6. Diurnal variations for PM_{10}, $PM_{2.5}$ and average PBL height in Gual Pahari (left) and Mukteshwar (right). Gual Pahari and Mukteshwar have different concentration and height scales.

where dust layers have been observed (e.g. Gautam et al., 2009; Kuhlmann and Quaas, 2010; Srivastava et al., 2011). It is also possible that the coarse particles were local wind-blown dust or dust from farming activity or road traffic (Marinoni et al., 2010).

3.4. Effect of boundary layer dynamics on aerosol concentrations

In addition to the horizontal winds, vertical transport of pollutions has been a common explanation for aerosol concentration cycles observed both at the foothills and at the slopes of the Himalayas (e.g. Pant et al., 2006; Dumka et al., 2008; Hyvärinen et al., 2009; Komppula et al., 2009; Beegum et al., 2009; Decesari et al., 2010; Marinoni et al., 2010; Gobbi et al., 2010; Sellegri et al., 2010; Gautam et al., 2011; Brun et al., 2011; Srivastava et al., 2011; Hegde and Kawamura, 2012). Also here the previous sections showed that both diurnal and annual aerosol concentration cycles at the Himalayan foothill site Mukteshwar can be explained by the boundary layer dynamics and the transport of pollutions from the plains to the foothills.

Starting from the annual cycles, Fig. 7 shows monthly averages of rainfall (district wise monthly rainfall data from the Hydromet Division of the India Meteorological Department (www.imd.gov.in; accessed June 2013) averaged over measurement sites as described in Hyvärinen et al. (2011a)), PM_{10} and $PM_{2.5}$ mass concentrations, and Mukteshwar trajectory altitude and Gual Pahari maximum daily PBL height (both in meters above sea level). Mukteshwar trajectory altitudes are higher than the maximum boundary layer heights at the plains during post-monsoon and winter seasons. Due to the limited vertical mixing and significant local and regional aerosol sources, the highest annual aerosol concentrations are seen at Gual Pahari, but Mukteshwar is above this pollution layer. When PBL height starts to increase after January, dilution decreases concentrations at Gual Pahari, but at the same time more and more pollutions reach the Mukteshwar station altitude until concentrations become similar after March. Monsoon rains have a clear effect on aerosol concentrations, which are decreased rapidly when the rains start, but the increase in Gual Pahari aerosol concentrations is even faster when the rainy season ends (Hyvärinen et al., 2011a, b). At that time, Mukteshwar is again above the pollution layer.

At first it looks like monthly aerosol mass concentrations in Mukteshwar depend directly on PBL height, but actually the higher PBL height means that Mukteshwar aerosol concentrations are approaching those at Gual Pahari. Fig. 8 shows how Mukteshwar to Gual Pahari $PM_{2.5}$ mass concentration and scattering coefficient ratios depend on the PBL height. Different averaging times ranging from one day to seasonal averages were examined, but the ratios were similar and only the noise increased with decreasing averaging time. Because PBL heights have rather crude spatial and temporal resolution, we have selected monthly averages. Different PBL heights including those for each station and between the stations were tried, but the average of Gual Pahari and Mukteshwar monthly PBL heights was selected as it had somewhat better correlation with the $PM_{2.5}$ mass ratio. Rains have a clear effect on aerosol concentrations, so months when either Gual Pahari or Mukteshwar monthly rainfall exceeds 50 mm were excluded from the linear fits; these rainy months are indicated by the open markers. The linear fits to the $PM_{2.5}$ and scattering data from the dry months (solid markers) show that the ratios depend strongly (Pearson's correlation coefficients, r, are 0.97 and 0.94 for $PM_{2.5}$ and scattering, respectively) on PBL height. The correlation is clear even if it does not account for the horizontal transport and the distance between the stations is 270 km. This indicates that Gual Pahari is a good representative of the Indo-Gangetic plains and vertical mixing is important in addition to surface winds (Hooda et al., 2014).

Fig. 8 includes also equivalent black carbon (EBC) ratio, which is only weakly dependent on the PBL height. It is possible that Gual Pahari EBC concentrations depend mainly on the local EBC emissions. In addition, the mixing of EBC is not as effective as that of the other aerosol types. When practically all EBC sources are at the ground level, secondary sulfate and organic aerosol formation happens at elevated altitudes where they are more efficiently spread over wider areas (Henriksson et al., 2011, 2013).

With the exception of the monsoon season when rains are affecting on aerosol concentrations, diurnal aerosol concentration cycles can be explained by the boundary layer dynamics. Fig. 6 showed that when PBL height increased during the day, dilution decreased Gual Pahari aerosol concentrations. At the same time, concentrations were first decreased in Mukteshwar due to dilution, but a clear increase was seen later in the afternoon when polluted air masses reached the station level. Such delay can be expected, because polluted air masses were most likely originating from the Indo-Gangetic plains, a few tens of kilometers SW from the Mukteshwar station. The same diurnal cycle was seen in Mukteshwar

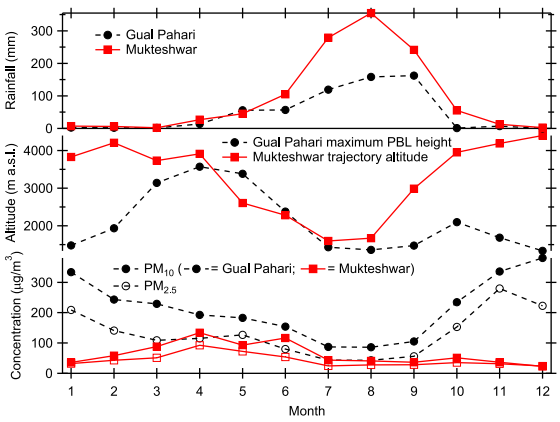

Fig. 7. Annual cycles for Mukteshwar (square markers and solid lines) and Gual Pahari (round markers and dashed lines) monthly rainfalls from IMD (see Hyvärinen et al. (2011a)), Gual Pahari maximum daily PBL height, Mukteshwar average trajectory altitude, and PM_{10} and $PM_{2.5}$ mass concentrations for both sites.

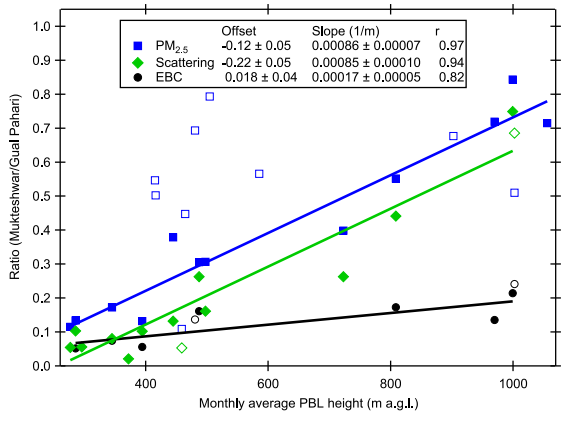

Fig. 8. The ratio of Mukteshwar to Gual Pahari monthly average $PM_{2.5}$, scattering coefficient and EBC concentration as a function of the average PBL height. Also shown are linear fits to the those data points where monthly rainfall in both stations is below 50 mm (solid markers). The open markers mean that the monthly rainfall exceeds 50 mm in either station.

relative humidity (Fig. 3), which increased in the afternoon when the humid air masses reached the station.

Boundary layer dynamics can explain the observed Mukteshwar and Gual Pahari aerosol concentrations and this explanation is also supported by the meteorological and trajectory data, but there are some limitations and uncertainties. For example, our study is limited to the foothill altitudes of about 2–3 km and locations close to the plains. Although similar diurnal and annual aerosol concentration cycles have been observed at the NCO-Pyramid station located at about 5 km altitude, transport of pollutions from the Indo-Gangetic plains may not be as important as the transport of pollutions with mountain and valley winds and the long-range (e.g. dust from the Thar or Taklamakan Deserts or from other parts of the Indian subcontinent) transport of pollutions (Decesari et al., 2010; Marinoni et al., 2010; Sellegri et al., 2010; Gobbi et al., 2010). Even if the basic aerosol properties can be explained well with the PBL height, details about aerosol properties including changes in the size distributions (e.g. EBC and fine particle mass fractions) are not that well understood. For example, a midday minimum was seen in Mukteshwar $PM_{2.5}$, but PM_{10} increased at the same time. It was hypothesized that these larger particles are dust possibly from higher altitudes, but further evidence such as measurements of particle chemical composition or vertical distributions are definitely needed.

4. Conclusions

Previous studies have noted that aerosols originating from the polluted Indo-Gangetic plains can reach the foothills and slopes of the Himalayas (e.g. Pant et al., 2006; Dumka et al., 2008; Hyvärinen et al., 2009; Marinoni et al., 2010; Ram et al., 2010; Brun et al., 2011; Gautam et al., 2011; Srivastava et al., 2012b) and thereby could have an effect on the south Asian monsoon. Here we have examined the transport of pollutions by comparing calculated backward trajectories and Planetary Boundary Layer (PBL) heights and measured meteorological and aerosol parameters from a Himalayan foothill site (Mukteshwar) and a site at the Indo-Gangetic plains (Gual Pahari). Unlike most of the previous studies, our high time resolution data covers more than two years of simultaneous measurements from the two stations; this means that we were able to examine seasonal variations and compare the measured and modeled parameters from the two stations. The comparison showed that aerosol concentrations at the foothill site are correlated with the spatially averaged PBL height. Together with the favorable synoptic scale circulation, this suggests a contribution of air mass transport from the plains. With the exception of the rainy season and winter, this short-range transport can be even more important than the local aerosol sources at the Himalayan foothills or the long-range transports from other parts of the Indian subcontinent. Planetary Boundary Layer (PBL) heights are lower during the cooler post-monsoon and winter months, so aerosol pollutions are accumulated to the plains, which are here represented by the Gual Pahari station. The Himalayan foothill (about 2 km above the nearby plains) site Mukteshwar, on the other hand, is mostly above the pollution layer. When mixing increases in the early spring, PBL height exceeds the average altitude of air masses arriving to Mukteshwar. As a result, concentrations are increased in Mukteshwar and decreased in Gual Pahari until they become similar. Monsoon rains decrease aerosol concentrations, but those are increased rapidly in Gual Pahari after the rainy season. The effects of boundary layer dynamics and air mass transport are also seen in the diurnal cycles. Namely, increased daytime mixing decreases aerosol concentrations in Gual Pahari and this is seen as an increase in Mukteshwar. Similar diurnal cycle was also seen in Mukteshwar relative humidity.

Acknowledgments

Measurements in the Gual Pahari station were funded by the European Integrated project on Aerosol Cloud Climate and Air Quality Interactions, EUCAARI. We are also grateful for The Ministry of Foreign Affairs of Finland for the funding of the Mukteshwar measurements. Timo Anttila and Ari Halm are acknowledged for technical assistance and Pekka Kolmonen is acknowledged for the Mukteshwar nephelometer truncation calculations. TERI's staff is acknowledged for their valuable routine maintenance of instruments in Gual Pahari and Mukteshwar stations.

References

Babu, S.S., Moorthy, K.K., Manchanda, R.K., Sinha, P.R., Satheesh, S.K., Vajja, D.P., Srinivasan, S., Kumar, V.H.A., 2011. Free tropospheric black carbon aerosol measurements using high altitude balloon: do BC layers build "their own homes" up in the atmosphere? Geophysical Research Letters 38, L08803.

Beegum, S.N., Moorthy, K.K., Babu, S.S., Satheesh, S., Vinoj, V., Badarinath, K., Safai, P., Devara, P., Singh, S., Vinod, Dumka, U., Pant, P., 2009. Spatial distribution of aerosol black carbon over India during pre-monsoon season. Atmospheric Environment 43, 1071–1078.

Bollasina, M., Nigam, S., Lau, K.M., 2008. Absorbing aerosols and summer monsoon evolution over South Asia: an observational portrayal. Journal of Climate 21, 3221–3239.

Bollasina, M.A., Ming, Y., Ramaswamy, V., 2011. Anthropogenic aerosols and the weakening of the south Asian summer monsoon. Science 334, 502–505.

Brun, J., Shrestha, P., Barros, A.P., 2011. Mapping aerosol intrusion in himalayan valleys using the moderate resolution imaging spectroradiometer (MODIS) and cloud–aerosol lidar and infrared pathfinder satellite observation (CALIPSO). Atmospheric Environment 45, 6382–6392.

Chung, C.E., Ramanathan, V., Kiehl, J.T., 2002. Effects of the South Asian absorbing haze on the northeast monsoon and surface–air heat exchange. Journal of Climate 15, 2462–2476.

Decesari, S., Facchini, M.C., Carbone, C., Giulianelli, L., Rinaldi, M., Finessi, E., Fuzzi, S., Marinoni, A., Cristofanelli, P., Duchi, R., Bonasoni, P., Vuillermoz, E., Cozic, J., Jaffrezo, J.L., Laj, P., 2010. Chemical composition of PM_{10} and PM_1 at the high-altitude Himalayan station Nepal climate observatory-pyramid (NCO-P) (5079 m a.s.l.). Atmospheric Chemistry and Physics 10, 4583–4596.

Dey, S., Di Girolamo, L., 2010. A climatology of aerosol optical and microphysical properties over the Indian subcontinent from 9 years (2000–2008) of multi-angle imaging spectroradiometer (MISR) data. Journal of Geophysical Research 115, D15204.

Dumka, U.C., Moorthy, K.K., Pant, P., Hegde, P., Sagar, R., Pandey, K., 2008. Physical and optical characteristics of atmospheric aerosols during ICARB at Manora Peak, Nainital: a sparsely inhabited, high-altitude location in the Himalayas. Journal of Earth System Science 117, 399–405.

Ganguly, D., Rasch, P.J., Wang, H., Yoon, J.H., 2012. Climate response of the South Asian monsoon system to anthropogenic aerosols. Journal of Geophysical Research: Atmospheres 117, D13209.

Gautam, R., Hsu, N.C., Lau, K.M., Kafatos, M., 2009. Aerosol and rainfall variability over the Indian monsoon region: distributions, trends and coupling. Annals of Geophysics 27, 3691–3703.

Gautam, R., Hsu, N.C., Tsay, S.C., Lau, K.M., Holben, B., Bell, S., Smirnov, A., Li, C., Hansell, R., Ji, Q., Payra, S., Aryal, D., Kayastha, R., Kim, K.M., 2011. Accumulation of aerosols over the Indo-Gangetic plains and southern slopes of the Himalayas: distribution, properties and radiative effects during the 2009 pre-monsoon season. Atmospheric Chemistry and Physics 11, 12841–12863.

GLOBE Task Team and others, 1999. In: Hastings, David A., Dunbar, Paula K., Elphingstone, Gerald M., Bootz, Mark, Murakami, Hiroshi, Maruyama, Hiroshi, Masaharu, Hiroshi, Holland, Peter, Payne, John, Bryant, Nevin A., Logan, Thomas L., Muller, J.-P., Schreier, Gunter, MacDonald, John S. (Eds.), The Global Land One-Kilometer Base Elevation (GLOBE) Digital Elevation Model, Version 1.0. National Oceanic and Atmospheric Administration, National Geophysical Data Center, 325 Broadway, Boulder, Colorado 80305–3328, U.S.A. Digital data base on the World Wide Web (URL: http://www.ngdc.noaa.gov/mgg/topo/globe.html) and CD-ROMs.

Gobbi, G.P., Angelini, F., Bonasoni, P., Verza, G.P., Marinoni, A., Barnaba, F., 2010. Sunphotometry of the 20062007 aerosol optical/radiative properties at the Himalayan Nepal climate observatory-Pyramid (5079 m a.s.l.). Atmospheric Chemistry and Physics 10, 11209–11221.

Hegde, P., Kawamura, K., 2012. Seasonal variations of water-soluble organic carbon, dicarboxylic acids, ketocarboxylic acids, and α-dicarbonyls in Central Himalayan aerosols. Atmospheric Chemistry and Physics 12, 6645–6665.

Henriksson, S.V., Pietikäinen, J.P., Hyvärinen, A.P., Räisänen, P., Kupiainen, K., Tonttila, J., Hooda, R., Lihavainen, H., Backman, L., Klimont, Z., Laaksonen, A., 2013. Spatial distributions and seasonal cycles of aerosol climate effects in India seen in global climate-aerosol model. Atmospheric Chemistry and Physics 13, 18031–18067.

Henriksson, S.V., Laaksonen, A., Kerminen, V.M., Räisänen, P., Järvinen, H., Sundström, A.M., de Leeuw, G., 2011. Spatial distributions and seasonal cycles of aerosols in India and China seen in global climate-aerosol model. Atmospheric Chemistry and Physics 11, 7975–7990.
Hooda, R.K., Hyvärinen, A.-P., Vestenius, M., Gilardoni, S., Sharma, V.P., Vignati, E., Paatero, P., Kulmala, M., Lihavainen, H., 2014. Atmospheric Aerosol Behaviour at Background of Delhi in Indo-Gangetic Plain (Under Review in Atmospheric Environment).
Hyvärinen, A.P., Lihavainen, H., Komppula, M., Panwar, T.S., Sharma, V.P., Hooda, R.K., Viisanen, Y., 2010. Aerosol measurements at the Gual Pahari EUCAARI station: preliminary results from in-situ measurements. Atmospheric Chemistry and Physics 10, 7241–7252.
Hyvärinen, A.P., Lihavainen, H., Komppula, M., Sharma, V.P., Kerminen, V.M., Panwar, T.S., Viisanen, Y., 2009. Continuous measurements of optical properties of atmospheric aerosols in Mukteshwar, northern India. Journal of Geophysical Research 114, D08207.
Hyvärinen, A.P., Raatikainen, T., Brus, D., Komppula, M., Panwar, T.S., Hooda, R.K., Sharma, V.P., Lihavainen, H., 2011a. Effect of the summer monsoon on aerosols at two measurement stations in Northern India – part 1: PM and BC concentrations. Atmospheric Chemistry and Physics 11, 8271–8282.
Hyvärinen, A.P., Raatikainen, T., Komppula, M., Mielonen, T., Sundström, A.M., Brus, D., Panwar, T.S., Hooda, R.K., Sharma, V.P., de Leeuw, G., Lihavainen, H., 2011b. Effect of the summer monsoon on aerosols at two measurement stations in Northern India – part 2: physical and optical properties. Atmospheric Chemistry and Physics 11, 8283–8294.
Hyvärinen, A.P., Vakkari, V., Laakso, L., Hooda, R.K., Sharma, V.P., Panwar, T.S., Beukes, J.P., van Zyl, P.G., Garland, R.M., Andreae, M.O., Pöschl, U., Petzold, A., 2013. Correction for a measurement artifact of the multi-angle absorption photometer (MAAP) at high black carbon mass concentration levels. Atmospheric Measurement Techniques 6, 81–90.
Komppula, M., Lihavainen, H., Hyvärinen, A.P., Kerminen, V.M., Panwar, T.S., Sharma, V.P., Viisanen, Y., 2009. Physical properties of aerosol particles at a Himalayan background site in India. Journal of Geophysical Research 114, D12202.
Komppula, M., Mielonen, T., Arola, A., Korhonen, K., Lihavainen, H., Hyvärinen, A.P., Baars, H., Engelmann, R., Althausen, D., Ansmann, A., Müller, D., Panwar, T.S., Hooda, R.K., Sharma, V.P., Kerminen, V.M., Lehtinen, K.E.J., Viisanen, Y., 2012. Technical note: one year of Raman-lidar measurements in Gual Pahari EUCAARI site close to New Delhi in India – seasonal characteristics of the aerosol vertical structure. Atmospheric Chemistry and Physics 12, 4513–4524.
Kuhlmann, J., Quaas, J., 2010. How can aerosols affect the Asian summer monsoon? Assessment during three consecutive pre-monsoon seasons from CALIPSO satellite data. Atmospheric Chemistry and Physics 10, 4673–4688.
Lau, K.M., Kim, M.K., Kim, K.M., 2006. Asian summer monsoon anomalies induced by aerosol direct forcing: the role of the Tibetan Plateau. Climate Dynamics 26, 855–864.
Marinoni, A., Cristofanelli, P., Laj, P., Duchi, R., Calzolari, F., Decesari, S., Sellegri, K., Vuillermoz, E., Verza, G.P., Villani, P., Bonasoni, P., 2010. Aerosol mass and black carbon concentrations, a two year record at NCO-P (5079 m, Southern Himalayas). Atmospheric Chemistry and Physics 10, 8551–8562.
Menon, S., Hansen, J., Nazarenko, L., Luo, Y., 2002. Climate effects of black carbon aerosols in China and India. Science 297, 2250–2253.
Moorthy, K.K., Satheesh, S.K., Babu, S.S., Dutt, C.B.S., 2008. Integrated campaign for aerosols, gases and radiation budget (ICARB): an overview. Journal of Earth System Science 117, 243–262.
Neitola, K., Asmi, E., Komppula, M., Hyvärinen, A.P., Raatikainen, T., Panwar, T.S., Sharma, V.P., Lihavainen, H., 2011. New particle formation infrequently observed in Himalayan foothills – why? Atmospheric Chemistry and Physics 11, 8447–8458.
Pant, P., Hegde, P., Dumka, U.C., Sagar, R., Satheesh, S.K., Moorthy, K.K., Saha, A., Srivastava, M.K., 2006. Aerosol characteristics at a high-altitude location in central Himalayas: optical properties and radiative forcing. Journal of Geophysical Research 111, D17206.
Panwar, T., Hooda, R.K., Lihavainen, H., Hyvärinen, A., Sharma, V., Viisanen, Y., 2013. Atmospheric aerosols at a regional background Himalayan site–Mukteshwar, India. Environmental Monitoring and Assessment 185, 4753–4764.
Ram, K., Sarin, M.M., Hegde, P., 2010. Long-term record of aerosol optical properties and chemical composition from a high-altitude site (Manora Peak) in central Himalaya. Atmospheric Chemistry and Physics 10, 11791–11803.
Ramanathan, V., Chung, C., Kim, D., Bettge, T., Buja, L., Kiehl, J.T., Washington, W.M., Fu, Q., Sikka, D.R., Wild, M., 2005. Atmospheric brown clouds: impacts on south Asian climate and hydrological cycle. Proceedings of the National Academy of Sciences 102, 5326–5333.
Ramanathan, V., Crutzen, P.J., Lelieveld, J., Mitra, A.P., Althausen, D., Anderson, J., Andreae, M.O., Cantrell, W., Cass, G.R., Chung, C.E., Clarke, A.D., Coakley, J.A., Collins, W.D., Conant, W.C., Dulac, F., Heintzenberg, J., Heymsfield, A.J., Holben, B., Howell, S., Hudson, J., Jayaraman, A., Kiehl, J.T., Krishnamurti, T.N., Lubin, D., McFarquhar, G., Novakov, T., Podgorny, I.A., O, J.A., Prather, K., Priestley, K., Prospero, J.M., Quinn, P.K., Rajeev, K., Rasch, P., Rupert, S., Sadourny, R., Satheesh, S.K., Shaw, G.E., Sheridan, P., Valero, F.P.J., 2001. Indian ocean experiment: an integrated analysis of the climate forcing and effects of the great Indo-Asian haze. Journal of Geophysical Research 106, 28371–28398.
Ramanathan, V., Li, F., Ramana, M.V., Praveen, P.S., Kim, D., Corrigan, C.E., Nguyen, H., Stone, E.A., Schauer, J.J., Carmichael, G.R., Adhikary, B., Yoon, S.C., 2007. Atmospheric brown clouds: hemispherical and regional variations in long-range transport, absorption, and radiative forcing. Journal of Geophysical Research 112, D22S21.
Sajani, S., Krishna Moorthy, K., Rajendran, K., Nanjundiah, R., 2012. Monsoon sensitivity to aerosol direct radiative forcing in the community atmosphere model. Journal of Earth System Science 121, 867–889.
Sarkar, S., Chokngamwong, R., Cervone, G., Singh, R., Kafatos, M., 2006. Variability of aerosol optical depth and aerosol forcing over India. Advances in Space Research 37, 2153–2159.
Satheesh, S.K., Moorthy, K.K., Babu, S.S., Vinoj, V., Dutt, C.B.S., 2008. Climate implications of large warming by elevated aerosol over India. Geophysical Research Letters 35, L19809.
Sellegri, K., Laj, P., Venzac, H., Boulon, J., Picard, D., Villani, P., Bonasoni, P., Marinoni, A., Cristofanelli, P., Vuillermoz, E., 2010. Seasonal variations of aerosol size distributions based on long-term measurements at the high altitude Himalayan site of Nepal climate observatory-pyramid (5079 m), Nepal. Atmospheric Chemistry and Physics 10, 10679–10690.
Singh, R.P., Dey, S., Tripathi, S.N., Tare, V., Holben, B., 2004. Variability of aerosol parameters over Kanpur, northern India. Journal of Geophysical Research 109, D23206.
Srivastava, A.K., Pant, P., Hegde, P., Singh, S., Dumka, U.C., Naja, M., Singh, N., Bhavanikumar, Y., 2011. The influence of a south Asian dust storm on aerosol radiative forcing at a high-altitude station in central Himalayas. International Journal of Remote Sensing 32, 7827–7845.
Srivastava, A., Singh, S., Tiwari, S., Kanawade, V., Bisht, D., 2012a. Variation between near-surface and columnar aerosol characteristics during the winter and summer at Delhi in the Indo-Gangetic Basin. Journal of Atmospheric and Solar-Terrestrial Physics 77, 57–66.
Srivastava, A.K., Singh, S., Pant, P., Dumka, U.C., 2012b. Characteristics of black carbon over Delhi and Manora peak – a comparative study. Atmospheric Science Letters 13, 223–230.
Srivastava, A.K., Bisht, D.S., Tiwari, S., 2014. Boundary layer aerosol characteristics at Mahabubnagar during CAIPEEX-IGOC: modeling the optical and radiative properties. Science of the Total Environment 468–469, 1093–1102.
Stohl, A., Seibert, P., 1998. Accuracy of trajectories as determined from the conservation of meteorological tracers. Quarterly Journal of the Royal Meteorological Society 124, 1465–1484.
Stohl, A., Wotawa, G., Seibert, P., Kromp-Kolb, H., 1995. Interpolation errors in wind fields as a function of spatial and temporal resolution and their impact on different types of kinematic trajectories. Journal of Climate and Applied Meteorology 34, 2149–2165.
Turner, A.G., Annamalai, H., 2012. Climate change and the South Asian summer monsoon. Nature Climate Change 2, 587–595.
Tyagi, A., Hatwar, H.R., Pai, D.S. (Eds.), 2009. Monsoon 2008, A Report. Government of India, India Meteorological Department.
Tyagi, A., Hatwar, H.R., Pai, D.S. (Eds.), 2010. Monsoon 2009, A Report. Government of India, India Meteorological Department.

Paper 4 (P4)

Journal of Geophysical Research: Atmospheres

RESEARCH ARTICLE
10.1029/2018JD029744

Driving Factors of Aerosol Properties Over the Foothills of Central Himalayas Based on 8.5 Years Continuous Measurements

R. K. Hooda[1,2], N. Kivekäs[1], E. J. O'Connor[1,3], M. Collaud Coen[4], J.-P. Pietikäinen[1], V. Vakkari[1], J. Backman[1], S. V. Henriksson[1], E. Asmi[1], M. Komppula[5], H. Korhonen[1], A.-P. Hyvärinen[1], and H. Lihavainen[1,6]

[1]Finnish Meteorological Institute, Helsinki, Finland, [2]The Energy and Resources Institute, New Delhi, India, [3]University of Reading, Reading, UK, [4]Federal Office of Meteorology and Climatology, Payerne, Switzerland, [5]Finnish Meteorological Institute, Kuopio, Finland, [6]Now at SIOS-KC, Longyearbyen, Norway

Abstract This study presents analysis of in situ measurements conducted over the period 2005–2014 in the Indian Himalayas to give a thorough overview of the factors and causes that drive aerosol properties. Aerosol extensive properties (namely, particle number concentration, scattering coefficient, equivalent black carbon, $PM_{2.5}$, and PM_{10}) have 1.5–2 times higher values in the early to late afternoon than during the night, and a strong seasonality. The interannual variability is ±20% for both $PM_{2.5}$ and total particle number concentration. Analysis of the data shows statistically significant decreasing trends of -2.3 μg m^{-3} $year^{-1}$ and -2.7 μg m^{-3} $year^{-1}$ for $PM_{2.5}$ and PM_{10}, respectively, over the study period. The mountainous terrain site (Mukteshwar, MUK) is primarily under the influence of air from the plains. This is due to convective transport processes that are enhanced by local and mesoscale topography, leading to pronounced valley/mountain winds and consequently to atmospheric boundary layer air lifting from the plains below. The transport from plains is evident in seasonal-diurnal patterns observed at MUK. The timing of the patterns corresponds with changes in turbulence and water vapor (*q*). According to our analysis, using these as proxies is a viable method for examining boundary layer influence in the absence of direct atmospheric boundary layer height measurements. Comparing the measurements with climate models shows that even regional climate models have problems capturing the orographic influence accurately at MUK, highlighting the importance of long-term direct measurements at multiple points to understand aerosol behavior in mountainous areas.

Key Points:
- Long-term aerosol observations were conducted in the central Himalaya, and turbulence and water vapor were used to describe mixing layer diurnal cycle
- Aerosol variables clearly present clusters of highest concentration during the afternoon hours in the premonsoon and postmonsoon season
- Transport and valley wind influence to the atmospheric boundary layer are the predominant reasons for the poor performance of climate models

Supporting Information:
- Supporting Information S1

Correspondence to:
R. K. Hooda,
rakesh.hooda@fmi.fi

Citation:
Hooda, R. K., Kivekäs, N., O'Connor, E. J., Collaud Coen, M., Pietikäinen, J.-P., Vakkari, V., et al. (2018). Driving factors of aerosol properties over the foothills of central Himalayas based on 8.5 years continuous measurements. *Journal of Geophysical Research: Atmospheres*, *123*, 13,421–13,442. https://doi.org/10.1029/2018JD029744

Received 3 OCT 2018
Accepted 9 NOV 2018
Accepted article online 14 NOV 2018
Published online 4 DEC 2018

Author Contributions:
Conceptualization: R. K. Hooda
Data curation: R. K. Hooda
Formal analysis: R. K. Hooda, N. Kivekäs, M. Collaud Coen, V. Vakkari
Funding acquisition: R. K. Hooda, A.-P. Hyvärinen, H. Lihavainen
Investigation: R. K. Hooda
Methodology: R. K. Hooda, E. J. O'Connor, M. Collaud Coen, A.-P. Hyvärinen, H. Lihavainen
Resources: R. K. Hooda, E. J. O'Connor
Supervision: R. K. Hooda, N. Kivekäs, A.-P. Hyvärinen
Validation: R. K. Hooda, M. Collaud Coen, J.-P. Pietikäinen, J. Backman, S. V. Henriksson
Visualization: R. K. Hooda, N. Kivekäs
(continued)

1. Introduction

Aerosols have been recognized as an important atmospheric constituent and an active climate forcing agent since the 1970s (Charlson et al., 1992; Twomey, 1977). Aerosols are highly nonuniform in the troposphere due to their relatively short residence times, variety of sources and sinks, and the chemical and microphysical processing that occurs in the atmosphere. Over the years, in spite of consistent improvements in instrumentation (both surface in situ and columnar measurements) and computational simulations, the single largest uncertainty continuous to be aerosols in the estimation of globally averaged total radiative forcing (Intergovernmental Panel on Climate Change, 2007, 2013). The uncertainty further increases over regional scale by a factor about 2–4 across the regions—for example, black carbon (BC) estimations (Bond et al., 2013).

Almost 50% of the Earth's land surface is covered by hilly and mountainous terrain (Meybeck et al., 2001), and 27% is defined as mountainous (altitude >1,500 m above sea level, asl; Messerli & Ives, 1997). Thus, surface in situ observatory stations on mountains and in remote areas are important in addition to measurements in lowlands. High-altitude stations provide information on background aerosol properties in a larger area, trends in aerosol concentrations and properties, and data for validating models. Moreover, these stations are important in studying climatologies of aerosol radiative properties and the influence of regional sources and processes. However, over mountainous terrain, the atmospheric structure becomes much more complicated and even a universal definition of convective boundary layer (CBL) height over mountains remains an ambiguous issue (De Wekker & Kossmann, 2015; Rotach et al., 2015; Serafin et al., 2018). Transport and mixing processes, such as those related to mountain waves (Smith et al., 2007) and thermally driven wind systems (Zardi & Whiteman, 2013) among others, affect CBL variability significantly.

Writing - original draft: R. K. Hooda, A.-P. Hyvärinen
Writing – review & editing: R. K. Hooda, N. Kivekäs, M. Collaud Coen, V. Vakkari, E. Asmi, M. Komppula, H. Korhonen, A.-P. Hyvärinen, H. Lihavainen

The role of aerosols over the south Asian region (Di Girolamo et al., 2004; Lelieveld et al., 2001) has been a topic of high interest for the past two decades, and it is increasingly recognized as being among the hotspots of aerosols and anthropogenic trace gases; the anthropogenic emissions are relatively high in this region and expected to further increase for the next few decades (Dubash et al., 2018; IIASA, 2015; Krotkov et al., 2016; Ohara et al., 2007; Rao et al., 2016). In India, several focused and thematic campaigns such as Indian Middle Atmosphere Programme (Moorthy et al., 1999), Indian Ocean Experiment (Ramanathan et al., 2001), Indian Space Research Organization's Geosphere Biosphere Program (ISRO, 2004), and Integrated Campaign for Aerosols, gases and Radiation Budget (Satheesh et al., 2008) were conducted in the past. These campaigns addressed the physicochemical properties of aerosols and their modulation by mesoscale and synoptic meteorological processes at different geographical regions (Moorthy et al., 2016). Another recent campaign, Ganges Valley Aerosol Experiment, was carried out at Nainital to measure radiative, cloud, convection, and aerosol characteristics over the mainland for a 10-month period in 2011–2012 (Dumka et al., 2015; Kotamarthi, 2010; Singh et al., 2016). In spite of these efforts, the campaigns were time specific, and only a sufficiently long time series of data would help in inferring climate change signals (Moorthy et al., 2016). It is noticeable also that India is absent from the global map of GAW stations (WMO/GAW, 2016).

Notably, systematic and long-term measurements of aerosol properties in the Gangetic-Himalayan region in India were also performed by the Indo-Finnish cooperation of the Finnish Meteorological Institute and The Energy and Resources Institute at their sites: in the Himalayas at Mukteshwar (MUK) since 2005 (Collaud Coen et al., 2018; Henriksson et al., 2014; Hyvärinen et al., 2009; Komppula et al., 2009; Neitola et al., 2011; Nieminen et al., 2018; Panwar et al., 2013; Raatikainen et al., 2014; Raatikainen et al., 2017) and in the Indo Gangetic Plains (IGP) at Gual Pahari (GP) since 2007 (Baars et al., 2016; Hyvärinen et al., 2010, Hyvärinen, Raatikainen, Brus, et al., 2011, Hyvärinen, Raatikainen, Komppula, et al., 2011, 2013; Hooda et al., 2016; Komppula et al., 2012). These studies infer seasonality of aerosol properties based on surface in situ and columnar measurements, new particle formation events, topography characteristics, and disintegration between local and regional sources. The details can be obtained from each article since a critical review is not attempted in the present work; however, what is investigated as part of the present study has been highlighted as follows.

In this study, 8.5 years of measured aerosol physical and optical properties at a Himalayan site are analyzed. Remote sensing aerosol networks in India—for example, Aerosol Radiative Forcing over India Network and AERONET (Aerosol Robotic Network—are aerosol measurement programs stared in early 2000, but to our knowledge, this data set at MUK represents the longest surface in situ aerosol observations from India which comprises physical and optical properties. We first provide an overview of the measurements, showing temporal variability of aerosol properties, which corroborate with the findings of distinct diurnal and seasonal cycles of our previous studies (refer above); however, those covered shorter time periods. We then focus on analyzing the possible factors and causes that drive aerosol diurnal, seasonal, and interannual variability and trends in aerosol properties at MUK. In particular, the long data set enables investigating the influence of valley/mountain winds and atmospheric boundary layer (ABL) dynamics on aerosol variability. For this purpose, a combination of micrometeorological observations of wind parameters, solar radiation, and water vapor is utilized. In addition, we used a global and a regional climate model to investigate how the changes in emission inventories over the study period relate to the observed long-term aerosol variability and to validate the climate model results against measurements at MUK.

2. Methods

2.1. Measurement Site

The measurement station, MUK (29°26´N, 79°37´E, 2,180 m asl) in India, is located in the foothills of the central Himalayas (Figure 1a). The site has a 180° view of the Himalayan ranges west, north, and east of the site; the nearest high peaks are approximately 90 km NE of the site. The area surrounding the site consists of low mountains (peaks 1,500–2,500 m asl) between the IGP (100–200 m asl) and the Himalayas (peaks 6,000–8,000 m asl; Figures 1b and S1 in the supporting information). The village of Mukteshwar, located 3 km NE of the measurement site and at a similar altitude, has ~800 inhabitants (Census of India, 2011). The nearest population centers are the town of Almora (1,650 m asl, 16 km N, population ~34,000) and Nainital (1,960 m asl, 25 km SW, population ~41,000) and the city of Haldwani (424 m asl, 32 km SW,

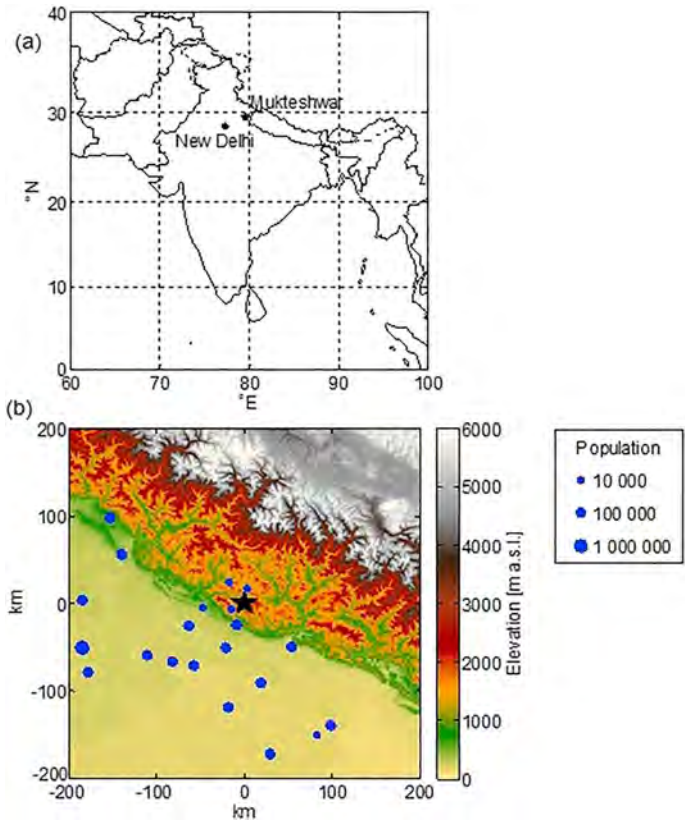

Figure 1. (a) Site location in India. (b) The location of Mukteshwar (denoted with star) and population centers (blue filled circles) on a 400 × 400 km topographic map (United States Geological Survey, 2016).

population ~150,000). The major metropolitan city Delhi (National Capital Territory), located in the IGP region (215 m asl, 250 km SW), has a population of ~16.8 million. Between Haldwani and Delhi, there are some industrial zones (Figure 1b), namely, the cities Kashipur and Rudrapur (70 km SW).

The IGP region is one of the most populated with over 900 million inhabitants. It is both highly fertile agricultural belt and a rapidly developing region of the Indian subcontinent. Furthermore, the geography of this region adds a considerable quantity of natural aerosols (windblown desert dust; Kumar, Kumar, et al., 2015, and reference therein) into the atmosphere from March to June, which coincides with anthropogenic ones, making the aerosol environment one of the most complex in the region (Moorthy et al., 2016). Crop residue burning over the IGP region is a common practice in clearing land during the harvesting period, resulting in highly seasonal agricultural particulate emissions (Kaskaoutis, Kumar, et al., 2014; Kumar et al., 2011; Rajput et al., 2014; Sahu et al., 2015; Singh & Kaskaoutis, 2014; Venkataraman et al., 2006). Considering the diverse fossil fuel use for domestic, industrial, and transport energy, and the open waste burning for disposal and heating purposes in this region (CPCB, 2010), especially over the IGP, the postmonsoon and winter seasons have also witnessed high pollution levels (Chakraborty et al., 2015; Hooda et al., 2016; Hyvärinen et al., 2010; Komppula et al., 2012). The elevated wintertime pollution levels as well as severe anthropogenic winter haze (Sati & Mohan, 2014) further coincide with the fog period (Ganguly et al., 2006; Gautam et al., 2007; Gautam & Singh, 2018), resulting in manifold increases in the complexity of aerosol composition over the region. These spatiotemporally diversified emissions are coupled with varying atmospheric dynamics, such as contrasting monsoons and varying ABL. All of this, together with the

complex topography, makes the Gangetic-Himalayan region's aerosol very difficult to fingerprint and model, and ultimately to implement effective mitigation strategies.

2.2. Aerosol Instrumentation and Data Processing

This study presents the aerosol time series from September 2005 to January 2014. The particle size distribution was measured using a differential mobility particle sizer (DMPS, Finnish Meteorological Institute assembled). A seven-wavelength (370 to 950 nm) Aethalometer (Magee Scientific AE-31) was used for measuring absorption coefficient (σ_{ap}) and equivalent black carbon (eBC) at λ = 880 nm, and an integrating nephelometer (Ecotech M 9003) measured the scattering coefficient (σ_{sp}) at λ = 525 nm. The particulate mass concentrations ($PM_{2.5}$ and PM_{10}) were measured with Thermo β attenuation mass monitors. The details of the instrumentation (supporting information Table S1) used in the present study, their maintenance and calibration protocols, and data logging are available in Hyvärinen et al. (2009) and Komppula et al. (2009). The ambient air sampling scheme and sample air conditioning (drying) adhered to the recommendations of World Meteorological Organization (WMO) (WMO/GAW, 2003, 2016) and have been detailed in our earlier publications (Hyvärinen et al., 2009; Komppula et al., 2009).

The DMPS data were divided into three characteristic particle size ranges of aerosol at MUK: 10- to 25-nm particles (nucleation-mode N_{nuc}) represent the most recently formed aerosol particles, 25- to 90-nm particles (Aitken-mode N_{ait}) represent fresher aerosol particles no more than a few days old, and 90- to 800-nm particles (accumulation-mode N_{acc}) are representative of aged aerosol particles (Komppula et al., 2009; Seinfeld & Pandis, 2006). In general, particle number size distributions observed at MUK (Komppula et al., 2009) were mostly unimodal (with the mode at approximately 100 nm). The sum of the particle number concentrations in the three particle size ranges is termed N_{tot}. The particle mass concentration was also calculated utilizing the submicron aerosol size spectra assuming spherical particles and a gravimetric density of 1.77 g/cm^3. The density value used is representative for remote/background aerosols and is close to the bulk densities of ammonium sulphate and nitrate, the main constituents of accumulation-mode particles (DeCarlo et al., 2004; Heintzenberg et al., 2011; Stock et al., 2011). The mass size ranges are termed as M_{nuc}, M_{ait}, and M_{acc} following the same diameter limits as in the number size distributions. The M_{acc} was calculated further for additional submicron particle mass concentration—for example, 90–200, 200–300, and 300–500 nm.

The truncation error inherent to the nephelometer was corrected using Mie scattering calculations following the guidelines of Anderson and Ogren (1998) and Moosmüller and Arnott (2003). The particle size range from 10 nm to the inlet cutoff diameter (i.e., 2.5 or 10 μm) was chosen for the correction using simultaneous (1.5 years) measured DMPS (mobility diameter) and Aerosol Particle Sizer, TSI 3321 (APS) (aerodynamic diameter) data. In May 2013, the common sample inlet was changed from $PM_{2.5}$ to PM_{10}. The selection of the overlapped size channels in DMPS and APS is following Asmi et al. (2016). The correction factors (based on deemed inlet cutoff diameter) were estimated for the hourly data and averaged for those days and months when measurement coverage was ≥50%—that is, 12 hr/day and 15 days/month, respectively. The correction factors were then applied to different periods over the entire study time, in accordance with the deemed inlet cutoff diameter installed for nephelometer measurements. The truncation error of the measured σ_{sp} varies between 11% and 12% across the seasons, and an error of up to 5%–15% is acceptable depending on the particle size (Anderson et al., 1996).

The aethalometer measurements are known to suffer from several artifacts (namely, multiple scattering enhancement on the filter tape corrected by using a C factor and loading effect referred to as the shadowing effect). The approach of Weingartner et al. (2003) for these artifact corrections was applied in the present analysis following Hyvärinen et al. (2009), utilizing a C factor of 2.14. However, Collaud Coen et al. (2010) and in year 2016, WMO/Global Atmosphere Watch (GAW) has evaluated new aethalometer correction schemes and concluded that the C factor used in most studies worldwide is too low and should be at least 2.9 (Collaud Coen et al., 2010) or 3.5 (WMO/GAW, 2016). The latter value is generally likely to be adopted, in principle, and has an uncertainty of approximately 25% (Müller, 2015; WMO/GAW, 2016). To keep our data set consistent with the previous analysis (Hyvärinen et al., 2009), we report our results with a C factor of 2.14 (Weingartner et al., 2003). However, the results with a C factor of 3.5 show repercussions on aerosol intensive properties (such as the single scattering albedo); thus, we have discussed these as well.

The single scattering albedo (SSA) using measured σ_{sp} (λ = 525 nm) and σ_{ap} (λ = 520 nm), and absorption Ångström exponent (α_{abs}) that describes the spectral dependence of light absorption by the aerosol (Müller et al., 2011) was calculated. The α_{abs} is the negative slope of the regression fit between the logarithm of the absorption coefficients and the logarithm of the wavelengths (seven wavelengths between 370 and 950 nm).

The annual coverage of valid and analyzable hourly averaged data (processed/screened) of different aerosol properties and meteorological parameters is presented in supporting information Table S1. During data processing, the meteorological and aerosol parameters were averaged to 1-hr resolution, taking into account only those hours when more than 50% of the time was covered by valid measurements.

To extract more information on the seasonally averaged diurnal cycles, the diurnal cycles of the aerosol parameters were separated from the monthly background values and are denoted as ${}_e\Delta$ and ${}_i\Delta$ for extensive and intensive, respectively. This was done by subtracting mean monthly minima of the diurnal values from each monthly diurnal cycle. This procedure forces the minimum value of the ${}_e\Delta$ to be zero for the diurnal cycles of each month. These minimum values were systematically observed early in the morning before sunrise. As the minimum values of aerosol intensive parameters were typically observed at different times of the day for different months and for different parameters, ${}_i\Delta$ was calculated by subtracting the mean monthly 5:00 a.m. value (representing the time before the onset of the increase in particle concentration) from each monthly cycle.

2.3. Meteorological Data and Mixing Layer

The measurements of meteorological parameters (i.e., temperature, pressure, relative humidity, wind speed, wind direction, and global solar irradiance) were done using MILOS500+ sensors (Vaisala). Daily precipitation data was collected from the India Meteorological Department weather station, less than 2 km NE of MUK. The seasonal classification adopted for MUK is winter (December to February), premonsoon (March to May), monsoon (July to August), postmonsoon (October to November), and the transition months between monsoon and other seasons (June and September). The solar zenith and azimuth angles were also calculated using the algorithm of Blanco-Muriel et al. (2001) for representation of sunrise and sunset time in aerosol variability cycles.

The specific humidity can be used as a passive tracer (Kowol-Santen et al., 2001; Serafin et al., 2018; Weigel et al., 2007) to examine the ABL dynamics. It was calculated using meteorological data as shown in equation (1), following Bolton, (1980), and used in the present study when direct measurements of mixing layer depth (height) at MUK are not available.

$$q = \frac{(0.622\times e)}{(p-(0.378\times e))}; e = 6.112\times \exp\left(\frac{(17.67\times \mathrm{Td})}{(\mathrm{Td}+243.5)}\right), \quad (1)$$

where q is the specific humidity in kg/kg, p is the surface pressure in hectopascals, e is the vapor pressure in hectopascals, Td = dew point in °C, and the final specific humidity units are in g/kg.

Together with q (referred to as water vapor in from here onwards), wind speed and direction and solar radiation were also used for investigating ABL dynamics at MUK. For part of the same period, water vapor was also measured at GP (28°26′N, 77°09′E, 243 m asl), located in the IGP region near Delhi at 270-km distance from MUK (Hooda et al., 2016). In wind parameters, we utilized wind direction variability (δ_{WD}) and relative wind speed variability (δ_{WSr}). The δ_{WD} was calculated as the average of the absolute differences in wind direction from 1 min to the next during the given hour. The δ_{WSr} was calculated similarly to δ_{WD}, but in the end, it was divided by the average wind speed that hour in order to retrieve a proxy that was independent of the mean wind speed. In the case of the water vapor (q), its variability was obtained by subtracting the monthly mean diurnal minima from the monthly mean diurnal cycle and denoted as ∂q. Further, to investigate the ABL air lifting from the plains below, we also examined ∂q at GP and utilized average diurnal cycle of water vapor at GP for each month for further analysis. The variability (denoted as ∂q) in water vapor at MUK and GP shows some unique differences (see Figures 5f and S2d, respectively). We assumed that ∂q at the GP site represents the typical water vapor values in the plains (IGP). Each hourly water vapor value at MUK was then subtracted from the corresponding hourly water vapor value at GP. This difference was noted as

ϕq. We assumed, as stated earlier, that early in the morning (5:00 a.m.), there is no mixing of air between the plains and MUK and noted the ϕq at 5:00 a.m. as ΔMPq, the undisturbed difference of q between MUK and the plains. The fraction of MUK air originating from the plains (Φq), a clear indicator, was then calculated according to equation (2):

$$\left[\Phi q = 1 - \frac{(q\mathrm{GP} - q\mathrm{MUK})}{(\Delta \mathrm{MP}q)}\right]; \tag{2}$$

2.4. Back Trajectories and Modeled Mixing Layer Depth

Lagrangian models are often used to investigate source-receptor relationships based on air mass movement from gridded meteorological data (Fleming et al., 2012). In order to investigate the origin of the air masses measured at MUK, 5-day back trajectories were calculated using the Hybrid Single-Particle Lagrangian Integrated Trajectory model version 4.9 (Draxler & Hess, 1998; Stein et al., 2015). The meteorological data used was the 1° National Center for Environmental Prediction (NCEP)/Global Data Assimilation System (GDAS) data set with 23 hybrid pressure levels (Kanamitsu, 1989). The 5-day back trajectories were calculated for every 3 hr (the temporal resolution of the GDAS data) over the years 2005–2014. The mixing layer depth was taken from the NCEP/GDAS and this is referred to as modeled mixing layer depth from here onwards.

2.5. Statistical Analysis

The statistical methods were used to analyze the trends of aerosol parameters at MUK and to verify the sensitivity of the trends results. Since the aerosol variables are approximately lognormally distributed, a nonparametric trend test and slope estimator, the seasonal Mann-Kendall (MK) test and the Sen's slope estimator (Collaud Coen et al., 2013), were applied to the daily data to detect potential long-term trends and their magnitudes for each month as well as for the whole data sets. The least mean squares (LMS) fit of the logarithm of the monthly median has been widely used for trends estimations (Collaud Coen et al., 2007; Collaud Coen et al., 2013), and this was also applied in the present analysis. With these statistical tools, a general picture of the aerosol long-term variability can be obtained. If a trend was detected by one of the methods, a generalized least squares (GLS) trend with either autoregressive or block bootstrap (ARB) confidence intervals (Asmi et al., 2013) was also applied to validate the trend and estimate its magnitude. The trend analysis was also performed with the same methods on the meteorological parameters as they were recorded, since these are usually normally distributed. The trend analysis performed on aerosol and meteorological parameters was for the period September 2005 to January 2014 (about 8.5 years), except for DMPS, aethalometer and nephelometer. In May 2013, the common sample inlet of these instruments was changed from $PM_{2.5}$ to PM_{10} leading to a break in the long-term data set of absorption and scattering coefficients. Thus, for these parameters, the trend analysis was applied to the period of September 2005 to May 2013 (about 7.8 years). The DMPS data could only be considered homogeneous from March 2006 to November 2012, and therefore, the trend analysis was applied to this shorter data set of about 6.8 years.

2.6. Global and Regional Model Simulations

The global aerosol-climate model ECHAM-HAMMOZ (version ECHAM6.1.0-HAM2.2.0-MOZ0.9.0) was used with interactive aerosols to simulate years 2004–2014 with T63 (~210 km/1.9° grid box) spatial resolution and 31 vertical levels (Zhang et al., 2012). ECHAM-HAMMOZ accounts for both direct and indirect aerosol effects. The model simulations were nudged (vorticity, divergence, temperature, and surface pressure) towards ERA-Interim data (Dee et al., 2011). For anthropogenic emissions, ECLIPSE (Evaluating the Climate and Air Quality Impacts of Short-Lived Pollutants (ECLIPSE)) emission data (IIASA, 2015) was used. Detailed treatment of the emissions in ECHAM-HAMMOZ, including the annual cycle imposed on the domestic sector emissions, can be found in Pietikäinen et al. (2015). The wildfire emissions were taken from Global Fire Emissions Database v4 (van der Werf et al., 2010) as monthly average fields. Other natural emissions were taken as shown in Stier et al. (2005) and Zhang et al. (2012). Natural as well as aircraft emissions were used, as in Matt et al. (2016).

The regional aerosol-climate model REMO-HAM (version REMO2009; Pietikäinen et al., 2012) with interactive aerosols was simulated for 2007–2011 including a spin-up time, using 0.22° (~25 km grid box) resolution with 27 vertical levels covering plains and the Himalayas in India. More details about the domain can be seen in Kumar, Kotlarski, et al. (2015). Currently, aerosols in REMO-HAM impact radiation only through clouds

Table 1
Seasonal/Annual Values (Mean ± SD) of Aerosol Extensive and Intensive Parameters at MUK

Aerosol property	Winter (DJF)	Premonsoon (MAM)	Monsoon (Jul–Aug)	Postmonsoon (ON)	Transition (Jun and Sep)	Annual
Extensive						
$PM_{2.5}$ ($\mu g/m^3$)	20 ± 10	40 ± 20	12 ± 10	22 ± 15	25 ± 15	25 ± 15
PM_{10} ($\mu g/m^3$)	25 ± 20	70 ± 40	20 ± 25	35 ± 25	40 ± 30	40 ± 30
eBC ($\mu g/m^3$)	0.85 ± 0.65	1.40 ± 0.85	0.35 ± 0.25	0.90 ± 0.60	0.70 ± 0.40	0.90 ± 0.60
$^{a}\sigma_{ap}$ (Mm^{-1}) 2.14	12 ± 9	20 ± 10	5 ± 3	12 ± 8	10 ± 6	12 ± 8
$^{a}\sigma_{ap}$ (Mm^{-1}) 3.5	7 ± 6	12 ± 7	3 ± 2	7 ± 5	6 ± 3	7 ± 5
σ_{sp} (Mm^{-1})	70 ± 60	110 ± 65	35 ± 30	75 ± 60	65 ± 40	75 ± 55
N_{tot} (cm^{-3})	2,700 ± 1,700	5,200 ± 2,850	1,650 ± 750	2,200 ± 1,100	2,600 ± 1,250	3,050 ± 1,650
N_{nuc} (cm^{-3})	90 ± 120	380 ± 600	40 ± 45	65 ± 85	80 ± 125	150 ± 200
N_{ait} (cm^{-3})	1,200 ± 820	2,290 ± 1520	840 ± 360	880 ± 550	1,240 ± 670	1,360 ± 850
N_{acc} (cm^{-3})	1,420 ± 950	2,550 ± 1450	770 ± 420	1,200 ± 600	1,320 ± 680	1,540 ± 880
Intensive						
α_{abs}	1.40 ± 0.5	1.25 ± 0.2	1.15 ± 0.3	1.20 ± 0.3	1.10 ± 0.3	1.25 ± 0.4
$^{b}SSA^{2.14}$	0.82 ± 0.06	0.84 ± 0.03	0.83 ± 0.07	0.83 ± 0.04	0.84 ± 0.06	0.83 ± 0.05
$^{b}SSA^{3.5}$	0.88 ± 0.05	0.90 ± 0.02	0.89 ± 0.06	0.89 ± 0.03	0.90 ± 0.05	0.89 ± 0.04
$PM_{2.5}/PM_{10}$	0.97 ± 0.63	0.68 ± 0.31	0.88 ± 0.73	0.94 ± 0.58	0.79 ± 0.55	0.85 ± 0.55
$eBC/PM_{2.5}$	0.06 ± 0.07	0.04 ± 0.03	0.07 ± 0.06	0.05 ± 0.07	0.04 ± 0.04	0.05 ± 0.05
N_{acc}/N_{tot}	0.5 ± 0.1	0.5 ± 0.1	0.4 ± 0.1	0.6 ± 0.1	0.5 ± 0.1	0.5 ± 0.1
N_{ait}/N_{acc}	1.3 ± 0.6	1.4 ± 0.8	1.8 ± 1.0	1.1 ± 0.6	1.4 ± 0.8	1.05 ± 0.6

Note. The 2.14 value of C (Weingartner et al., 2003) and 3.5 value of C (WMO/GAW, 2016) used in Weingartner correction (Weingartner et al., 2003) approach for the aethalometer. DJF = December to February; MAM = March to May; ON = October to November; SSA = single scattering albedo; eBC = equivalent black carbon. [a]For hourly data, the value of σ_{ap} is decreased by 40% on average (range 25% to 45%). [b]Single scattering albedo (SSA) is increased by 7% (range 3% to 10%) while using $C = 3.5$ instead of using $C = 2.14$ (see section 2.2 on C factor correction).

(indirect effects). The ERA-Interim data were used as lateral boundary for meteorology, and the data from ECHAM-HAMMOZ simulations (as above) were postprocessed for REMO's aerosol boundary forcing data. The same ECLIPSE aerosol emissions as discussed above were used in REMO-HAM. The shorter period of simulations in REMO-HAM versus ECHAM-HAMMOZ is due to the heavier computational burden as a result of higher resolution.

3. Results and Discussion

3.1. Aerosol Variability

We summarize first the characteristics of the observed aerosol variability over 8.5 years of continuous measurements. Distinct diurnal and seasonal cycles are observed for the extensive (particle number concentration, scattering coefficient, eBC, $PM_{2.5}$, and PM_{10}) and the intensive (α_{abs}, SSA, and geometric mean diameter [GMD]) aerosol parameters. The seasonal and diurnal variations exhibit many similarities during 8.5 years of measurements. The drivers of these variabilities are discussed in section 3.2.

3.1.1. Seasonal-Diurnal Cycle

Both extensive and intensive aerosol parameters manifest a pronounced month-dependent diurnal cycle. Table 1 displays a strong seasonality across the aerosol properties similar to that presented earlier (Hyvärinen et al., 2009; Komppula et al., 2009; Raatikainen et al., 2014) for optical and physical properties based on a data set of 2–3 years at MUK. Recently, Dumka et al. (2015) also perceived a similar seasonality in scattering and absorption coefficients at Nainital based on 10-month observations.

In premonsoon months, the concentration of extensive aerosol properties is consistently high over the course of the day with 1.5–2 times higher values in the early to late afternoon than during the night (Figure 2, left column). However, N_{nuc} is exceptional for different reasons (discussed later). The consistently higher values of aerosol, as seen in the left panel of Figure 2, exhibit attribution of high background/residual aerosol concentration in premonsoon, which may be misinterpreted as a weakened diurnal pattern. Notably in normalized analysis ($_{e}\Delta$ and $_{i}\Delta$ values; Figure 2, right column), the influence of long-range transported aerosols in the late afternoon dominates distinctly during premonsoon, when air masses from the plains reach MUK (see section 3.2). This is evidenced by relatively large amplitudes in N_{tot}, $PM_{2.5}$, eBC, and σ_{sp} values in corresponding time (Figure 2, right column). In the case of N_{nuc} (Figure 2c)

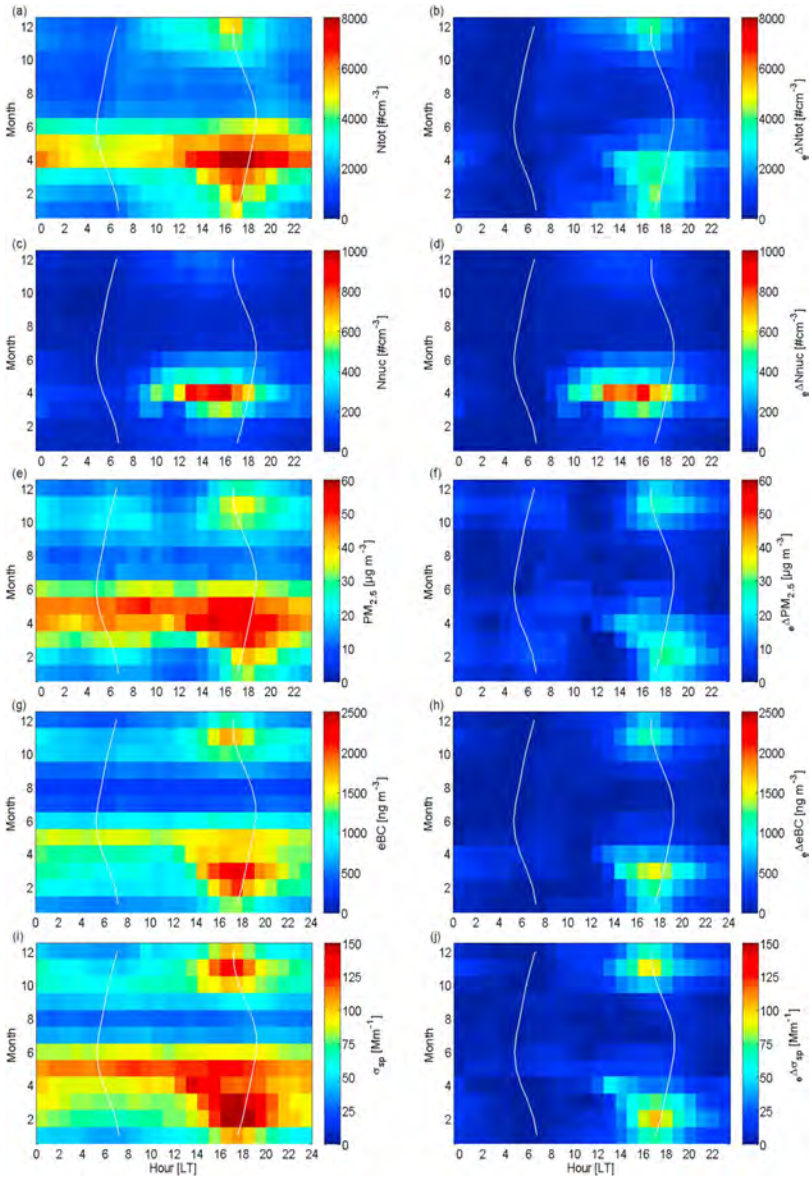

Figure 2. The diurnal-monthly aerosol extensive parameters representation in terms of both seasonal and diurnal variation (left column) and diurnal variation alone ($_e\Delta$; the minima of the diurnal values subtracted for each month [right column]). The sunrise and sunset time is shown with the white lines. eBC = equivalent black carbon.

and $_e\Delta N_{nuc}$ (Figure 2d), this shows a different behavior, being elevated only during afternoon in premonsoon, indicating new particle formation (NPF) events (Neitola et al., 2011).

In monsoon, the extensive parameter concentrations are low and constant; thus, no pronounced diurnal pattern is identified (Figure 2). Previous work (Hyvärinen, Raatikainen, Komppula, et al., 2011) has shown a

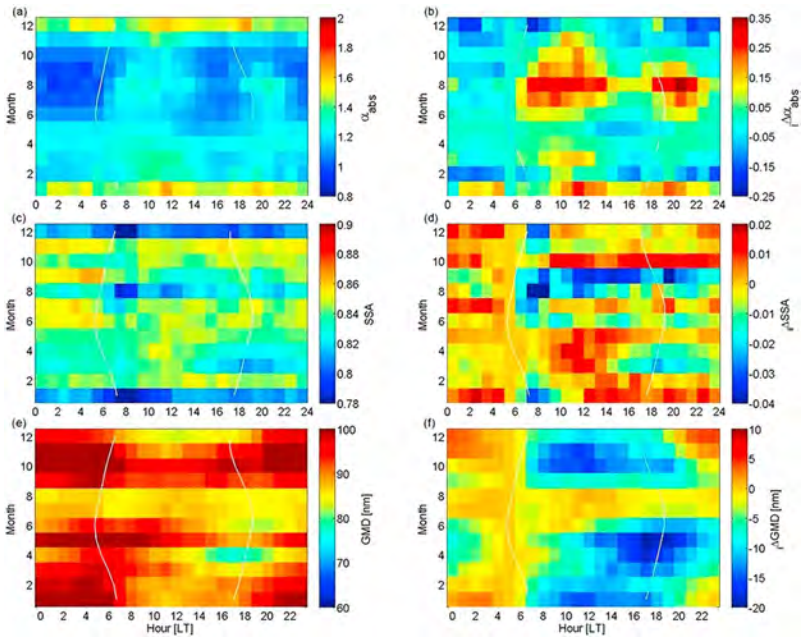

Figure 3. The diurnal–monthly aerosol intensive parameters representation at Mukteshwar in terms of both seasonal and diurnal variation (left column) and diurnal variation alone ($_j\Delta$; the 5 a.m. diurnal values subtracted for each month [right column]). The sunrise and sunset time is shown with the white lines. SSA = single scattering albedo; GMD = geometric mean diameter.

decrease of 40%–75% in average concentrations of aerosol physical and optical properties during monsoon relative to the premonsoon average concentration. In postmonsoon, particle mass and number concentrations elevate again to about twofold compared to monsoon, but lower than premonsoon values. In winter, a narrow decrease in aerosol concentrations relative to postmonsoon is noticed before a peak during premonsoon (Figure 2).

Figure 3 shows the seasonal cycle of the intensive parameters ($\alpha_{abs,}$ SSA, and GMD). The α_{abs} relative to $_j\Delta\alpha_{abs}$ is observed with small diurnal changes across the seasons. A high α_{abs} (Figures 3a and 3b) concurrently with low SSA (Figures 3c and 3d) shows the less scattering nature of the particles in winter. Moreover, some individual (hourly average) values of SSA registered as low as $<$0.6 in December and January, suggesting attribution of weak local or regional sources for absorbing aerosol emissions (Hyvärinen et al., 2009). In general, α_{abs} in fresh biomass burning smoke can vary from 1 to 10 (depending on the combustion process; Pokhrel et al., 2016). Thus, it is difficult to infer a plausible source only based on α_{abs}. But a ratio of N_{ait}/N_{acc} (supporting information Figure S8a) 1.0–1.5 times higher during the day time than the night time, together with $PM_{2.5}/PM_{10}$ ratio between 0.8 and 0.95, can be attributed to biomass emissions, such as burning dung cakes for heating and cooking purposes in the region (Komppula et al., 2009).

The values of SSA are relatively close to each other across the seasons (0.82 to 0.84; Table 1), indicating equal changes in source strength or removal processes of absorbing and scattering types of aerosols. The values of SSA are also low, up to 0.7 in August. However, contrary to winter, in August the dispersed and low SSA values in addition to the elevated N_{ait}/N_{acc} ratio (Table 1 and supporting information Figure S8a) imply wet scavenging of aged particles (Laakso et al., 2003). Moreover, we observe a clear difference in SSA during the November and March eBC peaks. In March, the mean SSA decreases from 0.85 to 0.81 as the BC-rich aerosol reaches MUK (Figure 3c). However, in November a small increase is seen in SSA in the afternoon hours (Figure 3c).

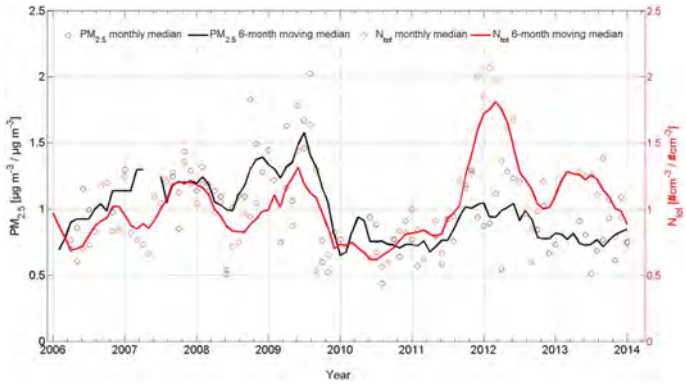

Figure 4. Monthly anomaly (dividing each monthly mean value by the 2005–2014 mean value for the given month) of aerosol variables. The parameters $PM_{2.5}$ and N_{tot} are unit less.

The GMD values for MUK are little bit higher than those observed elsewhere: for example, in Siberia, over 2006–2009 measurements (Heintzenberg et al., 2011), a site relatively undisturbed by anthropogenic influences, and in central North Carolina, in a forested suburban environment during September (Ziemba et al., 2010). The nighttime values of GMD at MUK are higher than the daytime values across the months. The GMD (Figure 3e) is stable at approximately 92 nm under more stagnant conditions in the winter (Herrmann et al., 2015) and distinctly high in monsoon (Figure 3f), obviously due to wet scavenging of large particles. A high ratio of eBC/$PM_{2.5}$ and N_{ait}/N_{acc} (Table 1 and supporting information Figure S8a) in monsoon relative to other seasons also manifests wet scavenging of large (aged) particles (Hyvärinen, Raatikainen, Komppula, et al., 2011). But a decrease in ratio of N_{ait}/N_{acc} concurrently with an increase in ratio of N_{acc}/N_{tot} (Table 1 and supporting information Figure S8b) and maxima in GMD (Figure 3e) with a distinct amplitude in ${}_{i}\Delta$GMD (Figure 3f) during postmonsoon might imply long-range transported plumes of stubble burning. The GMD is lowest at approximately 80 nm in premonsoon (specifically in April) due to NPF (supporting information Figure S10; Dal Maso et al., 2005; Komppula et al., 2009; Neitola et al., 2011). The ${}_{i}\Delta$GMD also shows distinctly very low values in early to late afternoon, especially in premonsoon.

3.1.2. Interannual Variability and Trend Analysis

The interannual variability in aerosol is distinct, and to get more insight into this variability, the relative deviations of monthly averaged values from the typical seasonal cycle were obtained with division of each monthly mean by respective monthly mean over the entire period 2005–2014.

The monthly anomalies in the interannual cycle are presented as an example for $PM_{2.5}$ and N_{tot} (Figure 4). The high values of $PM_{2.5}$ are in 2009 and N_{tot} is in both 2009 and 2012. The observed April–July monthly values of $PM_{2.5}$ in 2009 are as high as 80 $\mu g/m^3$, and N_{tot} is elevated to 6,000 $\#cm^{-3}$. Again in December 2011–2012 and January–March 2012, the aerosol particle number concentration increases up to 7,500 $\#cm^{-3}$, but $PM_{2.5}$ remains close to or even below the seasonal mean values. In the present analysis, on average the interannual variability of both $PM_{2.5}$ and N_{tot} is ±20%.

The trend analysis at MUK shows statistically significant negative trends at 95% confidence level with slopes of -19 $\mu g/m^3$ and of -23 $\mu g/m^3$ in $PM_{2.5}$ and PM_{10}, respectively, with both LMS and GLS/ARB methods. But MK analysis results in a statistically insignificant trend for both $PM_{2.5}$ and PM_{10}. The trend analysis result of N_{tot} has a positive slope, but not statistically significant (not shown here). In summary, all other aerosol parameters observed at MUK show no statistically significant trend, either with MK or LMS analysis. The ratio of eBC to $PM_{2.5}$ has a positive statistically significant trend of 2.44%/year corresponding to a slope of 0.06 ($\mu g/m^3(BC/PM_{2.5})$/7.7 years). However, eBC itself does not exhibit a statistically significant trend, so the observed trend in eBC/$PM_{2.5}$ is assumed to have been caused by the negative trend in $PM_{2.5}$.

In general, the absence of a statistically significant trend for the other aerosol parameters can be largely attributed to the length of the time period of continuous measurements in this study. As commented in

Collaud Coen et al. (2013), trends calculated on time series shorter than 8–10 years usually present larger slopes with great confidence intervals leading to statistically insignificant trends, since the results are too much influenced by the initial and final period together with possible outliers. Interestingly, in contrast to an increase in emission loads in India (Dubash et al., 2018; Krotkov et al., 2016; Rao et al., 2016), a decreasing trend of PM is investigated at MUK, as discussed above, which corresponds to a decrease in the interannual tendency of ABL (using modeled mixing layer depth) air transport to MUK from IGP (supporting information Figure S4). However, in-depth assessment of its reasons and linkages with aerosol variability could be a future task.

On trend analysis in India, CPCB (2012) showed varying trends for PM_{10} across 46 cities (population 1 million plus) based on their long-term (2000–2012) monitoring, while HEI (2017) indicated an increase in air pollution ($PM_{2.5}$) levels since 2010. Both these results have their own limitations in terms of a robust trend analysis approach and representation of monitoring locations for all of India.

3.2. Factors Driving the Aerosol Variability

3.2.1. Diurnal Cycle

The seasonal-diurnal plots in Figure 2 show a clear increase in all extensive aerosol parameters during late afternoon outside of the monsoon season. Raatikainen et al. (2014) identified similar patterns in aerosol patterns at MUK and used a modeled mixing depth in the plains to infer the transport of polluted air from IGP to MUK. It has previously been shown that convective mixing can transport polluted air from valleys and plains to high-altitude mountain sites (Baltensperger et al., 1997; Poltera et al., 2017; Raatikainen et al., 2014). It is known, however, that modeled mixing layer depths have uncertainties (supporting information Figure S3), especially in the mountain environment (Lehner & Rotach, 2018; Rotach et al., 2015); thus, here, due to the absence of direct measurements (Eresmaa et al., 2006) of the mixing layer depth, we use observed surface meteorological variables to determine the likely influence of boundary layer transport.

Figure 5 presents the monthly and diurnal median values in selected meteorological parameters at MUK: wind direction, wind speed, specific humidity, and solar irradiance. Outside of the monsoon season, the median wind direction (Figure 5a) has a very strong diurnal cycle, being predominantly NE-E (with 45% total contribution) during the day and N-NW (with 37% total contribution) at night. These wind directions are consistent with the alignment of the mountain ridges (Gohm et al., 2009; Pal et al., 2014; supporting information Figure S1). Figure 5 also presents the variability in winds and specific humidity, with a high variability indicating turbulence and hence an actively mixing boundary layer. The variability in wind speed and direction (Figures 5b and 5d) as well as specific humidity (Figure 5f) is much higher during the day, a consequence of the daytime convectively driven turbulent boundary layer (Stull, 1988). Strongly turbulent periods are associated with a reduction in horizontal wind speeds (Figure 5c). The strength of the turbulent mixing, indicated by the variability in each parameter, is determined by the sensible heat fluxes arising from solar irradiance (Figure 5g); good agreement between high solar irradiance and high variability in winds and specific humidity is the result of high solar irradiance generating high surface sensible heat fluxes and associated turbulent boundary layer. Note that the timing of maximum solar irradiance is, as expected, around solar noon on clear days whereas the maximum variability in winds and specific humidity is generally later in the afternoon (Prabha et al., 2012). The wind speed displays more variability than wind direction earlier in the day; however, and it is known that the boundary layer in mountainous regions has a more complex structure due to the interaction between flows at different scales (synoptic flow, valley wind, and slope flows; De Wekker & Kossmann, 2015; Ball, 1960; Tennekes, 1973; Serafin et al., 2018; Stull, 1973, 1988). At night, the variability is much lower since, in the absence of any thermal convection, any turbulent production is the result of wind shear (Serafin et al., 2018).

During the monsoon season, the diurnal pattern is heavily suppressed. In the night time the wind direction is SE (Figure 5a) since the summer monsoon circulation in India is more synoptic in scale (Kaskaoutis, Houssos, et al., 2014), and there is also more night time variability in wind speed and direction compared to other seasons. The solar irradiance at the surface is much reduced, producing weaker, surface-driven convective mixing; hence, the daytime variability in the winds and in specific humidity is not as strong as in the premonsoon and postmonsoon seasons. An additional source of turbulent mixing during the monsoon period is cloud-driven turbulence (Mehta et al., 2017).

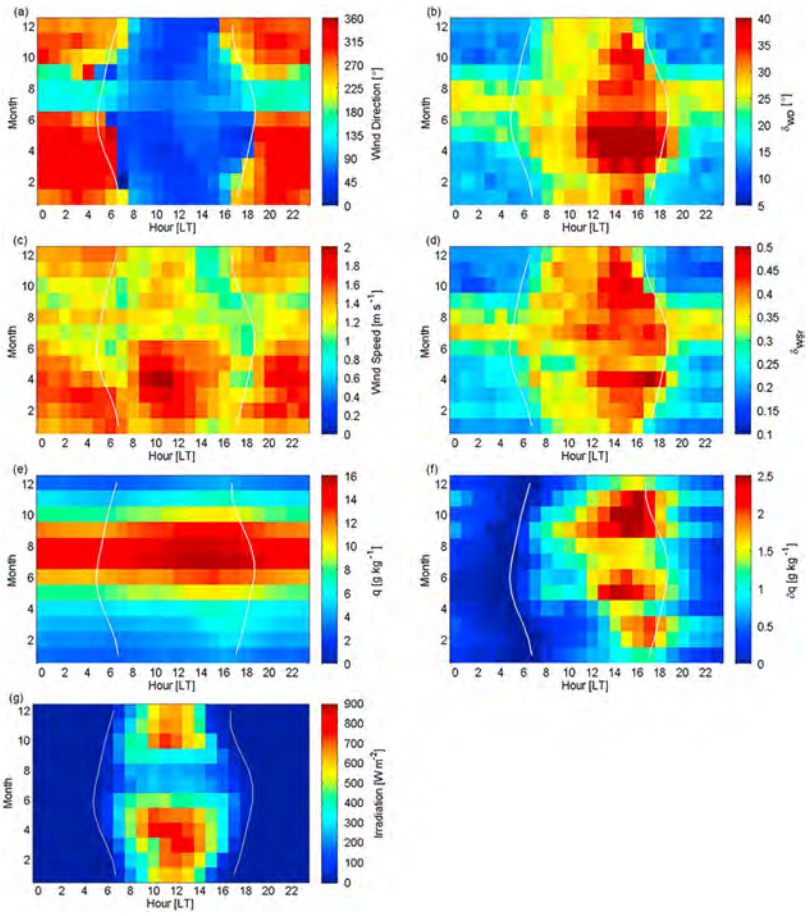

Figure 5. The diurnal-monthly median cycle of meteorological parameters at MUK: (a) wind direction, (b) wind direction variability (average of the absolute differences in wind direction from 1 min to the next during the given hour and represented as δ_{WD}), (c) wind speed, (d) wind speed variability (same way as δ_{WD}, but in the end divided by the average wind speed of that hour and represented as δ_{WSr}), (e) diurnal-monthly median of specific humidity, (f) diurnal median alone (subtracting the minima of each monthly cycle from all values of the respective cycle and represented as ∂q), (g) solar irradiation. The sunrise and sunset time is shown with the white lines.

However, the relative strength of boundary layer mixing alone is not sufficient to infer the mixing layer depth and thereby determine whether aerosol measurements at MUK are influenced by transport from the plains (IGP). The parameter Φq shown in Figure 6a is a much clearer indicator, as this uses the property that specific humidity is a conserved variable and is usually locally well mixed. Elevated values of Φq correspond very well with the observed 1.5–2 times increase in all extensive aerosol parameters at MUK seen in the early to late afternoon in Figure 2.

A weak peak in the morning is attributed to transport of air from the local valley, while the boundary layer is still growing, and the strong peak in the late afternoon relates to daytime transport of moist air masses from lower altitudes, mixed with the valley air (Figure 6a). Furthermore, the mixing layer influence is evaluated with different threshold values of Φq (0.25, 0.5, and 0.75) and compared to the maximum mixing depth (model based) in terms of the fraction of the days when MUK is under the influence of air from the plains

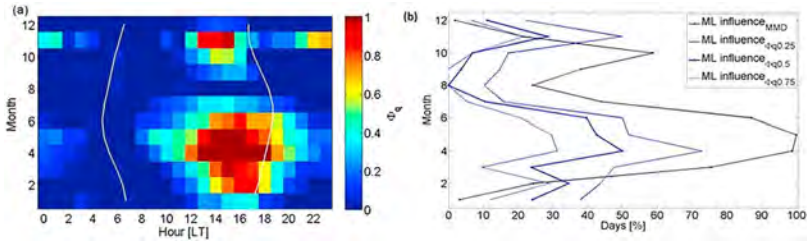

Figure 6. (a) Diurnal influence of atmospheric boundary layer (each hourly *q* value at Mukteshwar subtracted from the respective hourly *q* at Gual Pahari (in Indo Gangetic Plains) and divided by values at 5 a.m., represented as Φ*q*), (b) mixing layer influence as the average monthly fraction of days affected by air from Indo Gangetic Plains illustrated with maximum mixing depth and Φ*q* with three threshold values (0.25, 0.5, and 0.75) shown as blue thick line in middle (0.5), and as upper (0.25), and lower (0.75). The sunrise and sunset time in (a) is shown with the white lines.

(Figure 6b), indicating the mixing of air masses dominantly in premonsoon and postmonsoon. This is in agreement with previous findings that high regional pollution can be seen in dry months at elevated sites when the boundary layer is deep enough (Collaud Coen et al., 2013).

3.2.2. Seasonal and Interannual Variability

Broadly, the differentiation of seasons (premonsoon and postmonsoon) in India is based on the arrival and withdrawal phases of the classified precipitation level, and that might differ across the years. One of the suggested reasons is El Niño, which delays the onset of monsoon rains by inducing enhanced subsidence, persistent during the preonset phase, and advances the withdrawal by intensifying the horizontal cold air advection (Krishna Kumar et al., 2006; Xavier et al., 2007). The months of June and September, a mix of dry and rainy periods with transitional synoptic weather conditions and synoptic scale circulation, impeded a weaker diurnal aerosol cycle (Figure 2).

Figure 4 shows exceptionally high aerosol concentration in 2009 and 2012. A delay in onset of monsoon in 2009 might be due to El Niño event (Table 2), resulting relatively high aerosol concentration. Previously, Hyvärinen, Raatikainen, Brus, et al. (2011) and Hyvärinen, Raatikainen, Komppula, et al. (2011) examined the influence of monsoon on PM and BC concentrations along with optical and physical properties at MUK and identified less of a decrease in aerosol concentration during 2009 than 2006 and 2007. The air mass trajectories in anomaly month during 2009 (supporting information Figure S7) are typical of a dry and wet period and show a seasonal corroboration to that in other years. Although, 2012 has a negative rainfall anomaly, it is below the line for drought (IITM, 2017), suggesting the anomaly was not driven primarily due

Table 2
Year-Wise Details of ENSO Phase, Onset, and Withdrawal of Monsoon, and Cumulative Rainfall at MUK

Year	ENSO[a] phase	SW monsoon onset[b]	SW monsoon withdrawal[b]	Cumulative rainfall (mm) in parenthesis (%)[c]		Annual cumulative rainfall (mm)[d]
				JJAS	JA	
2005	—	16 June	28 Sept	990 (74)	580 (43)	1,330
2006	El Niño	30 June	27 Sept	680 (75)	455 (50)	910
2007	La Niña	18 June	02 Oct	785 (60)	450 (34)	1,320
2008	—	16 June	28 Sept	1,380 (91)	775 (51)	1,510
2009	El Niño	29 June	28 Sept	900 (68)	540 (41)	1,315
2010	La Niña	05 July	28 Sept	1,490 (88)	830 (49)	1,700
2011	La Niña	20 June	26 Sept	1,220 (82)	850 (57)	1,490
2012	—	05 July	25 Sept	920 (82)	660 (60)	1,115
2013	—	15 June	15 Oct	1,190 (74)	500 (31)	1,610
2014	El Niño	01 July	04 Oct	1,000 (64)	870 (55)	1,575

Note. ENSO = El Niño–Southern Oscillation; MUK = Mukteshwar.
[a]All India Summer Monsoon Rainfall: http://www.tropmet.res.in/~kolli/mol/Monsoon/frameindex.html. [b]India Meteorological Department, monsoon report. [c]Based on daily rainfall data (IMD, 2016; surface chemistry station at Mukteshwar); dashes refers to not classified; JJAS = June, July, August, and September (southwest *SW* monsoon period); JA = July and August. [d]Sum of JJAS (SW); and northeast (NE) monsoon (November–March); monsoon transition periods (April and May for the winter-to-summer transition, and in late September to October for the summer-to-winter transition).

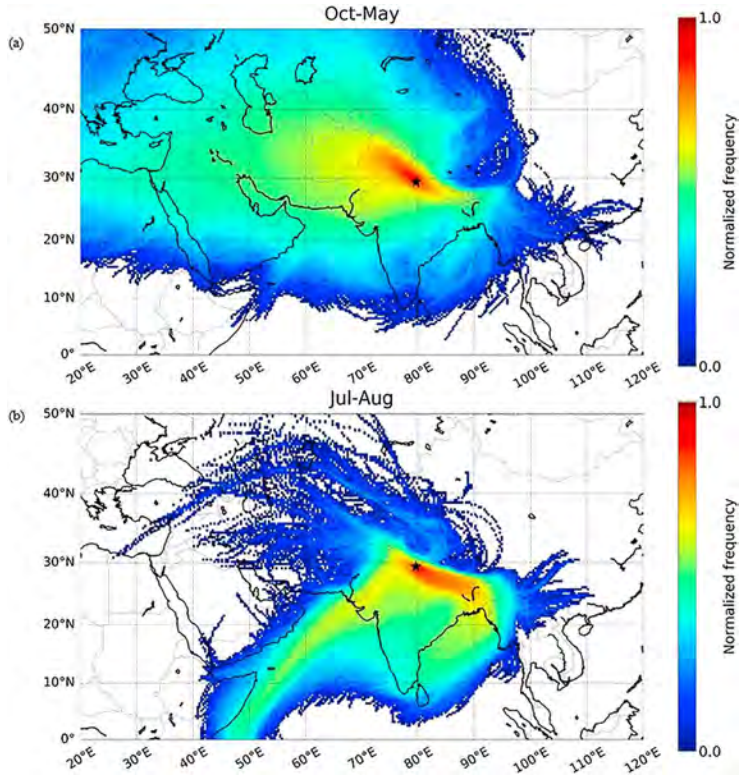

Figure 7. Normalized frequency of the trajectories, (a) dry period (October to May) and (b) monsoon (July and August).

to less rain. The air mass trajectories, however, are NW centered (supporting information Figure S7) and are short, with an average height above 4,000 m (range 2,500–7,500 m, not shown here; Komppula et al., 2009) along the Himalayan ridges. Therefore, for such altitudes where the aerosol layers are commonly associated with increases in sulfur dioxide (SO_2) and CCN (cloud condensation nuclei; Clarke et al., 2013), notably when SO_2 levels had been documented with increased emissions over the region (Li et al., 2017; Lu et al., 2013), this is likely to establish a linkage of the transport of such layers to MUK. However, this remains a future task for in-depth analysis. The ECHAM-HAM simulations also show an increasing pattern in N_{tot} (Figure 8). Notwithstanding, a plausible explanation of high N_{tot} and relatively low $PM_{2.5}$ values in 2012 could not be interpreted satisfactorily through the present analysis, even though PM_{10} values are also noticed to be relatively high in March 2012 (not shown here).

In contrast to 2009 and 2012, year 2010 and 2011 have La Niña events (Table 2), hence the highest annual cumulative precipitation, suggesting the lowest aerosol concentration. In monsoon, GMD shows a dip (Figure 3) that corroborates well with earlier findings of an efficient cleansing process of particles at MUK and GP (Hyvärinen, Raatikainen, Brus, et al., 2011, Hyvärinen, Raatikainen, Komppula, et al., 2011). This is attributed to nonuniform removal of particles due to cloud processes and wet scavenging by rain, which are more efficient for larger particles scavenging.

Outside the monsoon, the IGP suffers from intense dust storms originated from the arid and desert regions of southwest Asia (Iran, Afghanistan), Arabia, and the Thar desert blanketing IGP and the Himalayan foothills (Carrico et al., 2003; Duchi et al., 2014; El-Askary et al., 2006; Kaspari et al., 2009). Figure 7 shows normalized frequency of air mass origin before arriving at MUK and traveling over large regional population centers in

the IGP region (Komppula et al., 2009) carrying a considerable amount of windblown dust and agricultural burning aerosols (Dumka et al., 2015; Kumar, Kotlarski, et al., 2015). In the dry seasons (premonsoon and postmonsoon and winter), the trajectories show air masses arriving at MUK from the northwest and southwest sectors, but in general dominated by westerly air masses (Figure 7a). In the monsoon, the air masses originate from the Arabian Sea and Bay of Bengal and arrive at MUK by moving parallel to the Himalayas (Figure 7b). The air masses ascend such that the average altitude of the trajectory is lower than the end point altitude (not shown here). The humid marine air masses travel above IGP before reaching MUK. As the wet air mass rises to the altitude of MUK, the moisture condenses and rains down, effectively removing a lot of the particles (Figure 7b). The prevailing meteorological conditions and the marine humidity are the factors that differentiate the air masses, along with the fact that during premonsoon; there is a large amount of dust at middle and upper levels of the troposphere that is also transported over MUK.

Anthropogenic emissions, both local and distant are found to lead to significant climate impacts over India (Guo et al., 2016). The emissions of SO_2 (IIASA, 2011; Li et al., 2017), NO_x (Li et al., 2017), and $PM_{2.5}$ (Guttikunda & Jawahar, 2014; HEI, 2017; Rao et al., 2016) are increasing trends in India. The SO_2 and NO_x emissions are mainly released from the energy sector, road transport, and industries (IIASA, 2015). In the case of $PM_{2.5}$, the combustion of biomass for cooking (HEI, 2017) and emissions from coal-fired power plants (Guttikunda & Jawahar, 2014) are predominant. The emissions of BC and OM (organic matter) from the domestic sector in India show a slight decreasing or stable trend post-2010, and sulphates mainly from energy production and industries show a steep increasing trend after 2007 (IIASA, 2015).

The absolute emission strength at MUK is small in comparison to emissions over the Delhi region (supporting information Figure S6). The MUK area is often under the influence of long-range transported air masses from the IGP region, as discussed in the previous section, which results in long-range transported biomass burning aerosols (Dumka et al., 2015; Komppula et al., 2009; Kumar et al., 2011) and aged combustion-derived aerosols (Komppula et al., 2009; Raatikainen et al., 2017). The size-segregated correlation analysis reveals eBC mass contribution significantly in the size range $>$ 90 nm (supporting information Figure S9) and to that in 200–300 nm of the submicron aerosol mass spectra, suggesting attribution of aged combustion aerosol at MUK. The results are in corroboration with those observed in Hanle (Gogoi et al., 2014), a site in the western Himalayas at a higher altitude than MUK and potentially a receiver of aerosol aged further than that at MUK. Previously, Raatikainen et al. (2017) observed a similar eBC size distribution at MUK which is dominated by a mode at 210 nm during premonsoon season. The 5-day back air mass trajectories (Figure 7) also indicate long-range transported aerosol plumes at MUK. However, local anthropogenic emissions, although on a weak scale (domestic cooking and space heating), are also important. The local traffic emissions did not lead to a large aerosol load at MUK as we found no statistically robust cycle in weekday-weekend variability of extensive aerosol parameters. The values are within 1σ (standard deviation) across the months, confirming MUK to be located away from any high traffic density roads or cities. But the remote traffic emissions from the plains cannot be ruled out.

Besides mineral dust, another major source of MUK aerosol load is crop residue burning. The increased $PM_{2.5}$ and eBC concentrations in the afternoon hours during February–March and October–November (Figures 2e and 2g) agree with the seasonality of crop-residue burning at IGP (Kumar et al., 2011; Venkataraman et al., 2006). Domestic heating and cooking, which are also major sources of biomass burning aerosol in India (Bond et al., 2013), could have a similar signature to crop-residue burning with simultaneously increasing $PM_{2.5}$ and eBC. However, as the observed peaks in $PM_{2.5}$ and eBC (Figures 2f and 2h) occur during the harvesting months but not during the coldest months (December and January), we attribute these peaks to open crop-residue burning's impact on the air masses being transported from the plains to MUK. Dumka et al. (2015) observed a similar seasonality in scattering and absorption coefficients at Nainital, which was also attributed to long-range transported biomass burning aerosols. In northern India, rice residue burning is the main source of biomass burning aerosols in November, while in March, wheat residue burning prevails.

We observe a clear difference in SSA during the March and November eBC peaks. In March, the mean SSA decreases from 0.85 to 0.81 as the BC-rich aerosol reaches MUK (Figure 3c). However, in November a small increase is seen in SSA in the afternoon hours (Figure 3c). This is surprising, considering that in March, toward the end of the dry period, the amount of wind-blown dust is increasing and thus one would expect more scattering aerosol and higher SSA than in November.

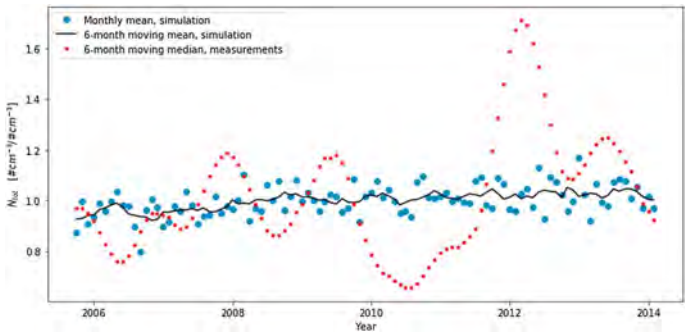

Figure 8. Monthly anomaly of N_{tot} in ECHAM-HAM simulations and in situ measurements at Mukteshwar.

A higher BC fraction in PM emissions from wheat residue burning compared to rice residue burning could explain the lower SSA in March. However, near-fire measurements (Ni et al., 2015; Zhang et al., 2015) do not indicate conclusive differences between the crops but report highly variable BC and $PM_{2.5}$ emissions. Another factor that may contribute to higher SSA in November is SOA formation. In November, biogenic emissions of SOA precursors are probably higher than in March. Additionally, SOA formation in crop residue burning plumes (Vakkari et al., 2018; Yokelson et al., 2009) may make a larger contribution in November than in March. Rice is cultivated mostly >200 km from MUK (Kaskaoutis, Kumar, et al., 2014), but wheat is grown also within 50–200 km of MUK; the longer transport would allow more time for in-plume SOA formation. However, this cannot be verified without further studies closer to the sources.

3.2.3. Modeled Aerosol Variability

In addition to observations, simulations are undertaken using two climate models with the same anthropogenic emissions but different spatial resolutions (ECHAM-HAMMOZ with a ~1.9° resolution and the regional model REMO-HAM with a 0.22° resolution). These simulations are used to evaluate the models' ability to capture the observed aerosols variability (refer to section 3.1) at MUK. In both models, the model level closest to the station altitude is chosen for the comparison following Pietikäinen et al. (2012). It should be mentioned that comparing a mountain station against models with terrain following hybrid pressure based coordinates is problematic unless the model spatial resolution is very high (approximately some kilometers). In this coordinate system, the horizontal transport of aerosols is too efficient in the lowest model layers—even at times when in reality there is no transport in the layer below the MUK station. This causes overestimation in the lowest model levels of mountainous areas and is the reason why we use the height-matched level (Li et al., 2014; Zou et al., 2016, and references therein). However, the height-matched level also has some errors as the terrain following vertical coordinate levels combined with the hydrostatic model does not produce enough vertical transport at mountainous regions. This causes some artificial dilution of the concentrations, but the error is much smaller than with the lowest level approach.

Figure 8 shows the monthly mean and 6-month moving mean of N_{tot} at MUK over the period 2005–2014 in the ECHAM-HAM simulations and the observations. The anomalies are compared for the different months of the years 2005–2014. The modeling results are comparable to the corresponding observational result of anomalies of N_{tot} (Figure 4). However, since the station stays within the ABL in the model and the artificial dilution does not allow the pollution load to build up sufficiently over the plain, the height-matched model level of MUK does not receive a strong enough pollution *pulse* when the ABL starts to grow and encompasses MUK in the premonsoon months. We do see that the later years of the period from 2005–2014 in general have higher N_{tot} concentrations with both observational and modeling results. Additionally, many of the interannual and interseasonal variability features—for example, the peaks in early 2009 and 2012 and the low values in late 2010 and late 2011—are captured reasonably well.

On the other hand, ECHAM-HAM overestimates the measured eBC values almost throughout the analyzed period and shows a reversed seasonality with the lowest concentrations during the premonsoon. A comparison of the modeled and measured eBC concentrations at MUK with the ECHAM-HAM and

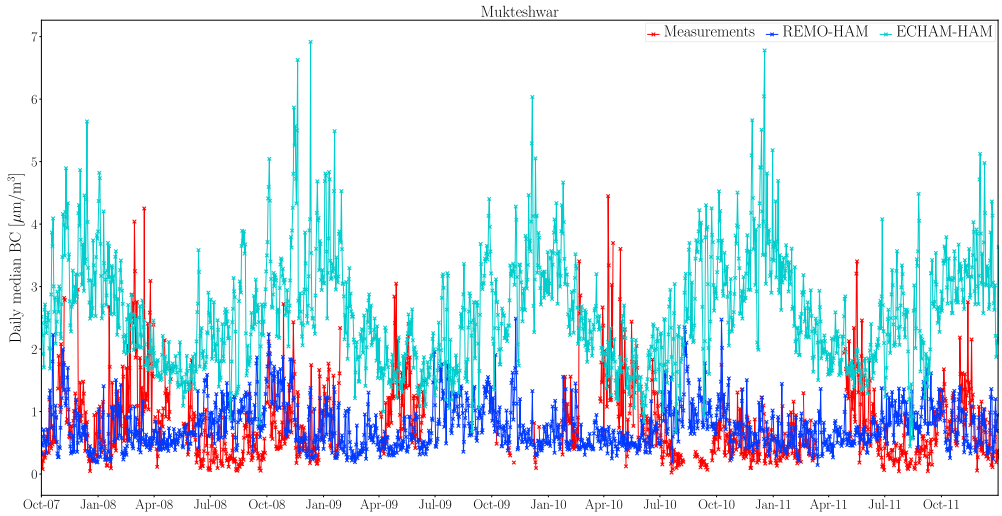

Figure 9. Daily median measured and modeled black carbon (BC) ground concentrations at Mukteshwar. The modeled values are from the height-matched levels.

REMO-HAM models, using the same emission inventory, is shown in Figure 9. The modeled overestimation is likely due to the coarse resolution of ECHAM-HAM, which flattens the orography and seems to artificially delay modeled precipitation so that it takes place at higher altitudes than MUK (analysis not shown). But the variability observed in measurements is captured reasonably well with the higher-resolution regional model REMO-HAM (Figure 9), apart from underestimating the measured peak concentrations during premonsoon and very slightly overestimating eBC during monsoon.

Notably, both models are able to capture the observed eBC concentrations over the IGP much more reliably (a comparison to GP is shown in supporting information Figure S11), indicating that the emission inventory does not have significant biases. This finding further indicates that transport and representation of the valley wind influence to ABL might be the main reason for the poor performance of ECHAM-HAM in modeling eBC at the mountainous MUK. Further issues include uncertainties in subgrid processes (like orographic thermal circulation) manifested in typical diurnal variation patterns, errors in model-predicted meteorology, aerosol processes, numerical model errors, and uncertainty in boundary conditions (Kumar, Barth, et al., 2015; Seibert et al., 2000). Moreover, inaccuracies in the local emissions estimations (Saikawa et al., 2017) are also possible.

4. Summary and Conclusions

We present the longest time series for in situ aerosol observations at a mountain site in India. The annual and seasonal values of aerosol extensive properties at MUK show high aerosol concentrations with respect to mountain sites worldwide, but still low in comparison to rural and urban sites elsewhere in India.

Typically, the strongest variability takes place over several consecutive months, indicating a seasonal phenomenon. The interannual variability of $PM_{2.5}$ and N_{tot} is ±20%, and we attribute the variability mostly to meteorology and climate changeability, and longer-term variations in emissions. Trend analysis shows statistically significant decreasing trends of -2.3 μg m^{-3} year^{-1} and -2.7 μg m^{-3} year^{-1} for $PM_{2.5}$ and PM_{10}, respectively. A decreasing interannual tendency for ABL air from IGP reaching MUK suggests a decrease in transport of pollution-laden air from the plains. However, investigating further this decreasing interannual tendency will be within the scope of future work.

All extensive aerosol parameters have 1.5–2 times higher values in early to late afternoon than in the night. Aerosol number concentration has a clear peak in the late afternoon and a minimum at 5:00 in the morning.

The seasonal variability is modulated due to fluctuations in different anthropogenic and natural sources, air mass flows, and/or wet scavenging. The long-range transported plumes of dust are pronounced in premonsoon, while stubble burning contributes in both premonsoon and postmonsoon. In premonsoon, notably the atmospheric NPF contributes in elevating total number concentration. The wet scavenging process in monsoon has significant influence on both extensive and intensive parameters of aerosols.

In this study, we used observed surface meteorological variables in the absence of direct measurements of the mixing layer depth to determine the likely influence of boundary layer transport to MUK. The results present the variability in winds and specific humidity, with a high variability indicating turbulence and hence an actively mixing boundary layer; however, during the monsoon season, the diurnal pattern is heavily suppressed.

But the relative strength of boundary layer mixing alone is not sufficient to infer the mixing layer depth and hence determine whether aerosol measurements at MUK are influenced by transport from the plains (IGP). Thus, in determining that variable, we use each hourly specific humidity both at MUK and GP (IGP), and referred as (Φq): the fraction of MUK air originating from the plains. The parameter Φq is a much clearer indicator, as this uses the property that specific humidity is a conserved variable and is usually locally well mixed. Elevated values of Φq correspond very well with the observed 1.5–2 times increase in all extensive aerosol parameters at MUK seen in the early to late afternoon. It concludes that the water vapor proxy matches reasonably well with aerosol variability over the course of the day and across the seasons. Further, it suggests that a weak peak in aerosol concentration in the morning could be due to air from the local valley, and the strong peak in the late afternoon may be dominantly related to daytime transport of moist air masses from lower altitude, mixed with the valley air. In summary, it suggests that the mixing of air masses via vertical and horizontal transport is significant in premonsoon and postmonsoon. The monsoon season is not captured well either with water vapor proxy or modeled mixing layer depth.

The global model ECHAM-HAM simulation with nudged meteorology reproduces the interannual, interseasonal, and long-term variability of N_{tot} reasonably well. The global model is struggling with modeling eBC concentrations in the mountainous region at MUK, while the regional model REMO-HAM managed to reproduce some of the main features of the variability. Both models reproduce the concentrations well over the IGP region (e.g., GP), indicating that emissions are not highly biased in the two models. This highlights the need of sufficient resolution and correct descriptions of transport processes when investigating mountainous regions. Efforts to increase resolution and improve process descriptions ought to improve the match between observational and modeling results further in future work.

Acknowledgments

This work was performed with financial support by the Ministry of Foreign Affairs of Finland, project grants (264242, 268004, 284536, and 287440) received from Academy of Finland, TEKES, Finland, and DBT, India, sponsored project TAQIITA (2634/31/2015), the Centre on Excellence in Atmospheric Science funded by the Finnish Academy of Sciences (307331), European Research Council Consolidator grant project (646857), and NordForsk Nordic Center of Excellence *eSTICC*. V.V. is beneficiary of an AXA Research Fund postdoctoral grant. The observational data used in this study are available freely from supporting information with due co-authorship or acknowledgment. The support of D. G., T. E. R. I. was always encouraging, and R. K. H. is thankful. The authors would like to thank the FMI colleague Timo Antila for his consistent technical assistance, and staff in Mukteshwar, TERI for their routine support in maintaining the observation station over the period. Comments from three anonymous reviewers are greatly appreciated.

References

Anderson, T. L., Covert, D. S., Marshall, S. F., Laucks, M. L., Charlson, R. J., Waggoner, A. P., et al. (1996). Performance characteristics of a high-sensitivity, three-wavelength, total scatter/backscatter nephelometer. *Journal of Atmospheric and Oceanic Technology*, *13*(5), 967–986. https://doi.org/10.1175/1520-0426(1996)013<0967:PCOAHS>2.0.CO;2

Anderson, T. L., & Ogren, J. A. (1998). Determining aerosol radiative properties using the TSI 3563 integrating Nephelometer. *Aerosol Science and Technology*, *29*(1), 57–69. https://doi.org/10.1080/02786829808965551

Asmi, A., Collaud Coen, M., Ogren, J. A., Andrews, E., Sheridan, P., Jefferson, A., et al. (2013). Aerosol decadal trends—Part 2: In situ aerosol particle number concentrations at GAW and ACTRIS stations. *Atmospheric Chemistry and Physics*, *13*(2), 895–916. https://doi.org/10.5194/acp-13-895-2013

Asmi, E., Kondratyev, V., Brus, D., Laurila, T., Lihavainen, H., Backman, J., et al. (2016). Aerosol size distribution seasonal characteristics measured in Tiksi, Russian Arctic. *Atmospheric Chemistry and Physics*, *16*(3), 1271–1287. https://doi.org/10.5194/acp-16-1271-2016

Baars, H., Kanitz, T., Engelmann, R., Althausen, D., Heese, B., Komppula, M., et al. (2016). An overview of the first decade of PollyNET: An emerging network of automated Raman-polarization lidars for continuous aerosol profiling. *Atmospheric Chemistry and Physics*, *16*(8), 5111–5137. https://doi.org/10.5194/acp-16-5111-2016

Ball, F. K. (1960). Control of inversion height by surface heating. *Quarterly Journal of the Royal Meteorological Society*, *86*, 983–994.

Baltensperger, U., Gäggeler, H. W., Jost, D. T., Lugauer, M., Schwikowski, M., Weingartner, E., & Seibert, P. (1997). Aerosol climatology at the high-alpine site Jungfraujoch, Switzerland. *Journal of Geophysical Research*, *102*(D16), 19,707–19,715. https://doi.org/10.1029/97JD00928

Blanco-Muriel, M., Alarcón-Padilla, D. C., López-Moratella, T., & Lara-Coira, M. (2001). Computing the solar vector. *Solar Energy*, *70*, 431–441.

Bolton, D. (1980). The Computation of Equivalent Potential Temperature. *Monthly Weather Review*, *108*(7), 1046–1053. https://doi.org/10.1175/1520-0493(1980)108<1046:TCOEPT>2.0.CO;2

Bond, T. C., Doherty, S. J., Fahey, D. W., Forster, P. M., Berntsen, T., DeAngelo, B. J., et al. (2013). Bounding the role of black carbon in the climate system: A scientific assessment. *Journal of Geophysical Research: Atmospheres*, *118*, 5380–5552. https://doi.org/10.1002/jgrd.50171

Carrico, C. M., Bergin, M. H., Shrestha, A. B., Dibb, J. E., Gomes, L., & Harris, J. M. (2003). The importance of carbon and mineral dust to seasonal aerosol properties in the Nepal Himalaya. *Atmospheric Environment*, *37*(20), 2811–2824. https://doi.org/10.1016/S1352-2310(03)00197-3

Census of India (2011). *Provisional population totals: rural-urban distribution Volume 2, Issue 1 of Census of India, 2011, India*. India: Office of the Registrar General & Census Commissioner.

Chakraborty, A., Bhattu, D., Gupta, T., Tripathi, S. N., & Canagaratna, M. R. (2015). Real-time measurements of ambient aerosols in a polluted Indian city: Sources, characteristics, and processing of organic aerosols during foggy and nonfoggy periods. *Journal of Geophysical Research: Atmospheres*, *120*, 9006–9019. https://doi.org/10.1002/2015JD023419

Charlson, R. J., Schwartz, S. E., Hales, J. M., Cess, R. D., Coakley, J. A., Hansen, J. E., & Hofmann, D. J. (1992). Climate forcing by anthropogenic aerosols. *Science*, *255*(5043), 423–430. https://doi.org/10.1126/science.255.5043.423

Clarke, A. D., Freitag, S., Simpson, R. M. C., Hudson, J. G., Howell, S. G., Brekhovskikh, V. L., et al. (2013). Free troposphere as a major source of CCN for the equatorial pacific boundary layer: Long-range transport and teleconnections. *Atmospheric Chemistry and Physics*, *13*(15), 7511–7529. https://doi.org/10.5194/acp-13-7511-2013

Collaud Coen, M., Andrews, E., Aliaga, D., Andrade, M., Angelov, H., Bukowiecki, N., et al. (2018). Identification of topographic features influencing aerosol observations at high altitude stations. *Atmospheric Chemistry and Physics*, *18*(16), 12,289–12,313. https://doi.org/10.5194/acp-18-12289-2018

Collaud Coen, M., Andrews, E., Asmi, A., Baltensperger, U., Bukowiecki, N., Day, D., et al. (2013). Aerosol decadal trends – Part 1: In situ optical measurements at GAW and IMPROVE stations. *Atmospheric Chemistry and Physics*, *13*(2), 869–894. https://doi.org/10.5194/acp-13-869-2013

Collaud Coen, M., Weingartner, E., Apituley, A., Ceburnis, D., Fierz-Schmidhauser, R., Flentje, H., et al. (2010). Minimizing light absorption measurement artifacts of the Aethalometer: Evaluation of five correction algorithms. *Atmospheric Measurement Techniques*, *3*(2), 457–474. https://doi.org/10.5194/amt-3-457-2010

Collaud Coen, M., Weingartner, E., Nyeki, S., Cozic, J., Henning, S., Verheggen, B., et al. (2007). Long-term trend analysis of aerosol variables at the high-alpine site Jungfraujoch. *Journal of Geophysical Research*, *112*, D13213. https://doi.org/10.1029/2006JD007995

CPCB (2010). *Air quality monitoring, emission inventory and source apportionment study for Indian Cities*. New Delhi, India: Central Pollution Control Board, Government of India.

CPCB. (2012). National ambient air quality status and trends in India −2010; NAAQMS/35/2011–2012.

Dal Maso, M., Kulmala, M., Riipinen, I., Wagner, R., Hussein, T., Aalto, P. P., & Lehtinen, K. E. J. (2005). Formation and growth of fresh atmospheric aerosols: Eight years of aerosol size distribution data from SMEAR II, Hyytiälä, Finland. *Boreal Environment Research*, *10*, 323–336.

De Wekker, S. F. J., & Kossmann, M. (2015). Convective boundary layer heights over mountainous terrain—A review of concepts. *Frontiers of Earth Science*, *3*, 77. https://doi.org/10.3389/feart.2015.00077

DeCarlo, P. F., Slowik, J. G., Worsnop, D. R., Davidovits, P., & Jimenez, J. L. (2004). Particle morphology and density characterization by combined mobility and aerodynamic diameter measurements. Part 1: Theory. *Aerosol Science and Technology*, *38*(12), 1185–1205. https://doi.org/10.1080/027868290903907

Dee, D. P., Uppala, S. M., Simmons, A. J., Berrisford, P., Poli, P., Kobayashi, S., et al. (2011). The ERA-interim reanalysis: Configuration and performance of the data assimilation system. *Quarterly Journal of the Royal Meteorological Society*, *137*(656), 553–597. https://doi.org/10.1002/qj.828

Di Girolamo, L., Bond, T. C., Bramer, D., Diner, D. J., Fettinger, F., Kahn, R. A., et al. (2004). Analysis of Multi-angle Imaging SpectroRadiometer (MISR) aerosol optical depths over greater India during winter 2001–2004. *Geophysical Research Letters*, *31*, L23115. https://doi.org/10.1029/2004GL021273

Draxler, R. R., & Hess, G. D. (1998). An overview of the HYSPLIT_4 modelling system for trajectories, dispersion, and deposition. *Australian Meteorological Magazine*, *47*, 295–308.

Dubash, N. K., Khosla, R., Rao, N. D., & Bhardwaj, A. (2018). India's energy and emissions future: An interpretive analysis of model scenarios. *Environmental Research Letters*, *13*(7), 074018. https://doi.org/10.1088/1748-9326/aacc74

Duchi, R., Cristofanelli, P., Marinoni, A., Bourcier, L., Laj, P., & Calzolari, F. (2014). Synoptic-scale dust transport events in the southern Himalaya. *Aeolian Research*, *13*, 51–57. https://doi.org/10.1016/j.aeolia.2014.03.008

Dumka, U. C., Kaskaoutis, D. G., Srivastava, M. K., & Devara, P. C. S. (2015). Scattering and absorption properties of near-surface aerosol over Gangetic–Himalayan region: The role of boundary-layer dynamics and long-range transport. *Atmospheric Chemistry and Physics*, *15*(3), 1555–1572. https://doi.org/10.5194/acp-15-1555-2015

El-Askary, H., Gautam, R., Singh, R. P., & Kafatos, M. (2006). Dust storms detection over the indo-Gangetic basin using multi sensor data. *Advances in Space Research*, *37*(4), 728–733. https://doi.org/10.1016/j.asr.2005.03.134

Eresmaa, N., Karppinen, A., Joffre, S. M., Räsänen, J., & Talvitie, H. (2006). Mixing height determination by ceilometer. *Atmospheric Chemistry and Physics*, *6*(6), 1485–1493. https://doi.org/10.5194/acp-6-1485-2006

Fleming, Z. L., Monks, P. S., & Manning, A. J. (2012). Review: Untangling the influence of air-mass history in interpreting observed atmospheric composition. *Atmospheric Research*, *104-105*, 1–39. https://doi.org/10.1016/j.atmosres.2011.09.009

Ganguly, D., Jayaraman, A., Rajesh, T. A., & Gadhavi, H. (2006). Winter-time aerosol properties during foggy and nonfoggy days over urban center Delhi and their implications for shortwave radiative forcing. *Journal of Geophysical Research*, *111*, D15217. https://doi.org/10.1029/2005JD007029

Gautam, R., Hsu, N. C., Kafatos, M., & Tsay, S.-C. (2007). Influences of winter haze on fog/low cloud over the indo-Gangetic plains. *Journal of Geophysical Research*, *112*, D05207. https://doi.org/10.1029/2005JD007036

Gautam, R., & Singh, M. K. (2018). Urban heat island over Delhi punches holes in widespread fog in the indo-Gangetic Plains. *Geophysical Research Letters*, *45*, 1114–1121. https://doi.org/10.1002/2017GL076794

Gogoi, M. M., Moorthy, K. K., Kompalli, S. K., Chaubey, J. P., Babu, S. S., Manoj, M. R., et al. (2014). Physical and optical properties of aerosols in a free tropospheric environment: Results from long-term observations over western trans-Himalayas. *Atmospheric Environment*, *84*, 262–274. https://doi.org/10.1016/j.atmosenv.2013.11.029

Gohm, A., Harnisch, F., Vergeiner, J., Obleitner, F., Schnitzhofer, R., Hansel, A., et al. (2009). Air pollution transport in an Alpine Valley: Results from airborne and ground-based observations. *Boundary-Layer Meteorology*, *131*(3), 441–463. https://doi.org/10.1007/s10546-009-9371-9

Guo, L., Turner, A. G., & Highwood, E. J. (2016). Local and Remote Impacts of Aerosol Species on Indian Summer Monsoon Rainfall in a GCM. *Journal of Climate*, *29*(19), 6937–6955. https://doi.org/10.1175/JCLI-D-15-0728.1

Guttikunda, S. K., & Jawahar, P. (2014). Atmospheric emissions and pollution from the coal-fired thermal power plants in India. *Atmospheric Environment*, *92*, 449–460. https://doi.org/10.1016/j.atmosenv.2014.04.057

HEI (2017). State of global air, A special report on global exposure to air pollution and its disease burden. https://www.stateofglobalair.org/sites/default/files/SOGA2017_report.pdf

Heintzenberg, J., Birmili, W., Otto, R., Andreae, M. O., Mayer, J.-C., Chi, X., & Panov, A. (2011). Aerosol particle number size distributions and particulate light absorption at the ZOTTO tall tower (Siberia), 2006–2009. *Atmospheric Chemistry and Physics*, *11*(16), 8703–8719. https://doi.org/10.5194/acp-11-8703-2011

Henriksson, S. V., Pietikäinen, J.-P., Hyvärinen, A.-P., Räisänen, P., Kupiainen, K., Tonttila, J., et al. (2014). Spatial distributions and seasonal cycles of aerosol climate effects in India seen in a global climate–aerosol model. *Atmospheric Chemistry and Physics*, *14*(18), 10,177–10,192. https://doi.org/10.5194/acp-14-10177-2014

Herrmann, E., Weingartner, E., Henne, S., Vuilleumier, L., Bukowiecki, N., Steinbacher, M., et al. (2015). Analysis of long-term aerosol size distribution data from Jungfraujoch with emphasis on free tropospheric conditions, cloud influence, and air mass transport. *Journal of Geophysical Research: Atmospheres*, *120*, 9459–9480. https://doi.org/10.1002/2015JD023660

Hooda, R. K., Hyvärinen, A.-P., Vestenius, M., Gilardoni, S., Sharma, V. P., Vignati, E., et al. (2016). Atmospheric aerosols local-regional discrimination for a semi-urban area in India. *Atmospheric Research*, *168*, 13–23. https://doi.org/10.1016/j.atmosres.2015.08.014

Hyvärinen, A.-P., Lihavainen, H., Komppula, M., Panwar, T. S., Sharma, V. P., Hooda, R. K., & Viisanen, Y. (2010). Aerosol measurements at the Gual Pahari EUCAARI station: Preliminary results from in situ measurements. *Atmospheric Chemistry and Physics*, *10*(15), 7241–7252. https://doi.org/10.5194/acp-10-7241-2010

Hyvärinen, A.-P., Lihavainen, H., Komppula, M., Sharma, V. P., Kerminen, V.-M., Panwar, T. S., & Viisanen, Y. (2009). Continuous measurements of optical properties of atmospheric aerosols in Mukteshwar, northern India. *Journal of Geophysical Research*, *114*, D08207. https://doi.org/10.1029/2008JD011489

Hyvärinen, A.-P., Raatikainen, T., Brus, D., Komppula, M., Panwar, T. S., Hooda, R. K., et al. (2011). Effect of the summer monsoon on aerosols at two measurement stations in northern India – Part 1: PM and BC concentrations. *Atmospheric Chemistry and Physics*, *11*(16), 8271–8282. https://doi.org/10.5194/acp-11-8271-2011

Hyvärinen, A.-P., Raatikainen, T., Komppula, M., Mielonen, T., Sundström, A.-M., Brus, D., et al. (2011). Effect of the summer monsoon on aerosols at two measurement stations in northern India – Part 2: Physical and optical properties. *Atmospheric Chemistry and Physics*, *11*(16), 8283–8294. https://doi.org/10.5194/acp-11-8283-2011

Hyvärinen, A.-P., Vakkari, V., Laakso, L., Hooda, R. K., Sharma, V. P., Panwar, T. S., et al. (2013). Correction for a measurement artifact of the multi-angle absorption photometer (MAAP) at high black carbon mass concentration levels. *Atmospheric Measurement Techniques*, *6*(1), 81–90. https://doi.org/10.5194/amt-6-81-2013

International Institute for Applied Systems Analysis (IIASA) (2011). World outlook report, Emissions of air pollutants for the world energy outlook 2011 energy scenarios, http://pure.iiasa.ac.at/9766/1/XO-11-028.pdf. (Accessed in Mar 2017.)

International Institute for Applied Systems Analysis (IIASA) (2015). http://www.iiasa.ac.at/web/home/research/researchPrograms/air/Global_emissions.html. (accessed in June 2015.)

Indian Institute of Tropical Meteorology (IITM) (2017). All India Summer Monsoon Rainfall (AISMR) http://www.tropmet.res.in/~kolli/mol/Monsoon/frameindex.html. (accessed in Jan 2017.)

India Meteorological Department (IMD) (2016). Personal communication.

Intergovernmental Panel on Climate Change (2007). Climate change 2007: The physical science basis. In S. Solomon, D. Qin, M. Manning, Z. Chen, M. Marquis, K. B. Averyt, et al. (Eds.), *Contribution of Working Group I to the Fourth Assessment Report of the Intergovernmental Panel on Climate Change* (pp. 153–171). Cambridge, UK and New York: Cambridge University Press.

Intergovernmental Panel on Climate Change (2013). Climate change 2013: The physical science basis. In T. F. Stocker, D. Qin, G.-K. Plattner, M. Tignor, S. K. Allen, J. Boschung, A. Nauels, Y. Xia, V. Bex, & P. M. Midgley (Eds.), *Contribution of Working Group I to the Fifth Assessment Report of the IPCC* (pp. 675–686). Cambridge, United Kingdom: Cambridge University Press.

Indian Space Research Organisation (ISRO) (2004). Special Land Based Campaign on Aerosols. http://www.isro.gov.in/update/04-feb-2004/special-atmospheric-aerosol-campaign-launched. (accessed in Jan 2017.)

Kanamitsu, M. (1989). Description of the NMC Global Data Assimilation and Forecast System. *Weather and Forecasting*, *4*(3), 335–342. https://doi.org/10.1175/1520-0434

Kaskaoutis, D. G., Houssos, E. E., Goto, D., Bartzokas, A., Nastos, P. T., Sinha, P. R., et al. (2014). Synoptic weather conditions and aerosol episodes over Indo-Gangetic Plains, India. *Climate Dynamics*, *43*(9-10), 2313–2331. https://doi.org/10.1007/s00382-014-2055-2

Kaskaoutis, D. G., Kumar, S., Sharma, D., Singh, R. P., Kharol, S. K., Sharma, M., et al. (2014). Effects of crop residue burning on aerosol properties, plume characteristics, and long-range transport over northern India. *Journal of Geophysical Research: Atmospheres*, *119*, 5424–5444. https://doi.org/10.1002/2013JD021357

Kaspari, S., Mayewski, P. A., Handley, M., Kang, S., Hou, S., Sneed, S., et al. (2009). A high-resolution record of atmospheric dust composition and variability since A.D. 1650 from a Mount Everest ice core. *Journal of Climate*, *22*(14), 3910–3925. https://doi.org/10.1175/2009JCLI2518.1

Komppula, M., Lihavainen, H., Hyvärinen, A.-P., Kerminen, V.-M., Panwar, T. S., Sharma, V. P., & Viisanen, Y. (2009). Physical properties of aerosol particles at a Himalayan background site in India. *Journal of Geophysical Research*, *114*, D12202. https://doi.org/10.1029/2008JD011007

Komppula, M., Mielonen, T., Arola, A., Korhonen, K., Lihavainen, H., Hyvärinen, A.-P., et al. (2012). Technical note: One year of Raman-lidar measurements in Gual Pahari EUCAARI site close to New Delhi in India – Seasonal characteristics of the aerosol vertical structure. *Atmospheric Chemistry and Physics*, *12*(10), 4513–4524. https://doi.org/10.5194/acp-12-4513-2012

Kotamarthi, V. R. (2010). Ganges valley aerosol experiment: Science and operations plan. DOE/SC-ARM-10-019, available at: http://www.arm.gov/publications/programdocs/doe-sc-arm-10-019.pdf?id=25. (Accessed on 10 August 2016).

Kowol-Santen, J., Beekmann, M., Schmitgen, S., & Dewey, K. (2001). Tracer analysis of transport from the boundary layer to the free troposphere. *Geophysical Research Letters*, *28*(15), 2907–2910. https://doi.org/10.1029/2001GL012908

Krishna Kumar, K., Rajagopalan, B., Hoerling, M., Bates, G., & Cane, M. (2006). Unraveling the mystery of Indian monsoon failure during El Niño. *Science*, *314*(5796), 115–119. https://doi.org/10.1126/science.1131152

Krotkov, N. A., McLinden, C. A., Li, C., Lamsal, L. N., Celarier, E. A., Marchenko, S. V., et al. (2016). Aura OMI observations of regional SO_2 and NO_2 pollution changes from 2005 to 2015. *Atmospheric Chemistry and Physics*, *16*(7), 4605–4629. https://doi.org/10.5194/acp-16-4605-2016

Kumar, P., Kotlarski, S., Moseley, C., Sieck, K., Frey, H., Stoffel, M., & Jacob, D. (2015). Response of Karakoram-Himalayan glaciers to climate variability and climatic change: A regional climate model assessment. *Geophysical Research Letters*, *42*, 1818–1825. https://doi.org/10.1002/2015GL063392

Kumar, R., Barth, M. C., Pfister, G. G., Nair, V. S., Ghude, S. D., & Ojha, N. (2015). What controls the seasonal cycle of black carbon aerosols in India? *Journal of Geophysical Research: Atmospheres*, *120*, 7788–7812. https://doi.org/10.1002/2015JD023298

Kumar, R., Naja, M., Satheesh, S. K., Ojha, N., Joshi, H., Sarangi, T., et al. (2011). Influences of the springtime northern Indian biomass burning over the Central Himalayas. *Journal of Geophysical Research*, *116*, D19302. https://doi.org/10.1029/2010JD015509

Kumar, S., Kumar, S., Kaskaoutis, D. G., Singh, R. P., Singh, R. K., Mishra, A. K., et al. (2015). Meteorological, atmospheric and climatic perturbations during major dust storms over indo-Gangetic Basin. *Aeolian Research*, *17*, 15–31. https://doi.org/10.1016/j.aeolia.2015.01.006

Laakso, L., Hussein, T., Aarnio, P., Komppula, M., Hiltunen, V., Viisanen, Y., & Kulmala, M. (2003). Diurnal and annual characteristics of particle mass and number concentrations in urban, rural and Arctic environments in Finland. *Atmospheric Environment*, *37*(19), 2629–2641. https://doi.org/10.1016/S1352-2310(03)00206-1

Lehner, M., & Rotach, M. W. (2018). Current challenges in understanding and predicting transport and exchange in the atmosphere over mountainous terrain. *Atmosphere*, *9*(7), 276. https://doi.org/10.3390/atmos9070276

Lelieveld, J., Crutzen, P. J., Ramanathan, V., Andreae, M. O., Brenninkmeijer, C. A. M., Campos, T., et al. (2001). The Indian Ocean experiment: Widespread air pollution from South and Southeast Asia. *Science*, *291*(5506), 1031–1036. https://doi.org/10.1126/science.1057103

Li, C., McLinden, C., Fioletov, V., Krotkov, N., Carn, S., Joiner, J., et al. (2017). India is overtaking China as the World's largest emitter of anthropogenic sulfur dioxide. *Scientific Reports*, *7*(1), 14304. https://doi.org/10.1038/s41598-017-14639-8

Li, Y., Wang, B., Wang, D., Li, J., & Dong, L. (2014). An orthogonal terrain-following coordinate and its preliminary tests using 2-D idealized advection experiments. *Geoscientific Model Development*, *7*(4), 1767–1778. https://doi.org/10.5194/gmd-7-1767-2014

Lu, Z., Streets, D. G., de Foy, B., & Krotkov, N. A. (2013). Ozone monitoring instrument observations of interannual increases in SO_2 emissions from Indian coal-fired power plants during 2005–2012. *Environmental Science & Technology*, *47*(24), 13,993–14,000. https://doi.org/10.1021/es4039648

Matt, F. N., Burkhart, J. F., & Pietikäinen, J.-P. (2016). Modelling hydrologic impacts of light absorbing aerosol deposition on snow at the catchment scale. *Hydrology and Earth System Sciences*, *2016*, 1–35. https://doi.org/10.5194/hess-2016-551

Mehta, S. K., Ratnam, M. V., Sunilkumar, S. V., Rao, D. N., & Krishna Murthy, B. V. (2017). Diurnal variability of the atmospheric boundary layer height over a tropical station in the Indian monsoon region. *Atmospheric Chemistry and Physics*, *17*(1), 531–549. https://doi.org/10.5194/acp-17-531-2017

Messerli, B., & Ives, J. (Eds) (1997). *Mountains of the world: A global priority*. New York, London: Parthenon.

Meybeck, M., Green, P., & Vörösmarty, C. (2001). A new typology for mountains and other relief classes. *Mountain Research and Development*, *21*(1), 34–45. https://doi.org/10.1659/0276-4741(2001)021[0034:ANTFMA]2.0.CO;2

Moorthy, K., Niranjan, K., Narasimhamurthy, B., Agashe, V. V., & Krishna Murthy, B. V. (1999). Aerosol climatology over India: 1. ISRO GBP MWR Network and database, ISRO-GBP Sci. Rep. 03-99, Indian Space Res. Organ., Bangalore.

Moorthy, K. K., Satheesh, S. K., Sarin, M. M., & Panday, A. K. (2016). South Asian aerosols in perspective: Preface to the special issue. *Atmospheric Environment*, *125*, 307–311. https://doi.org/10.1016/j.atmosenv.2015.10.073

Moosmüller, H., & Arnott, W. P. (2003). Angular truncation errors in integrating nephelometry. *Review of Scientific Instruments*, *74*(7), 3492–3501. https://doi.org/10.1063/1.1581355

Müller, T. (2015). Development of correction factors for Aethalometers AE31 and AE33, ACTRIS-2 WP3 Workshop, Athens 10–12 November 2015.

Müller, T., Henzing, J. S., de Leeuw, G., Wiedensohler, A., Alastuey, A., Angelov, H., et al. (2011). Characterization and intercomparison of aerosol absorption photometers: Result of two intercomparison workshops. *Atmospheric Measurement Techniques*, *4*(2), 245–268. https://doi.org/10.5194/amt-4-245-2011

Neitola, K., Asmi, E., Komppula, M., Hyvärinen, A.-P., Raatikainen, T., Panwar, T. S., et al. (2011). New particle formation infrequently observed in Himalayan foothills – Why? *Atmospheric Chemistry and Physics*, *11*(16), 8447–8458. https://doi.org/10.5194/acp-11-8447-2011

Ni, H., Han, Y., Cao, J., Chen, L.-W. A., Tian, J., Wang, X., & Wang, P. (2015). Emission characteristics of carbonaceous particles and trace gases from open burning of crop residues in China. *Atmospheric Environment*, *123*, 399–406. https://doi.org/10.1016/j.atmosenv.2015.05.007

Nieminen, T., Kerminen, V.-M., Petäjä, T., Aalto, P. P., Arshinov, M., Asmi, E., et al. (2018). Global analysis of continental boundary layer new particle formation based on long-term measurements. *Atmospheric Chemistry and Physics*, *18*(19), 14,737–14,756. https://doi.org/10.5194/acp-18-14737-2018

Ohara, T., Akimoto, H., Kurokawa, J., Horii, N., Yamaji, K., Yan, X., & Hayasaka, T. (2007). An Asian emission inventory of anthropogenic emission sources for the period 1980–2020. *Atmospheric Chemistry and Physics*, *7*(16), 4419–4444. https://doi.org/10.5194/acp-7-4419-2007

Pal, S., Lee, T. R., Phelps, S., & De Wekker, S. F. J. (2014). Impact of atmospheric boundary layer depth variability and wind reversal on the diurnal variability of aerosol concentration at a valley site. *Science of the Total Environment*, *496*, 424–434. https://doi.org/10.1016/j.scitotenv.2014.07.067

Panwar, T. S., Hooda, R. K., Lihavainen, H., Hyvärinen, A. P., Sharma, V. P., & Viisanen, Y. (2013). Atmospheric aerosols at a regional background Himalayan site—Mukteshwar, India. *Environmental Monitoring and Assessment*, *185*(6), 4753–4764. https://doi.org/10.1007/s10661-012-2902-8

Pietikäinen, J.-P., Kupiainen, K., Klimont, Z., Makkonen, R., Korhonen, H., Karinkanta, R., et al. (2015). Impacts of emission reductions on aerosol radiative effects. *Atmospheric Chemistry and Physics*, *15*(10), 5501–5519. https://doi.org/10.5194/acp-15-5501-2015

Pietikäinen, J.-P., O'Donnell, D., Teichmann, C., Karstens, U., Pfeifer, S., Kazil, J., et al. (2012). The regional aerosol-climate model REMO-HAM. *Geoscientific Model Development*, *5*(6), 1323–1339. https://doi.org/10.5194/gmd-5-1323-2012

Pokhrel, R. P., Wagner, N. L., Langridge, J. M., Lack, D. A., Jayarathne, T., Stone, E. A., et al. (2016). Parameterization of single-scattering albedo (SSA) and absorption Ångström exponent (AAE) with EC/OC for aerosol emissions from biomass burning. *Atmospheric Chemistry and Physics*, *16*(15), 9549–9561. https://doi.org/10.5194/acp-16-9549-2016

Poltera, Y., Martucci, G., Collaud Coen, M., Hervo, M., Emmenegger, L., Henne, S., et al. (2017). PathfinderTURB: An automatic boundary layer algorithm. Development, validation and application to study the impact on in situ measurements at the Jungfraujoch. *Atmospheric Chemistry and Physics*, *17*(16), 10,051–10,070. https://doi.org/10.5194/acp-17-10051-2017

Prabha, T. V., Karipot, A., Axisa, D., Kumari, B. P., Maheskumar, R. S., Konwar, M., et al. (2012). Scale interactions near the foothills of Himalayas during CAIPEEX. *Journal of Geophysical Research*, *117*, D10203. https://doi.org/10.1029/2011JD016754

Raatikainen, T., Brus, D., Hooda, R. K., Hyvärinen, A.-P., Asmi, E., Sharma, V. P., et al. (2017). Size-selected black carbon mass distributions and mixing state in polluted and clean environments of northern India. *Atmospheric Chemistry and Physics*, *17*(1), 371–383. https://doi.org/10.5194/acp-17-371-2017

Raatikainen, T., Hyvarinen, A.-P., Hatakka, J., Panwar, T. S., Hooda, R. K., Sharma, V. P., & Lihavainen, H. (2014). The effect of boundary layer dynamics on aerosol properties at the indo-Gangetic plains and at the foothills of the Himalayas. *Atmospheric Environment*, *89*, 548–555. https://doi.org/10.1016/j.atmosenv.2014.02.058

Rajput, P., Sarin, M. M., Sharma, D., & Singh, D. (2014). Characteristics and emission budget of carbonaceous species from postharvest agricultural-waste burning in source region of the indo-Gangetic plain. *Tellus B*, *66*, ID 21026.

Ramanathan, V., Crutzen, P. J., Lelieveld, J., Mitra, A. P., Althausen, D., Anderson, J., et al. (2001). Indian Ocean experiment: An integrated analysis of the climate forcing and effects of the great indo-Asian haze. *Journal of Geophysical Research*, *106*(D22), 28,371–28,398. https://doi.org/10.1029/2001JD900133

Rao, S., Klimont, Z., Leitao, J., Riahi, K., van Dingenen, R., Reis, L. A., et al. (2016). A multi-model assessment of the co-benefits of climate mitigation for global air quality. *Environmental Research Letters*, *11*(12), 124013. https://doi.org/10.1088/1748-9326/11/12/124013

Rotach, M. W., Gohm, A., Lang, M. N., Leukauf, D., Stiperski, I., & Wagner, J. S. (2015). On the vertical exchange of heat, mass, and momentum over complex, mountainous terrain. *Frontiers in Earth Science*, *3*, 76. https://doi.org/10.3389/feart.2015.00076

Sahu, L. K., Sheel, V., Pandey, K., Yadav, R., Saxena, P., & Gunthe, S. (2015). Regional biomass burning trends in India: Analysis of satellite fire data. *Journal of Earth System Science*, *124*(7), 1377–1387. https://doi.org/10.1007/s12040-015-0616-3

Saikawa, E., Kim, H., Zhong, M., Avramov, A., Zhao, Y., Janssens-Maenhout, G., et al. (2017). Comparison of emissions inventories of anthropogenic air pollutants and greenhouse gases in China. *Atmospheric Chemistry and Physics*, *17*(10), 6393–6421. https://doi.org/10.5194/acp-17-6393-2017

Satheesh, S. K., Moorthy, K. K., Babu, S. S., Vinoj, V., & Dutt, C. B. S. (2008). Climate implications of large warming by elevated aerosol over India. *Geophysical Research Letters*, *35*, L19809. https://doi.org/10.1029/2008GL034944

Sati, A. P., & Mohan, M. (2014). Analysis of air pollution during a severe smog episode of November 2012 and the Diwali festival over Delhi, India. *International Journal of Remote Sensing*, *35*(19), 6940–6954. https://doi.org/10.1080/01431161.2014.960618

Seibert, P., Beyrich, F., Gryning, S.-E., Joffre, S., Rasmussen, A., & Tercier, P. (2000). Review and intercomparison of operational methods for the determination of the mixing height. *Atmospheric Environment*, *34*(7), 1001–1027. https://doi.org/10.1016/S1352-2310(99)00349-0

Seinfeld, J., & Pandis, S. (2006). *Atmospheric chemistry and physics: From air pollution to climate change*, (II ed.). New York: John Wiley & Sons, Inc.

Serafin, S., Adler, B., Cuxart, J., De Wekker, S. F. J., Gohm, A., Grisogono, B., et al. (2018). Exchange processes in the atmospheric boundary layer over mountainous terrain. *Atmosphere*, *9*(3), 102. https://doi.org/10.3390/atmos9030102

Singh, N., Solanki, R., Ojha, N., Janssen, R. H. H., Pozzer, A., & Dhaka, S. K. (2016). Boundary layer evolution over the central Himalayas from radio wind profiler and model simulations. *Atmospheric Chemistry and Physics*, *16*(16), 10,559–10,572. https://doi.org/10.5194/acp-16-10559-2016

Singh, R. P., & Kaskaoutis, D. G. (2014). Crop residue burning: A threat to south Asian air quality. *Eos Transactions American Geophysical Union*, *95*(37), 333–334. https://doi.org/10.1002/2014EO370001

Smith, R. B., Doyle, J. D., Jiang, Q., & Smith, S. A. (2007). Alpine gravity waves: Lessons from MAP regarding mountain waves generation and braking. *Quarterly Journal of the Royal Meteorological Society*, *133*(625), 917–936. https://doi.org/10.1002/qj.103

Stein, A. F., Draxler, R. R., Rolph, G. D., Stunder, B. J. B., Cohen, M. D., & Ngan, F. (2015). NOAA's hysplit atmospheric transport and dispersion modeling system. *Bulletin of the American Meteorological Society*, *96*(12), 2059–2077. https://doi.org/10.1175/BAMS-D-14-00110.1

Stier, P., Feichter, J., Kinne, S., Kloster, S., Vignati, E., Wilson, J., Ganzeveld, L., et al. (2005). The aerosol-climate model ECHAM5-HAM. *Atmospheric Chemistry and Physics*, *5*(4), 1125–1156. https://doi.org/10.5194/acp-5-1125-2005

Stock, M., Cheng, Y. F., Birmili, W., Massling, A., Wehner, B., Müller, T., et al. (2011). Hygroscopic properties of atmospheric aerosol particles over the eastern Mediterranean: Implications for regional direct radiative forcing under clean and polluted conditions. *Atmospheric Chemistry and Physics*, *11*(9), 4251–4271. https://doi.org/10.5194/acp-11-4251-2011

Stull, R. B. (1973). Inversion rise model based on penetrative convection. *Journal of the Atmospheric Sciences*, *30*(6), 1092–1099. https://doi.org/10.1175/1520-0469(1973)030<1092:IRMBOP>2.0.CO;2

Stull, R. B. (1988). *An introduction to boundary layer meteorology, Atmospheric Sciences Library*, (p. 666). Dordrecht: Kluwer Academic Publishers. https://doi.org/10.1007/978-94-009-3027-8

Tennekes, H. (1973). A model for the dynamics of the inversion above a convective boundary layer. *Journal of the Atmospheric Sciences*, *30*(4), 558–567. https://doi.org/10.1175/1520-0469(1973)030<0558:AMFTDO>2.0.CO;2

Twomey, S. (1977). The influence of pollution on the shortwave albedo of clouds. *Journal of the Atmospheric Sciences*, *34*(7), 1149–1152. https://doi.org/10.1175/1520-0469(1977)034<1149:TIOPOT>2.0.CO;2

United States Geological Survey (2016). https://ngmdb.usgs.gov/ngmdb/ngmdb_home.htm. (Accessed in Jan 2017.)

Vakkari, V., Beukes, J. P., Dal Maso, M., Aurela, M., Josipovic, M., & van Zyl, P. G. (2018). Major secondary aerosol formation in southern African open biomass burning plumes. *Nature Geoscience*, *11*(8), 580–583. https://doi.org/10.1038/s41561-018-0170-0

van der Werf, G. R., Randerson, J. T., Giglio, L., Collatz, G. J., Mu, M., Kasibhatla, P. S., et al. (2010). Global fire emissions and the contribution of deforestation, savanna, forest, agricultural, and peat fires (1997–2009). *Atmospheric Chemistry and Physics*, *10*(23), 11,707–11,735. https://doi.org/10.5194/acp-10-11707-2010

Venkataraman, C., Habib, G., Kadamba, D., Shrivastava, M., Leon, J.-F., Crouzille, B., et al. (2006). Emissions from open biomass burning in India: Integrating the inventory approach with high-resolution Moderate Resolution Imaging Spectroradiometer (MODIS) active-fire and land cover data. *Global Biogeochemical Cycles*, *20*, GB2013. https://doi.org/10.1029/2005GB002547

Weigel, A. P., Chow, F. K., & Rotach, M. W. (2007). The effect of mountainous topography on moisture exchange between the "surface" and the free atmosphere. *Boundary-Layer Meteorology*, *125*(2), 227–244. https://doi.org/10.1007/s10546-006-9120-2

Weingartner, E., Saathoff, H., Schnaiter, M., Streit, N., Bitnar, B., & Baltensperger, U. (2003). Absorption of light by soot particles: Determination of the absorption coefficient by means of aethalometers. *Journal of Aerosol Science*, *34*(10), 1445–1463. https://doi.org/10.1016/S0021-8502(03)00359-8

World Meteorological Organization/Global Atmosphere Watch (WMO/GAW) (2003). Aerosol measurement procedures, guidelines and recommendations, Edition 2003, GAW Report No. 153, http://library.wmo.int/pmb_ged/wmo-td_1178.pdf

World Meteorological Organization/Global Atmosphere Watch (WMO/GAW). (2016). Aerosol measurement procedures, guidelines and recommendations, 2nd Edition 2016, GAW Report No. 227, https://library.wmo.int/doc_num.php?explnum_id=3073

Xavier, P. K., Marzin, C., & Goswami, B. N. (2007). An objective definition of the Indian summer monsoon season and a new perspective on the ENSO–monsoon relationship. *Quarterly Journal of the Royal Meteorological Society*, *133*(624), 749–764. https://doi.org/10.1002/qj.45

Yokelson, R. J., Crounse, J. D., DeCarlo, P. F., Karl, T., Urbanski, S., Atlas, E., et al. (2009). Emissions from biomass burning in the Yucatan. *Atmospheric Chemistry and Physics*, *9*(15), 5785–5812. https://doi.org/10.5194/acp-9-5785-2009

Zardi, D., & Whiteman, C. D. (2013). Diurnal mountain wind systems. In F. Chow, S. F. J. De Wekker, & B. Synder (Eds.), *Mountain weather research and forecasting: Recent progress and current challenges*, (pp. 35–119). New York, NY: Springer.

Zhang, K., O'Donnell, D., Kazil, J., Stier, P., Kinne, S., Lohmann, U., et al. (2012). The global aerosol-climate model ECHAM-HAM, version 2: Sensitivity to improvements in process representations. *Atmospheric Chemistry and Physics*, *12*(19), 8911–8949. https://doi.org/10.5194/acp-12-8911-2012

Zhang, T., Wooster, M. J., Green, D. C., & Main, B. (2015). New field-based agricultural biomass burning trace gas, $PM_{2.5}$, and black carbon emission ratios and factors measured in situ at crop residue fires in Eastern China. *Atmospheric Environment*, *121*, 22–34. https://doi.org/10.1016/j.atmosenv.2015.05.010

Ziemba, L. D., Griffin, R. J., Cottrell, L. D., Beckman, P. J., Zhang, Q., Varner, R. K., et al. (2010). Characterization of aerosol associated with enhanced small particle number concentrations in a suburban forested environment. *Journal of Geophysical Research*, *115*, D12206. https://doi.org/10.1029/2009JD012614

Zou, X., Li, Y., Li, J., & Wang, B. (2016). Advection errors in an orthogonal terrain-following coordinate: Idealized 2-D experiments using steep terrains. *Atmospheric Science Letters*, *17*(3), 243–250. https://doi.org/10.1002/asl.650

Atmos. Chem. Phys., 17, 371–383, 2017
www.atmos-chem-phys.net/17/371/2017/
doi:10.5194/acp-17-371-2017

Atmospheric Chemistry and Physics
Open Access
EGU

Size-selected black carbon mass distributions and mixing state in polluted and clean environments of northern India

Tomi Raatikainen[1], David Brus[1], Rakesh K. Hooda[1,2], Antti-Pekka Hyvärinen[1], Eija Asmi[1], Ved P. Sharma[2], Antti Arola[3], and Heikki Lihavainen[1]

[1]Finnish Meteorological Institute, Helsinki, Finland
[2]The Energy and Resources Institute, Delhi, India
[3]Finnish Meteorological Institute, Kuopio, Finland

Correspondence to: Tomi Raatikainen (tomi.raatikainen@fmi.fi)

Received: 20 May 2016 – Published in Atmos. Chem. Phys. Discuss.: 24 June 2016
Revised: 29 November 2016 – Accepted: 15 December 2016 – Published: 9 January 2017

Abstract. We have measured black carbon properties by using a size-selected single-particle soot photometer (SP2). The measurements were conducted in northern India at two sites: Gual Pahari is located at the Indo-Gangetic Plain (IGP) and Mukteshwar at the Himalayan foothills. Northern India is known as one of the absorbing aerosol hot spots, but detailed information about absorbing aerosol mixing state is still largely missing. Previous equivalent black carbon (eBC) mass concentration measurements are available for this region, and these are consistent with our observations showing that refractory black carbon (rBC) concentrations are about 10 times higher in Gual Pahari than those at Mukteshwar. Also, the number fraction of rBC-containing particles is higher in Gual Pahari, but individual rBC-containing particles and their size distributions are fairly similar. These findings indicate that particles at both sites have similar local and regional emission sources, but aerosols are also transported from the main source regions (IGP) to the less polluted regions (Himalayan foothills). Detailed examination of the rBC-containing particle properties revealed that they are most likely irregular particles such as fractal aggregates, but the exact structure remains unknown.

1 Introduction

Absorbing aerosols are warming the global climate, but uncertainties are still significant partly due to the lack of detailed experimental data on aerosol spatial and temporal distributions and their physical properties (Stocker et al., 2013; Bond et al., 2013). Broadly defined, black carbon (BC) is typically the main absorbing aerosol component in submicron aerosols and its radiative effects depend on absolute concentrations and mixing state, which describes how BC is distributed within the aerosol particles (Bond and Bergstrom, 2006; Petzold et al., 2013; Lack et al., 2014). Although BC mass concentrations are often measured, the information about the mixing state is currently limited. For some sources the freshly emitted BC can be almost pure black carbon, but rapid atmospheric processing leads to mixed particles containing significant mass fractions of other typical aerosol species such as sulphate and organics. The inclusion of non-absorbing components may cause an increase to BC absorption by a so-called lensing effect, but this also depends on the structure of the particle (e.g., Adachi et al., 2010; Cappa et al., 2012; He et al., 2015; Peng et al., 2016). In addition to the direct radiative effect, aerosol water uptake depends on the volume fraction of soluble aerosol species as pure BC is hydrophobic. Some absorbing aerosol particles can act as a cloud condensation nuclei (CCN), which means that BC can have an effect on cloud properties (an indirect climate effect). Therefore, knowing the mixing state is highly important when assessing the climate effects of BC.

Recent development of single-particle instruments capable of detecting BC (e.g., Cross et al., 2010; Lack et al., 2014) has provided detailed information about the BC mixing state. One widely used instrument for this purpose is the single-particle soot photometer, SP2 (Stephens et al., 2003; Schwarz et al., 2006; Moteki and Kondo, 2007), developed by Droplet Measurement Technologies (Boulder, CO,

USA). This instrument uses the laser-induced incandescence technique to detect so-called refractory black carbon (rBC), which is the fraction of the absorbing carbonaceous material that has boiling point close to 4000 K and emits visible light when heated to that temperature (Petzold et al., 2013; Lack et al., 2014). The rBC mass can be detected accurately for most particle types (e.g., Slowik et al., 2007; Cross et al., 2010), while determining the size of the particle containing both rBC and non-refractory material requires significant assumptions about the particle properties (e.g., Taylor et al., 2015). These uncertainties dealing with determining the particle sizes are further reflected in calculations of mixing state parameters such as the rBC volume fraction in each particle and the number fraction of rBC-containing particles.

Due to the significant local and regional emissions and prevailing meteorological conditions, northern India is one of the global absorbing aerosol hot spots (Ramanathan et al., 2007). The low frequency of rainfall during the winter and spring months allows the accumulation of aerosol pollution, which can be observed as a brown cloud (Ramanathan et al., 2001, 2007). Although the absorbing dust aerosol is mainly from natural origin, anthropogenic emissions such as biofuel burning and road traffic produce large amounts of black carbon. Aerosol concentrations are decreased significantly when the monsoon rains arrive (typically between mid-June and July in northern India). However, it has been suspected that the increased aerosol absorption could have an effect on the monsoon (e.g., Menon et al., 2002; Bollasina et al., 2008, 2011; Gautam et al., 2009; Lau et al., 2010; Ganguly et al., 2012; D'Errico et al., 2015; Boos and Storelvmo, 2016), which has great importance for the whole of South Asia. In spite of the potential importance of the absorbing aerosol, little information has been published about the BC mixing state in India.

The main purpose of this study is to provide new and detailed information about the rBC mixing state in northern India, focusing on two different environments: polluted Indo-Gangetic Plain and relatively clean Himalayan foothills. Comparing these observations gives us additional experimental information about processes affecting the transport and uplift of absorbing aerosol from the plains towards Himalayan foothills. Observations are made with a new measurement system where differential mobility analyzer (DMA) is used to size-select ambient particles before measuring rBC properties with an SP2. This system provides size-resolved information about rBC mixing state parameters including rBC number fractions and rBC mass in each particle. Also, comparing the DMA-selected particle size with that measured by the SP2 gives additional information about particle morphology.

2 Methods

2.1 Measurement sites

Mixing state of the rBC aerosol was measured in northern India in Mukteshwar, Nainital (29.47° N, 79.65° E; 2180 m a.s.l. (above sea level)), and Gual Pahari, Gurgaon (28.43° N, 77.15° E; 243 m a.s.l.), during the spring and premonsoon season 2014. Figure 1 shows the station locations. The measurements were started in Mukteshwar (9 February–31 March 2014) and then the instruments were moved to Gual Pahari (3 April–14 May 2014). Mukteshwar is a relatively clean site at the foothills of the central Himalayas about 2 km above the Indo-Gangetic Plain (IGP), and Gual Pahari station is located at the plains close to Delhi, where aerosol concentrations are significantly higher (e.g., Hyvärinen et al., 2009, 2010; Komppula et al., 2009; Panwar et al., 2013; Raatikainen et al., 2014; Hooda et al., 2016).

2.2 Measurement setup

Refractory black carbon (rBC) concentrations and mixing state parameters were measured by an SP2 (Revision C* with eight channels), manufactured by the Droplet Measurement Technologies (Boulder, CO, USA), which was connected to a differential mobility particle sizer (DMPS). Details of the DMPS-SP2 measurement setup, data analysis and a series of consistency tests are given in the Supplement. Briefly, the DMPS is composed of a differential mobility analyzer (DMA) and a condensation particle counter (CPC). The DMA selects narrow particle mobility size ranges from dried ($RH \approx 25\,\%$) polydisperse ambient particles (sampled through PM_{10} inlet line) and the CPC measures their number concentrations. Particle number concentrations are recorded for 30 logarithmically spaced mobility diameters (from about 20 to 650 nm) during a 32 min scan (60 s in each mobility diameter and 120 s between scans). The actual ambient particle number size distribution is then inverted from the CPC observations by the user defined routines (Wiedensohler et al., 2012). The inversion routines account mainly for the effects of the DMA transfer function and particle charging efficiencies, including multiply charged particles.

The SP2 (see, e.g., Stephens et al., 2003; Schwarz et al., 2006; Moteki and Kondo, 2007) was connected in parallel to the CPC to the outlet of the DMA. The SP2 measures number concentrations of particles with and without rBC for each mobility diameter. Any particle can be identified from the scattered laser light, while only the rBC-containing particles emit visible light (incandescence). It is expected that the incandescence is originating from rBC, because clear evidence of other refractory species such as mineral dust was not observed (e.g., varying ratios between wide and narrow band incandescence signals). Scattering and incandescence signal peak heights are proportional to the particle-scattering cross section and rBC mass, respectively. The measured

Figure 1. Locations of Gual Pahari (red marker) and Mukteshwar (blue marker) measurement stations.

single-particle rBC masses (0.3–380 fg quantification range) were converted to rBC volume equivalent diameters (briefly just rBC core diameter) by using 1800 kg m^{-3} density (70–740 nm diameter range). These diameters are used even when it is well known that the ambient rBC is not necessarily spherical or compact (e.g., Bond and Bergstrom, 2006; Peng et al., 2016). Number and volume mean rBC core diameters, average rBC mass concentration, and average number concentration of particles with and without rBC were calculated from the single-particle data for each mobility diameter. In addition, the number fraction of particles containing rBC was calculated from the number concentrations of particles with and without rBC. Number (with and without rBC) and rBC mass size distributions were calculated from the corresponding mobility bin average number and mass concentrations using an applied inversion method. The DMPS inversion method is not directly suitable for SP2 data, because noise from mobility size bins close to the SP2 detection limit would have propagated to the relevant size bins. Therefore, we used the DMPS inversion results (number size distributions calculated from the CPC concentrations) to calculate size-dependent scaling factors that convert SP2 concentrations to corresponding size distributions (see the Supplement). Briefly, the size- and scan-dependent scaling factor is the inverted size distribution divided by the original CPC concentrations, but we have calculated the mode of the scaling factor for each mobility size bin to reduce the variability and to make the SP2 results less dependent on the availability of the CPC data. This correction accounts for the effects of the DMA transfer function and particle charging efficiencies including multiply charged particles based on a typical particle size distribution. Multiply charged particles also have a small effect on the number and volume mean rBC core diameters, but these have been ignored based on visual examination of the rBC core size distributions (see Sect. 3.2).

Current measurement setup has some similarities with those used by Zhang et al. (2016), Liu et al. (2013) and McMeeking et al. (2011), who coupled a SP2 with a volatility tandem differential mobility analyzer (VTDMA) and hygroscopicity tandem differential mobility analyzer (HTDMA). The VTDMA measures particle size distributions after exposing size-selected (200, 250, 300 and 350 nm) particles to 300 °C temperature (Zhang et al., 2016). The same size-selected particles are also measured by the SP2, allowing comparison between rBC core size distributions and those measured by the VTDMA. In the HTDMA-SP2 setup used by McMeeking et al. (2011) and Liu et al. (2013), size-selected particles (147, 193 and 286 nm in the first study and 163 and 259 nm in the second study) are exposed to a high RH (∼ 90 %) and then measured by the SP2. There are also studies where the SP2 has been placed behind different types of classifiers such as the aerosol particle mass (APM) analyzer or the centrifugal particle mass analyzer (CPMA) (e.g., Ohata et al., 2016). The main advantages of the current

DMPS-SP2 setup is that the mobility size resolution is better (30 logarithmic size bins from about 20 to 650 nm) and this allows the calculation of rBC mass and number size distributions.

Consistency tests showed that the SP2 over counted particles compared with the parallel CPC measurements, which is a known issue for this specific SP2 (Supplement). Multiplying all SP2 concentrations by a factor of 0.82 caused the SP2 and CPC number concentrations levels to be similar, with just noise-like variability. Consistency tests also showed that the DMA-selected mobility sizes are in good agreement with those measured by the SP2 (particles without rBC) although a weak dependency on the SP2 temperature was observed (known issue for all SP2s). Comparison between rBC mass concentration with the optically detected (Aethalometer) equivalent BC (eBC) mass concentration from Mukteshwar showed a strong correlation between mass concentrations (absolute values are not directly comparable) and that their ratio was independent of the SP2 temperature. Finally, laser power analysis showed that the average scattering signal was 93 and 41 % from the original calibration value at Mukteshwar and Gual Pahari, respectively. Especially the latter drop in scattering signal could indicate critical drop in laser power. However, additional calculations showed that the reduced laser power is high enough for detecting rBC from particles with mobility sizes above 200 nm. These consistency tests show that the instrument setup and the data analysis methods provide accurate size-resolved rBC size distributions and mixing state parameters.

3 Results

Any SP2 can measure rBC core mass distributions (i.e., rBC mass concentration as a function of rBC core volume equivalent diameter) with high time resolution; however, the current size-selected measurements give this information for each DMA-selected mobility diameter. Knowing the particle (mobility) size simplifies the calculations especially for rBC-containing particles, which evaporate when traveling through the laser beam. For those particles, leading-edge-only (LEO) methods (e.g., Gao et al., 2007; Metcalf et al., 2012; Laborde et al., 2012) can be used to calculate the optical size from the scattered laser light, but the calculations require additional particle position information and the results depend on the assumed particle structure and optical parameters. In the following calculations particle size is represented by the DMA-selected mobility diameter. However, optical and mobility sizes are compared in Sect. 3.6 to obtain additional information about particle morphology.

Size-selected measurements allow the detailed examination of the rBC homogeneity, i.e., the variability in the rBC core size within each mobility size bin (Sect. 3.2). Since this level of detail is not typically needed, we will focus on the particle properties averaged for each DMA-selected mobility size bin. These values are used to calculate rBC number and mass size distributions and size-dependent rBC mixing state parameters (number fraction of particles containing rBC and the average rBC core size in those particles) for each size scan. Their average values are described in Sects. 3.3 and 3.4 and diurnal cycles in Sect. 3.5. First, we give an overview of the measured parameters and their time variations using the total rBC mass concentration as an example (Sect. 3.1).

3.1 Total rBC mass concentration time series

As an example of the measured parameters and their time variations, the total rBC mass concentration time series from the site at the polluted Indo-Gangetic Plain (Gual Pahari) and the relatively clean site at the Himalayan foothills (Mukteshwar) are shown in Fig. 2. Time series of the other parameters, which will be described below, are shown in the Supplement. The average rBC mass concentrations and their standard deviations are 11 ± 11 and $1.0 \pm 0.6\,\mu g\,m^{-3}$ for Gual Pahari and Mukteshwar, respectively. Figure 2 shows that the rBC mass concentrations are highly variable, which is the reason for the high standard deviations (absolute measurement uncertainties are close to 20 % (e.g., Laborde et al., 2012), and the variability is dominated by their diurnal cycles. Statistically significant long-term trends or weekly cycles cannot be found. Detailed examination of the diurnal variations in the total rBC mass and the other measured rBC mixing state parameters will be given in Sect. 3.5.

3.2 Size-selected rBC homogeneity

Examining size-selected rBC core size distributions can show how homogeneous these rBC-containing particles are. The selected mobility size must be large enough so that the thickly coated rBC can be detected but still small enough to represent the accumulation-mode particles. Examination of the available mobility sizes showed that the 360 nm mobility diameter is optimal for this purpose (the limits are shown in the Supplement). Figure 3 shows the campaign-average rBC core number size distributions from particles with 360 nm DMA-selected mobility diameter (variability shown in the Supplement). When Gual Pahari rBC core size distribution is mostly unimodal (mode at about 180 nm), that at Mukteshwar is clearly bimodal, where the smaller mode is located at about 110 nm and the other dominating mode is at about 210 nm. Changing the DMA-selected diameter to a larger or smaller value does not reveal any additional modes and the same larger mode is always dominating. The modes are relatively wide mainly due to the width of DMA transfer function (the full width at half maximum is about 45 nm for the 360 nm mobility size). The tails of the size distributions are related to the instrument noise (below 85 nm and above 300 nm) and multiply charged particles (above 300 nm), but they have small contributions to the mobility size bin mean values that are used in the following sections (86 and 92 %

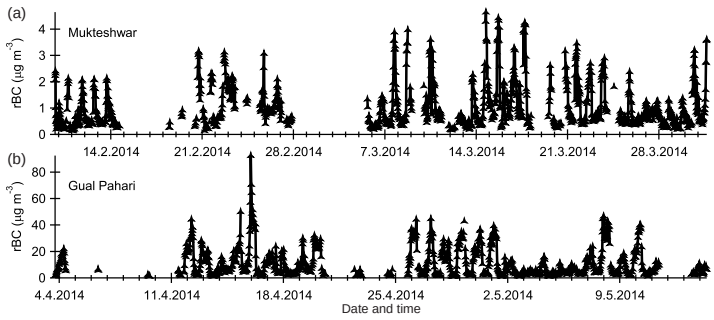

Figure 2. Total rBC mass concentration time series from Mukteshwar **(a)** and Gual Pahari **(b)**.

of the particles between 85 and 300 nm in Gual Pahari and Mukteshwar, respectively). In general, the modes at about 200 nm seem to be quite similar for Gual Pahari and Mukteshwar, while the smaller mode at about 110 nm is clearly seen only at Mukteshwar.

Figure 3 shows the campaign-average core size distributions for the 360 nm mobility diameter, but we have also calculated those for each size scan. Mukteshwar rBC core number size distribution seems to be bimodal most of the time. The number fraction of the larger rBC particles (those larger than 140 nm from the 85–300 nm core size range) varies between 0.5 and 0.8. The fluctuations are irregular, covering several days, and mainly for this reason there are no significant diurnal variations (not shown). Since rBC homogeneity within a DMA-selected mobility size bin is information that is too detailed for most practical applications, the following calculations are based on rBC properties averaged for each mobility size bin in each scan.

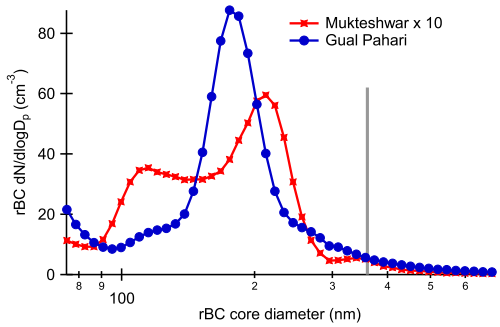

Figure 3. Campaign average rBC core number size distributions for the 360 nm DMA-selected mobility diameter (indicated by the vertical gray line) from Mukteshwar (multiplied by a factor of 10) and Gual Pahari. Standard deviations are approximately equal to the average concentration values when concentrations are larger than 1 cm^{-3}, while smaller concentrations mean increasing standard deviations.

3.3 Average rBC size distributions

Figure 4 shows the campaign-average rBC core mass and number size distributions from the both measurement sites. The gap at about 300 nm is caused by discontinuous high- and low-gain rBC mass calibration parameterizations. Due to the significant diurnal variations, which will be discussed later, the average mass and number size distributions have standard deviations (not shown) that are proportional to the observed size bin mean values. It is evident from Fig. 4 that the number size distributions are not fully resolved due to the about 70 nm rBC core size detection limit. Therefore, we will focus on the rBC mass size distributions. These have similar shapes except that the concentrations at Gual Pahari are about 10 times higher than those at Mukteshwar. Both mass distributions peak at around 210 nm, but these have relatively high concentrations of larger particles, especially at Gual Pahari. Large particles are also observed in the number and mass size distributions measured by the DMPS (shown in the Supplement). Bimodal lognormal distributions fitted to the mass distributions are shown with three (both modes and the total) thin blue (Mukteshwar) and green (Gual Pahari) lines in Fig. 4. The fits show that the peak diameters of the main modes are 195 and 202 nm, and the main modes cover 76 and 93 % of the observed rBC mass in Gual Pahari and Mukteshwar, respectively. Because only the tails of the modes with larger particles are seen (their peak diameters are larger than the rBC core detection limit, 740 nm), it is not possible to quantify their contributions to the total rBC mass.

Figure 4 shows the campaign-average distributions, but we have also calculated those for each mobility scan. Although the mass distributions are somewhat skewed, these can be described relatively well by lognormal distributions. We have therefore calculated the time series of total rBC mass concentrations (shown in Fig. 2) and geometric mass mean diameters and standard deviations (shown in the Supplement). The average size distribution parameters and their standard devia-

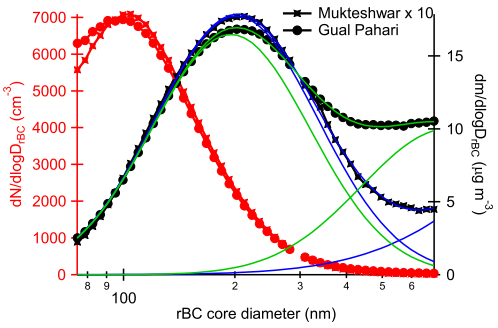

Figure 4. Campaign average rBC mass (black, right axis) and number (red, left axis) size distributions for Mukteshwar (lines with circles) and Gual Pahari (lines with crosses). The thin lines are bimodal lognormal fits including both modes and the total fitted mass (blue line for Mukteshwar and green line for Gual Pahari). Mukteshwar number and mass size distributions have been multiplied by a factor of 10. Standard deviations are approximately 80 % (Mukteshwar) or 100 % (Gual Pahari) of the bin mean number and mass. The gap at about 300 nm is caused by discontinuous high- and low-gain rBC mass calibration parameterizations.

tions from both measurement sites are shown in Table 1. The diurnal variations in the key rBC size distribution and mixing state parameters are shown in Sect. 3.5.

Previous SP2 studies have reported rBC core size distribution parameters from various environments (e.g., summary in Huang et al., 2012), but to our knowledge there are no previously published results from India. However, equally high rBC concentrations are observed in China, and there SP2 studies have shown that rBC core peak diameters are close to 220 nm (Huang et al., 2011, 2012; Wang et al., 2014), which is in good agreement with the current observations (peaks at about 210 nm). Huang et al. (2011) and Wang et al. (2014) have also observed bimodal rBC size distributions, but the larger particles (> 400 nm) have significantly higher contribution in India. In general, mass mean diameters are relatively similar at least compared with concentrations which vary by several orders of magnitude, depending heavily on local and regional emission sources.

3.4 Average rBC mixing state

Mixing state can be described by two parameters that are directly measured by the SP2: number fraction of particles containing rBC ($N_{\mathrm{rBC}}/N_{\mathrm{total}}$) and rBC mass in these particles, which is here represented by the rBC core diameter (volume equivalent diameter based on 1800 kg m^{-3} rBC density). Because core diameters showed some variability (Fig. 3), we have calculated both number and volume mean rBC core diameters ($D_{\mathrm{rBC},N}$ and $D_{\mathrm{rBC},V}$). We also present their ratios with the mobility diameters (D_m). Since these particles may not be spherical (some indirect evidence is given in Sect. 3.6), rBC core to mobility diameter ratios should not be taken as an exact measure of the rBC volume fraction. These parameters depend on mobility size and time, but the time series are correlated. Therefore, conclusions can be made using only one time series and mean values for each mobility size. Again, we use the 360 nm mobility size to represent the typical accumulation-mode particles.

Table 1. Campaign average values (±standard deviations) describing rBC mass size distributions (total mass and geometric mass mean diameter and standard deviation) and mixing state (number and volume mean core diameters, those normalized by the mobility size (D_m), and number fraction of particles containing rBC). The mixing state parameters are calculated for the 360 nm mobility size bins.

Parameter	Gual Pahari	Mukteshwar
Total rBC (μg m^{-3})	11 ± 11	1.0 ± 0.6
GMD $\mathrm{d}m/\mathrm{d}\log D_{\mathrm{rBC}}$ (nm)	249 ± 30	217 ± 13
GSD $\mathrm{d}m/\mathrm{d}\log D_{\mathrm{rBC}}$	0.246 ± 0.014	0.221 ± 0.014
$D_{\mathrm{rBC},N}$ (nm)	185 ± 8	178 ± 12
$D_{\mathrm{rBC},N}/D_m$	0.51 ± 0.02	0.50 ± 0.03
$D_{\mathrm{rBC},V}$ (nm)	221 ± 14	205 ± 16
$D_{\mathrm{rBC},V}/D_m$	0.61 ± 0.04	0.57 ± 0.04
$N_{\mathrm{rBC}}/N_{\mathrm{total}}$	0.46 ± 0.12	0.31 ± 0.05

The campaign-average mixing state parameters and their standard deviations for the 360 nm mobility size are shown in Table 1. As expected, the rBC number fraction is somewhat larger in Gual Pahari (polluted region) than in Mukteshwar (regional background), but the rBC-containing particles seem to have similar rBC core diameters. It could have been expected that rBC core size decreases when secondary aerosol species such as organics and sulfate condense to existing particles during their transport to Mukteshwar, but this effect is not clearly seen, although it may contribute to the observed bimodal rBC core size distribution seen in Fig. 3. It seems that the observed rBC properties are common for the whole region due to the similar emission sources and relatively short times for aging (more likely hours than days). For example, air masses in the upper troposphere or in remote regions can have spent several days without any contact to rBC sources.

There are some previous studies that describe the rBC mixing state with this level of details. It is evident that most particles do not contain detectable amounts of rBC anywhere (e.g., Kondo et al., 2011; Reddington et al., 2013; Dahlkötter et al., 2014; Raatikainen et al., 2015), but the current number fractions of rBC-containing particles (46 and 31 % for the 360 nm mobility size at Gual Pahari and Mukteshwar, respectively) seem to be the highest so far. For example, our previous results from the Finnish Arctic show that 24 % of the particles from 350–450 nm optical diameter range contain rBC and this is already a relatively large fraction (Raatikainen et al., 2015). In India, the high num-

ber fraction of rBC-containing particles is resulting from the significant regional black carbon emissions. The observed rBC core to particle diameter ratios ($D_{\mathrm{rBC},V}/D_m \sim 0.6$ and $D_{\mathrm{rBC},N}/D_m \sim 0.5$ from Table 1), whose cube is rBC volume fraction in a spherical compact particle, are larger than those observed for aged aerosol (e.g., Raatikainen et al., 2015; Dahlkötter et al., 2014), but match with the lowest values found for fresh emissions (e.g., Kondo et al., 2011; Schwarz et al., 2008; Sahu et al., 2012; Metcalf et al., 2012). For example, Metcalf et al. (2012) found thickly coated rBC from an urban plume with rBC core to particle diameter ratios ranging from about 0.51 to 0.59 (145 nm rBC cores with 50–70 nm coating thicknesses). Although the agreement is good, it should be noted that our particle size is based on the mobility diameter, while most other studies use the optical diameter from the LEO method. We will show later (Sect. 3.6) that mobility sizes are larger than optical sizes, which means that our rBC core to particle (optical) diameter ratios actually represent fresh emissions.

Mixing state parameters are somewhat size-dependent and this can be parameterized using the size-selected measurements. Figure 5 shows the averaged size-dependent mixing state parameters (number- and volume-based rBC core diameters and number fractions of particles containing rBC) and simple parameterizations. The lowest particle sizes where the SP2 detection limit has a significant effect on the results have been excluded from the fits (indicated by the smaller marker below ∼ 200 nm particle size). Also, the largest particle size in Mukteshwar has also been excluded due to the low number of observed particles. In general, the trends in the rBC mixing state parameters are similar for Gual Pahari and Mukteshwar, which indicates fairly similar local and regional rBC sources.

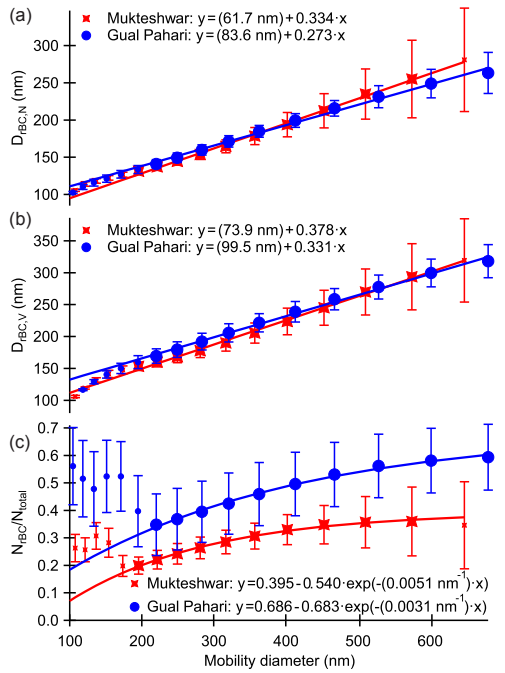

Figure 5. Size dependent rBC mixing state parameters for Gual Pahari and Mukteshwar. Panel **(a)** shows the number mean rBC core volume equivalent diameters and **(b)** shows those based on the rBC volume. Panel **(c)** shows rBC particle number fractions. Solid lines are the fits to the data (ignoring bad data points indicated by the smaller marker size). Error bars indicate ±1 standard deviation limits.

3.5 Diurnal cycles

Figure 6 shows the diurnal cycles of the rBC mass distribution (total mass and geometric mass mean diameter and standard deviation) and mixing state (rBC core to mobility diameter ratio and the number fraction of particles containing rBC for the 360 nm mobility size) parameters. The number-based diameter ratios and size distribution parameters are not shown, because these have similar diurnal variations with the mass- and volume-based parameters. The total rBC mass concentrations have significant diurnal variations, while those for the mean diameter and distribution width are modest. From the rBC mixing state parameters, which are not directly related to the mass distribution, only the rBC particle number fractions have clear diurnal cycles, while the rBC core to mobility diameter ratio is practically constant. The strong diurnal variability in the rBC mass concentrations is in good agreement with those of equivalent black carbon observed in our previous studies and by others (e.g., Komppula et al., 2009; Hyvärinen et al., 2009, 2010; Panwar et al., 2013; Raatikainen et al., 2014). Increased vertical mixing is the main reason for the daytime decrease in rBC mass in Gual Pahari and this can also explain the decrease in rBC number fraction. In general, Gual Pahari and Mukteshwar rBC aerosols are relatively similar except that the Gual Pahari aerosol has an order of magnitude higher concentration and the number fraction of particles containing rBC is about 50 % larger compared with those from Mukteshwar.

3.6 Morphology of rBC-containing particles

Black carbon or soot particles are initially aggregates composed of several primary BC particles, which diameters are in the order of a few tens of nanometers (e.g., Sorensen, 2001). These fresh aggregates can contain some amounts of a non-refractory material, but the fraction increases with time when atmospheric vapors condense to the soot particles and when the particle grows by coagulation. Increasing non-refractory fraction makes these particles more spherical. In addition, aggregates can be compacted when particles absorb water vapor and become droplets (e.g., Zhang et al., 2008; Pagels et al., 2009). As a result, core–shell structure can be a valid approx-

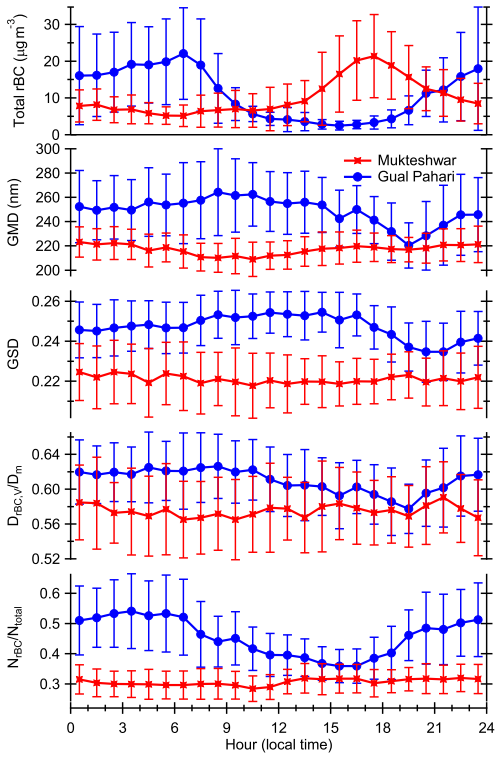

Figure 6. Diurnal cycles of rBC core mass size distribution parameters (total mass concentrations and geometric mass mean diameter and standard deviation), rBC core to mobility diameter ratios and fractions of particles containing rBC. The diameter ratios and fractions are calculated for the 360 nm mobility size. Error bars indicate ±1 standard deviation limits. Mukteshwar total rBC mass concentration and its standard deviation have been multiplied by a factor of 10.

imation for the aged aerosol, but it is not clear whether this is the case in India, where the aerosol is relatively fresh. The SP2 can provide some information about the morphology of the rBC-containing particles.

First, the SP2 can detect if a particle disintegrates in the laser beam into rBC and non-rBC fragments. This can happen if the rBC core is close to the particle surface or when rBC is attached to the surface of another particle (Sedlacek et al., 2012; Moteki et al., 2014). However, our measurements show that such disintegrating particles have negligible concentrations.

There are also studies reporting bare rBC particles (e.g., Huang et al., 2012), but the current rBC core volume equivalent diameters are always well below mobility diameters. However, it is possible that the rBC particles have low densities or that the particles are irregular aggregates. At least qualitative information about the particle shape can be obtained by comparing the DMA-selected mobility and SP2-derived optical sizes. Optical size is based on the measured or reconstructed (see below) intensity of the scattered laser light and a theoretical correction to the scattering accounting for the difference between calibration (ammonium sulfate) and ambient aerosol structures and optical properties. Accurate sizing requires information about particle structure, but clear differences (e.g., much larger than the typical ±20 % sizing uncertainty) between optical and mobility sizes indicate non-spherical particles such as aggregates.

Optical size based on a LEO method

Optical sizes are estimated using LEO methods (e.g., Gao et al., 2007; Metcalf et al., 2012; Laborde et al., 2012). In earlier studies, the authors use the leading edge of the scattering signal, which is still unaffected by the evaporation of the non-refractory material, to reconstruct the unperturbed scattering signal. Current method is the same as the method used in our previous study (Raatikainen et al., 2015): here the leading edge is the part of the signal where laser beam intensity is 0.07–3 % of the maximum, and the Gaussian scattering (laser beam) profile and peak position are calculated by averaging those from 100 previous particles that do not have detectable incandescence signal. Scattering signal peak height is solved by fitting the Gaussian profile to the signal from the leading edge (e.g., Gao et al., 2007). The scattering cross section is calculated from the signal peak height by using the scattering calibration, and optical particle size is calculated from the scattering cross section by using the Mie theory (linear interpolation between the limits of pure ammonium sulfate (refractive index $m = 1.48 - i0$) and a mixed particle ($m = 1.715 - i0.395$) with rBC core to particle diameter ratio of 0.6).

The current LEO analysis suffered from a systematic noise signal, which increased the variability in the results and seemed to cause a systematic bias when the instrument temperature was below 30 °C (see the Supplement). Also, the decrease in laser power when the SP2 was transported from Mukteshwar to Gual Pahari decreased the success rate of the LEO fits from 98.6 to 90.9 % (for rBC-containing particles from the 360 nm mobility size bin). Due to these uncertainties, we focus on the 360 nm mobility size bin and use data from instrument temperatures between 30 and 35 °C. These results seem to be reliable, but potential biases cannot be fully ruled out.

For the 360 nm mobility size and when the instrument temperature is between 30 and 35 °C, the campaign-average LEO-derived optical particle diameters for rBC-containing particles are 245 ± 10 and 234 ± 20 nm for Mukteshwar and Gual Pahari, respectively. For reference, corresponding sizes for particles without rBC are 360 ± 25 and 359 ± 17 nm, which are in good agreement with those without the LEO

method (356 ± 7 and 361 ± 11 nm) and the selected mobility diameter (360 nm). It is clear that the average optical size is significantly smaller than the mobility size, which shows that the rBC-containing particles are not spherical. Further examination of the single-particle data can reveal additional details about individual particles. Figure 7 shows the dependency of the optical size on the rBC core size by means of a probability density map (normalized by the maximum probability density). The rBC core size population is clearly bimodal in Mukteshwar (see Sect. 3.2), and it seems that the smaller rBC cores are thickly coated (core to optical diameter ratio approx. 0.4), while the larger rBC cores are thinly coated (core to optical diameter ratio close to unity). The only clear rBC mode in Gual Pahari seems to be thinly coated. The red markers and error bars show the effect of refractive index on the calculated optical size; the upper limit is based on ammonium sulfate refractive index ($m = 1.48 - i0$) and the lower limit is based on that of pure rBC ($m = 2.26 - i1.26$ from Moteki et al., 2010). Additional uncertainties arise from the particle morphology (e.g., He et al., 2015) and scattering model (e.g., He et al., 2016). Even when considering these large potential uncertainties, the optical sizes are smaller than the mobility sizes, which show that rBC-containing particles are not spherical. Especially the thinly coated particles are most likely highly fractal soot aggregates. Such aggregates typically have low volume fractions of non-refractory material, but the exact fractions cannot be determined without detailed information about particle morphology and optical properties (e.g., He et al., 2016).

Zhang et al. (2016) used similar measurement setup (VTDMA-SP2) in northern China about 60 km from Beijing. They have found closely matching LEO-calculated optical and mobility sizes, which indicates spherical particle shape, and internally mixed particles with low rBC volume fraction (161 nm mass equivalent rBC core size for 350 nm mobility size). Although the rBC concentrations have similar magnitudes in northern China and India, rBC-containing particles seem to have different properties most likely due to different sources.

4 Conclusions

Refractory black carbon (rBC) mass distributions and mixing state parameters were measured using a size-selected single-particle soot photometer (SP2) in northern India during spring 2014. The size-selected results were obtained by connecting a SP2 to the outlet of a differential mobility analyzer (DMA), which classifies particles according to their mobility size. The measurements were made in a relatively clean regional background site at the Himalayan foothills (Mukteshwar) and at a relatively polluted site close to Delhi (Gual Pahari). To our knowledge, this is the first publication showing size-selected rBC mass distributions and mixing state parameters for this region.

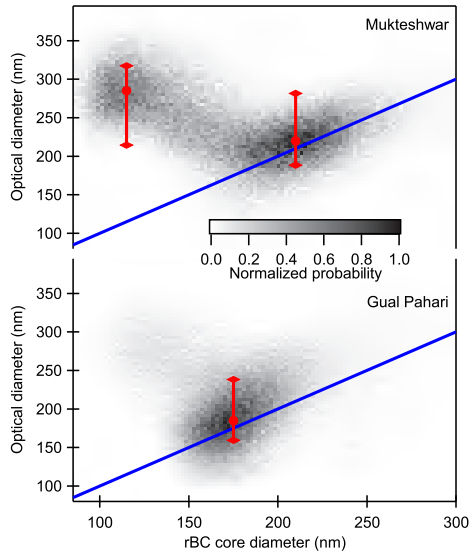

Figure 7. Distributions of single-particle optical and rBC core diameters for the 360 nm mobility size and 30–35 °C instrument temperature range (probabilities normalized by the maximum values). The blue lines indicate equal rBC and optical diameters. The red markers represent the mode center points and the error bars are based on calculations using different optical constants (ammonium sulfate and rBC).

The measurements show that 46 ± 12 and 31 ± 5 % of the accumulation-mode particles contain observable amounts of rBC in Gual Pahari and Mukteshwar, respectively. Just as the absolute rBC concentrations (11 ± 11 and $1.0 \pm 0.6\,\mu g\,m^{-3}$ in Gual Pahari and Mukteshwar, respectively), the rBC particle number fraction is higher at the source region (represented by Gual Pahari) and lower at elevated altitudes (Mukteshwar). Although literature data about rBC mixing state are limited (e.g., Raatikainen et al., 2015; Dahlkötter et al., 2014; Reddington et al., 2013), the observed number fractions of particles containing rBC are the highest reported so far.

The observed rBC particles are likely to contain non-refractory materials such as sulfate and organics, but the exact volume fractions could not be quantified, because these particles are not spherical. Current rBC volume equivalent to mobility diameter ratios (number mean $D_{rBC,N}/D_m$ are 0.51 ± 0.02 and 0.50 ± 0.03 for Gual Pahari and Mukteshwar, respectively) would mean that spherical particles have lower rBC volume fractions than expected for fresh particles (e.g., Schwarz et al., 2008; Sahu et al., 2012). However, optical sizes determined using a leading-edge-only (LEO) method were significantly smaller than the mobility diameters, which indicates that the rBC-containing particles are highly irregular ones such as fractal aggregates. The rBC di-

ameter to optical size ratios (~ 0.8 at Gual Pahari and ~ 0.7 at Mukteshwar) are closer to value expected for fresh aerosol, but these calculations are also limited by the fact that the optical size is based on assumed optical parameters and spherical core–shell structure. The exact calculation of particle composition is not possible without additional details about particle structure.

Although individual particles seem to be quite similar in Gual Pahari and Mukteshwar, the total rBC concentrations are about 10 times higher at the more polluted site, Gual Pahari, than those at the regional background site, Mukteshwar. Also, a larger fraction of the particles contain rBC in Gual Pahari than in Mukteshwar. One explanation for the similarity is that some aerosol sources are common for the whole region (e.g., crop residue and biofuel burning and cooking). The other is that a significant fraction of the rBC seen in Mukteshwar can be originating from the densely populated Indo-Gangetic Plain represented by Gual Pahari (Raatikainen et al., 2014).

Detailed information about the black carbon mixing state is needed for assessing and improving the performance of climate models in simulating their evolution and radiative effects. SP2 is one of the few instruments that can provide detailed information about the rBC mixing state. The accuracy of the mixing state parameters can be further improved by size-selecting the particles before measurements with the SP2; this method is especially suitable for polluted areas, where good counting statistics are guaranteed.

5 Data availability

Data are available upon request from the contact author, Tomi Raatikainen (tomi.raatikainen@fmi.fi).

The Supplement related to this article is available online at doi:10.5194/acp-17-371-2017-supplement.

Acknowledgements. The authors would like to acknowledge the Academy of Finland (project numbers 264242, 268004 and 284536), Academy of Finland Centre of Excellence Program (project number 272041) and KONE foundation for the financial support. We thank the local TERI staff for 24/7 work at Mukteshwar aerosol research station.

Edited by: A. Petzold
Reviewed by: three anonymous referees

References

Adachi, K., Chung, S. H., and Buseck, P. R.: Shapes of soot aerosol particles and implications for their effects on climate, J. Geophys. Res., 115, D15206, doi:10.1029/2009JD012868, 2010.

Bollasina, M., Nigam, S., and Lau, K.-M.: Absorbing Aerosols and Summer Monsoon Evolution over South Asia: An Observational Portrayal, J. Climate, 21, 3221–3239, doi:10.1175/2007JCLI2094.1, 2008.

Bollasina, M. A., Ming, Y., and Ramaswamy, V.: Anthropogenic Aerosols and the Weakening of the South Asian Summer Monsoon, Science, 334, 502–505, doi:10.1126/science.1204994, 2011.

Bond, T. C. and Bergstrom, R. W.: Light Absorption by Carbonaceous Particles: An Investigative Review, Aerosol Sci. Tech., 40, 27–67, doi:10.1080/02786820500421521, 2006.

Bond, T. C., Doherty, S. J., Fahey, D. W., Forster, P. M., Berntsen, T., DeAngelo, B. J., Flanner, M. G., Ghan, S., Kärcher, B., Koch, D., Kinne, S., Kondo, Y., Quinn, P. K., Sarofim, M. C., Schultz, M. G., Schulz, M., Venkataraman, C., Zhang, H., Zhang, S., Bellouin, N., Guttikunda, S. K., Hopke, P. K., Jacobson, M. Z., Kaiser, J. W., Klimont, Z., Lohmann, U., Schwarz, J. P., Shindell, D., Storelvmo, T., Warren, S. G., and Zender, C. S.: Bounding the role of black carbon in the climate system: A scientific assessment, J. Geophys. Res.-Atmos., 118, 5380–5552, doi:10.1002/jgrd.50171, 2013.

Boos, W. R. and Storelvmo, T.: Near-linear response of mean monsoon strength to a broad range of radiative forcings, P. Natl. Acad. Sci. USA, 113, 1510–1515, doi:10.1073/pnas.1517143113, 2016.

Cappa, C. D., Onasch, T. B., Massoli, P., Worsnop, D. R., Bates, T. S., Cross, E. S., Davidovits, P., Hakala, J., Hayden, K. L., Jobson, B. T., Kolesar, K. R., Lack, D. A., Lerner, B. M., Li, S.-M., Mellon, D., Nuaaman, I., Olfert, J. S., Petäjä, T., Quinn, P. K., Song, C., Subramanian, R., Williams, E. J., and Zaveri, R. A.: Radiative Absorption Enhancements Due to the Mixing State of Atmospheric Black Carbon, Science, 337, 1078–1081, doi:10.1126/science.1223447, 2012.

Cross, E. S., Onasch, T. B., Ahern, A., Wrobel, W., Slowik, J. G., Olfert, J., Lack, D. A., Massoli, P., Cappa, C. D., Schwarz, J. P., Spackman, J. R., Fahey, D. W., Sedlacek, A., Trimborn, A., Jayne, J. T., Freedman, A., Williams, L. R., Ng, N. L., Mazzoleni, C., Dubey, M., Brem, B., Kok, G., Subramanian, R., Freitag, S., Clarke, A., Thornhill, D., Marr, L. C., Kolb, C. E., Worsnop, D. R., and Davidovits, P.: Soot Particle Studies–Instrument Inter-Comparison–Project Overview, Aerosol Sci. Tech., 44, 592–611, doi:10.1080/02786826.2010.482113, 2010.

Dahlkötter, F., Gysel, M., Sauer, D., Minikin, A., Baumann, R., Seifert, P., Ansmann, A., Fromm, M., Voigt, C., and Weinzierl, B.: The Pagami Creek smoke plume after long-range transport to the upper troposphere over Europe – aerosol properties and black carbon mixing state, Atmos. Chem. Phys., 14, 6111–6137, doi:10.5194/acp-14-6111-2014, 2014.

D'Errico, M., Cagnazzo, C., Fogli, P. G., Lau, W. K. M., von Hardenberg, J., Fierli, F., and Cherchi, A.: Indian monsoon and the elevated-heat-pump mechanism in a coupled aerosol-climate model, J. Geophys. Res.-Atmos., 120, 8712–8723, doi:10.1002/2015JD023346, 2015.

Ganguly, D., Rasch, P. J., Wang, H., and Yoon, J.-H.: Climate response of the South Asian monsoon system to an-

thropogenic aerosols, J. Geophys. Res.-Atmos., 117, D13209, doi:10.1029/2012JD017508, 2012.

Gao, R. S., Schwarz, J. P., Kelly, K. K., Fahey, D. W., Watts, L. A., Thompson, T. L., Spackman, J. R., Slowik, J. G., Cross, E. S., Han, J.-H., Davidovits, P., Onasch, T. B., and Worsnop, D. R.: A Novel Method for Estimating Light-Scattering Properties of Soot Aerosols Using a Modified Single-Particle Soot Photometer, Aerosol Sci. Tech., 41, 125–135, doi:10.1080/02786820601118398, 2007.

Gautam, R., Hsu, N. C., Lau, K.-M., and Kafatos, M.: Aerosol and rainfall variability over the Indian monsoon region: distributions, trends and coupling, Ann. Geophys., 27, 3691–3703, doi:10.5194/angeo-27-3691-2009, 2009.

He, C., Liou, K.-N., Takano, Y., Zhang, R., Levy Zamora, M., Yang, P., Li, Q., and Leung, L. R.: Variation of the radiative properties during black carbon aging: theoretical and experimental intercomparison, Atmos. Chem. Phys., 15, 11967–11980, doi:10.5194/acp-15-11967-2015, 2015.

He, C., Takano, Y., Liou, K.-N., Yang, P., Li, Q., and Mackowski, D. W.: Intercomparison of the GOS approach, superposition T-matrix method, and laboratory measurements for black carbon optical properties during aging, J. Quant. Spectrosc. Ra., 184, 287–296, doi:10.1016/j.jqsrt.2016.08.004, 2016.

Hooda, R., Hyvärinen, A.-P., Vestenius, M., Gilardoni, S., Sharma, V., Vignati, E., Kulmala, M., and Lihavainen, H.: Atmospheric aerosols local–regional discrimination for a semi-urban area in India, Atmos. Res., 168, 13–23, doi:10.1016/j.atmosres.2015.08.014, 2016.

Huang, X.-F., Gao, R. S., Schwarz, J. P., He, L.-Y., Fahey, D. W., Watts, L. A., McComiskey, A., Cooper, O. R., Sun, T.-L., Zeng, L.-W., Hu, M., and Zhang, Y.-H.: Black carbon measurements in the Pearl River Delta region of China, J. Geophys. Res.-Atmos., 116, D12208, doi:10.1029/2010JD014933, 2011.

Huang, X.-F., Sun, T.-L., Zeng, L.-W., Yu, G.-H., and Luan, S.-J.: Black carbon aerosol characterization in a coastal city in South China using a single particle soot photometer, Atmos. Environ., 51, 21–28, doi:10.1016/j.atmosenv.2012.01.056, 2012.

Hyvärinen, A.-P., Lihavainen, H., Komppula, M., Sharma, V. P., Kerminen, V.-M., Panwar, T. S., and Viisanen, Y.: Continuous measurements of optical properties of atmospheric aerosols in Mukteshwar, northern India, J. Geophys. Res., 114, D08207, doi:10.1029/2008JD011489, 2009.

Hyvärinen, A.-P., Lihavainen, H., Komppula, M., Panwar, T. S., Sharma, V. P., Hooda, R. K., and Viisanen, Y.: Aerosol measurements at the Gual Pahari EUCAARI station: preliminary results from in-situ measurements, Atmos. Chem. Phys., 10, 7241–7252, doi:10.5194/acp-10-7241-2010, 2010.

Komppula, M., Lihavainen, H., Hyvärinen, A.-P., Kerminen, V.-M., Panwar, T. S., Sharma, V. P., and Viisanen, Y.: Physical properties of aerosol particles at a Himalayan background site in India, J. Geophys. Res., 114, D12202, doi:10.1029/2008JD011007, 2009.

Kondo, Y., Matsui, H., Moteki, N., Sahu, L., Takegawa, N., Kajino, M., Zhao, Y., Cubison, M. J., Jimenez, J. L., Vay, S., Diskin, G. S., Anderson, B., Wisthaler, A., Mikoviny, T., Fuelberg, H. E., Blake, D. R., Huey, G., Weinheimer, A. J., Knapp, D. J., and Brune, W. H.: Emissions of black carbon, organic, and inorganic aerosols from biomass burning in North America and Asia in 2008, J. Geophys. Res.-Atmos., 116, D08204, doi:10.1029/2010JD015152, 2011.

Laborde, M., Mertes, P., Zieger, P., Dommen, J., Baltensperger, U., and Gysel, M.: Sensitivity of the Single Particle Soot Photometer to different black carbon types, Atmos. Meas. Tech., 5, 1031–1043, doi:10.5194/amt-5-1031-2012, 2012.

Lack, D., Moosmüller, H., McMeeking, G., Chakrabarty, R., and Baumgardner, D.: Characterizing elemental, equivalent black, and refractory black carbon aerosol particles: a review of techniques, their limitations and uncertainties, Anal. Bioanal. Chem., 406, 99–122, doi:10.1007/s00216-013-7402-3, 2014.

Lau, W. K. M., Kim, M.-K., Kim, K.-M., and Lee, W.-S.: Enhanced surface warming and accelerated snow melt in the Himalayas and Tibetan Plateau induced by absorbing aerosols, Environ. Res. Lett., 5, 025204, doi:10.1088/1748-9326/5/2/025204, 2010.

Liu, D., Allan, J., Whitehead, J., Young, D., Flynn, M., Coe, H., McFiggans, G., Fleming, Z. L., and Bandy, B.: Ambient black carbon particle hygroscopic properties controlled by mixing state and composition, Atmos. Chem. Phys., 13, 2015–2029, doi:10.5194/acp-13-2015-2013, 2013.

McMeeking, G. R., Good, N., Petters, M. D., McFiggans, G., and Coe, H.: Influences on the fraction of hydrophobic and hydrophilic black carbon in the atmosphere, Atmos. Chem. Phys., 11, 5099–5112, doi:10.5194/acp-11-5099-2011, 2011.

Menon, S., Hansen, J., Nazarenko, L., and Luo, Y.: Climate Effects of Black Carbon Aerosols in China and India, Science, 297, 2250–2253, doi:10.1126/science.1075159, 2002.

Metcalf, A. R., Craven, J. S., Ensberg, J. J., Brioude, J., Angevine, W., Sorooshian, A., Duong, H. T., Jonsson, H. H., Flagan, R. C., and Seinfeld, J. H.: Black carbon aerosol over the Los Angeles Basin during CalNex, J. Geophys. Res.-Atmos., 117, D00V13, doi:10.1029/2011JD017255, 2012.

Moteki, N. and Kondo, Y.: Effects of Mixing State on Black Carbon Measurements by Laser-Induced Incandescence, Aerosol Sci. Tech., 41, 398–417, doi:10.1080/02786820701199728, 2007.

Moteki, N., Kondo, Y., and Nakamura, S.: Method to measure refractive indices of small nonspherical particles: Application to black carbon particles, J. Aerosol Sci., 41, 513–521, doi:10.1016/j.jaerosci.2010.02.013, 2010.

Moteki, N., Kondo, Y., and Adachi, K.: Identification by single-particle soot photometer of black carbon particles attached to other particles: Laboratory experiments and ground observations in Tokyo, J. Geophys. Res.-Atmos., 119, 1031–1043, doi:10.1002/2013JD020655, 2014.

Ohata, S., Schwarz, J. P., Moteki, N., Koike, M., Takami, A., and Kondo, Y.: Hygroscopicity of materials internally mixed with black carbon measured in Tokyo, J. Geophys. Res.-Atmos., 121, 362–381, doi:10.1002/2015JD024153, 2016.

Pagels, J., Khalizov, A. F., McMurry, P. H., and Zhang, R. Y.: Processing of Soot by Controlled Sulphuric Acid and Water Condensation–Mass and Mobility Relationship, Aerosol Sci. Tech., 43, 629–640, doi:10.1080/02786820902810685, 2009.

Panwar, T., Hooda, R. K., Lihavainen, H., Hyvärinen, A., Sharma, V., and Viisanen, Y.: Atmospheric aerosols at a regional background Himalayan site–Mukteshwar, India, Environ. Monit. Assess., 185, 4753–4764, doi:10.1007/s10661-012-2902-8, 2013.

Peng, J., Hu, M., Guo, S., Du, Z., Zheng, J., Shang, D., Levy Zamora, M., Zeng, L., Shao, M., Wu, Y.-S., Zheng, J., Wang, Y., Glen, C. R., Collins, D. R., Molina, M. J., and Zhang, R.: Markedly enhanced absorption and direct radiative forcing of black carbon under polluted urban environments, P. Natl. Acad. Sci. USA, 113, 4266–4271, doi:10.1073/pnas.1602310113, 2016.

Petzold, A., Ogren, J. A., Fiebig, M., Laj, P., Li, S.-M., Baltensperger, U., Holzer-Popp, T., Kinne, S., Pappalardo, G., Sugimoto, N., Wehrli, C., Wiedensohler, A., and Zhang, X.-Y.: Recommendations for reporting "black carbon" measurements, Atmos. Chem. Phys., 13, 8365–8379, doi:10.5194/acp-13-8365-2013, 2013.

Raatikainen, T., Hyvärinen, A.-P., Hatakka, J., Panwar, T., Hooda, R., Sharma, V., and Lihavainen, H.: The effect of boundary layer dynamics on aerosol properties at the Indo-Gangetic plains and at the foothills of the Himalayas, Atmos. Environ., 89, 548–555, doi:10.1016/j.atmosenv.2014.02.058, 2014.

Raatikainen, T., Brus, D., Hyvärinen, A.-P., Svensson, J., Asmi, E., and Lihavainen, H.: Black carbon concentrations and mixing state in the Finnish Arctic, Atmos. Chem. Phys., 15, 10057–10070, doi:10.5194/acp-15-10057-2015, 2015.

Ramanathan, V., Crutzen, P. J., Lelieveld, J., Mitra, A. P., Althausen, D., Anderson, J., Andreae, M. O., Cantrell, W., Cass, G. R., Chung, C. E., Clarke, A. D., Coakley, J. A., Collins, W. D., Conant, W. C., Dulac, F., Heintzenberg, J., Heymsfield, A. J., Holben, B., Howell, S., Hudson, J., Jayaraman, A., Kiehl, J. T., Krishnamurti, T. N., Lubin, D., McFarquhar, G., Novakov, T., andI. A. Podgorny, J. A. O., Prather, K., Priestley, K., Prospero, J. M., Quinn, P. K., Rajeev, K., Rasch, P., Rupert, S., Sadourny, R., Satheesh, S. K., Shaw, G. E., Sheridan, P., and Valero, F. P. J.: Indian Ocean Experiment: An integrated analysis of the climate forcing and effects of the great Indo-Asian haze, J. Geophys. Res., 106, 28371–28398, 2001.

Ramanathan, V., Li, F., Ramana, M. V., Praveen, P. S., Kim, D., Corrigan, C. E., Nguyen, H., Stone, E. A., Schauer, J. J., Carmichael, G. R., Adhikary, B., and Yoon, S. C.: Atmospheric brown clouds: Hemispherical and regional variations in long-range transport, absorption, and radiative forcing, J. Geophys. Res., 112, D22S21, doi:10.1029/2006JD008124, 2007.

Reddington, C. L., McMeeking, G., Mann, G. W., Coe, H., Frontoso, M. G., Liu, D., Flynn, M., Spracklen, D. V., and Carslaw, K. S.: The mass and number size distributions of black carbon aerosol over Europe, Atmos. Chem. Phys., 13, 4917–4939, doi:10.5194/acp-13-4917-2013, 2013.

Sahu, L. K., Kondo, Y., Moteki, N., Takegawa, N., Zhao, Y., Cubison, M. J., Jimenez, J. L., Vay, S., Diskin, G. S., Wisthaler, A., Mikoviny, T., Huey, L. G., Weinheimer, A. J., and Knapp, D. J.: Emission characteristics of black carbon in anthropogenic and biomass burning plumes over California during ARCTAS-CARB 2008, J. Geophys. Res.-Atmos., 117, D16302, doi:10.1029/2011JD017401, 2012.

Schwarz, J. P., Gao, R. S., Fahey, D. W., Thomson, D. S., Watts, L. A., Wilson, J. C., Reeves, J. M., Darbeheshti, M., Baumgardner, D. G., Kok, G. L., Chung, S. H., Schulz, M., Hendricks, J., Lauer, A., Kärcher, B., Slowik, J. G., Rosenlof, K. H., Thompson, T. L., Langford, A. O., Loewenstein, M., and Aikin, K. C.: Single-particle measurements of midlatitude black carbon and light-scattering aerosols from the boundary layer to the lower stratosphere, J. Geophys. Res.-Atmos., 111, D16207, doi:10.1029/2006JD007076, 2006.

Schwarz, J. P., Gao, R. S., Spackman, J. R., Watts, L. A., Thomson, D. S., Fahey, D. W., Ryerson, T. B., Peischl, J., Holloway, J. S., Trainer, M., Frost, G. J., Baynard, T., Lack, D. A., de Gouw, J. A., Warneke, C., and Del Negro, L. A.: Measurement of the mixing state, mass, and optical size of individual black carbon particles in urban and biomass burning emissions, Geophys. Res. Lett., 35, L13810, doi:10.1029/2008GL033968, 2008.

Sedlacek, A. J., Lewis, E. R., Kleinman, L., Xu, J., and Zhang, Q.: Determination of and evidence for non-core-shell structure of particles containing black carbon using the Single-Particle Soot Photometer (SP2), Geophys. Res. Lett., 39, L06802, doi:10.1029/2012GL050905, 2012.

Slowik, J. G., Cross, E. S., Han, J.-H., Davidovits, P., Onasch, T. B., Jayne, J. T., Williams, L. R., Canagaratna, M. R., Worsnop, D. R., Chakrabarty, R. K., Moosmüller, H., Arnott, W. P., Schwarz, J. P., Gao, R.-S., Fahey, D. W., Kok, G. L., and Petzold, A.: An Inter-Comparison of Instruments Measuring Black Carbon Content of Soot Particles, Aerosol Sci. Tech., 41, 295–314, doi:10.1080/02786820701197078, 2007.

Sorensen, C. M.: Light Scattering by Fractal Aggregates: A Review, Aerosol Sci. Tech., 35, 648–687, doi:10.1080/02786820117868, 2001.

Stephens, M., Turner, N., and Sandberg, J.: Particle identification by laser-induced incandescence in a solid-state laser cavity, Appl. Optics, 42, 3726–3736, doi:10.1364/AO.42.003726, 2003.

Stocker, T., Qin, D., Plattner, G.-K., Tignor, M., Allen, S., Boschung, J., Nauels, A., Xia, Y., Bex, V., and Midgley, P. (Eds.): Climate Change 2013: The Physical Science Basis. Contribution of Working Group I to the Fifth Assessment Report of the Intergovernmental Panel on Climate Change, Cambridge University Press, Cambridge, United Kingdom and New York, NY, USA, 1535 pp., 2013.

Taylor, J. W., Allan, J. D., Liu, D., Flynn, M., Weber, R., Zhang, X., Lefer, B. L., Grossberg, N., Flynn, J., and Coe, H.: Assessment of the sensitivity of core/shell parameters derived using the single-particle soot photometer to density and refractive index, Atmos. Meas. Tech., 8, 1701–1718, doi:10.5194/amt-8-1701-2015, 2015.

Wang, Q., Schwarz, J. P., Cao, J., Gao, R., Fahey, D.W., Hu, T., Huang, R.-J., Han, Y., and Shen, Z.: Black carbon aerosol characterization in a remote area of Qinghai–Tibetan Plateau, western China, Sci. Total Environ., 1, 151–158, doi:10.1016/j.scitotenv.2014.01.098, 2014.

Wiedensohler, A., Birmili, W., Nowak, A., Sonntag, A., Weinhold, K., Merkel, M., Wehner, B., Tuch, T., Pfeifer, S., Fiebig, M., Fjäraa, A. M., Asmi, E., Sellegri, K., Depuy, R., Venzac, H., Villani, P., Laj, P., Aalto, P., Ogren, J. A., Swietlicki, E., Williams, P., Roldin, P., Quincey, P., Hüglin, C., Fierz-Schmidhauser, R., Gysel, M., Weingartner, E., Riccobono, F., Santos, S., Grüning, C., Faloon, K., Beddows, D., Harrison, R., Monahan, C., Jennings, S. G., O'Dowd, C. D., Marinoni, A., Horn, H.-G., Keck, L., Jiang, J., Scheckman, J., McMurry, P. H., Deng, Z., Zhao, C. S., Moerman, M., Henzing, B., de Leeuw, G., Löschau, G., and Bastian, S.: Mobility particle size spectrometers: harmonization of technical standards and data structure to facilitate high quality long-term observations of atmospheric particle number size

distributions, Atmos. Meas. Tech., 5, 657–685, doi:10.5194/amt-5-657-2012, 2012.

Zhang, R., Khalizov, A. F., Pagels, J., Zhang, D., Xue, H., and McMurry, P. H.: Variability in morphology, hygroscopicity, and optical properties of soot aerosols during atmospheric processing, P. Natl. Acad. Sci. USA, 105, 10291–10296, doi:10.1073/pnas.0804860105, 2008.

Zhang, Y., Zhang, Q., Cheng, Y., Su, H., Kecorius, S., Wang, Z., Wu, Z., Hu, M., Zhu, T., Wiedensohler, A., and He, K.: Measuring the morphology and density of internally mixed black carbon with SP2 and VTDMA: new insight into the absorption enhancement of black carbon in the atmosphere, Atmos. Meas. Tech., 9, 1833–1843, doi:10.5194/amt-9-1833-2016, 2016.

ILMATIETEEN LAITOS
METEOROLOGISKA INSTITUTET
FINNISH METEOROLOGICAL INSTITUTE

FINNISH METEOROLOGICAL INSTITUTE
Erik Palménin aukio 1
P.O. Box 503
FI-00560 HELSINKI
tel. +358 29 539 1000
WWW.FMI.FI

FINNISH METEOROLOGICAL INSTITUTE
CONTRIBUTIONS No. 150
ISBN 978-952-336-069-3 (paperback)
ISSN 0782-6117
Erweko 2019

ISBN 978-952-336-070-9 (pdf)
Helsinki 2019